Department of Architecture
and Built Environment

SIMULATION OF PHOTOVOLTAIC AIRFLOW WINDOWS FOR INDOOR THERMAL AND VISUAL COMFORT AND ELECTRICITY GENERATION

Abdullah Haredy
BArch, MSc

Thesis submitted to the University of Nottingham for
the degree of Doctor of Philosophy
March 2016

ABSTRACT

The alleviation of heating (in winter), cooling (in summer), artificial lighting and electricity use in office facilities is defined as a bioclimatic trend that offers sustainable building practice through a semi-transparent building integrated photovoltaic thermal envelope as a photovoltaic airflow window system. This thesis aims to produce synthesised design and strategies for the use of a proposed airflow window unit in office building in any given location and to maximise use of the renewable energy. Computational Fluid Dynamics (CFD), namely ANSYS Fluent 14.0, and ECOTECT have been employed to model the mechanical and natural ventilation of an office building integrated with a semi-transparent photovoltaic airflow window and the daylighting impact of various PV transparent degrees (15, 20, 25, 30 and 35 per cent) on the interior space, respectively, for winter and summer conditions.

The use of such software has urged to establish a validation analysis a priori in order to ascertain the applicability of the tools to the targeted examination. The validation process involved a comparison of the results of CFD turbulence models, first, against benchmark and, second, against results of literature for identical component. The results of ECOTECT, in terms of daylight factor and illuminance level, were also compared against the results of Daysim/radiance, Troplux and BC/LC found in the literature. Excellent agreement was attained from the comparison of the results with errors less than 10 per cent.

The study presents results of modelling of the airflow window system integrated into an office room for energy efficiency and adequate level of thermal and visual comfort. Results have revealed that the combination of mechanical and buoyancy induced flow spreads the heat internally warming the space to be thermally acceptable during the heating season whilst the mechanical convection is a main force for the cooling season. The thermal and visual comfort was compared for different PV airflow window transparent levels to determine the optimum PV transparency for the office space. Moreover, time-dependant and steady state conditions were imposed to predict the

thermal and air behaviour for more elaborate investigation. The transient analysis was carried out, in sequential and individual base, according to the solar irradiance of each minute of working period, 8am-4pm (winter) and 5am-7pm (summer). The results obtained from transient and steady state, for both seasons, were compared and revealed negligible impact of transient effect.

The PV electricity output was calculated from each transparency level under each condition, summer and winter (transient and steady). The predicted flow patterns, temperature distribution and the daylight factors in the room have been used to determine the most appropriate opening locations, sizes and system specifications for maintaining a comfortable indoor environment. The simulation investigation show that, for the proposed window model, optimum thermal and visual performance can be achieved from the PV transparency level of 20 per cent, during the heating season, and from the PV transmittance of 15 per cent, during the cooling season, where the PV output is highest. However the PV transparencies of 25, 30 and 35% can be reliable under altered conditions of operation.

ACKNOWLEDGEMENTS

This honoured work could not have been completed without people who I have in communicate with at the University of Nottingham. Thus, it is quite demanding to express my sincere gratitude towards these wonderful figures.

I would like to thank my main supervisor, Dr Guohui Gan, for his continuing guidance and inspiration towards the achievement of my doctoral degree. He had a great contribution of visioning this study showing appreciated patience to advice throughout the work; Dr Mohamed Gadi, my second supervisor for providing valuable input; Dr Robin Wilson for allowing me to involve in his ECOTECT class that was beneficial towards my studies.

I would also like to thank the staff of the Department of the Built Environment, especially the IT team for giving advice and helping with computer programming and technical issues that I had encountered during my work.

I am highly grateful to Baha University, Baha, Kingdom of Saudi Arabia represented in Saudi Arabia Cultural Bureau in London, United Kingdom for the financial support (through payments of tuition fees, living expenses and incentive allowances) towards this academic achievement.

Finally, and most important of all, I am most thankful for the infinite love and support that my family has always granted me, during my studies at the University of Nottingham and my whole life.

TABLE OF CONTENTS

LIST OF FIGURES

LIST OF TABLES

LIST OF ABBREVIATIONS

AC:	Alternating current
ASHRAE:	American Society of Heating, Refrigeration, and Air-Conditioning Engineers
BCO:	The British Council for Offices
BESTEST:	Building Energy Simulation Test
BIPV:	Building-integrated photovoltaics
BIPV/T:	Building-integrated photovoltaics thermal system
CFD:	Computational fluid dynamics
CRI:	Color rendering index
CCT:	Correlated color temperature
CIBSE:	Chartered Institution of Building Services Engineers
DC:	Direct current
FDM:	Finite Difference Method
FEM:	Finite Element Method
FVM:	Finite Volume Method
HVAC:	Heating, Ventilation, and Air Conditioning
PV:	Photovoltaic
PCMs:	Phase Change Materials
PIV:	Particle image velocimetry
SST:	Shear-stress transport
SPD:	Spectral power distribution
SPVHG:	Semi-transparent Photovoltaic Heat Gain
STPV:	Semi-transparent Photovoltaic
STBIPV:	Semi-transparent building-integrated photovoltaics
STBIPV/T:	Semi-transparent building-integrated photovoltaics thermal system
ST:	Solar transmittance
UK:	United Kingdom
USA:	United States of America
USD:	United States dollar
WWR:	Window to wall ratio

NOMENCLATURE

A	opening area (m^2)
A_{inlet}	refers to the area of the inlet (m^2)
A_{outlet}	refers to the area of the outlet (m^2)
C_P	specific heat of air (J/kg K)
C_d	discharge coefficient
D	plate spacing (m)
D_H	hydraulic diameter (m)
G	incident solar radiation on the PV surface (W/m^2)
G_m	monthly mean incident solar radiation on the PV surface (W h/m^2)
G_g	solar radiation levels incident on the window double glazing (W/m^2)
G_P	solar radiation levels incident on the PV panels (W/m^2)
G_r	Grashof Number
g	gravitational acceleration (m/s2)
$\mathbf{g}_{trans}$	coefficient of transmitted radiation gain to the interior
$\mathbf{g}_{vent}$	coefficient of absorbed radiation gain in the ventilated gap
$\bar{\mathbf{g}}_{trans}$	monthly mean coefficients of transmitted radiation gain to the interior
$\bar{\mathbf{g}}_{vent}$	monthly mean coefficients of absorbed radiation gain in the ventilated gap
h_c	heat transfer coefficient (W/m^2k)
h_{cg}	convective heat transfer coefficient for heat transfer from the double glazing to the air gap (W/m^2 K)
h_{cp}	The convective heat transfer coefficient for heat transfer from the PV panel to the air gap (W/m^2 K)
h_r	long wave radiation heat exchange coefficient between the PV panel and the double glazing window (W/m^2 K)
k_{air}	thermal conductivity of air (W/m.K)
m	ventilated air flow rate (kg/s)
$\overline{Nu}$	mean Nusselt number
$\overline{Nu}_{lam}$	mean laminar Nusselt number
$\overline{Nu}_{turb}$	mean turbulent Nusselt number
$\mathbf{P}_{\text{inlet}}$	refers to the perimeter of the inlet (m^2)
$\mathbf{P}_{outlet}$	refers to the perimeter of the outlet (m^2)
ΔP	pressure difference across the opening (Pa)
P_r	Prandtl number
Q	ventilation rate (m^3/s)
Q_E	the rate of electrical power generation by the PV panels (W/m^2)
Q_{trans}	net rate thermal energy to the room (W/m^2)
Q_{vent}	ventilation heat gain (W/m^2)
Re	Reynolds number
Re_{forced}	forced convection Reynolds number
Re_{free}	free convection Reynolds number
T_{amb}	ambient air temperature (°C)
T_g	glass window temperature (°C)
T_m	mean air temperature in the air gap (°C)
T_P	PV panel temperature (°C)
T_{room}	room air temperature (°C)
T_{ref}	reference temperature of the element (°C)
U_g	thermal transmittance between the double glazing and the room space (W/m^2 K)
U_P	thermal transmittance between the PV panel and ambient (W/m^2 K)
U_{vent}	heat loss from interior to ventilation air (W/m^2 K)
U_{trans}	heat loss from the room (W/m^2 K)
$\bar{U}_{vent}$	monthly mean heat loss from interior to ventilation air (W h/m^2 K)
$\bar{U}_{trans}$	monthly mean heat loss from the room (W h/m^2 K)

GREEK SYMBOLS

$\boldsymbol{\beta}$	coefficient of thermal expansion (K^{-1})
$\boldsymbol{\rho}$	air density (kg/m^3)
$\boldsymbol{\alpha_p}$	PV absorptivity level
$\boldsymbol{\tau_p}$	PV transparency level
$\boldsymbol{\eta}$	PV electricity conversion efficiency
$\boldsymbol{\mu}$	dynamic viscosity (kg/ms)
$\boldsymbol{v}$	air velocity (m/s)
$\boldsymbol{\upsilon}$	kinematic viscosity of air (m^2/s)

CHAPTER 1 BACKGROUND

1.1 INTRODUCTION

Buildings are accountable for a large portion of consumption of resources and energy in addition to production of a substantial amount of environmental pollutants. Building envelope is a major component that is responsible for transmitting heat between the environment outside and inside a space, thus, it is essential to carefully balance heat loss and gain during the design process and accurately identify its properties. Nowadays, the dedication towards saving energy using advanced building envelope design criteria and techniques has become extensively a priority issue. In developed countries, residential and commercial buildings consume 20–40 per cent of all primary energy (Perez-Lombard et al. 2008). The population growth, the long-term occupation and the importance of providing satisfactory levels of building comfort have raised the concerns about saving energy in buildings that will extend to continue for the future. In the European Union, 20 per cent of the energy saving would be potentially achieved by improving the energy efficiency that accounts for 60 billion euros a year (Blok et al. 2001; Blok 2004).

A building design must be feasible to preserve acquired heat during the heating season and to lose heat during the cooling season. There are two different routes of heat loss or heat gain: fabric heat losses and ventilation heat losses. Fabric heat losses occur when the heat transfers from the warm interior through the building envelope to the cold exterior. This transference is attributed to the mechanisms of convection, conduction, and radiation of heat transfer. The other form of losses, ventilation route, occurs when the inside warm air is replaced by the outside cold air through the building openings. Therefore, careful attention must be directed to the solar access and building façade design strategies and construction forms would then minimize excessive energy consumption of the building.

To this end, a building must be considered as a whole. From this perspective examinations on how the site, form, materials and structure should be performed to explore possible reduction on energy consumption whilst maintaining comfort.

Furthermore, the importance of daylight needs to be taken into consideration for energy savings. Natural light is a rewarding use of solar energy, thus, responsible envelope design should be considered to provide sufficient daylight. However, the dangers of glare and overheating must be avoided. Therefore, façade design and ventilation are two of key elements to a successful strategy. As part of this, low-e double-glazed windows have been used to control the solar radiation during the day. Energy efficient façade design which makes use of available solar energy has great potential today for enormous applications in the built environment with significant savings in conventional and non-renewable energy of 50 per cent in residential buildings with appropriate approach (Nakahara et al. 1995).

Numerous energy saving techniques in window technology have been improved and developed to mitigate the fenestration total transmittance (Han et al. 2010) achieving satisfactory daylight and noise requirements. These techniques include the application of multiple-glazed façades, low-conductivity substitute fill gases, tinted glazing, switchable glazing, spectrally selective coatings, low-emissivity coatings, windows with Phase Change Materials (PCMs) viz photochromatics, thermochromatics, and more advanced techniques that have been proposed to keep the building energy consumption minimal for Heating, Ventilation, and Air Conditioning (HVAC).

Being a simple and practical concept, the technology of multiple-glazed ventilated façades has been the most promising building configuration. It utilizes solar radiation to reduce the energy consumption and increase thermal performance of a building which is achieved as a result of the fact that the solar radiation incident onto the glass surface translates into electrical and desired daylight sources as well as thermal energy for the heating seasons. Moreover, the air flow between the façade panes can represent a critical role on energy savings. This bioclimatic solution proposal has been recently booming due to its remarkable development among others and attracted strong dedication from the energy and building scientific community which already has devoted massive efforts with relation to the system performance (Lloret et al. 1995; Reijenga et al. 1997; Mei et al. 2003; Infield et al. 2004).

This chapter introduces an extensive background of the topic of this study. The research objectives, scope, and limitations are given. The research hypothesis is formulated; the significance of the subject is underlined by performing a CFD simulation analysis of a proposed ventilated photovoltaic window unit, the fact behind the motivation of conducting this research is explained, and an outline of the entire document is presented.

1.2 BACKGROUND

The representation of the ventilated multiple-layer façades falls under two categories: double-skin façade and airflow window. Both are comprised of two or more glazing panes where air can flow either by natural, forced or mixed convection providing space heating (when extracting the preheated air between the cavities) and electrical energy (via photovoltaic solar cells integration) and natural lighting.

1.2.1 DOUBLE-SKIN FAÇADE

Le Corbusier, the French architect, brought the first double glazing unit that consisted of glass membranes sealed hermetically with 12mm air gap in 1935 (Wigginton et al. 2000). The unit, named "Thermopane", was applied to all solar homes in USA designed by Chicago Architect George Fred Keck. The double glazing units were analysed over the first half of 20^{th} century to enable people to understand the building energy efficiency. By 1960s, double glazing units were significantly approved and marketed (Wigginton et al. 2000). The significant development of double glazing system was in 1961 with the completion of Wallasay School that its façade consisted of two glass walls with 600mm air gap that enables daylight and provides solar energy. The outer wall was clear and the inner was translucent containing reversible panels. These panels were black in one side and polished aluminium on the other. The building was naturally ventilated (Wigginton et al. 2000). Trombe Michel Wall was the first solar wall that built in 1882 by Morse (Wigginton et al. 2000). As Morse was aware of the sun's rays passing through glass and falling upon an opaque metal that can be warmed and then produces thermal energy, Morse ended up to construct such an energy efficient envelope (what is known today a

Trombe-Michel Wall). The wall consisted of three layers: an outer glass pane, an opaque metal right behind it, both attached to the masonry wall of the house, the third was an insulation layer. The cavity openings were in both the top and the bottom incorporated with adjustable flaps that were located at the top and the bottom of the masonry wall as well. The adjustable flaps enable the wall to work in several ways; the cold air can be driven from the bottom opening and preheats between the cavities to reach the interior space through the top opening; the air inside the room could pass through the heated opaque metal to run inside the room if the outside air was too cold and both the top and the bottom flaps should be closed. However, the inner top flap should be closed and the outer top flap should be opened if the room was too hot (Wigginton et al. 2000).

The need to improve glazing resistance to heat transfer to the building through the façade led to the application of extra glazing layer during the 1970s as the first use of double skin Façade. The double skin façade consists of two glass skins, inner and outer panes with airflow chamber. Air can flow naturally or mechanically between the inner and the outer skin through the cavity to improve the energy performance of a building. Moreover, the double skin façade system can be utilised as a source of electrical energy and shading device when integrated with photovoltaic cells. PV can be encapsulated to the outer glazing layer to exploit the picked up heat within the cavity by the air stream which yields to increase the efficiency of PV module's power output. (Roberts et al. 2009). PV modules are applicable to integrate with residential and commercial buildings that can be supplemented by the power taken from the electrical grid to contribute as a source of electricity that can minimise building energy consumption; PV can further put power back when electricity is not in need by the building for future use. Double-skin façade is best suited for building-integrated PV cells. This can be configured as part of the outdoor, facing the sun directly, and transparent (glazing) or opaque (insulating) walls are placed as part of the indoor skin. However, more output power can be produced from rooftop PV panels due to the smaller angels of incidence and from vertical south-facing façades in winter, in the northern hemisphere. PV modules efficiency

decrease when cell temperatures are increased. Thus, it is critical to maintain the PV panel's temperature moderate.

1.2.2 AIRFLOW WINDOW

The notion of airflow window goes back to September 27, 1956 when a Swedish invention was filed for an architectural element that conserves energy and improves air quality by venting exhaust room air through an opening chamber between double glass membranes (Aitken 1981). Although the double-skin façade is expensive to apply in residential buildings, airflow windows are affordable for installation to enhance thermal performance of a building and to provide adequate perimeter space comfort. They can bring buildings to a significant level of energy efficient performance. The mechanism of airflow window can be either mechanical or natural (Baker et al. 2000) depending on the airflow pattern and window structure. Figure 1.1 shows five modes of operation for airflow windows: supply, exhaust, indoor air curtain, outdoor air curtain, and dual airflow window (Gosselin et al. 2008a). The supply mode Figure 1.1 (a) circulates the outside fresh air into the space, whilst the solar radiation heats the air between the cavities. Thus, the mode is for heating seasons. For cooling seasons, the exhaust air mode Figure 1.1 (b) is best suited because it cools window panels and the room by removing heat accumulated between the cavity and inside the room by extracting the inside air through the cavity to outside space. Another winter mode is the indoor air curtain window Figure 1.1 (c); this mode uses solar radiation to heat indoor air. The outdoor curtain window Figure 1.1 (d) uses solar radiation to heat the window panels in winter. However, both indoor and outdoor curtain windows do not exchange air between indoor and outdoor. To trap more solar radiation, sometimes venetian blinds are added into the cavity to improve the thermal performance. The dual airflow window Figure 1.1 (e) combines two airflow paths, inner and outer path. The inner path circulates the inside air to outside; the outer path ventilate the inside space with fresh outdoor air. There is a heat exchange in this mode which is the mid-glazing.

In summary, it is imperative to consider how the climate, of where the building will be situated, is estimated in order to predict the energy consumption of a prospective building, thus, the excess energy consumption can be minimized by enhancing the design of the building. Despite climate could further be moderated through the building fabric when it is harsh, the need for energy consumption is still essential to maintain internal conditions. In other word, therefore, the greater moderation of the climate for internally acceptable conditions, the less energy consumption is overridden.

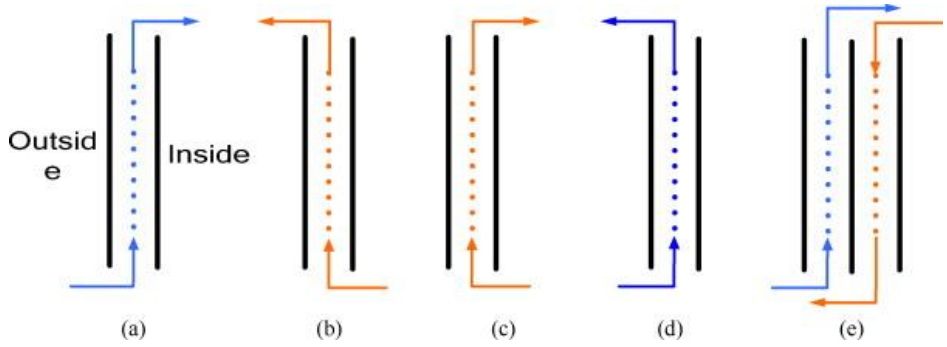

Figure 1.1: operating modes of airflow windows: (a) supply mode, (b) exhaust mode, (c) indoor air curtain mode, (d) outdoor air curtain mode, (e) dual airflow mode (adapted from Wei et al. (2010))

1.3 SOLAR PHOTOVOLTAIC ENERGY

The photovoltaic power generation system comprises primarily of different elements such as cells, mechanical and electrical connected items for controlling its power output. The electricity, expected to be generated from the PV cells when the sun is vertically positioned on a clear day, is measured in peak kilowatts (kWp). A group of photovoltaic panels can form an electricity generation system that come in forms such as PV panels, batteries (for off-grid systems), charge controller, inverter and/ or export electricity meter. The incorporated energy in the materials that are essential for manufacturing a 2.1 kWp BIPV system is displayed in Figure 1.2. PV panel can be formed from these cells that are grouped together and form variety of PV panel sizes where the smallest can generate few watts to the largest the reach over 3kW in size (Parida et al. 2011). Batteries can store the generated electricity for future demand, though the electricity can be converted to alternating current (the type of electricity that commonly used

throughout the world (AC)) and exported to the grid (Parida et al. 2011). The grid can feed building utilities with the electricity via the exporter meter. However, buildings can be more independent with PV's from the national grids.

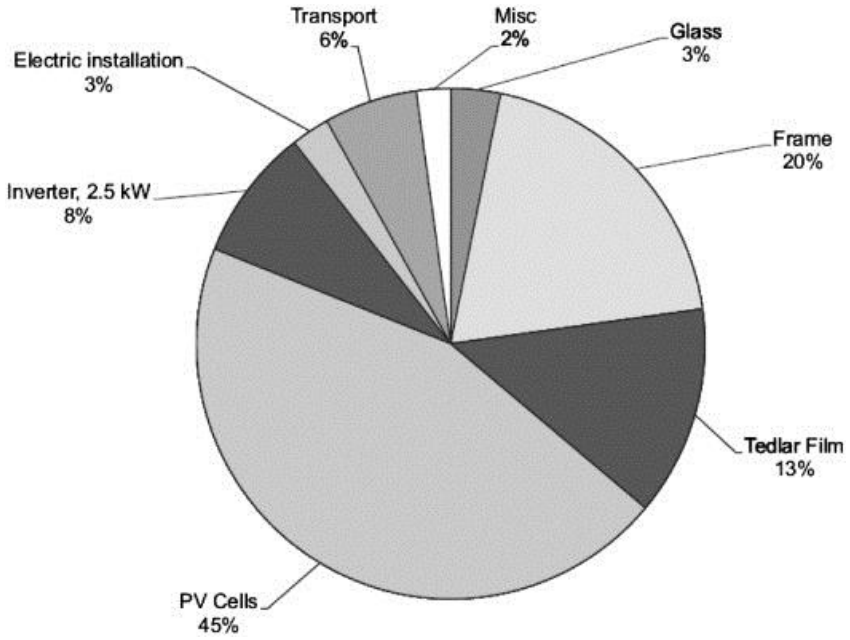

Figure 1.2 : The incorporated energy in the materials that are essential for manufacturing a 2.1 kWp BIPV system (reproduced from Hammond et al. (2012))

1.3.1 PV'S TYPES AND COSTS

Buildings predominantly use two types of PVs: polycrystalline and monocrystalline. The former are the most dominated components in-use whereas the latter are slightly high in cost and slightly more efficient. PV's produce electricity in the form of direct current (the electricity that moves from negative charges to positive charges through a conducting material (DC)) whilst buildings use alternative current (AC) electricity, thus, inverter is involved to change the produced electricity to (AC) (Hall 2008).

Despite photovoltaics are leading-edge systems for energy efficient buildings, their costs are higher than other solutions. For PV efficiencies of 4.5-6 per cent, in the early 1950s, the solar cells cost 286 USD/W (Yoon et al. 2011). Significant rise of silicon price was, since then, noticed due to the increased demand for solar panel. Thus, other materials and thinner silicon were utilised to maintain reasonable cost. Fortunately, the price is expected to gradually decrease as manufactures adopted large scale of production. One watt installation of PV panel can cost USD 6.50-7.50 as an average, in early 2006,

including inverters, mounts and electrical devices (Peng et al. 2011). However, the PV array costs can be offset thanks to replacing the expensive cladding materials with PV cells.

1.3.2 APPLICATION OF PHOTOVOLTAICS INTO MULTIPLE-GLAZED VENTILATED FAÇADES

The integration of photovoltaic into multiple-glazed façades has been further applied to different types of building. The initiatives of the United States million solar rooftop, Japanese 70,000 residential PV rooftop and European 500,000 PV programmes, are the penetrated factors of mainstream electricity market (IEA 1998). The 100,000 rooftop programme in Germany were launched at the beginning of 1999 to create a huge market for some 500 MW of PV modules; the programme is much greater than the total world module shipments of around 152 MW in 1997 (Curry 1998). The large PV companies such as BP Solar, Solarex, Shell/Pilkington, Kyocera, Sharp, Canon and Pacific Solar have driven the building integrated photovoltaic (BIPV) system development and growth to success.

PV panels can be secured into the outer skin of the façade unit using a metal structure, whilst the air flow behind the panel cools down the solar cells which improves their efficiency. More than just providing electrical energy, the integration of photovoltaic solar cells is a statement about innovative architecture as well as aesthetically-pleased engineering design (Roberts et al. 2009). Recently, a more advanced building integrated photovoltaic technology has become important and effective tool that provides thermal comfort beside the electrical energy and daylighting (BIPV/T). The technology aims to reduce costs and to minimize energy loads of both electricity and space heating. Two possible classifications for building integrated photovoltaic thermal systems (BIPV/T) are semi-transparent or opaque type. Figure 1.3 presents detailed classifications. BIPV/T systems are considered as an attractive technology for sustainable buildings (Agrawal et al. 2010).

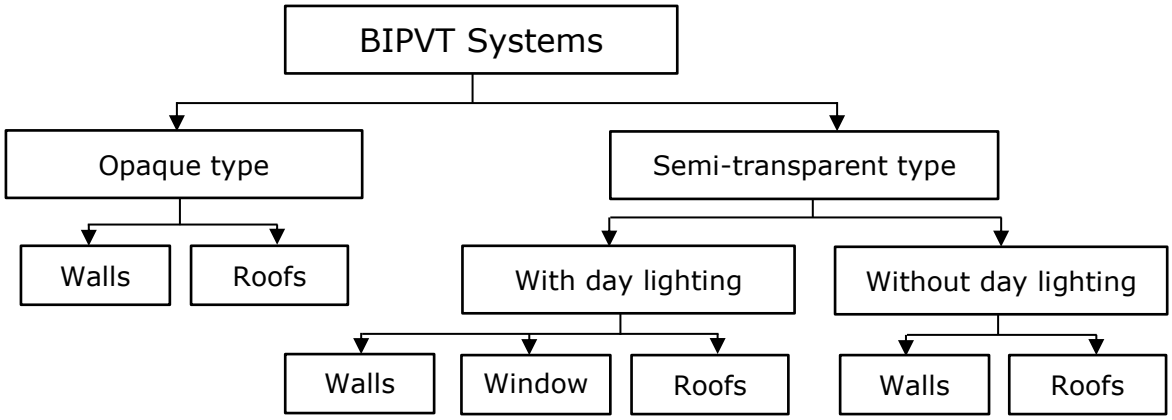

Figure 1.3: Classification of BIPVT systems

1.4 FORCES OF AIRFLOW BETWEEN AIRFLOW WINDOW FAÇADES CAVITIES

Airflow window façade can depend on two ventilation processes to supply and extract air from indoor space: mechanical and natural ventilation operations where the latter is attributed to two forms of driving forces as wind-induced or buoyancy-induced flow. The difference between the two mechanisms, mechanical and natural, is that the former has a fan as dominated force for the airflow. Obviously, a fan can provide controlled flow rates that result in reduced surface temperatures. Thus, mechanically ventilated façade can work more efficiently as HVAC system of the building (Jiru et al. 2008). However, when the façade unit is naturally ventilated, three important aspects can dominate its performance: solar radiation availability, proper orientation, and local conditions. For example, when airflow windows are installed in a building in Barcelona, 12 per cent of heating loads would be saved, whereas only two per cent of total energy consumption would be reduced in Stuttgart and Loughborough (Mei et al. 2003). Therefore, careful attention must be paid to these factors in building design in order to maintain acceptable indoor air quality. Failure to meet the proper airflow windows standards and considerations may result in inadequate level of occupant comfort.

Extensive evaluation of the thermal performance of natural and mechanical ventilation for multiple layers has been conducted (Chen 1995; Baker et al. 2000; Zöllner et al. 2002; Faggembauu et al. 2003a and 2003b; McEvoy et al. 2003; Posner et al. 2003; Manz et al. 2004; Park et al. 2004a; Saelens et al. 2004; Till 2004; Hien et al. 2005;

Safer et al. 2005; Balocco et al. 2006; Southall et al. 2006; Liao et al. 2007; Eicker et al. 2008; Jiru et al. 2008; Haase et al. 2009a; Wei et al. 2010). Some studies relied on experimental measurements (McEvoy et al. 2003; Till 2004; Eicker et al. 2008) and others applied numerical models (Chen 1995; Baker et al. 2000; Zöllner et al. 2002; Faggembauu et al. 2003a and 2003b; Posner et al. 2003; Manz et al. 2004; Park et al. 2004a; Saelens et al. 2004; Hien et al. 2005; Safer et al. 2005; Balocco et al. 2006; Southall et al. 2006; Liao et al. 2007; Jiru et al. 2008; Haase et al. 2009a; Wei et al. 2010) for investigation into the performance and the optimum design criteria and climatic and working parameters of such energy efficient systems. The massive sources available on numerical studies of airflow windows indicate that the most predominant tools to evaluate the airflow window are CFD and energy balance models.

1.5 COMPUTATIONAL FLUID DYNAMICS (CFD) CODE

Since the purpose of this simulation is to understand the complexity of fluid dynamic and thermal energy of building integrated semi-transparent photovoltaic airflow window, the CFD code, ANSYS Fluent 14.0, is used for this study. DesignModeler, the pre-processor program, is a standard tool for formulating the geometry model. The mixing flow phenomena within the airflow window has urged for three-dimensional modelling instead of two-dimensional as the former can release accurate estimations as well as the ability of adapting such a complex flow except that it is time consuming. Unstructured meshes were generated.

The flow within a multiple layers of BIPV semi-transparent component falls under the turbulent flow classification (Bakker 2012). Therefore, a suitable turbulent mathematical model must be thoughtfully defined to process the calculations for the basic conservation equations of mass, momentum and energy that are incorporated in Fluent 14.0. The equations are solved in a sequence or segregated order to iteratively reach the convergence state which is the end of solution process. Literature is considerably loaded with studies, such as Awbi (1998 and 2013), that employed the standard k-ε model for the calculations as the most appropriate turbulence model. However, it is insufficient for

modelling turbulence in the supply mode of airflow flow window and in non-circular duct (Ansys 2011; Bakker 2012) which both belong to the case in this study. The shear stress transport turbulence model (SST k-ω) was developed by Menter (1994) to be effectively combine the robustness and the accuracy of the standard k-ε in the near-wall region with the free-stream independence of the model. The SST k-ω is similar to the standard k-ε model, yet, it is refined to a degree that can conform to a wide class of flows to be more accurate and reliable. Bhamjee et al. (2012) applied an SST k-ω model with enhanced wall treatment to investigate a three-dimensional geometry of a supply air window.

1.6 PROBLEM STATEMENT

The excessive energy consumption of buildings underlies the bridging of unwanted heat gains and heat loss through windows and transparent façades between buildings and the outside environment. As such, it is imperative to consider specific design criteria for solar heat gains resources in buildings to optimise and allow energy efficient level of thermal and visual performance.

1.7 MOTIVATION

The need for a system that achieves reasonable reduction in cooling and heating loads during the summer and winter seasons, respectively, in order to save energy has driven the built environment professionals to innovate a semi-transparent building-integrated photovoltaic thermal system (STBIPV/T). This system can provide a wide class of opportunities for innovative architectural design, and it can be an architecturally sleek element. It can further work as thermal provider in the form of heated air, and as efficient electricity generator by conserving the absorbed solar radiation by PV cells. Furthermore, the maximising of its efficiency in generating electricity is due to the forced ventilation around the PV panel that moderates its temperature. (Petter Jelle et al. 2012).

A huge variety of solutions would be achieved by developing such a system. Future developments are attributed to key factors namely low production cost, low environmental impacts, and higher efficiency. For more advanced technology, PV

materials should be developed to lead in a more advanced STBIPV/T that can form semi-transparent elements of fenestration. These transparent modules can be utilized for buildings construction components as façades or glass ceilings to create different visual effects (Petter Jelle et al. 2012).

1.8 THESIS HYPOTHESIS

The hypothesis that will be tested in this study has been formulated in analogy to the hypotheses put forward by Liao et al.(2007), Hadlock (2006), and Nemati (2009) in their researches and papers to study the performance and potentials of (BIPV/T) that have been constructed at Concordia University, Montreal, Quebec, Canada in order to optimise thermal comfort, heating and cooling loads, natural daylight, and energy consumption through the use of advanced fenestration system in the building's envelope.

1.9 STUDY OBJECTIVES

The study intends to perform a numerical analysis of semi-transparent building-integrated photovoltaic thermal (STBIPV/T) airflow window system, Figure 1.4, for both hot and cold climate conditions as determined by various influencing factors. A methodology needs to be developed for conducting this analytical study. The following objectives need to be accomplished for this study:-

1) To develop a thermal model and also numerical thermo fluid model using CFD for the system;
2) To develop a daylighting assessment model for the building with the system;
3) To evaluate the performance of the STBIPV/T system using parametric analysis to identify the influence of PV transparency and flow rate on the indoor comfort;
4) To analyse the effects of separation distance between the glass panes and the incident solar radiation on the STBIPV/T system in order to identify the optimal values that contributes to reduction of heat gains towards the inside environment in summer and maximize heat gains in winter;
5) To determine the effect of PV transparency on visual comfort;
6) To perform parametric analyses to clearly show the relationship of multiple

variables of the energy performance of STBIPV/T so simulation can guide to identify the design requirements and the appropriate climate criteria for the proposed system;

7) To optimise the design for the PV airflow window based on the requirements for minimum energy use and maximum comfort in buildings.

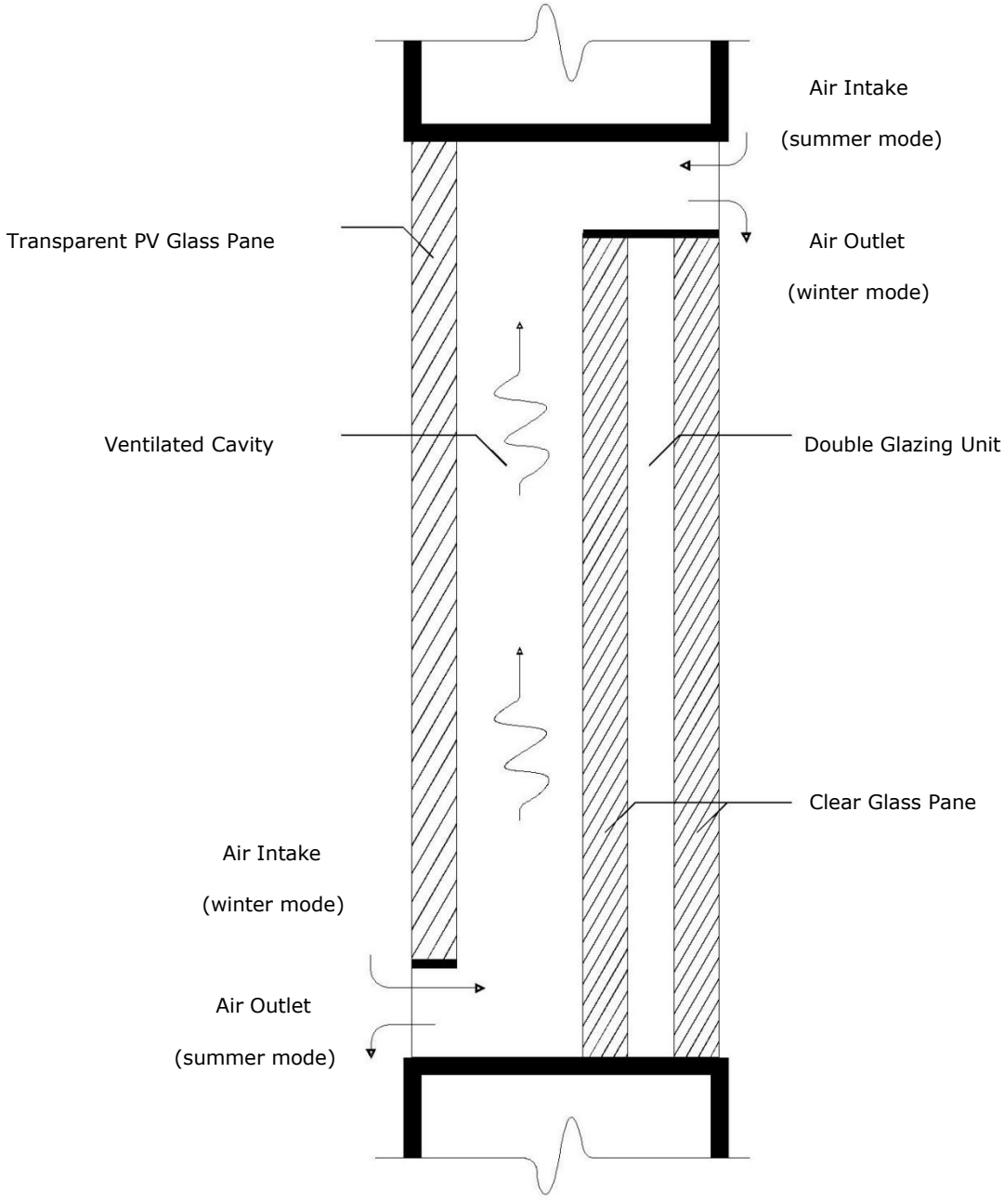

Figure 1.4: Schematic of the proposed (STBIPV/T) system for the study

1.10 THESIS STRUCTURE

This thesis consists of 11 chapters. Following are brief descriptions of the contents of each chapter.

- **Chapter 1**- Background sets the stage for the thesis by introducing the concept of the semi-transparent building integrated photovoltaic thermal system (STBIPV/T) and the problem that is examined in this study. The objectives and hypothesis are formulated.
- **Chapter 2**- Literature Review provides the framework of the current knowledge. Related literature is reviewed and important studies from relevant disciplines and their methods are presented.
- **Chapter 3**- Analytical method displays the figures of multiple variables and results of different inputs and different climate zone.
- **Chapter 4**- CFD turbulence models Validation presents the computational analysis of the prospective models using ANSYS Fluent 14.0 with relation to the STBIPV/T system employing the inputs obtained from the relevant literature and comparing the results from literature and predictions.
- **Chapter 5-** Daylighting tool validation presents the comparison between the results of ECOTECT and other daylighting simulation programs.
- **Chapter 6-** Airflow window model set up presents the description for the airflow window computational model and its solution criteria from the previous studies in relevant literature and best practice guides.
- **Chapter 7**- Design Optimisation specifies the detailed properties and the design criteria for efficient energy consumption and adequate level of comfort in buildings for the intended system during the winter period.
- **Chapter 8**- Design Optimisation for the intended system during the summer period.
- **Chapter 9**- Impact of internal heat gains on thermal and ventilation performances of airflow window presents the comparison between the thermal and ventilation behaviour when with an without the internal heat sources.

- **Chapter 10-** Impact of transient treatment on thermal and ventilation performances of airflow window presents comparison between the thermal and ventilation behaviour of the time-dependant and steady state operation for the window unit.
- **Chapter 11**- Conclusion and Recommendations concludes the document with a review of the thesis hypothesis and how the study contributes to the body of knowledge, gives a summary of the thesis results and points out areas of further research.

CHAPTER 2 LITERATURE REVIEW

In this chapter, a brief overview of research pertaining to photovoltaic (Curry 1998) ventilated façade including airflow windows will be presented. The topics for the literature review will cover major related studies, evaluations, and analyses for investigation of solar-optical, heat transfer, and optimisation of PV ventilated façade. A number of researchers have investigated several factors that affect the mechanism of such a component under different conditions and for different buildings. Heat transfer and airflow were the most prominent factors.

2.1 NATURAL VENTILATION RESEARCH

Faggembauu et al (2003a and 2003b) introduced a specific numerical code for evaluating a naturally ventilated multiple-glazed area in Mediterranean weather conditions. The study was based on a time-dependent and a one-dimensional meshing for the channel and different slid zones and carried out over the course of one year.

Saelens et al. (2004) restricted their study on reaching the optimum values of boundary conditions and modelling parameters. The study focused on the accurate implementation of inlet temperature when simulating double skin façade using CFD.

Haase et al. (2009a) studied the possibility of maintaining solar heat gains through a ventilated façade during the warm and humid weather. A simulation model was used through TRANSY and TRNFLOW to evaluate the effectiveness of various control strategies of energy consumptions. Because the exhaust airflow is a pivotal factor, it was exclusively evaluated for a new proposed airflow window of an office building. For comparison, the curtain wall system was taking into account. It was found that controlling the exhaust airflow reduced cooling loads. Thus, ventilated façade loads mitigation is attributed to the improved airflow control.

Assessments that based on experimental set up and simulation models to conduct calibration studies between single and double-skin façade in order to explore the effectiveness of installing extra one glass pane to the façade have shown excellent agreement. Hien et al. (2005) calibrated the performance of a double glazed façade

against a single glazed façade taking into account three factors: energy consumption, thermal comfort, and condensation. The authors recommended the installation of a mechanical fan to keep moderate surface temperatures and to remove condensation in the air chamber.

Eicker et al. (2008) presented experimental and computer simulation analyses to evaluate the single and double glazed façades under summer climate conditions. It was revealed that both can efficiently achieve energy savings with some restrictions for solar radiations and supplying fresh air.

Till (2004) conducted, for a long-term, an empirical study on three different high-rise buildings with ventilated façade individually to examine the energetic performance. Each building was treated in different conditions: naturally ventilated double façade applied without installation of cooling equipment; naturally ventilated double façade considered with restricted installation of cooling equipment; mechanically ventilated double façade applied with restricted installation of cooling equipment. The evaluation affirmed the feasibility of either concepts of natural ventilation for high-rise buildings without equipment's installation and further studies to be performed for the concepts of restricted installed cooling equipment, indoor climate, and boundary conditions implementation.

Høseggen et al. (2008) introduced how to model a double-skin façade with controllable windows and hatches for natural ventilation in computer algorithm (ESP-r). Results showed that the energy demand in the conventional window is 20 per cent higher than the double-skim façade.

Wong et al. (2008a) presented a CFD attempt to investigate the feasibility of ventilating an 18-story high-rise office building naturally through double-skin façade under hot and humid climate conditions. The study indicated that the application of double-skin façade is efficient for naturally ventilated towers.

Chow et al. (2009b) verified a theoretical model via the ESP-r simulation platform against field measurements to identify findings on the energy of a naturally ventilated

semi-transparent photovoltaic glazing. It was found that significant reduction on air conditioning power consumption when compared to the conventional single absorptive glazing system.

Tanaka et al. (2009) implemented a field measurement analysis to quantitatively investigate the influence of the ventilation opening and the shade condition on three dimensional thermal characteristics and cooling load reduction in hot weather condition. The performance of naturally ventilated double-skin envelope achieved 20-25 1/h of maximum air change rate through the bottom to the top opening and 25 per cent reduction of solar heat gain compared with those of non-natural ventilation configurations.

Xu et al. (2007) investigated the effectiveness of naturally ventilated double-skin system for an actual house in Kitakyushu, Japan. Thermal behaviour in the double-skin cavity and its impact on air-conditioning load in rooms, and the temperature distribution were observed. The study proved that the double-skin system is feasible for energy saving for houses with different operation modes under multiple climate zones.

Gratia and De Herde (2004d; 2004c and 2004a and 2004b and 2007a and 2007b; 2007c; 2007d) applied a computational fluid dynamics code (TAS) to evaluate an office building equipped with naturally ventilated double skin façade during a sunny summer day in terms of façade and wind orientation and the degree of wind protection. The authors further took into account the impact of several parameters: solar radiation level, orientation and shading devices application, interior façade to opaque wall/window ratio, colour of shading devices and of interior façade, wind speed, DSF cavity width, glazing type in the interior façade and opening in the DSF on the trend of the mean air temperature within the gap. The studies simultaneously proved that the installation of DSF always contributes in significant cooling load consumption, thus, proposed natural cooling strategies should be applied to DSF in order to minimize the energy loads.

2.2 MECHANICAL VENTILATION RESEARCH

Theoretical and experimental attempts have been presented on evaluations on mechanically ventilated multiple-layer façades to analyse their potential of being possible energy resources. (Chen 1995; Baker et al. 2000; Zöllner et al. 2002; McEvoy et al. 2003; Posner et al. 2003; Manz et al. 2004; Safer et al. 2005; Balocco et al. 2006; Southall et al. 2006; Liao et al. 2007; Jiru et al. 2008). In most of these studies (Manz et al. 2004; Safer et al. 2005; Southall et al. 2006; Liao et al. 2007; Gosselin et al. 2008c), CFD predictions were used to validate empirical measurements. Thus, computational analyses are the predominant method of investigating multiple-glazed façades behaviour. However, in some cases (Zöllner et al. 2002; Balocco et al. 2006), mathematical correlations were employed for validation process.

Baker et al. (2000) performed an evaluation study on theoretical model of heat exchange conditions within the airflow window that was calibrated against results from a test cell. It was concluded that a limited correlation between solar intensity and the extent of the temperature gradient within the window was substantially modified by the external wind speed.

Zöllner et al. (2002) investigated the time and the local averaged overall heat transfer coefficients for solar radiation augmented turbulent mixed convection flows in transparent vertical channel. Mainly, the study concluded that the reduction of outside temperature can increase the average mean Nusselt number whereas it can decrease where the solar irradiation increases.

Chen (1995), and Posner et al. (2003) applied several flow modelling assumptions and procedures in indoor air flow simulations to BIPV/T. McEvoy et al. (2003) conducted series of tests using a PASSYS test cell to identify the optimum values for air flow window characteristics, the best suited pane low-e coating within the glazing assembly. The study revealed that the pre-heating performance reduction was a function of ventilation rate increase.

Safer et al. (2005) applied CFD modelling approach to assess the air movement within the ventilated façade channel equipped with venetian blind. The author presented a parametric analysis to explore the impact of different parameters: air outlet position, blind position, and slat tilt angel. Subsequently, Southall et al. (2006) carried out further analysis using a whole building dynamic thermal modelling tool such as, CFD and ESP-r, a test cell, and a laboratory.

Gosselin et al. (2008a) suggested a new computational method to simplify the evaluation process. CFD and coded radiation calculations were employed to identify the values of airflow and heat transfer through an airflow window. Data was obtained from a dual-airflow window system to validate the proposed computer code. Computer predictions and measurements were perfectly matched.

Corgnati et al. (2007) showed the results of a comprehensive empirical assessment of an actual transparent façade performance with device-induced air flow and an HVAC system. Due to further improvements required for the façade's thermo fluid dynamic behaviour and exploring its shortcomings, the study took into account the impact on the enhanced comfort conditions and the energy savings.

Saelens et al. (2008) introduced different strategies of reaching the optimum energy efficiency of multiple- layer facades. The strategies were implemented using the software TRNSYS 15.3 and their values compared with the results of conventional cladding systems under typical Belgian climate conditions.

Serra et al. (2010) assessed the energy efficiency and the thermal comfort performance of climate façade with a forced ventilated air gap using the TWINS (Testing Window Innovative System) test facility. Based on the study, it is possible to affirm that in terms of energy efficiency and thermal comfort performance issues, the climate façade presented a better performance than the active façade.

Fallahi et al. (2010) presented a new concept of conventional double-skin façade integrated with passive thermal mass technique to improve the system's energy efficiency and thermal behaviour achieving overheating problem mitigation in the warmer

season and reduction of heating load during the cold dominated weather. Thermal performance of DSF was predicted utilizing a numerical model. The results indicated that significant energy savings can be achieved in summer and winter when installing a mechanically ventilated DSF.

In summary, despite the efficient performance of the promising façade systems, when installed in a building to save significant energy on cooling loads and achieve higher air change rate with different modes of operation under multiple climate conditions various control strategies should be implemented for air flow, air quality, supplying fresh air, solar radiation and the installation of shading device in order to bring them to the optimum performance. The most important of all is that adding a fan to force air movement between the façade's layers can improve their function by combating the possible condensation inside the air cavity and mitigating overheating of the glass façades.

2.3 VISUAL EFFECTS OF INTEGRATING PHOTOVOLTAIC SOLAR CELLS INTO MULTIPLE-LAYER FAÇADES

Visual aspects are thought-provoking factors throughout a building design phase for glazing components that cover its façades and apertures. Glass cladding is the main building's port where daylight can be transmitted through to the interior environment. Thus, it is important to strike an appropriate balance between daylight requirements and energy performance when integrating semi-transparent photovoltaic solar cells to a building with multiple-glazed skins. Three basic values are ordinarily presented in the semi-transparent photovoltaic (STPV) modules datasheets: heat transfer, visible light transmittance, and electric power generation. In addition, as an added benefit to the opaque PV modules of just producing electricity and reducing solar heat gain, the semi-transparent PV modules provide a sufficient daylighting access that alleviates lighting energy consumption which, in turn, yield to offset cooling loads. These modules are an aesthetic factor for the façade architecture design as well as color perception in indoor environment (Lynn et al. 2012).

To ensure adequate visual comfort of occupants, responsible care must be taken when characterizing color neutrality and color rendering for architectural glass/glazing (Wilson 2006), (Oelhafen et al. 2005), and (Manav 2007), however, these parameters are insufficient for assessing STPV modules behaviour. They are rather suitable to examine human response to color (Lee et al. 2007), (Bellia et al. 2011). In the visible range of 380 *nm* to 780 *nm*, solar irradiance contains daylight with spectral power distribution (SPD). Inside a space, visual comfort and color perception rely on the SPD of the light transmitted into a room. As the spectral transmission properties of glazing can affect the illumination quality of SPD, it can be specified by correlated color temperature (CCT) and color rendering index (CRI) (Lynn et al. 2012). Adequate level of Daylighting of an interior space is attributed to accurate identification of visible transmittance (Diomidov et al.) and of the semi-transparent PV modules; yet, daylight cannot be elaborated in terms of opaque PV components since they provide no access to the visible transmittance. Furthermore, the solar transmittance (ST) is an essential element to be responsibly investigated to balance the semi-transparent building integrated photovoltaic thermal behaviour (Li et al. 2009; Lynn et al. 2012).

Lynn et al. (2012) specified the color rendering properties of light sources through six semi-transparent PV glazing modules using the CIE test color method. These modules were configured as segments of glass-PV-glass where PV layer was laminated inside a double glazed unit. Two incident angles of 0.8 and 45° degrees, under laboratory conditions, were employed to specify the color rendering index. The study indicated that to combine appropriate visual comfort and aesthetic factors for façade materials, CRI must be above 90 for all angles of incidence.

Miyazaki et al. (2005) concentrated their studies on optimising façades visual comfort and proved that the semi-transparent building integrated photovoltaic can provide efficient electrical energy and facilitate daylighting schemes that conserve building energy expenditures.

Chow et al. (2007) applied an EnergyPlus simulation model to evaluate the natural light performance of a semi-transparent photovoltaic solar cells integrated to a ventilated

window of a small office space located in Hong Kong with respect to façade orientation glazing materials. The study revealed that more lighting load savings can be achieved in the SW direction where the lowest in the SE direction. The percentage savings of power loads of artificial lighting was in the range of 23-63%.

Wong et al. (2008b) established an EnergyPlus model to investigate the effect of direct daylight illuminance accessing through the poly-crystalline (P-Si) semi-transparent PV panel in five different regions in Japan for residential buildings. Excellent agreement was obtained between predictions and measurements.

Li et al. (2009) carried out an evaluation on a generic reference office building to explore the thermal and visual properties, energy performance and financial aspects of its semi-transparent PV facade. The authors also made an experimental attempt on case studies on an atrium integrated with semi-transparent photovoltaic solar cells to evaluate the contribution of the solar scheme to facilitating daylight and conserving lighting energy loads. The authors utilized the conventional daylight factor approach with the skies under overcast conditions to predict the internal daylight illuminance.

Robinson et al. (2009) conducted a simulation-based study to integrate the impact of integrated semi-transparent photovoltaic façade area ratio on the lighting loads from artificial lighting to allow daylight in order to mitigate the heat gain produced from the ordinary electrical lighting. The study presented the results of daylight illuminance and power generation for the façade in terms of different orientations and PV manufacturer's efficiencies to produce relevant designs standards for this technology community.

Colsmann et al. (2011) calculated the transparency color rendering index and color perception of semi-transparent organic solar cells incorporating a blend of PSBTBT to determine the possibility of this combination for actual window applications.

It can be concluded that several aspects can play a crucial role when identifying the visual comfort level of a see-through building integrated solar panel: angle of incidence, glazing materials, façade orientation, and façade area ratio. Two dominant analytical methods could be applied to evaluate the color rendering index (CRI) of the light sources

accessing through the semi-transparent photovoltaic solar cell panels: CIE color models and the conventional daylight factor approach, however, accurate prediction of the CRI can balance visual comfort and aesthetic factor of the solar unit. The Computer-based daylighting analyses (employing EnergyPlus and ECOTECT) and field measurement studies have concluded that considerable lighting energy savings and power conservation are attributed to facilitating daylight into the building to replace the artificial lighting equipped with strategies of implementation such as shading devices and coated glazing for different building elements and climatic conditions. Thus, such a replacement leads to a reduction of heat gain obtained from the bio-lighting which in turn accounts for minimized cooling loads.

The data that have been presented revealed comprehensive results that guide the energy professionals in their work. However, more studies are required to optimise this technology performance especially for the impact of shading by surrounding buildings.

2.4 HEAT TRANSFER ANALYSES

Significant amount of research and development work has been done on thermal and electrical performance of façades integrated with photovoltaic solar cell (Vats et al. ; Clarke et al. 1996; Moshfegh et al. 1996; Moshfegh et al. 1998; Krauter et al. 1999; Eicker et al. 2000; Sandberg et al. 2002; Gan et al. 2004; Charron et al. 2006; Gan 2006; Liao et al. 2007; Fung et al. 2008; Chow et al. 2009b; Gan 2009b and 2009a; Han et al. 2009; Li et al. 2009; Agrawal et al. 2011; Vats et al. 2011; Yoon et al. 2011). Glazing architecture component would experience three possible actions when exposed to solar rays namely reflection, transmission and absorption. Thus, the imperative focus, when analysing thermal performance for such a system, should investigate thermal transmittance and solar heat gain (U- and g- value). This involves particularly the evaluation of solar heat flux that reflects from, transmits through and absorbs by each glass pane of the glazing unit. The combination of the two construction segments, PV cells and ventilated cavities, maximizes PV modules efficiency (Infield et al. 2004).

Edwards (1977) applied an effective computational method to represented the solar-optical properties of the glazing layers based on a recursive summation to a number of glazing layers. The author assumed that a beam radiation source (I_b) can be a source of beam reflection and transmission, and a diffuse radiation source (I_d) can be a source of diffuse reflection and transmission.

The representation of thermal properties of a ventilation façade complicates its heat transfer estimation process. It entails a complex modelling of combined pressure and temperature differential regimes and external wind flow, most difficult of all, the heat transfer across vented air when buoyant flow is dominated. Therefore, sophisticated development work has been published by Balocco (2002), Institute (2002), Krauter et al. (1999), Sandberg and Moshfegh (1998; 2002), and Mei et al. (2002); Mei et al. (2003) to explore simple but effective approaches to simplify the calculation process of the thermal performance of such a ventilated façades.

S. Belharat et al. (1996), P.F. Abreu et al. (1998), Larsson et al. (1999), and Henŕıquez (2002), illustrated two-dimensional model to calculate the heat transfer through ventilated multiple window panes considering transient treatment. Due to the mixed flow conditions of heat transfer process, it is complex to estimate the convective heat transfer coefficients within the cavity of building integrated photovoltaic thermal (BIPV/T) system.

Mei et al. (2003) validated and developed transient model BIPV/T system of Mataro public library, Barcelona, Spain. The system consisted of an outer PV façade that absorbs directly the incident solar radiation and an inner glass double pane unit in the computer program TRNSYS (A TRaNsient SYstem simulation program).

Infield et al. (2004) described different approaches to provide architects, building designers and building services engineers with simple methodologies to estimate thermal behaviour of ventilated façades. Attention was paid to the heat transfer through the façade of Mataró library in Spain.

Clarke et al. (1996) and Krauter et al. (1999) restricted their studies to steady state model to evaluate the energy performance of multiple layers glazing PV façades. Infield,

Mei et al. (1999; 2004) performed dynamic and steady state analyses based on numerical solutions to maximize the potential thermal performance of a PV ventilated façade.

Xamán et al. (2005) presented a two-dimensional numerical model to examine the fluid flow and heat transfer by laminar and turbulent natural convection in a tall cavity. Nusselt numbers were calculated under a steady state condition for the rectangular cavity of aspect ratio of 20, 40 and 80. Experimental results were considered to calibrate the calculations of Rayleigh numbers in the range of 10^2 to 10^8 that obtained by the finite volume approach.

Ismail et al. (2005) formulated two-dimensional transient model to evaluate a double-sheet ventilated glass window. The two-dimensional transient model took into account the physical phenomena present in the heat and flow processes as well as the actual boundary conditions whilst in normal operation. The model was solved by finite difference approach and the alternating direction implicit scheme. Ismail et al. (2006) also presented a one-dimensional and unsteady model to evaluate the thermal performance of a double-sheet mechanically ventilated glass window. Based on the results of the numerical simulation considering the global energy balance, it was concluded that lower mean solar heat gain and the shading coefficients are the function of higher mass flow rate whereas the high inlet air temperature deteriorates the window thermal behaviour.

Ji et al. (2008) analysed a double-skin façade with between the pane Venetian blind for natural ventilation. A CFD two-dimensional model investigated the heat transfer by convection, conduction and radiation through the DSF component. The model considered a series of angles of the Venetian blind (0^0, 30^0, 45^0, 60^0 and 80^0). The study showed marginal impact of the blind on the convective heat transfer coefficient at the glazing panes.

Xu et al. (2008) carried out an exhaustive study of heat transfer behaviour across a double-skin envelope with Venetian blinds between the façade gap. The governing

equations of mass, momentum and energy were calculated for the façade system by comprising heat balance, optical and CFD model. The analysis indicated that the more complex natural ventilation exists inside the cavity system with the shading device, which cannot be reflected with the simplified model.

Fung et al. (2008) performed an experimental attempt to validate a one-dimensional transient heat transfer model, the Semi-transparent Photovoltaic Heat Gain (SPVHG) model, for heat transfer calculations. The results proved the implementation of SPVHG for simulating different scenarios. Wright et al. (2008) proposed a simplified one-dimensional model of the conjugate heat transfer whereas Dalal et al. (2009) compared their results that showed excellent agreement with a full conjugate CFD predictions when they conducted a one-dimensional study to analyse a double paned window with a between-pane pleated shade.

Kim et al. (2009) carried out an empirical and a computer algorithm evaluation of the contribution of a double-skin envelope to the heating energy savings in a naturally ventilated three-floor office building in a winter climate condition. It showed that the double-skin envelope can function to effectively increase thermal resistance and reduce heat transfer which leads to a reduced the heating energy consumption in heating seasons.

Guardo et al. (2009) conducted an evaluation studies on the Active Transparent Façade (ATF) to observe the effect of several construction and operation parameters such as optical properties of the materials, geometrical relations of the façade or flow stream conditions with regards to energy savings, measured as a reduction of the solar load entering the building. The study revealed that optical properties have significant impact on minimizing solar load gain. Furthermore, it was seen that the efficiency of ATF in terms of heat transfer into the building is a function of geometrical dimensions. For the examined cases, improvements in the reduction of solar load gains cannot be achieved by an increase on the turbulence intensity.

Fuliotto et al. (2010) applied a numerical evaluation to study heat transfer and air flow in a double-skin façade. The authors introduced a decoupling approach and CFD to capture the effects of solar radiation and complex flow on the façade system. Estimations were similar to the measurements obtained from a test cell room equipped with DSF.

2.5 NUMERICAL MODELS FOR MULTIPLE-LAYER FAÇADES

Generally, the behaviour of a façade is a function of four variations that identify its ventilation gains and transmission losses depending on solar heat flux and temperature profiles namely the heat loss from the room, U_{trans}, the heat loss from interior to ventilation air, U_{vent}, the directly transmitted radiation gains to the interior, g_{trans}, the absorbed radiation gains, g_{vent}, These are expressed as follows (Infield et al. 2004):

$$\boldsymbol{Q_{trans}} = \boldsymbol{g_{trans}}\mathbf{G} - \boldsymbol{U_{trans}}(\boldsymbol{T_{room}} - \boldsymbol{T_{amb}}) \quad 2.1$$

$$\boldsymbol{Q_{vent}} = \boldsymbol{g_{vent}}\mathbf{G} - \boldsymbol{U_{vent}}(\boldsymbol{T_{room}} - \boldsymbol{T_{inlet}}) \quad 2.2$$

Where Q_{trans} is the net rate of energy gains to the room $(\mathrm{W/m^2})$, G is the incident solar radiation on the PV surface $(\mathrm{W/m^2})$, Q_{vent} is the energy gains to the ventilation air $(\mathrm{W/m^2})$, T_{room} is the room temperature (K), and T_{amb} is the outside ambient temperature (K).

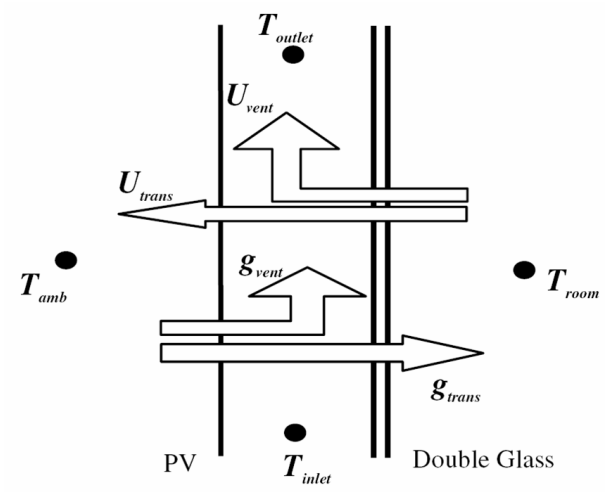

Figure 2.1: Heat transfer for ventilated façade (reproduced from Infield et al., 2004)

Figure 2.1 shows the energy flows with respect to each factor. There are two gains and two losses. Gains are represented by g_{trans} and g_{vent} where the radiation is transmitted

through and absorbed by the glass panes reaching the interior space and pre heating the ventilation air whereas U_{trans} and U_{vent} indicate heat losses from inside the room to outside ambient and to heat ventilation air, respectively.

2.6 THE MAIN SIMULATION SCHEMES FOR MULTIPLE-LAYER FAÇADE

The multiple-layered façades can transform part of the incident sunlight into electricity directly or by transmitting the thermal energy into the building using electrical or mechanical equipment (pumps, fans, valves, control equipment's), thus, prior equipping a building with multiple-layered façade units, an optimal thermal performance of the units must be achieved through investigation studies with suitable simulation approaches from the aspects of building orientation, units' design and ventilation rate.

2.6.1 LUMPED MODEL

The establishment of lumped model for multiple-layer façade can be easily applied to study the naturally ventilated unit based on a variable prediction technique and empirical measurements of a test cell element (Park et al. 2004a). Experimental data is a solid base for prediction technique to collectively identify the several unknown convective heat transfer coefficients between the unit's skins and the air gap. The model represents each layer within the façade unit and its cavity with a single node as well as the overall optimum values of the façade system characteristics (Park et al. 2004b). Park et al. (2004a) also presented a new modelling approach based on a postulated "minimalistic" lumped model to evaluate the simulation model of double-skin façade system with controlled rotating louvers and ventilation openings. The authors monitored the results on a full-scale element which revealed the accuracy of the new approach and its validation of use.

2.6.2 ZONAL APPROACH

The zonal approach is less complicated than CFD models and the accuracy is better than the lumped model. Modelling more complex buildings with zonal approach is possible

with less programming and computational efforts, thus, the simulation of building integrated multiple-glazed skins is feasible for evaluating such a unit (Jiru et al. 2008).

Jiru et al. (2008) employed the methodologies and applications of Zonal approach modelling air flow and temperature of a mechanically ventilated double-skin façade with inside Venetian blinds. The estimated temperature distributions were validated against empirical values. Moreover, parametrical analyses were done to capture the effect of height, flow rate, and installation of shading device on the temperature balance between the inside and the outside. It was affirmed that zonal method is valid for studying DSF performance as it works faster at minimum computational resources.

Lou et al. (2012) carried out empirical and numerical modelling to investigate the wind tunnel test for series wind pressure on corridor of double-skin façade of a tall rectangular buildings. Field measurements were observed for four cases of air corridor width. The zonal models were developed to predict the pressure coefficients for strip and L-shaped double-skin façade. The estimated values were validated against empirical data and satisfactory agreement was obtained.

López et al. (2012) assessed the thermal and air flow potential experimentally of opaque ventilated façade and validated the measurements against numerical predictions using a zonal approach software.

For investigating pressure process on building façades, zonal approach can be replaced with the usually adopted wind tunnel method. Furthermore, it could be refined and extended to include thermal stack effects, in addition to aerodynamic pressure for ventilation assessment of multiple-layer façades.

2.6.3 AIRFLOW NETWORK MODEL

The airflow network model is able to predict the heat and air flows within each element of the multiple-layer façade: glass panes, shading device, and inside and outside air space (Tanimoto et al. 1997). The network scheme establishes a network of nodes to introduce rooms, parts of rooms, and system components when estimating the fluid flow of a building and relevant (HVAC) systems. It represents the distributed flow paths such

as cracks, doors, pipes, pumps, ducts, and fans with intermodal connections where each node is acquired a non-linear equation (Hensen et al. 2002). Thus, a computer code can be written to iteratively solve the simultaneous equations for flow rates in branches at nodes and conservation of mass flow through the network (Aynsley 1997). Gratia et al (2004d; 2004c) coupled the airflow network models with energy simulation to evaluate a naturally ventilated multiple-glazed skins façade. Furthermore Gratia et al. (2004a) and Stec et al. (2005) applied the models to investigate the energy performance of the façade system.

Haase et al. (2009b) described coupled computational codes, thermal building simulations (TRNSYS) and nodal air flow network simulation (COMIS) to evaluate multiple ventilated double-skin facades designs for an office building in Lisboa. For validation purposes, results were calibrated against measured obtained from the reference building. The predictions of surface and air temperatures and experimental data were in excellent agreement. Results indicated that potential energy savings can be accomplished by different DSF configurations.

The network model coupled with energy simulation has been used by Wei et al. (2010). The authors implemented a network model successfully in the validated Energy Plus and developed it in order to justify the two-dimensional heat transfer in a dual-airflow window under actual climates. By comparing with measured temperatures of the window and the energy demand of a test cell with window under actual weather conditions, the heat transfer through the vertical and the cross sectional direction were validated as well as the modified Energy Plus program. This investigation proved that such a dynamic window is able to consume less heating energy especially in cold weather. It was also revealed that the experimented dual-airflow window was relatively insufficient for cooling purposes, unless otherwise the air quality of the building is improved. Therefore, the dual-airflow window is recommended for heating functions only.

The network method is more suited for studying the multiple-layer façades design associated work. However, the model is restricted to only bulk flow estimation unless otherwise combined with CFD that provides information about the nature of the flow

pattern. In addition, when analysing the pressure-flow relationships with the naturally ventilated façade unit, the integration with energy simulation programming codes is required to simplify the calculation of the established non-linear equations in each node.

2.6.4 COMPUTATIONAL FLUID DYNAMIC METHOD

Fluid flow and heat transfer are the most critical phenomena that need to be analysed for the airflow windows in order to achieve systems optimisation. Thus, a powerful technique is required for performing these evaluations.

CFD is suited to numerically analyse systems that transfer heat, circulate fluid and involved associated phenomena such as chemical reactions by computer algorithm simulation. This simulation is based fundamentally on replacing the differential equations governing the fluid flow and heat transfer from the principles of conservation of mass, momentum and energy (Patankar 1980; Versteeg et al. 2007; ANSYS 2009). Different numerical methods are applicable to obtain approximate solutions for governing equations such as the Finite Difference Method (FDM), Finite Element Method (FEM) and the Finite Volume Method (FVM) where the latter is the most employed code (Patankar 1980; Versteeg et al. 2007; ANSYS 2009).

The numerical modelling is a concept of discretising a flow path into cells, called control volume, via meshing progress within the computational domain. Generally, simulation tools solve conservation equations for all unknown transport variables (velocity, temperature, etc) and predict an approximate solution for either flow cases: turbulent or laminar (ANSYS 2009). Three basic conservation equations can calculate values for laminar flow: mass and momentum equations are for fluid dynamics and energy equation is for heat transfer whilst the turbulent flow requires additional transport equations that rely on iterative predictions and turbulence quantities (Patankar 1980; Versteeg et al. 2007).

2.6.5 NON-DIMENSIONAL ANALYSIS

The applicability of Non-dimensional analysis is valid for studying the multiple-layer façade in either case of ventilation: natural or mechanical. When transient condition is regarded, these factors are expressed as follows (Infield et al. 2004):

$$\boldsymbol{Q_{vent}} = \boldsymbol{\bar{g}_{vent} G_m - \bar{U}_{vent} \left(\bar{T}_{room} - \bar{T}_{amb} \right) n_h} \quad 2.3$$

$$\boldsymbol{Q_{trans}} = \boldsymbol{\bar{g}_{trans} G_m - \bar{U}_{trans} \left(\bar{T}_{room} - \bar{T}_{amb} \right) n_h} \quad 2.4$$

where n_h is the number of hours per month and the bar over each factor indicate the monthly mean values of the parameter, Q_{vent} is monthly ventilation heat gain $(\mathrm{W\,h/m^2})$, Q_{trans} is monthly net rate thermal energy to the room $(\mathrm{W\,h/m^2})$. The transient condition can be commonly treated with non-dimensional Nusselt number (Nu) to estimate the convective heat transfer coefficient. The associated number can be described as follows (Incropera et al. 1990):

$$\boldsymbol{\bar{N}u} = \sqrt{\boldsymbol{\bar{N}u_{lam}^2 + \bar{N}u_{turb}^2}} \quad 2.5$$

with

$$\boldsymbol{\bar{N}u_{lam}} = \boldsymbol{0.644\sqrt{Re}\sqrt[3]{Pr}}, \quad 2.6$$

$$\boldsymbol{\bar{N}u_{turb}} = \frac{\boldsymbol{0.037 Re^{0.8} Pr}}{\boldsymbol{1 + 2.444 Re^{-0.1}\left(Pr^{\frac{2}{3}} - 1 \right)}} \quad 2.7$$

$$\boldsymbol{\mathrm{Re}} = \sqrt{\boldsymbol{Re_{force}^2 + Re_{H,free}^2}} \quad 2.8$$

$$\boldsymbol{\mathrm{Re}_{forced}} = \frac{\boldsymbol{vH}}{\boldsymbol{v}}, \boldsymbol{\mathrm{Re}_{H,free}} = \sqrt{\frac{\boldsymbol{Gr_H}}{\boldsymbol{2.5}}} \quad 2.9$$

Convective heat transfer coefficient can be calculated from the Nusselt number:

$$\boldsymbol{h_c} = \frac{\boldsymbol{\bar{N}u\ k_{air}}}{\boldsymbol{D}} \quad 2.10$$

Balocco (2004) applied a non-dimensional analysis to a naturally ventilated double-skin façade to evaluate its thermal energy performance. The study revealed that non-dimensional numbers estimated by simulation, empirical measurements, and obtained

and validated correlation functions were in excellent agreement. In addition, Balocco et al. (2006) obtained 12 non-dimensional numbers to analyse a mechanically ventilated double glass façade and a validation analysis was done with empirical data.

It is clear that this method describes a process by dimensionless parameters that identify that process at all scales. Moreover, the approach is valid to adapt different weather conditions, aspect ratios, shading devices as well as different thermo-physical characteristics of each layer within the façade.

2.6.6 CONTROL VOLUME APPROACH

The control volume approach is based on transient simulation of ventilated and conventional façades where each façade is divided into a number of control volume. Based on the finite volume method, the continuous governing equations produce the discrete equations for each control volume. The method reflects only the effect of one-dimensional discretization for the air cavity in the flow direction and each skin of the façade in the indoor-outdoor direction. Furthermore, long-term analysis can be done with this approach for heat flux and temperature distributions in the façade. In addition, the method allows advanced elements to be integrated into the façade such as phase change materials, selective surfaces and special glazing. To better achieve accurate data in reasonable programming time, this scheme is the best suited for such analysis.

Several aspects can bring the heat transfer phenomenon through the multiple-glazed skins façades to its optimum behaviour: façade's geometrical dimension, high mass flow rate, façade's orientation. These three factors can mainly affect the transference process of the sunlight solar radiation into efficient source of bioclimatic energy such as electricity and space heating. Thus, careful attention must be paid when analysing the performance of the prospective façade units.

2.7 AIR FLOW RATE REPRESENTATION

Air flow is one of the most critical physical phenomena that affect the performance of a ventilated double glazing unit. Several design criteria that can affect the air flow patterns have been extensively investigated in the literature: solar protection (Safer et al. 2005),

gap width (Moshfegh et al. 1998; Balocco 2002; Sandberg et al. 2002), opening size (Gratia et al. 2004a), driven force (Gan 2010b), and building orientation (Gratia et al. 2004b).

Sandberg et al. (2002) investigated the air gaps behind solar cells located on vertical façades to obtain analytical values for four parameters: mass flow rate, velocity, temperature rise and location of neutral height (location where the ambient air pressure and the pressure in the air gap are equal). Behaving as bulk flow, the flow was considered either turbulent or laminar, assuming that velocity and temperature are uniform across the air gap and only affected by the height channel. Several variations were assumed for both the geometry of the air gap and the location of the solar module. Buoyant flows were exclusively considered with aerodynamic end losses considerations. By identifying a configuration factor, varying between 0 and 1, the location of solar cell panel was taken into account. Radiation-redistributed heat within the air gap was investigated. The study concluded that the solar cell location was a function of geometrical configuration where the aspect ratio is larger than 60. Assuming constant heat input to the air gap and varied location of the solar cell, the obtained analytical values for the evaluated parameters were validated against measurements made using a full-scale module. Great agreement was observed.

Gan (2006) investigated three types of open cavities to optimise the natural ventilation of buildings. Numerical simulation was carried out using CFD package to evaluate the buoyancy-driven air flow and flow rates in solar chimney, double façade, and Trombe wall. Satisfactory agreement was observed between the simulation results and previous data available in the literature. The author further investigated the cavity width on the buoyant ventilation rate for solar chimney and double façade to generate the optimum cavity width. For solar chimney of 6m high, the optimum width was 0.55-0.6m. Hence, highest buoyant flow rate could be supplied. For double façade of multiple-storeys, the ventilation rate increased and decreased with the cavity width and the floor level from bottom to top, respectively. However, installing photovoltaic into a double façade improved the quality of natural ventilation whereas minimizing the flow rate variation

with storey level. Gan (2010b) also simulated an office building to investigate the interaction between wind- and buoyancy-induced natural ventilation; two wings of offices and a central atrium were the building's configuration. The author compared the predicted natural ventilation rate obtained from the simulation with the calculated ventilation rate, predicated on the estimated pressure, using the following equation:

$$\boldsymbol{Q} = \boldsymbol{C_d}\, \boldsymbol{A}\sqrt{\frac{\boldsymbol{2\Delta P}}{\boldsymbol{\rho}}} \qquad 2.11$$

where Q is the ventilation rate (m^3/s), C_d is the discharge coefficient, A is the opening area (m^2), ΔP is the pressure difference across the opening (Pa) and ρ is the air density (kg/m^3).

It was observed that the air flow behaviour, in the building with buoyancy-induced natural ventilation, would be affected adversely by wind. The investigation also indicated that buoyancy can obtain simultaneous upwind wing assistance and downwind wing opposition by wind, however, wind-induced air flow can be only opposed by buoyancy in both wings. To obtain favourable air flow motion in naturally ventilated buildings, the study recommended either intelligent control of window openings or optimum design for wind-induced ventilation.

Generally, different aspects should be considered when studying the air flow for multiple-skin façade. First, the wind effect since it distributes the pressure around the building that changes the air flow rate. Second, buoyancy effect, especially when combined with the pressure, it can change the direction of the air flow. Finally, time and location have an impact on the air flow as well.

2.8 AIRFLOW WINDOW

Hadlock (2006) developed and validated a numerical model for an airflow window, with a roller blind installed inside the cavity, which is the upper section of the Photowatt configuration of the experimental system at Concordia University, shown in Figure 2.2, which its lower part consists of an opaque portion of a ventilated PV façade. The author carried out the study through three stages: model validation for forced convection

between parallel plates; radiation examination for different glazing layers (single, double and triple) due to the natural convection; comparing the experimental data, collected from the Solar Lab at Concordia University, against the numerical model.

Liao et al. (2007) succeeded Hadlock (2006) with a CFD simulation for the lower part of the test cell of Solar Lab, the opaque Photovoltaic façade. The authors established the flow as two dimensional and primarily turbulent because of the cavity framing, entrance, effects, and wind gusts. A two-dimensional CFD model was applied using properties of a test cell to evaluate the heat transfer due to the forced convection with fan-driven air flow for the lower part of the unit. The k-Ɛ turbulence model was utilized for turbulent flow, convective heat transfer in the cavity, the buoyancy effect, and the long-wave radiation between boundary surfaces. The authors further applied the particle image velocimetry (PIV) to the experimental measurements of the velocity profiles in the BIPV system cavity, and suitable match was found with CFD model predictions.

Nemati (2009) succeeded Liao et al. (2007) with numerical and experimental analysis for the Spheral-solar configuration, that consists of a mechanically ventilated façade with between-the-panes venetian blind (as an upper part) and between-the-panes PV panel (as a lower part), which is a part of the test cell of the Solar Lab at Concordia University, shown in Figure 2.3. The study presented a development and validation of solar-optical and CFD models at different blind slat angles and fan speeds to examine the fluid flow and heat transfer inside the system.

Figure 2.2: Concordia University experimental system, reproduced from Liao et al. (2007)

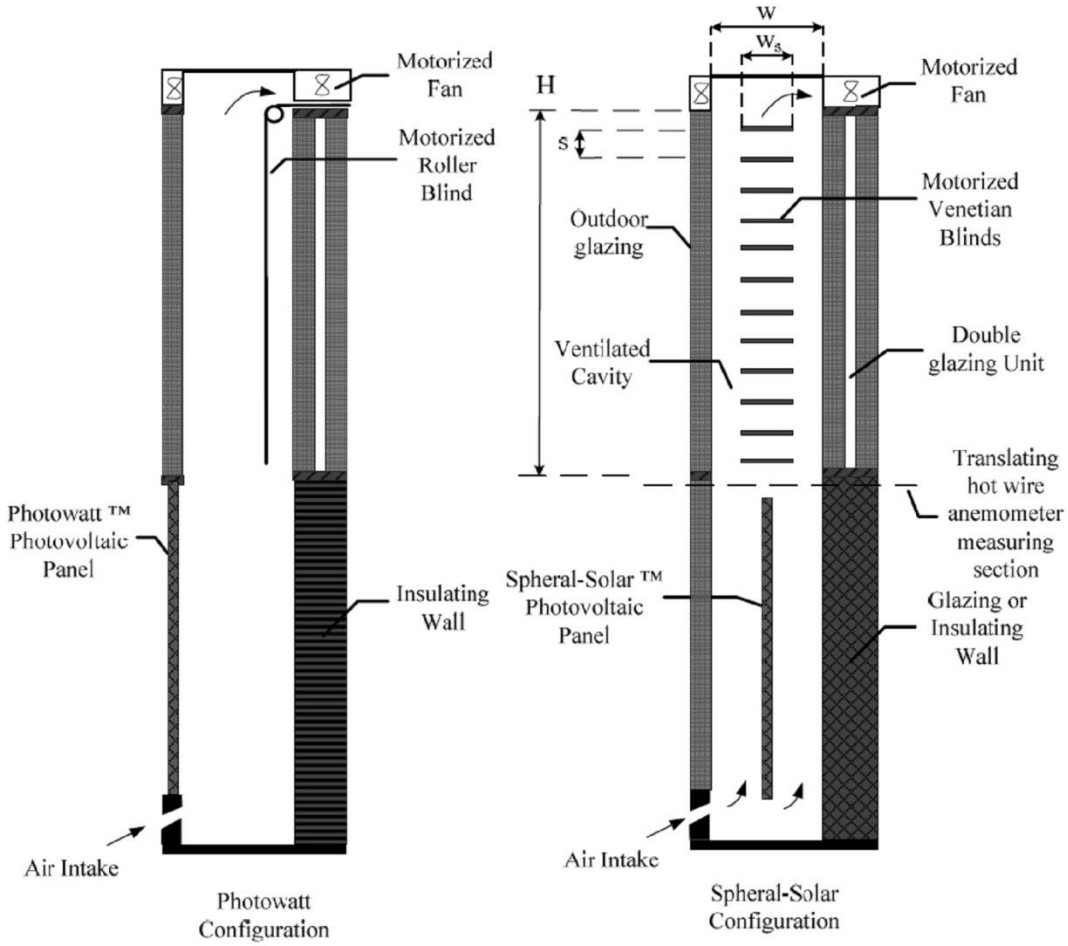

Figure 2.3: Schematic of the two BIPV/T test cell at Concordia University: Photowatt^{tm} on the left and Spheral-Solar^{TM} on the right, reproduced from Nemati (2009)

2.9 MODELS VALIDATION

Considerable attention has been paid to CFD models validation analyses in the literature in the last few decades (Shia-hui et al. 1995; Aydin 2000; McEvoy et al. 2000; Southall et al. 2000; K.T. Hollands 2001; Diomidov et al. 2002; McEvoy et al. 2003; Ismail et al. 2005; Safer et al. 2005; Aydın 2006; Ismail et al. 2006; Southall et al. 2006; Congress 2008; Gosselin et al. 2008b; Gosselin et al. 2008c; Jiru et al. 2008; Strachan et al. 2008a; Strachan et al. 2008b; Xu et al. 2008; Chow et al. 2009a; Handbook 2009; Carlos et al. 2010; Chow et al. 2010; Wei et al. 2010; Carlos et al. 2011). These numerical validations analyses were mainly verified with empirical measurements. Gan (2009b) ascertained the reliability of two-dimensional CFD model for buoyant fluid flow and heat transfer in a tall open cavity against values produced by Moshfegh et al. (1998). The author revealed that CFD technique is applicable to predict the optimum value for air gap.

Pasut et al. (2012) calibrated CFD results with experimental measurements from the literature (Mei et al. 2007) for naturally ventilated double skin façade DSF. They evaluated the performance of k-ε and k-ω turbulence models in terms of air flow patterns, air temperature, air velocity distributions and heat flux from the gap into the room. The authors found that CFD is sufficient for their work. In addition, they recommended the two-dimensional CFD instead of three-dimensional CFD model since the former gave similar predictions with less time consumption. More specifically, they advised for k-ε RNG for stable simulation results. Bhamjee et al. (2012) validated three-dimensional CFD model experimentally taking into account the velocity field, flow field and temperature rise in a supply air window. Qualitatively, the authors proved that CFD predictions were reliable.

From the aforementioned studies and more in the literature (Ye et al. 1999; Safer et al. 2005; Hadlock 2006; Pappas et al. 2008; Nemati 2009; Bhamjee 2012), CFD codes can demonstrate reliable predictions for a given system to characterise its behaviour, features and energy consumption.

The geometry of parallel plate has been evaluated widely throughout relevant literature investigating heat transfer and internal flow using mathematical correlations (Keshock et al. 1963; Churchill et al. 1973b; Churchill et al. 1973a; Garimella et al. 2000; Agrawal et al. 2010). Nickolay et al. (2002) described the local and overall Nusselt number for fully developed flow between parallel plates. They derived a correlation for the overall Nusselt number from continuous functions and then calculated the corresponding local Nusselt number from that correlation.

Yovanovich (2004) developed a new empirical formula to predict local and average Nusselt numbers in the combined entrance region of non-circular ducts and channel for both boundary conditions, uniform wall temperature and uniform wall flux. Comparison was made between the model predictions and numerical data for relevant literature and a good agreement was obtained with differences of 15 per cent.

Al-Amri et al. (2012) carried out an evaluation analysis to present the effect of a surface radiation on the developing laminar mixed-convection flow of a transparent gas between two asymmetrically heated vertical parallel plates. The authors illustrated the radiation effect on several factors including average friction factor and Nusselt number using dimensionless governing equations. Hamdan (2013) performed mathematical analysis for isothermal parallel plates channel completely that was filled with porous media. The author developed empirical correlations to relate friction factor and Nusselt number to Darcy and Forchheimen coefficient. He revealed that the coefficient is reliable to describe accurate results.

2.10 DYLIGHTING

Respective daylighting research papers have carried out several types of daylighting algorithm validation analyses. Some have implemented program-to-program analysis, and others have handled empirical validation analysis. Each one has its choice of daylighting software package. Hviid et al. (2008) compared BC/LC simulation tool, formed by (Nielsen et al. 2005), with Radiance, formed by (Ward et al. 1998). Loutzenhiser et al. (2007) calibrated results from DOE-2 and EnergyPlus against field

measurements. Ramos et al. (2010) validated the EnergyPlus program outputs with Daysim/Radiance and Troplux outputs. Reinhart et al. (2009) compared daylight simulation results generated by 3ds Max and Daysim. Vangimalla et al. (2011) validated the accuracy of ECOTECT for daylighting simulation against field measurements.

ECOTECT can be interacted easy with its Graphical User Interface (GUI) (Crawley et al. 2008) and produce reliable results for daylighting estimations (Al-Sallal 2007). As a result, the daylighting computational algorithm will be applied for this work after validating its estimations. In order to properly validate it, different studies (considered using different daylighting simulation tools and experimental models in their evaluations) have been chosen for using their input specifications for ECOTECT and comparing its outputs against theirs.

2.11 SUMMARY

A comprehensive literature review of available studies investigated recently relating to multiple-layer façade unit that involves the sustainable building design to improve occupants' comfort level whilst conserving energy consumption and excessive power expenditure. The review looks at first into background and the mechanism of air flow inside the system and then into three categories with respect to the major phenomena that the system encounters with: solar-optical, heat flux, and air flow. The common conclusion that can be drawn is that even though a variety of models available in the literature for airflow windows, most of them make use of simplified physical assumptions. Furthermore, the effects of visual aspects, and other source of heat gains such as occupants have not thoroughly been investigated.

Concerning the research methods, the main existing approaches on thermodynamic and fluid dynamic of multiple-layer façade unit have been depicted here. Clearly, two factors dominate the methods' performance: accuracy and computing time. Therefore, careful attention must be paid when choosing the method to study the unit in terms of visual and thermal comfort, heat transfer, and air flow since accurate prediction is crucial for the optimum performance and design of the façade system.

Currently, semi-transparent photovoltaic is becoming a niche application and is incorporating into ventilated facades of office and commercial buildings. Prominent representations of such technology are for the Mataro Public library in Spain (Lloret et al. 1995), and the De Klein Arade Boxtel in the Netherland (Reijenga et al. 1997). Furthermore, the photovoltaic airflow empirical unit of the Soalr Lab at Concordia University, Canada was based in the separation of an opaque PV and clear glazing as two parts (upper and lower) as well as internal shading device, located between the panes. Moreover, the research, on the airflow window incorporated with semi-transparent photovoltaics in the aspect of daylighting, power saving and thermal comfort effect, progress has been slow. Thus, it is essential to carry out a research that focus mainly on airflow window integrated with semi-transparent photovoltaic, as one unit, that can be a source of power, space heating and cooling, and daylighting (through the transparency level of the PV). The research should aim to quantify the PV window unit power generation, thermal comfort, and visual behaviour. This study also aims to be as a reference for specifying a standard CFD model properties and investigation methods.

Next chapter will present calculation models to be developed to represent the impact of different aspects on a current PV system that is similar the proposed unit in the study.

CHAPTER 3 ANALYTICAL METHOD

This chapter exploits a current system, that its concept similar to the proposed unit in the thesis, represented in Mataro Puplic Library in Spain as a multiple-layered ventilated façade integrated with semi-transparent PV solar cells, and examines the thermal behaviour of the system in different location, the city of London, and condition, summer and winter. It further exposes the unit to variable parameters such as cavity width and height, gap size, air velocity, and ambient temperature to explore the effect on the façade elements temperature such as PV panel, clear glass, and outlet temperature. Moreover, a calculation of the steady state formulas will be included since the window unit will be predominantly examined throughout the study under the steady state condition. This chapter offers an investigation to the feasibility of the steady state method with different parameters and reveals potential idea of the type of findings that will be ultimately discovered from the airflow window system.

3.1 MATARO LIBRARY FAÇADE

The public library at Mataro near Barcelona, Spain is a prominent example of a ventilated PV façade. It has been built as a prototype thermal photovoltaic building equipped with multifunctional photovoltaic modules contributing in minimising the energy consumption of thermal and electricity power. This south faced elevation, as seen in Figure 3.1, is 6 m high by 37.5 m wide. It comprises 20 kWp of multi-crystalline PV cells within a clear glass-glass laminate giving a semi-transparent appearance to the outer skin of the façade. The façade is completed by a 140 mm ventilation air space and conventional clear double glazing to the interior where outside air is drawn from the base of the façade and circulated through the gap (venting the preheated air between the cavity) to an upper air collector which is connected to the building ventilation system, illustrated in Figure 3.2. Within this technological building element, a vast part of the library's electricity and heating is generated. Also, the various building floors can feature proper daylight via PV transparency. Table 3.1 presents the thermal properties of the Mataro Library façade.

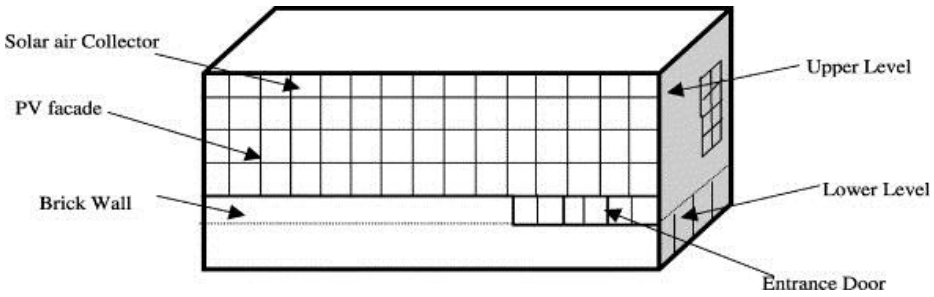

Figure 3.1 : The view of the building showing the south and east elevations (reproduced from Mei et al. (2003))

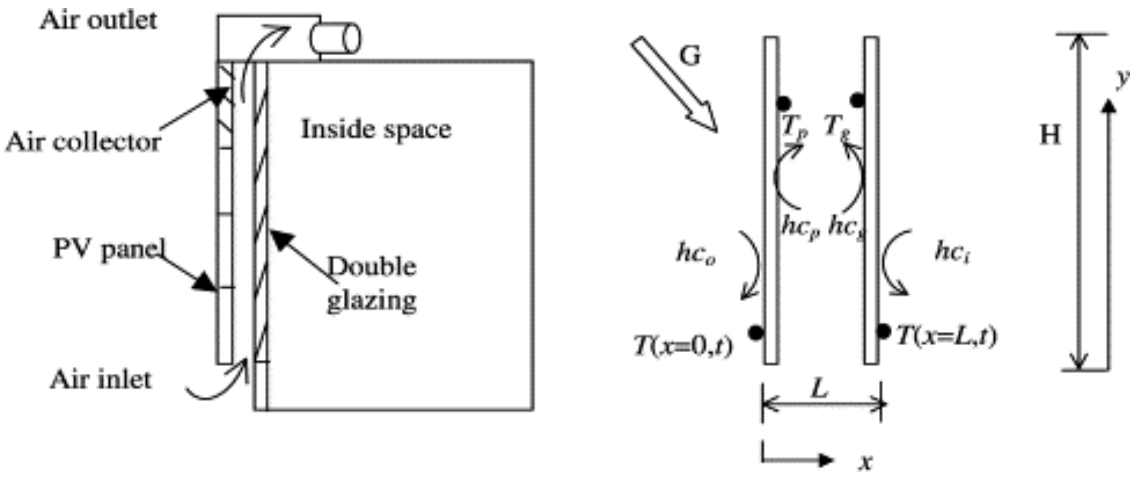

Figure 3.2: The configuration of Mataro façade (reproduced from Mei et al. (2003))

Table 3.1 : Thermal Properties of the PV Mataro façade (Mei et al. 2003)

	Left side wall			Air gap layer 4	**Right side wall**		
	Layer**1**	Layer**2**	Layer**3**		Layer**5**	Layer**6**	Layer**7**
Material	Glazed	PV	Glazed	Air	Glazed	Air	Glazed
Conductivity (W/m k)	0.8	0.8	0.8		0.8	0.021	0.8
Density (kg/m^3)	2500	2500	2500		2500	1	2500
Capacity (J/K)	1000	1000	1000		1000	1000	1000
Width (m)	0.004	0.0045	0.004	0.14	0.004	0.012	0.004

3.2 STEADY STATE FORMULAS

The steady state approach can be employed for quantifying the heat transfer through the proposed window unit in this study. The equations can be mainly considered for assessing the thermal behaviour of a multiple-layered window unit relying on either U- or R-value of each pane of the window. For steady-state thermal transmission calculation within a multiple-layer façade integrated with photovoltaic, the energy balance equations are as follows (Eicker et al. 1999):

for PV panel:

$$\mathbf{G}_p - \mathbf{U}_p\left(\mathbf{T}_p - \mathbf{T}_{amb}\right) - \mathbf{h}_{cp}\left(\mathbf{T}_p - \mathbf{T}_m\right) - \mathbf{h}_r\left(\mathbf{T}_p - \mathbf{T}_q\right) - Q_E = 0 \quad 3.1$$

for double glazing:

$$\mathbf{G}_g - \mathbf{U}_g\left(\mathbf{T}_g - \mathbf{T}_{room}\right) - \mathbf{h}_{cg}\left(\mathbf{T}_g - \mathbf{T}_m\right) - \mathbf{h}_r\left(\mathbf{T}_g - \mathbf{T}_p\right) = 0 \quad 3.2$$

for air flow rate in the gap:

$$\mathbf{h}_{cp}(\mathbf{T}_p - \mathbf{T}_m) + \mathbf{h}_{cg}\left(\mathbf{T}_g - \mathbf{T}_m\right) = \mathbf{m}\mathbf{C}_p \frac{d\mathbf{T}_m}{dx} \quad 3.3$$

The above listed equations have been applied for parametric analyses to gauge the effect of the several parameters such as gap size, window height, summer and winter solar irradiances, summer and winter temperatures, and air velocities under the effect of the city of London, United Kingdom instead of Barcelona, Spain. The simulations for the façade unit are based on hourly climate data obtained from the CIBSE guide A, the environmental design. The hourly data has been generated from monthly average of global horizontal radiation and temperature. The incident solar energy available to the PV arrays is determined by the global and diffuse irradiance on the horizontal plane. For the PV panel simulation, the shading effect is neglected.

3.3 PARAMETRIC ANALYSES

In order substantiate the steady state approach applicability, parametric analyses will be carried out to investigate the impacts of different parameters such as gap size, window height, ventilation rate, air temperature, and the heat transfer coefficient for different climate conditions. Hence, to distinctly detect such an impact, the investigation was carried out individually for each parameter that was applied variably meanwhile the other parameters were treated constantly. The fixed values of the parameters were similar to those inputted in the Mei et al. (2003), an extensive study that was presented for Mataro façade and employed the hourly vertical global solar radiations of Mataro, Spain for winter and summer time, (for the cavity width and height and air velocity, however, incident solar radiation and inlet temperature were of the city of London for winter and summer season at noon time) whilst assuming gradual increase and decrease for the

varied values that give a chance for different variation trends of the ventilated system and outlet temperature. Inputs data are tabulated in Table 3.2.

Examining the effect of these aspects can reveal the correlation between them and the system behaviour. Ultimately, results can be translated into design standards for the PV unit under the effect of multiple weathers during the winter and summer seasons. With each parameter, the thermal trend of PV and the clear glass (behind the PV panel) as well the outlet temperature will be predicted as they exemplify the performance of the whole passive solar element.

Table 3.2: Inputs data for winter and summer

	Parameter				
Weather	**Gap width d (m)**	**Gap Height H (m)**	**Air velocity V (m/s)**	**Solar radiation G (W)**	**Ambient temperature Tamb (°C)**
Winter	0.14	2.2	0.6	707.36	5.9
Summer	0.14	2.2	0.6	538.36	24.5

Parameter Variations							
d (m)	**H (m)**	**V (m/s)**	**Operation Time (h)**	**G (W)**		**Tamb (°C)**	
				Winter	**Summer**	**Winter**	**Summer**
0.06	1.1	0.1	05	0	62	0.7	16.8
0.14	2.2	0.15	06	0	91	0.7	18.5
0.22	3.4	0.2	07	0	107	1.8	20.1
0.3	4.5	0.3	08	18.3	210	2.3	21.5
0.38	5.6	0.35	09	300	342	3.7	22.7
0.46	6.7	0.4	10	523	448	4.7	23.6
0.54	7.8	0.5	11	656	516	5.5	24.4
0.62	8.9	0.55	12	707	538	5.9	24.5
0.7	10	0.6	13	678	511	5.8	24.4
0.78	11.1	0.7	14	568	438	5.3	24.2
0.86	12.2	0.75	15	372	328	4.3	23.5
0.94	13.3	0.8	16	24	194	3.7	22.5
1.02	14.4	0.9	17	0	106	3.3	19.3
1.1	15.6	0.95	18	0	89	3	17.9
1.18	16.7	1	19	0	57	2.7	16.8

3.3.1 CAVITY WIDTH AND HEIGHT EFFECT

Concerning the gap size, varied from 0.06m to 1.18m, its effect is shown in Figure 3.3 on the PV panel and back glass temperatures for both seasons due to 0.6m/s air velocity. It can be noticed that the increase of PV panel and back glass temperatures were a function of increasing cavity width which drives the outlet temperatures gradually from its maximum to its minimum providing cooler ventilation. However, the PV performance is still effective as the average PV temperature was 33^0C, in winter, and 44^0C, in summer.

The back glass temperature, when all cavity variations were applied, was 22^0C and 35^0C as an average of winter and summer, respectively. The effect of cavity width on the outlet temperature with 0.6m/s air velocity, presented in Figure 3.4, oppose to that on PV temperature. The reduction of the outlet temperature, of winter and summer, was attributed to the increase of cavity width. The outlet temperature obtained was 7^0C, as a winter average (thermally unacceptable with a maximum of 11^0C and a minimum of 6^0C), and 25^0C, as a summer average. This resulted from the more flow with the thicker cavity.

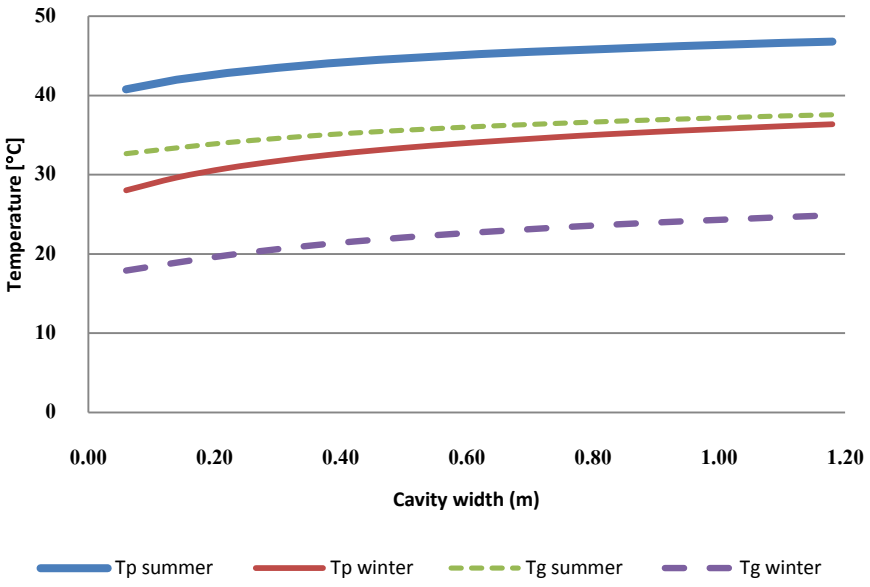

Figure 3.3: The prediction of PV panel and back glass temperatures affected by gap size

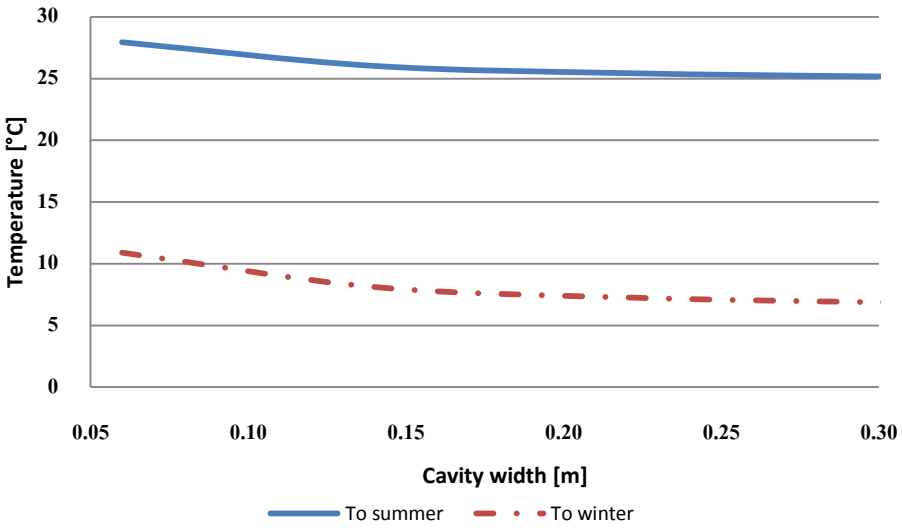

Figure 3.4: The prediction of outlet temperatures affected by cavity width

Similarly, when the height variations, varied from 1.1m to 16.7m with an air velocity of 0.6m/s, of the cavity were applied for both weather as shown in Figure 3.5 which presents the effect on the PV panel and back glass temperatures, the increase of PV and back glass temperature were proportional to the increase of cavity height. The winter average PV temperature was 32^{0}C and 44^{0}C for the summer average whilst the back glass temperature possessed winter average temperature of 22^{0}C and summer average of 35^{0}C. However, PV panel was maintained properly ventilated and within a moderate temperature.

Figure 3.6 shows the effect of cavity height on the outlet temperature with 0.6m/s air velocity under the effect of both seasons. It can be seen that the taller the cavity, the warmer outlet temperature is attained and vice versa. The average outlet temperature found in winter was 13^{0}C, for most of the heights utilised (≤ 15.6m) with a maximum of 19^{0}C and a minimum of 7^{0}C, however, the height of 16.7m fulfilled the required level of comfort with an outlet temperature of 20^{0}C. On the other hand (during the cooling season), the heights range from 2.2m to 16.7m revealed overheated outlet temperature with a highest of 35^{0}C and a lowest of 26^{0}C, however, the height of 1.1m achieved thermal comfort with outlet temperature of 25^{0}C. In summary, the taller the cavity the

more effective PV performance can be obtained as well the higher outlet temperature that is beneficial for heating season.

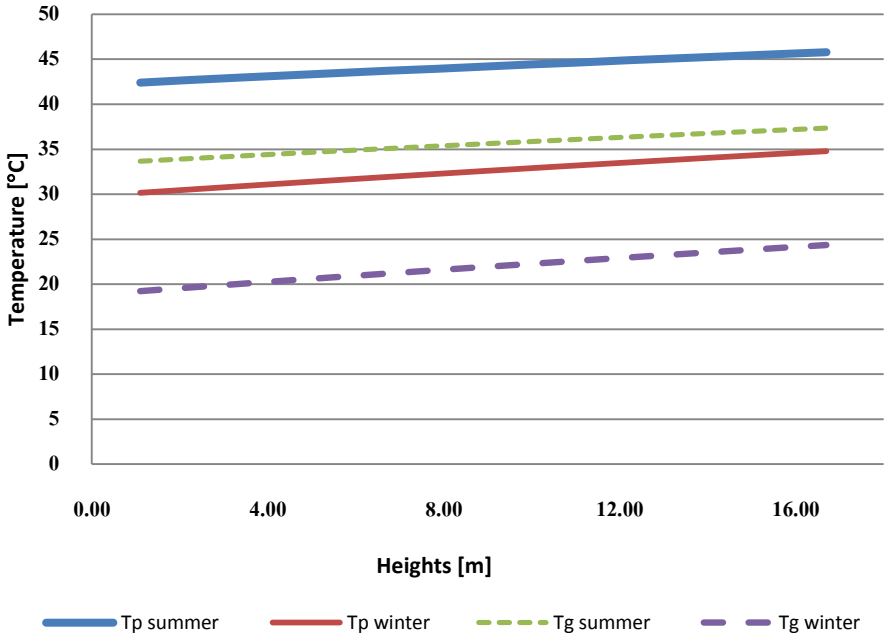

Figure 3.5: The prediction of PV panel and back glass temperatures affected by heights

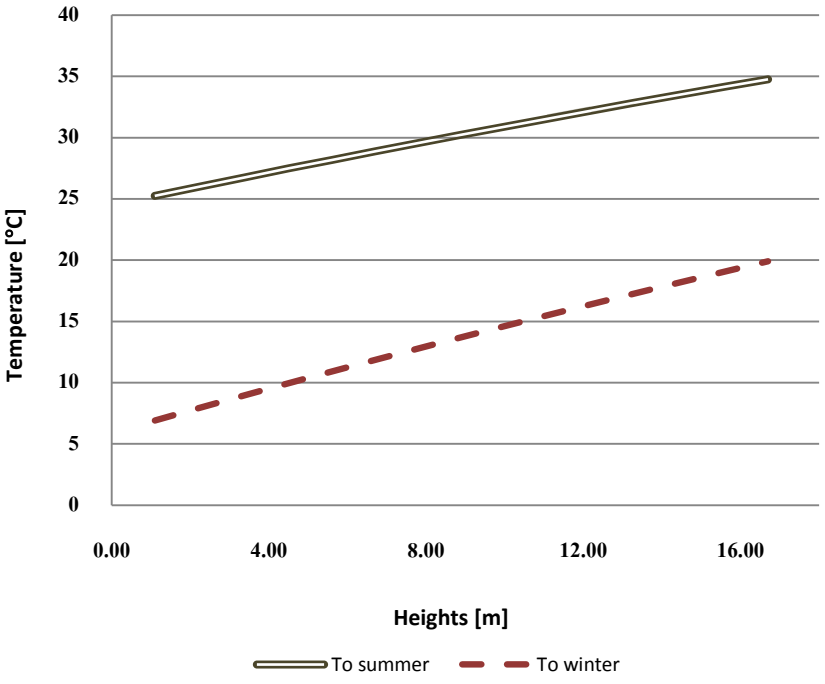

Figure 3.6: The prediction of outlet temperatures affected by heights

3.3.2 AIR VELOCITY EFFECT

The variation in the estimated PV and back glass heat distribution of different air velocities is shown in Figure 3.7. It is indicated that the increase of air velocity can cool down the PV panel and the back glass temperature gradually from a maximum to a minimum value in both weathers with an average of 33^{0}C in winter. However, velocities ≤ 0.15m/s can cause PV panel overheating when its temperature exceeds 45^{0}C whilst velocities ≥ 0.2m/s can maintain the PV panel as efficient. On the other hand, in the summer, the PV average temperature was 45^{0}C which is still acceptable for PV efficiency, yet, velocities ≤ 0.4m/s escalated the temperature above the normal operating temperature whilst velocities ≥ 0.5m/s suppressed PV overheating.

Figure 3.8 presents the effect of different air flow velocities on the outlet temperature for cooling and heating weather. From what is shown, the increase of the air velocity appear to counteract the outlet temperature behaviour as it decreased from the highest (on the lesser velocity) and increased to the lowest (on the maximum velocity). The average of outlet temperature revealed in winter was 9^{0}C (improper degree) with a maximum of 13^{0}C and a minimum of 7^{0}C. However, during the cooling period, some velocities ≥ 0.95m/s achieved the accepted thermal level whilst velocities ≤ 0.9m/s elevated the outlet temperature from 26^{0}C to 30^{0}C.

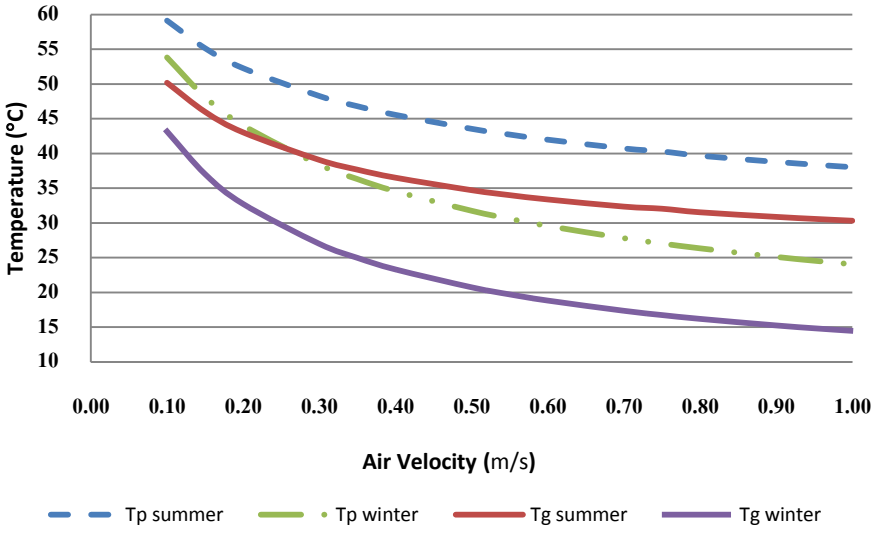

Figure 3.7 : The prediction of PV panel and back glass temperatures affected by air velocities

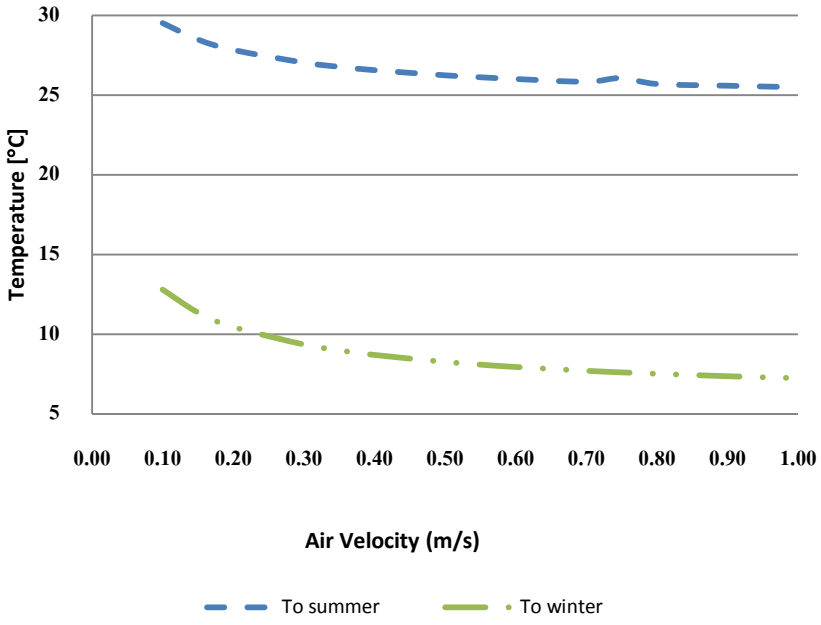

Figure 3.8: The prediction of outlet temperatures affected by air velocities

3.3.3 AMBIENT AIR TEMPERATURE EFFECT

The effect of ambient air temperature, from the early morning until the evening (the operation hours), and with a fixed incident solar radiation of summer condition (538W/m²) on the temperature of the PV panel and the back glass is presented in Figure 3.9. It can be noticed that the PV and the glass in the back were well ventilated during the working period. The back glass average temperature was 31°C with a highest and lowest value of 34°C and 27°C, respectively. The PV average temperature was 40°C with a maximum of 43°C and a minimum of 36°C meaning that the PV is still work as efficient during the day. In addition, indoor thermal comfort was obtained in some of the working time in most of the day, in the early morning and late afternoon, where the outlet temperature did not exceed 25°C and varied from 19°C to 25°C as shown in Figure 3.10. However, between 10am – 2pm (temperature was 24°C) useful thermal level for preheating was noticed.

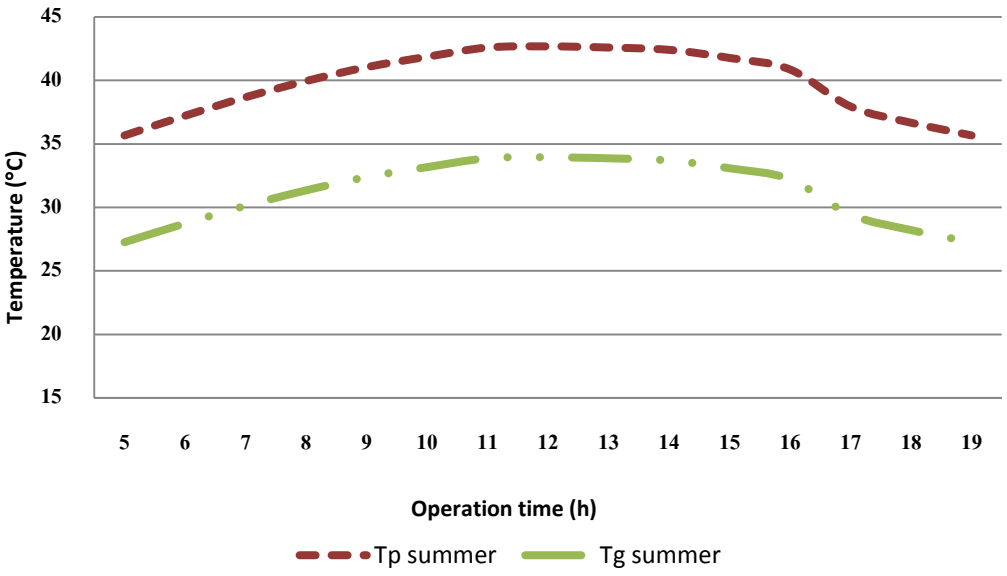

Figure 3.9: The prediction of PV panel and back glass temperatures affected by Ambient Temperature

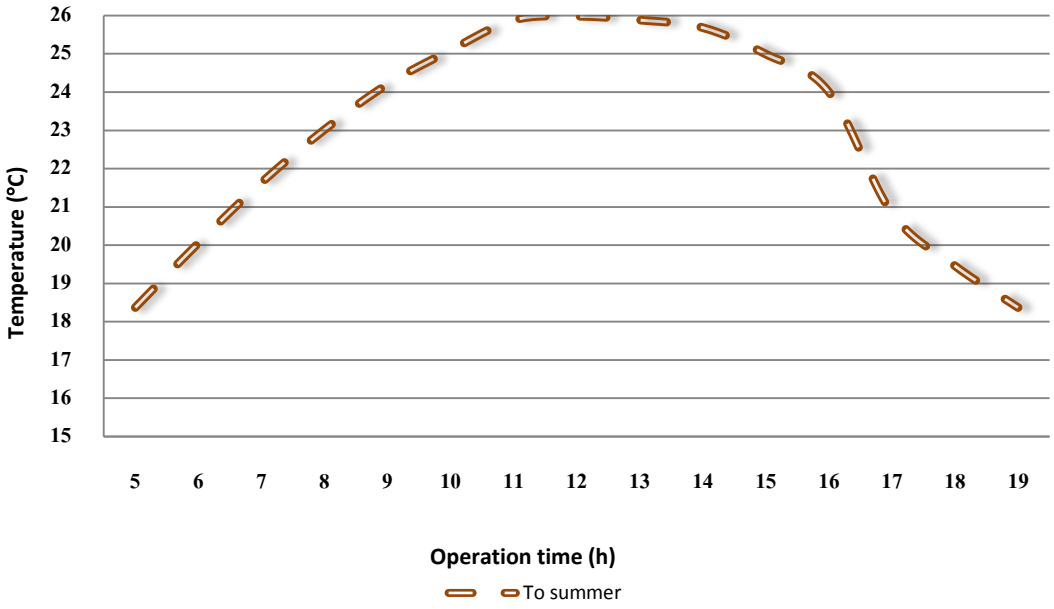

Figure 3.10: The prediction of outlet temperature affected by Ambient Temperature

Likewise, it is shown in Figure 3.11, including the trends of PV panel and the clear glass of temperature values under the effect of winter ambient temperature with a fixed incident solar radiation of 707W/m², that PV performance was efficient during the daytime (operation time) with an average temperature of 28°C and a highest degree of 31°C and a lowest of 26°C. The clear glass average temperature was 18°C where at noon time the temperature reached up to 20°C while 15°C at the early morning.

However, the outlet temperature values presented in Figure 3.12 shows that the maximum temperature found (at noon time) was 8°C. This might be a problem for the specified parameters for this analysis, yet, upon some parameters modification and deep investigation, the required thermal standards would be fulfilled.

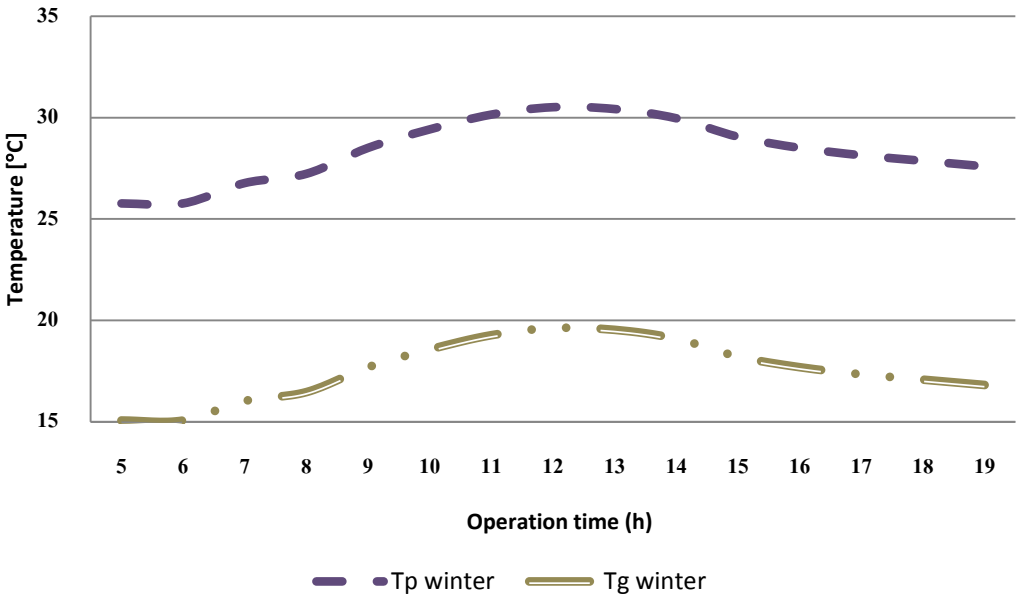

Figure 3.11: The prediction of PV panel and back glass temperatures affected by Ambient Temperature

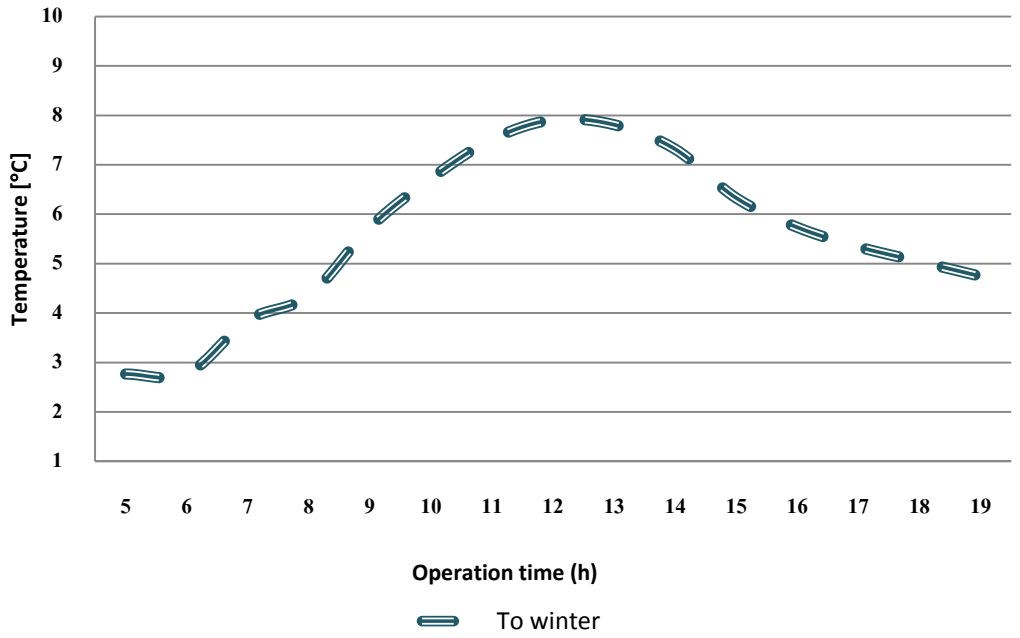

Figure 3.12: The prediction outlet temperatures affected by Ambient Temperature

3.3.4 SOLAR RADIATION

Figure 3.13 shows the effect of varied incident solar radiations on the PV panel and back glass temperature according to the winter weather. It can be observed that the PV unit can work efficiently during the operation time in winter as its average temperature was 15°C with a maximum of 31°C and a minimum of 7°C. However, the glass pane behind the PV was properly ventilated but the temperature was less than that for the PV with an average temperature of 12°C and a peak of 20°C and a lowest of 9°C. This is due to the absorptivity and transmissivity factors of the PV panel in the front as it absorbs most of the incident solar radiation and transmits the rest to the back glass which ultimately, both solar and thermal heat flux, reflect on the inside space comfort and partially determine the quality of a building thermal and visual comfort. As a result, indoor thermal comfort was not obtained as shown in Figure 3.14 from the estimations of outlet temperature affected by solar radiation. The maximum outlet temperature found was 8°C, and the minimum was 6°C.

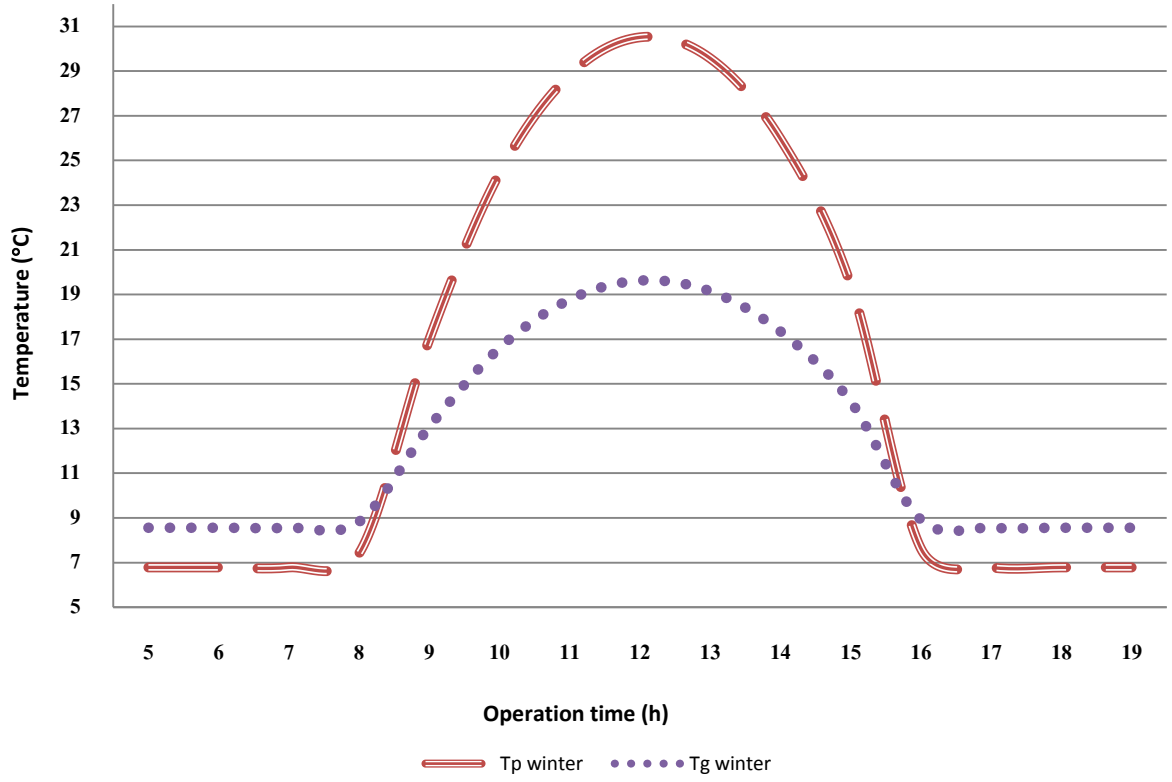

Figure 3.13: The prediction of PV panel and back glass temperatures affected by Solar Radiation in winter time

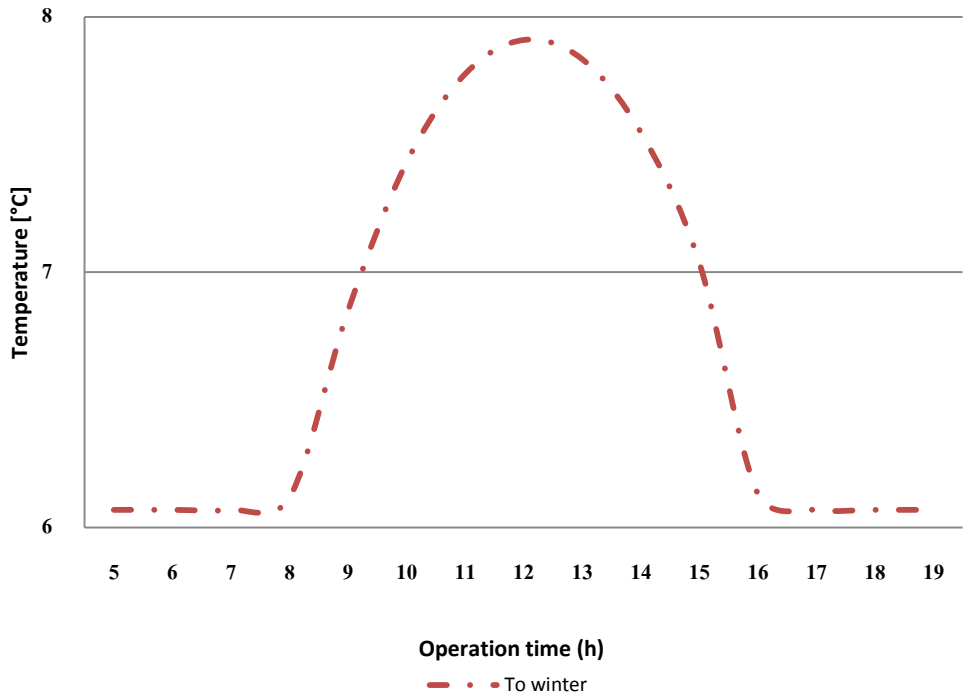

Figure 3.14: The prediction of outlet temperatures affected by Solar Radiation in winter time

Similarly, the PV performance was noticed to be efficient during the summer as shown in Figure 3.15 from the trends of PV panel and back glass temperature values under the impact of summer incident solar radiation despite its temperature was higher than that for the PV in winter with maximum degree was 43°C and the minimum was 27°C with an average of 33°C. In addition, the back glass average temperature was 29°C with a peak degree of 34°C and a lowest of 26°C. Therefore, indoor thermal comfort was fulfilled as presented in Figure 3.16 from the trend of the outlet temperature due to the summer solar radiation that revealed a maximum of 26°C and a minimum of 25°C. This increment is totally attributed to the higher heat flux of the summer time even though the incident solar radiation of summer is less than it is in winter.

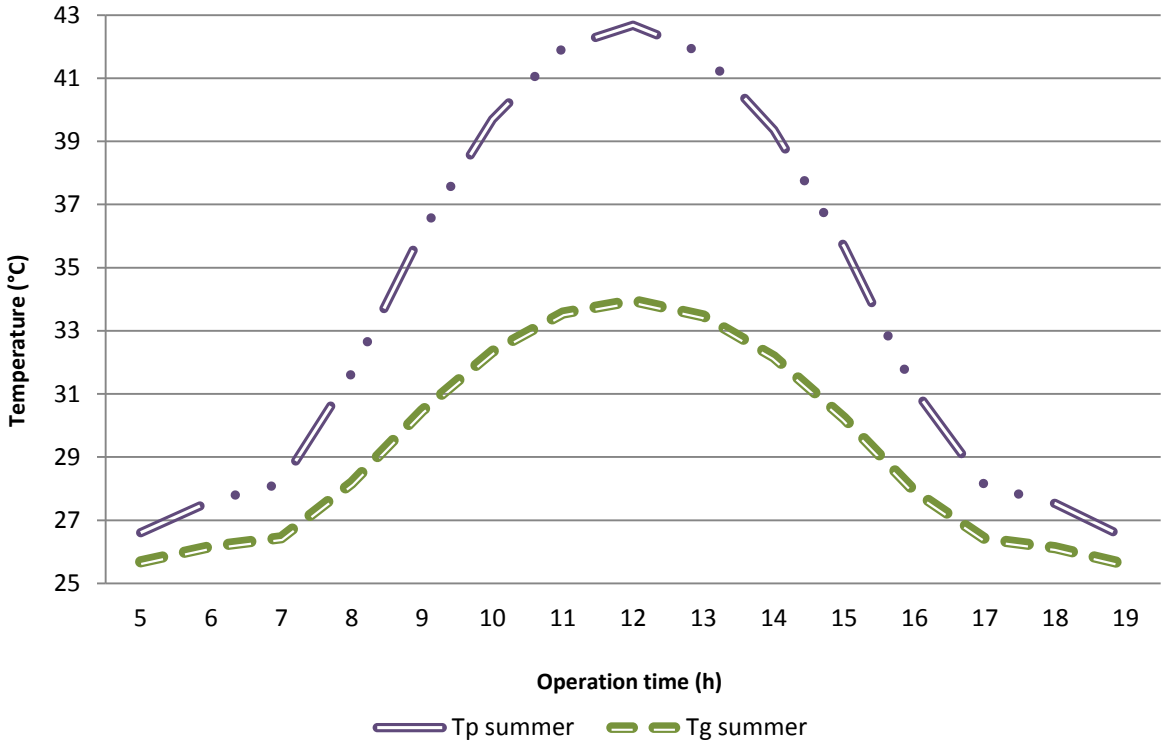

Figure 3.15: The prediction of PV panel and back glass temperatures affected by Solar Radiation in summer time

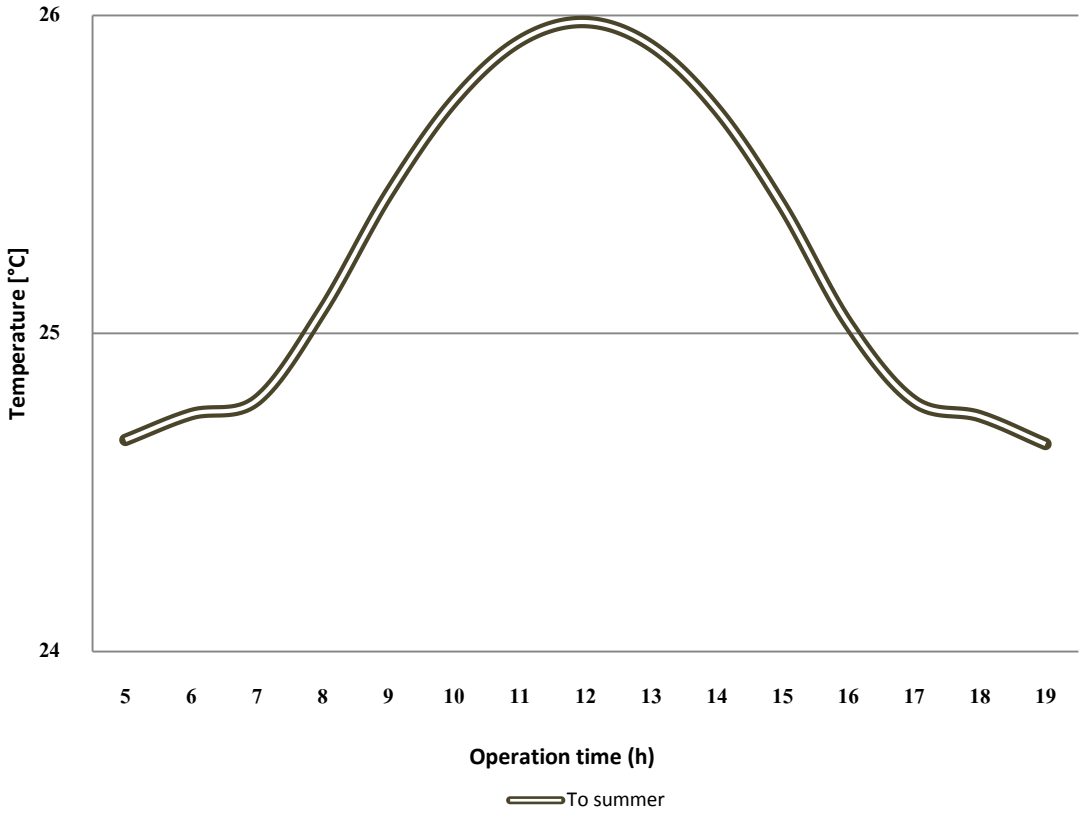

Figure 3.16: The prediction of outlet temperatures affected by Solar Radiation in summer time

3.4 SUMMARY

In this chapter a current semi-transparent PV ventilated façade of, ascribable to the influence of forced convection, was analytically exposed to a validation analysis, first, and then to parametric examination to evaluate the impact of the variations of diverse parameters (incident solar radiation, cavity width and height, ambient temperature and air velocity) that are decisive in the success of efficient performance of this bioclimatic building component during the summer and winter seasons. Then, findings will reflect on the thesis stream direction of investigation for the proposed airflow window as it is quite similar to the discussed PV unit. It was most pronounced that each parameter disclosed an aspect to be concentrated on as follows:

- Any given cavity width and height would be practical for ventilating PV panel and increasing the outlet temperature, however, condition alterations, mainly air flow velocity and air flow driving force, should be investigated and individually assigned for each season, summer and winter;
- The penetration of solar radiation of the PV unit depends on the PV transparency degree which quantifies the PV power output and indoor visual level. Hence, different PV transparencies must be evaluated from the aspects of power generation and daylighting.

Given the validation analysis for the steady state formula and the potential outcomes from an existing semi-transparent PV ventilated façade system in this chapter, the reliability of different CFD models will be ascertained against results that obtained from relevant literature and benchmark.

CHAPTER 4 MODELS VALIDATION

4.1 INTRODUCTION

Fluid flow and heat transfer are the most critical phenomena that need to be analysed for the airflow windows in order to achieve design optimisation. CFD is suited to numerically analyse systems that transfer heat, circulate fluid and associated phenomena such as chemical reactions by computer algorithm simulation. This simulation is based fundamentally on recasting the differential equations governing the fluid flow and heat transfer from the principles of conservation of mass, momentum and energy to a conservative form (Patankar 1980; Versteeg et al. 2007; ANSYS 2009). Different numerical methods are applicable to obtain approximate solutions for governing equations such as the Finite Difference Method (FDM), Finite Element Method (FEM) and the Finite Volume Method (FVM) where the latter is the most employed code (Patankar 1980; Versteeg et al. 2007; ANSYS 2009).

In order to understand the complexity of fluid dynamic and thermal energy of a building component such as an airflow window, the CFD code will be used for this analysis that is represented in ANSYS Fluent 14.0 (ANSYS 2009) using FVM. Thus, a validation analysis will be carried out a priori to ascertain the reliability of CFD codes for evaluating the system by validating CFD model results, firstly, by comparison the CFD results with benchmark, obtained from BEJAN (2003), of flat parallel plate with relation to airflow window, and secondly, against results in relevant literature.

4.2 CFD NUMERICAL MODELLING

The numerical modelling is a concept of discretising a flow path into cells, called control volume, via meshing progress within the computational domain. Each cell is introduced as an equation that is produced from sequential conservation calculations (Patankar 1980; Versteeg et al. 2007). Generally, simulation tools solve conservation equations for all unknown transport variables (velocity, temperature, etc) and predict an approximate solution for either flow cases: turbulent or laminar (ANSYS 2009). Three basic conservation equations can calculate values for laminar flow: mass and momentum

equations are for fluid dynamic and energy equation is for heat transfer whereas the turbulent flow requires additional transport equations that rely on iterative predictions and turbulence quantities (Patankar 1980; Versteeg et al. 2007). The governing equations for two dimensional steady state fluid dynamic and heat transfer are (Patankar 1980; Versteeg et al. 2007):

The continuity equation:

$$\frac{\partial}{\partial x}(\rho u) + \frac{\partial}{\partial y}(\rho v) = 0 \quad 4.1$$

The X-momentum transport equation:

$$\frac{\partial}{\partial x}(\rho u u) + \frac{\partial}{\partial y}(\rho u v) = -\frac{\partial P}{\partial x} + \frac{\partial}{\partial x}\left(\mu \frac{\partial u}{\partial x}\right) + \frac{\partial}{\partial y}(\mu \frac{\partial u}{\partial y}) \quad 4.2$$

The Y-momentum transport equation:

$$\frac{\partial}{\partial x}(\rho u v) + \frac{\partial}{\partial y}(\rho v v) = -\frac{\partial P}{\partial y} - \rho g \beta \left(T - T_{ref}\right) + \frac{\partial}{\partial x}(\mu \frac{\partial v}{\partial x}) + \frac{\partial}{\partial y}(\mu \frac{\partial v}{\partial y}) \quad 4.3$$

The energy conservation equation:

$$\frac{\partial}{\partial x}(\rho u T) + \frac{\partial}{\partial y}(\rho v T) = \frac{\partial}{\partial x}(\frac{K}{C_p}\frac{\partial T}{\partial x}) + \frac{\partial}{\partial y}(\frac{K}{C_p}\frac{\partial T}{\partial y}) \quad 4.4$$

Where x is the axis direction (m), u is the velocity in the x direction, v is the velocity in Y direction, β is the coefficient of thermal expansion (K^{-1}), μ is the dynamic viscosity ($(\mathrm{kg/ms})$, ρ is the air density (kg/m^3), C_p is the heat capacity (J/kg), T is the element temperature (K), T_{ref} is the reference temperature of the element (K), g is the gravitational acceleration (m/s^2), and K is the flow index, dimensionless. Fluent 14.0 was used to simulate the heat transfer and fluid flow in the airflow windows. Standard k-ε model with enhanced wall treatment were used due to the facts that its use was recommended in (Ansys 2011) as a standard model for turbulent flow due to its robustness, economy, and reasonable accuracy for a class range of turbulent flows.

4.3 VALIDATION ANALYSIS AGAINST BENCHMARK FOR FLOW IN PARALLEL PLATES

This section presents a validation analysis for CFD models' predictions against empirical correlations results in terms of the overall mean Nusselt number for a forced convection,

isothermal, vertical channel with relation to airflow window. The uniform wall temperature condition was considered and the correlations are (BEJAN 2003):-

$$\mathrm{Nu} = 0.023.\mathbf{Re}^{\mathbf{4/5}}\,\mathbf{Pr}^{\mathbf{0.4}} \qquad 4.5$$

The Nusselt number can also be calculated from CFD simulation using

$$\mathrm{Nu} = h\,D_h/\,k = [\mathrm{q}/\,(\mathrm{T_{out}} - \mathrm{T_{in}})]\,D_h/\,k \qquad 4.6$$

Where Nu is the Nusselt number, Re is Reynolds number ($Re = \mathrm{v.d}/\nu$), Pr is Prandtl number, h is the heat transfer coefficient (W/m^2.K), k is the thermal conductivity (W/mk), D_h is the hydraulic diameter (m), q is the heat flux (W/m^2), $\mathrm{T_{out}}$ is the outlet temperature (K), and $\mathrm{T_{in}}$ is the inlet temperature (K). A wide range of velocities, from 0.1 to 1m/s with an interval of 0.05m/s, were employed for comparison where flow types, laminar, turbulent or transitional were used to determine the suitable CFD model for the velocities. The CFD predictions have been obtained for heat flux from three different mesh sizes, original (size of 603366 cells) and two other refinements (first with size of 101400 cells and second with size of 241344 cells) as depicted in Figure 4.1, Figure 4.2 and Figure 4.3. The mesh size was increasing with each refinement to the point of acquiring finer mesh in order to obtain mesh-independent solution. Mesh independency will be explored by comparing the difference in Nusselt numbers (revealed between the CFD predicted Nusselt numbers under the original mesh and the first refinement) versus the difference in Nusselt numbers (found between the CFD estimated Nusselt numbers under the first and the second refinements).

Bottom Top

Figure 4.1: Original mesh near the bottom and the top of the vertical channel

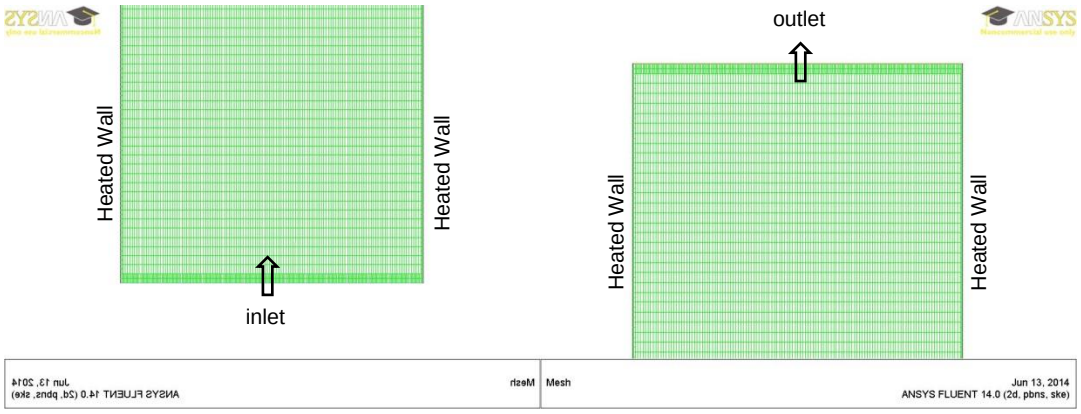

Bottom Top

Figure 4.2: First mesh refinement near the bottom and the top of the vertical channel

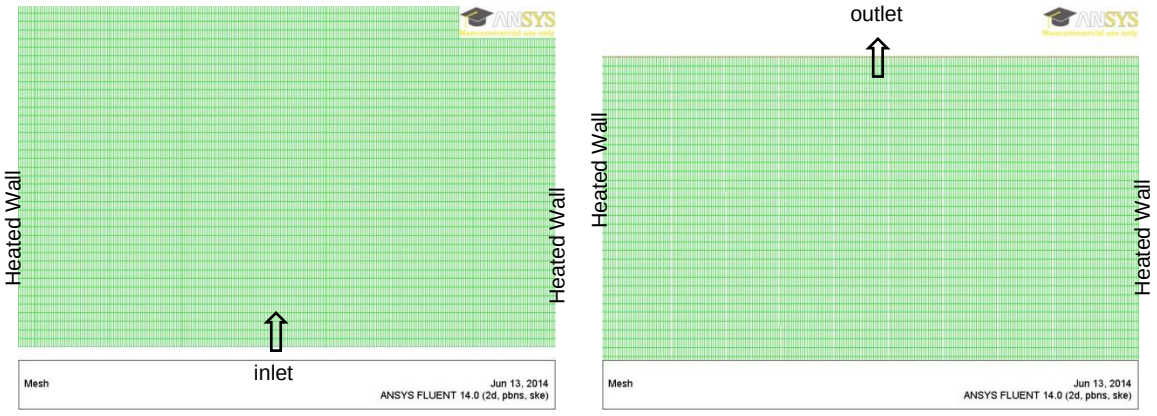

Bottom Top

Figure 4.3: Second mesh refinement near the bottom and the top of the vertical channel

4.4 RESULTS AND DISCUSSION

The predicted results of the Nusselt number were compared with those calculated from the empirical formulas. The model accuracy criteria used to evaluate the difference between mathematical calculations and numerical predictions are in compliance with the best practice guides. This model quantifies the relative error between estimations and calculations. If this error is less than or equal to 10 per cent, the predicted data will be considered as acceptable.

Figure 4.4 presents the comparison between overall mean Nusselt numbers calculated using empirical formulas and CFD model for the original mesh with the percentage errors between both results. It shows that both trends are similar as they rise gradually with the velocity increase. The overall average percentage error is 13 per cent where at velocities < 0.65m/s the relative error exceeds 10 per cent. However, the error is 10 per cent at velocities ≥ 0.65m/s. The large difference at low velocities might result from the absence of the buoyancy force which introduced the effect of fan-induced flow only. At low velocity the buoyancy could play a significant role in the cavity flow. This can be construed as all velocities are feasible for this type of model upon design modifications and driving force and condition considerations. Figure 4.5 shows the effect of different mesh sizes on the CFD predicted Nusselt numbers resulting from the flow through two parallel plates. It can be seen that the effect of mesh size is negligible where the errors between each size are maintained below 10 per cent.

In summary, the computed heat flux produced Nusselt numbers that generally are comparable with calculated data. The model can be employed to predict the airflow patterns, air temperature and air velocity distributions, and heat flux through the air channel into the inside space.

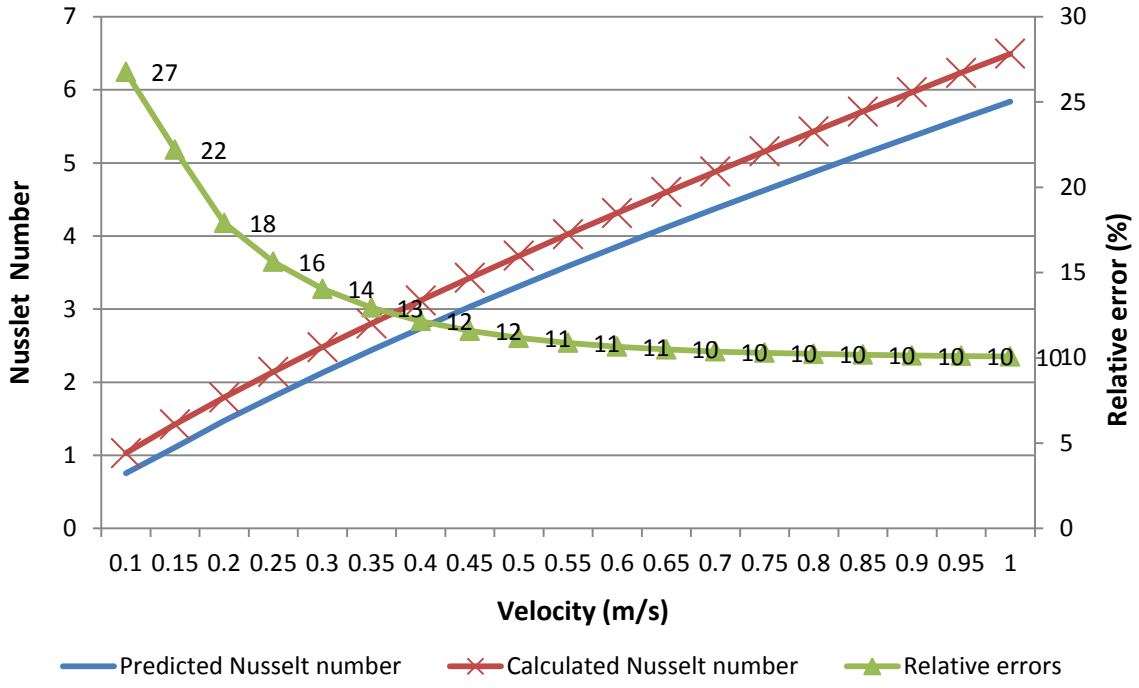

Figure 4.4: Comparison between overall mean Nusselt numbers calculated by empirical formulas and CFD model for the original mesh

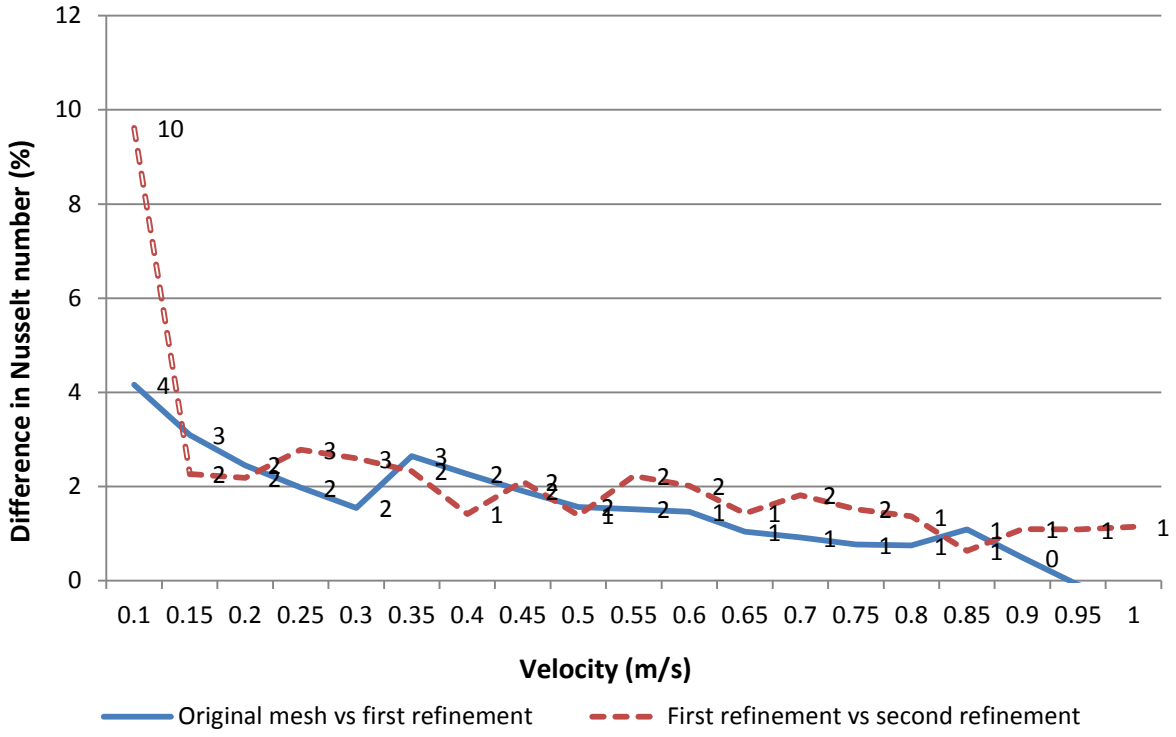

Figure 4.5: Effect of mesh size

4.5 VALIDATION ANALYSIS FOR AIRFLOW WINDOW

In this validation work the same methodology and inputs described above for modelling the air temperature distributions were used. Since the two-dimensional CFD model gives the same results compared to a three-dimensional model (Pasut et al. 2012) and the overall mesh size for such an extended three-dimensional computational domain would be excessively large, the two-dimensional model was the best choice for this work. The view of the two-dimensional model geometry is depicted in Figure 4.6. The validation analyses were restricted to case one and case two that represent the forced flow scenarios in Bhamjee et al. (2012), because they are similar to the flow mechanism of the proposed system in this content. Velocities were specified in this validation, in contrast to (Bhamjee et al. 2012), when they were considered unknown and the pressure was identified instead. They were calculated based on the resultant volumetric flow rate from Bhamjee et al. (2012) and defined by $v = v`/A$ (Han 2012) where $v$ is the velocity; $v`$ is the volumetric flow rate; A is the flow area.

Three different CFD models were employed for simulations. The models were k-ε with enhanced wall treatment, SST k-ω and SST Transition. Each simulation included three different mesh volumes: original volume (6579 cells) and two refinements (first with a volume of 33069 cells and second with a size of 88029 cells) that illustrated in Figure 4.6, Figure 4.7, Figure 4.8, Figure 4.10, Figure 4.11 and Figure 4.12 and three asymmetric ingress and egress temperature conditions ($T_{in} = 289.305$K and $T_{out} = 293.02$K; $T_{in} = 288.5$K and $T_{out} = 323.15$K; $T_{in} = 286$K and $T_{out} = 306$K). For each mesh size, rake lines were specified to obtain data for comparison and to regenerate finer meshes. In each simulation, a comparison of estimated temperature difference between the inlet and outlet for case one and case two in three different mesh sizes was carried out each with produced temperature difference value between the inlet and outlet in only when T_{in} was 289.305K and T_{out} was 293.02K (Bhamjee et al. 2012). For the other two temperature conditions, comparisons were made between predictions of original and added rake plots.

The work extended for further validation analysis to calibrate the temperature measurements at the outlet produced in Bhamjee et al. (2012). The CFD model applied for this simulation was k-ε with enhanced wall treatment since it is a standard CFD model (ANSYS 2009). The simulation was examined for three times. The first included similar temperature conditions to the paper and the other two considered climatic improvements at the inlet and outlet to capture the effect of the temperatures on the model reliability.

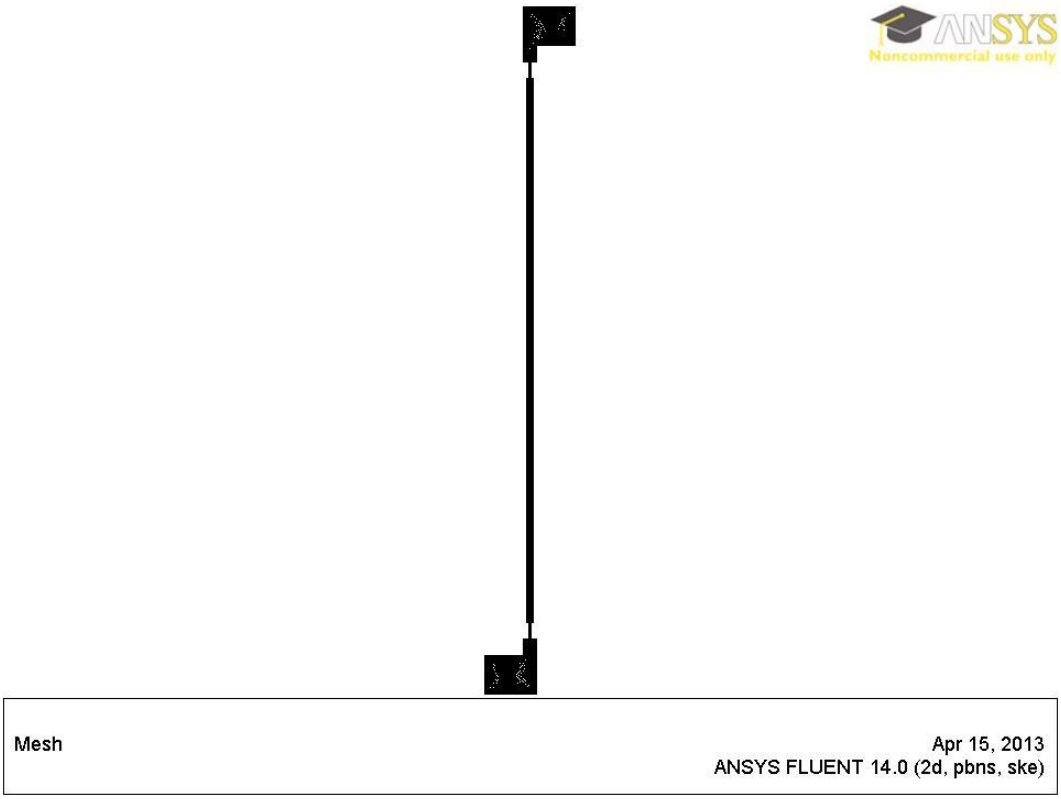

Figure 4.6: View of the Two-Dimensional CFD Model Geometry

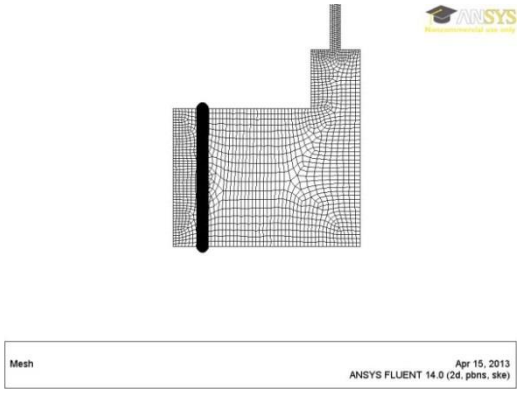

Figure 4.7: Original mesh at the inlet and rake

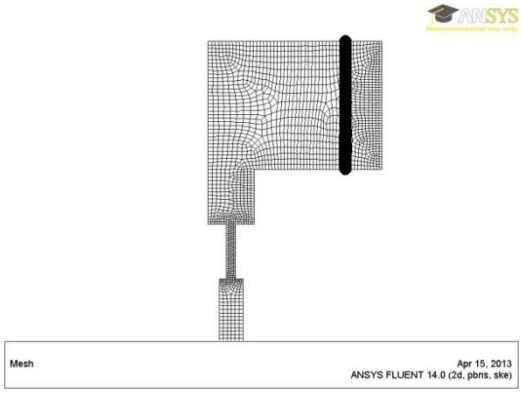

Figure 4.8: Original mesh at the outlet and rake

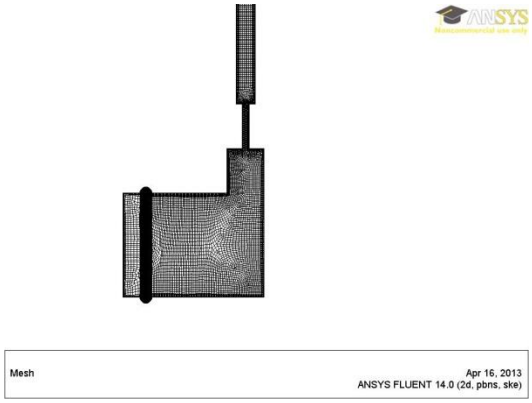

Figure 4.9: First mesh refinement at the inlet and rake

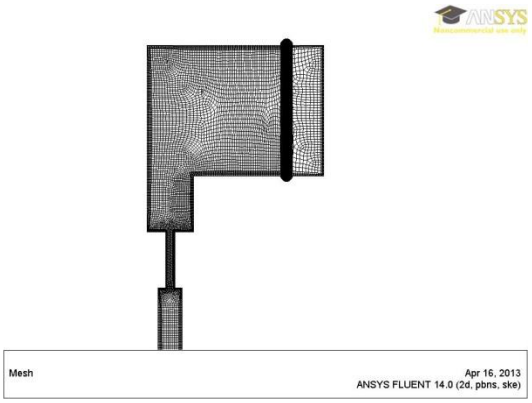

Figure 4.10: First mesh refinement at the outlet and rake

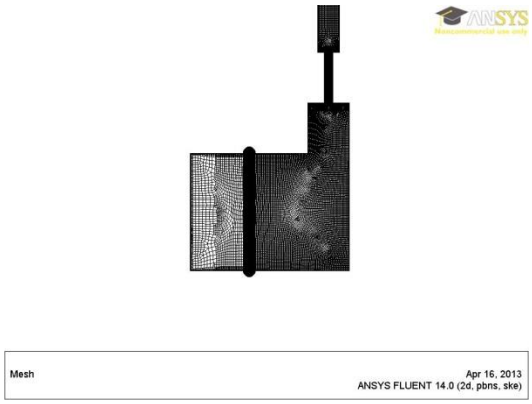

Figure 4.11: Second mesh refinement at the inlet and rake

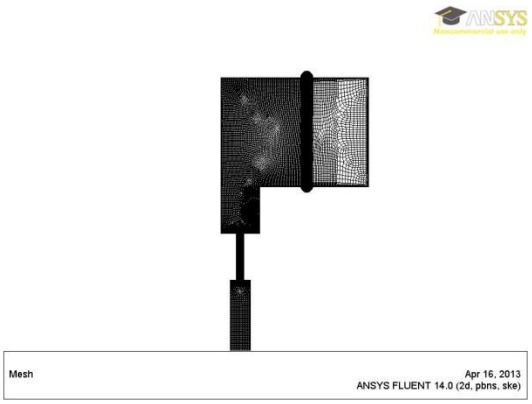

Figure 4.12: Second mesh refinement at the outlet and rake

4.5.1 SUPPLY AIR WINDOW DESCRIPTION

As mentioned previously, data will be employed from Bhamjee et al. (2012) of a supply air window to validate CFD models. The cavity of the window consisted of a heated vertical channel and open to the outside and inside environment as depicted in Figure 4.14. The dimensions of the system are illustrated in Figure 4.13. The system was modelled in three-dimensional CFD model utilising ANSYS Fluent 14.0 to investigate the velocity field, temperature distributions and thermal performance under forced flow (fan-induced air flow between the cavity), and natural flow (density changes – induced air flow between the cavity). Modelling was carried out for experimental model of a supply air window for a three-dimensional heat and fluid flow. The mesh consisted of nine

million hexahedral cells constructed by Cooper scheme in the cavity and perforations. That was produced by cell growth from the perforation into the rest of the flow path. The cell size was constant (1.4mm) for final simulations.

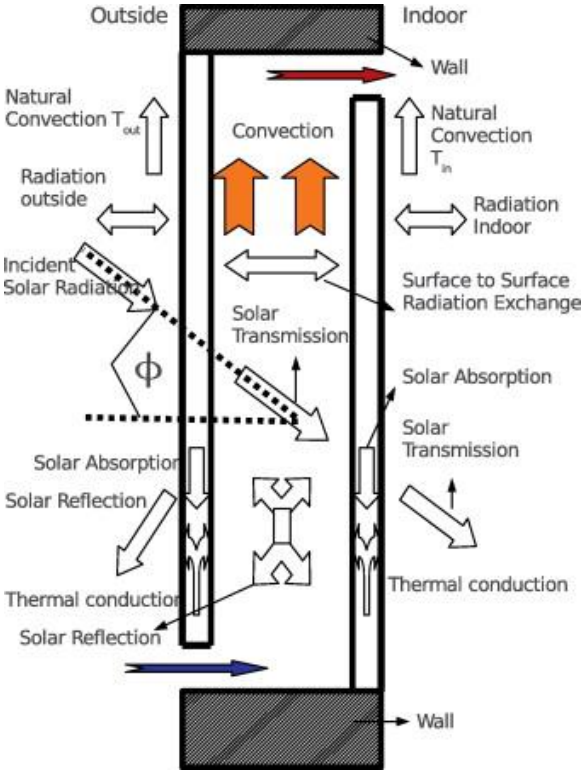

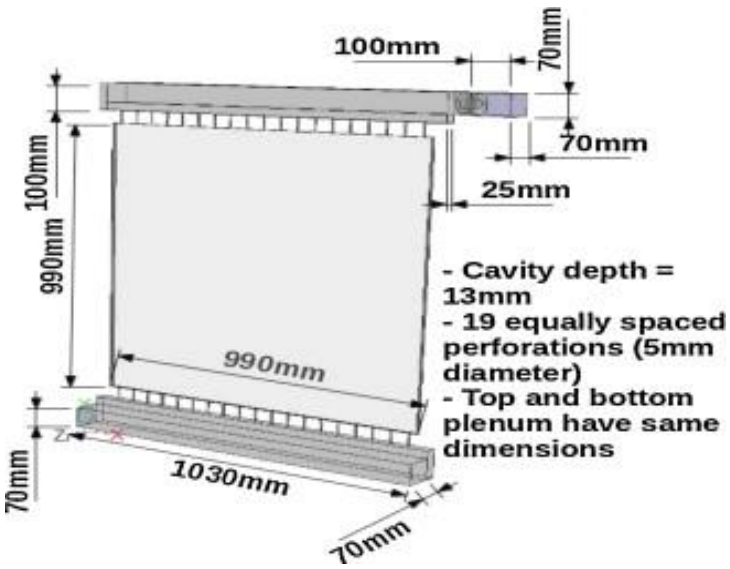

Figure 4.13: Dimensions of CFD model geometry

Figure 4.14: Physics of the supply Air Window

There were three types of boundary-fan, inlet and outlet. The perforations, ducts, plenums, glass panes and window cavity were labelled as aluminium walls except the two glass panes were assigned as glass walls. On the fluid side of all walls (thin walls), the no slip condition was applied. Both glass panes were provided heat via solar radiation with convection boundary condition. Walls were identified surface roughness. The surface roughness height for the glass was taken to be $3 * 10^{-7}$m and that for the aluminium to be $2.4 * 10^{-7}$m (Blevins 1984). The free stream temperature ($T_{\infty,outside}$) was identified at the inlet ($T_{inlet,meas}$) for all surfaces exposed to the outside of the empirical model whilst the surfaces facing the inside of the empirical model was identified as the temperature measured inside the model ($T_{room,meas}$) from the free stream temperature ($T_{\infty,inside}$). The employed turbulence models were the k-ε model and the SST k-ω model. The turbulence

intensity was specified as 10 per cent for inlet and outlet. The hydraulic diameter was calculated for the inlet by the following:

$D_{H,inlet} = 4P_{inlet}/A_{inlet}$ = 0.0631m where P_{inlet} refers to the perimeter of the inlet and A_{inlet} refers to the area of the inlet. Likewise, for the outlet the hydraulic diameter was 0.0822m by $D_{H,outlet} = 4P_{outlet}/A_{outlet}$ where P_{outlet} refers to the perimeter of the outlet and A_{outlet} refers to the area of the outlet. The fan boundary represented the fan as a face that was characterised with pressure jump, tangential and radial velocity. Details of further simulation characteristics and its material properties are given in Bhamjee (2012). The simulation was operated within gravity conditions with gravitational constant (g=9.81 m/s^2) in the negative y-direction. Because the airflow window meant to be investigated in a supply mode only under heating conditions (T_{in}>T_{out}), results were winter conditions dependant.

4.5.2 SOLUTION METHODS

Models were simulated as three-dimensional in a steady state using double precision and pressure based solvers. The simple segregated solver was applied for pressure velocity coupling. Each spatial discretization factor was specified different solution scheme. The second order upwind scheme was employed for the momentum, energy, turbulent kinetic energy and specific dissipation rate. For pressure, PRESTO was used. Gradient was reconstructed by the last squares cell based method.

4.5.3 EMPLOYING k-ε TURBULENCE MODEL WITH ENHANCED WALL TREATMENT

This section presents the calculated differences between the air temperature at the inlet and outlet for original and rake lines inside the cavity of the simulated supply air window employing k-ε turbulence model with enhanced wall treatment at three different mesh sizes where $T_{in} = 289.305$K. That is presented within two figures: Figure 4.15 where the velocity = 5.22 m/s; Figure 4.16 where the velocity = 5.17 m/s. Each figure shows the percentage errors with calculated differences between similar air temperature predicted

at the inlet and outlet for a typical system and parameters in (Bhamjee et al. 2012) except that the enhanced wall treatment was used by the SST k-ω turbulence model. Moreover, the section offers the calculated differences between the air temperature at the inlet and outlet for original and rake lines employing typical model for typical system at three different mesh sizes with two consecutive refinements on the temperature at the inlet and outlet to exclusively validate the performance of k-ε turbulence model with enhanced wall treatment. In addition, it shows the percentage errors between results obtained from original and rake lines. The first refinement assumed $T_{in} = 288.15$K and $T_{out} = 323.15$K and the second assumed $T_{in} = 286$K and $T_{out} = 306$K.

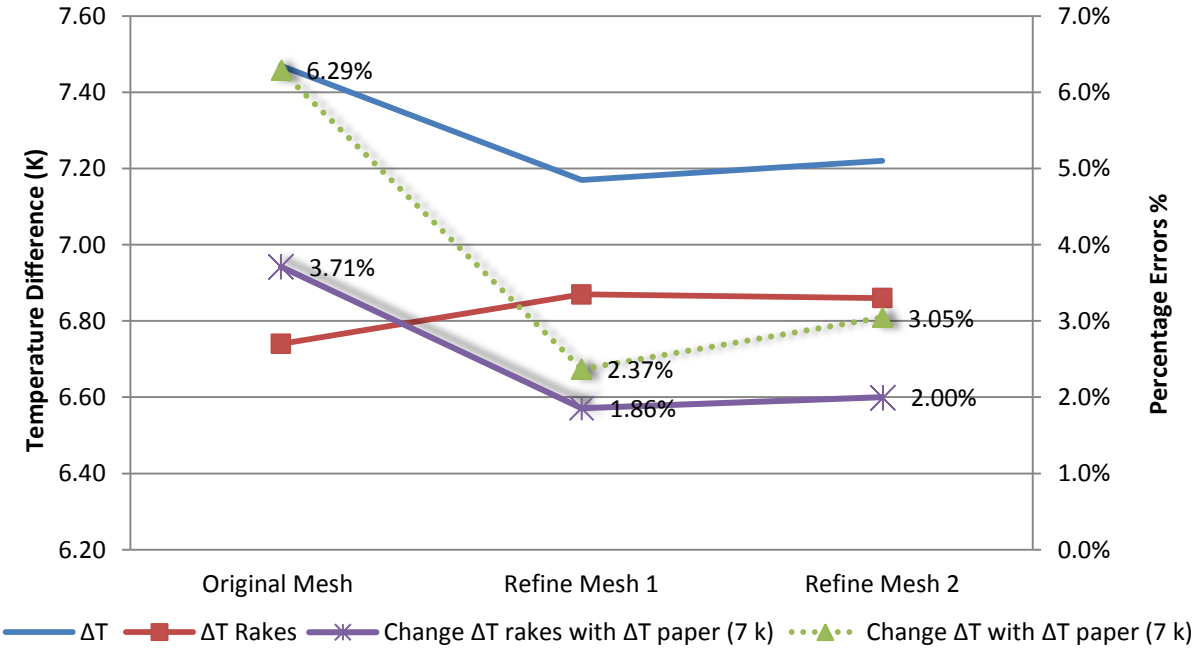

Figure 4.15 : Comparison of ΔT in different meshes for Case One (velocity =5.22 m/s) using k-ε Model & Enhanced Wall Treatment with Ti = 289.305K compared with ΔT = 7K in the paper

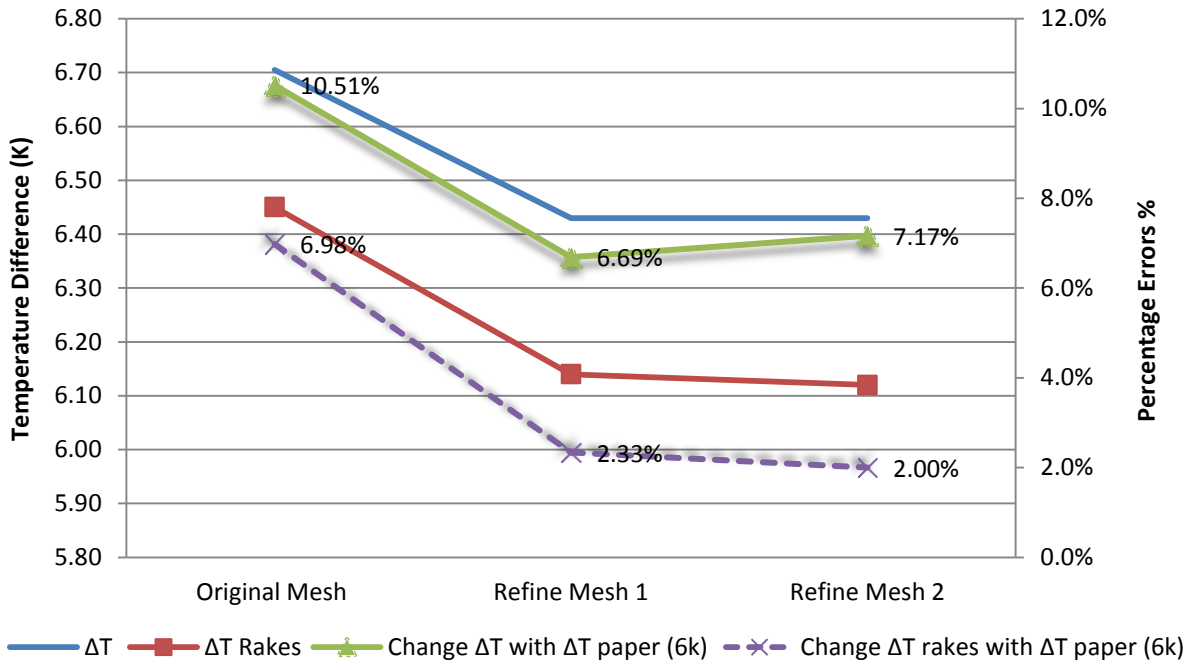

Figure 4.16 : Comparison of ΔT in different meshes for Case two (velocity = 5.17 m/s) using k-ε Model & Enhanced Wall Treatment with Ti = 289.305K compared with ΔT = 6K in the paper

4.5.4 RESULTS AND DISCUSSION

Figure 4.15 shows the difference between the temperature values at the inlet and outlet as calculated from the predicted temperatures, applying k-ε turbulence model and Enhanced Wall Treatment for case one, for original and rake lines at each mesh size. The figure indicates that the errors obtained between the temperature differences are in the range of the acceptable limit, 10 per cent. Furthermore, the mesh refinement impact, on the estimations, is trivial. However, the larger error revealed from the original mesh whilst the error becomes even smaller with finest mesh. The overall average error between the paper and the model predictions for the original lines is 3.9 per cent, and it is 2.52 per cent for the rake lines. Likewise, Figure 4.16 presents similar results for case two under the use of k-ε turbulence model and Enhanced Wall Treatment. It can be seen that the predicted inlet and outlet temperatures have slightly equal differences to those revealed in the paper with acceptable errors averaged with 8.12 per cent for original lines and 3.77 per cent for the rake lines.

Comparing these results to those produced in (Bhamjee et al. 2012), a scarce difference between both results can be observed. In addition, a uniform trend of both original and

rake lines give slight tapering percentage errors from the original mesh to the second mesh refinement represented with acceptable errors. Indeed, it can be noticed that the simulation is resistant to the complexity of different meshes. Also, rake lines have a relatively slight impact on the temperatures to be tapered compare to the differences between the temperatures calculated from original lines. For both results of original and rake lines produced when velocity = 5.22 m/s or 5.17 m/s, it appears that agreement can be obtained between the results of the two models (k-ε with enhanced wall treatment and SST k-ω) since the latter estimated approximately similar temperature values. Table 4.1 presents the comparison of ΔT in different meshes for case one and two.

Table 4.1: The comparison of ΔT in different meshes for case one and two using k-ε model and Enhanced Wall Treatment with Ti = 289.305K

ORIGINAL MESH						
Cases	**Velocities (m/s)**	**ΔT paper (K) (Bhamjee et al. 2012)**	**ΔT (K)**	**Change with paper (Bhamjee et al. 2012)**	**ΔT Rakes (K)**	**Change with paper (Bhamjee et al. 2012)**
1	**5.22**	**7.00**	**7.47**	6.29%	**6.74**	3.71%
2	**5.17**	**6.00**	**6.71**	10.51%	**6.45**	6.98%
REFINED MESH 1						
Cases	**Velocities (m/s)**	**ΔT paper (Bhamjee et al. 2012)**	**ΔT (K)**	**Change with paper (Bhamjee et al. 2012)**	**ΔT Rakes (K)**	**Change with paper (Bhamjee et al. 2012)**
1	**5.22**	**7.00**	**7.17**	2.37%	**6.87**	1.86%
2	**5.17**	**6.00**	**6.43**	6.69%	**6.14**	2.33%
REFINED MESH 2						
Cases	**Velocities (m/s)**	**ΔT paper (Bhamjee et al. 2012)**	**ΔT (K)**	**Change with paper (Bhamjee et al. 2012)**	**ΔT Rakes (K)**	**Change with paper (Bhamjee et al. 2012)**
1	**5.22**	**7.00**	**7.22**	3.05%	**6.86**	2.00%
2	**5.17**	**6.00**	**6.43**	7.17%	**6.12**	2.00%

4.5.5 k-ε WITH ENHANCED WALL TREATMENT EXCLUSIVE VALIDATION

The CFD k-ε model and enhanced wall treatment is not sensitive to the air temperature improvements. Figure 4.17 shows the negligible variations of the differences between the temperature predictions at the inlet and outlet where $T_{in} = 288.15K$ and $T_{out} = 323.15K$ for original and rake lines at different mesh volumes with higher velocity. For both surface

patterns, the differences between temperatures seem to be consistent and resistant to mesh complexity with average of 30.51 per cent and 29.23 per cent for original and rake lines, respectively. The same is true with regard to percentage errors between these values at the magnitude of each mesh. They seem to be trivial and the average is 4.19 per cent. Similar values are observed in Figure 4.18 when velocity was lower with values presented in Figure 4.17. The average difference between the air temperature at the inlet and outlet is 30.51 per cent for original surface, and it is 29.23 per cent for rake line. The average percentage error between these values is 4.19 per cent.

Similar results can be observed for the CFD k-ε model with enhanced wall treatment to the air temperature refinements in Figure 4.19 where $T_{in} = 286K$, $T_{out} = 306K$ and higher velocity. It offers relatively small variations of the differences between the temperature predictions at the inlet and outlet for original and rake lines at different magnitudes of the mesh. Consequently, it can be observed that the differences between temperatures are trivial for each surface plot.

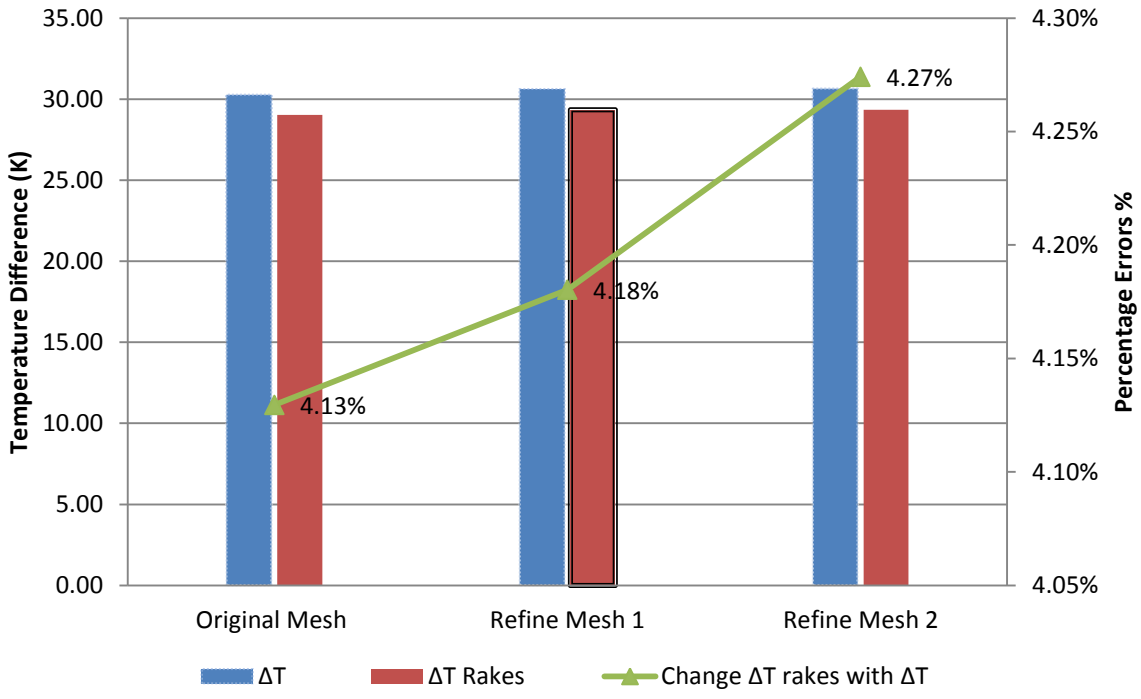

Figure 4.17 : Comparison of ΔT in different meshes for Case One (velocity = 5.22 m/s) using k-ε Model & Enhanced Wall Treatment with Ti = 288.15, To = 323.15 (K)

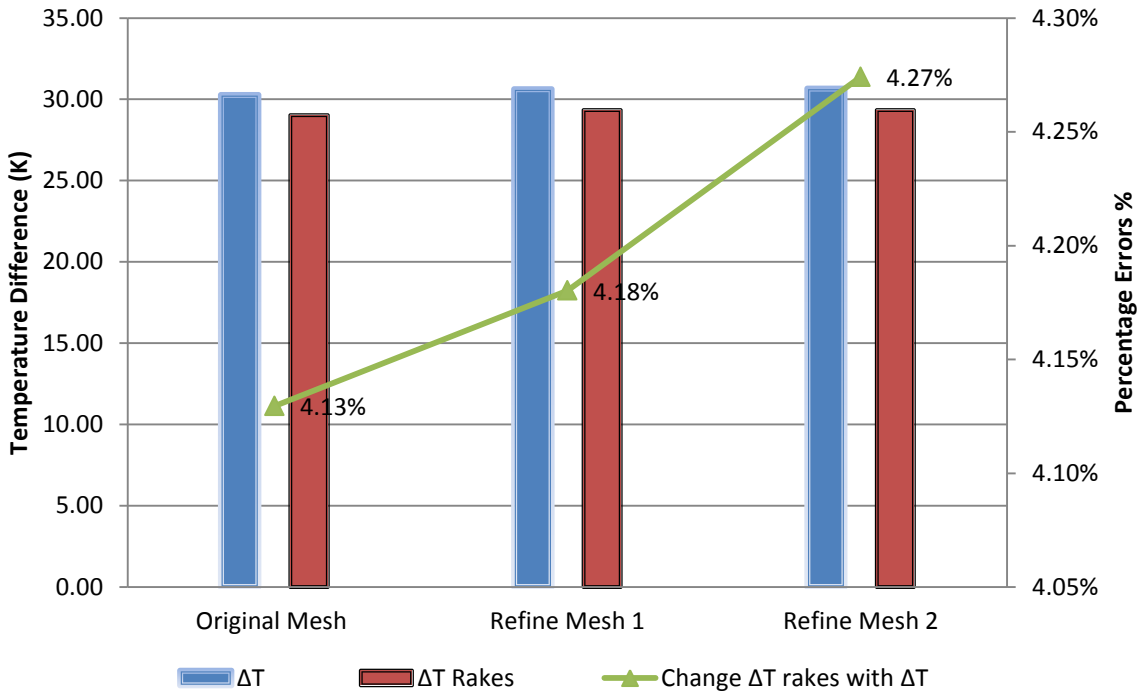

Figure 4.18 : Comparison of ΔT in different meshes for Case two (velocity= 5.17m/s) using k-ε Model & Enhanced Wall Treatment with Ti = 288.15K, To = 323.15K

Moreover, mesh complexity does not affect the differences between temperatures as they appear relatively similar at each mesh size. The average difference between the temperatures is 16.83 per cent for original surfaces, and it is 16.29 per cent for rake line. Similarly, the percentage errors between these values at the magnitude of each mesh are slightly different with average of 3.21 per cent. In the same way, Figure 4.20 offers similar observations, when velocity was 5.17 m/s, compare to observations in Figure 4.19. The average difference between the air temperatures at the inlet and outlet are 16.84 per cent and 16.2 per cent for original and rake patterns, respectively. The average percentage error between these values is 3.83 per cent.

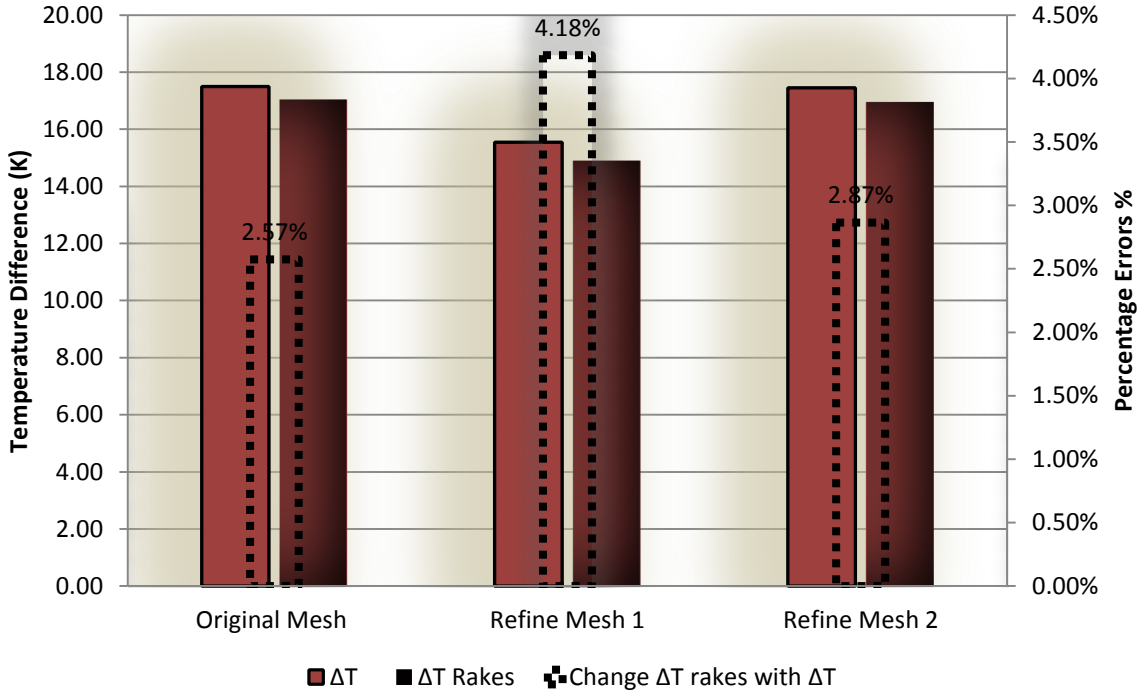

Figure 4.19 : Comparison of ΔT in different meshes for Case One (velocity=5.22 m/s) using k-ε Model & Enhanced Wall Treatment with Ti = 286K, To = 306K

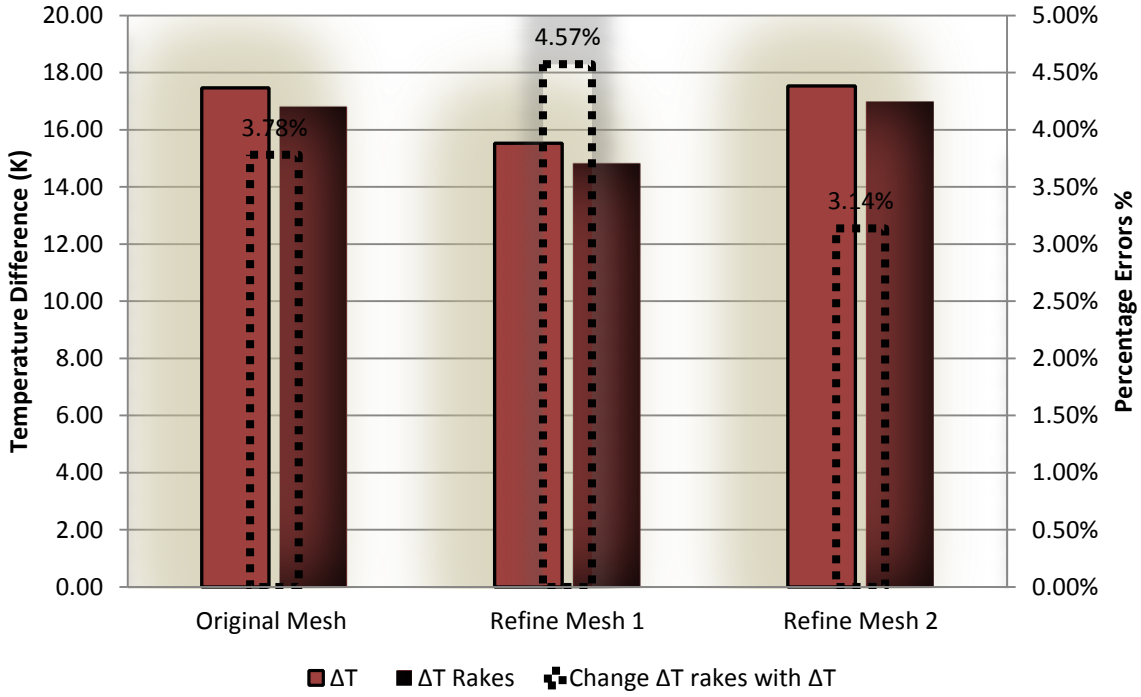

Figure 4.20 : Comparison of ΔT in different meshes for Case two (velocity = 5.17 m/s) using k-ε Model & Enhanced Wall Treatment with Ti = 286K, To = 306K

4.5.6 EMPLOYING SST k-ω CFD MODEL

In this section, the air temperatures at the inlet and outlet of the supply air window model were quantified by SST k-ω turbulence model for original and rake lines at the magnitudes of three different meshes where $T_{in} = 289.305$K. Then, the differences between the air temperatures at the inlet and outlet were calculated for both surfaces and presented as figures. Typical inputs and parameters of forced convection cases in (Bhamjee et al. 2012) were used in this simulation except that the turbulence model employed was SST k-ω model and results were produced for each case separately. Each result profile depicted the differences between the temperatures at the inlet and outlet and the percentage errors with those differences calculated in (Bhamjee et al. 2012).

Furthermore, the section extends to discuss an exclusive validation for the SST k-ω model with only two consecutive developments on the temperature at the inlet and outlet depicting calculated differences between these weather conditions for original and rake lines at three different mesh volumes. Moreover, it shows the percentage errors between results obtained from original and rake lines. The first refinement ($T_{in} = 288.15$K, $T_{out} = 323.15$K) and the second refinement ($T_{in} = 286$K, $T_{out} = 306$K) were anticipated for this simulation.

4.5.7 RESULTS AND DISCUSSION

Figure 4.21 sets forth the differences between the temperatures at the inlet and outlet, as calculated from the quantified temperatures, applying SST k-ω turbulence model for case one, for original and rake lines at each mesh size. It can be noticed that each mesh volume indicates that the estimations and the literature results are in acceptable agreement with errors below the limit level weather from the original, averaged with 7.33 per cent, or the rake lines, averaged with 6.24 per cent. In contrast, relatively larger errors between the results of the prediction and literature obtained, presented in Figure 4.22, for the case two with an average of 9.91 per cent for the original lines. However, agreement is still achieved between the both results since the percentage change fall below 10 per cent. Thus, the differences between the temperature patterns at

the inlet and outlet of original and rake lines are relatively similar and in agreement with those patterns produced in (Bhamjee et al. 2012) for both cases one and two meaning that accuracy can be fulfilled from the turbulence model of SST k-ω for flow between cavities. In addition, the simulation assures a stable level of estimations with mesh complexity refinements and added rakes, yet negligible impact on the temperature differences can be noticed at the rake lines. Table 4.2 shows the comparison of ΔT in different meshes for case one and two.

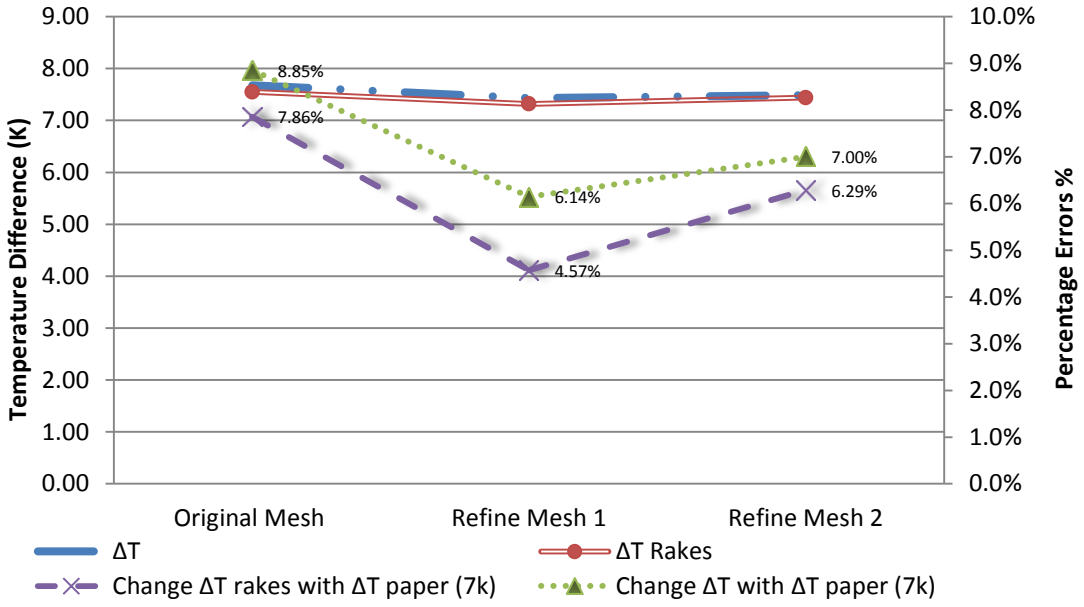

Figure 4.21: Comparison of ΔT in different meshes for Case One (velocity = 5.22 m/s) using SST k-ω with Ti = 289.305K, To = 293.02K compared with ΔT = 7K in the paper

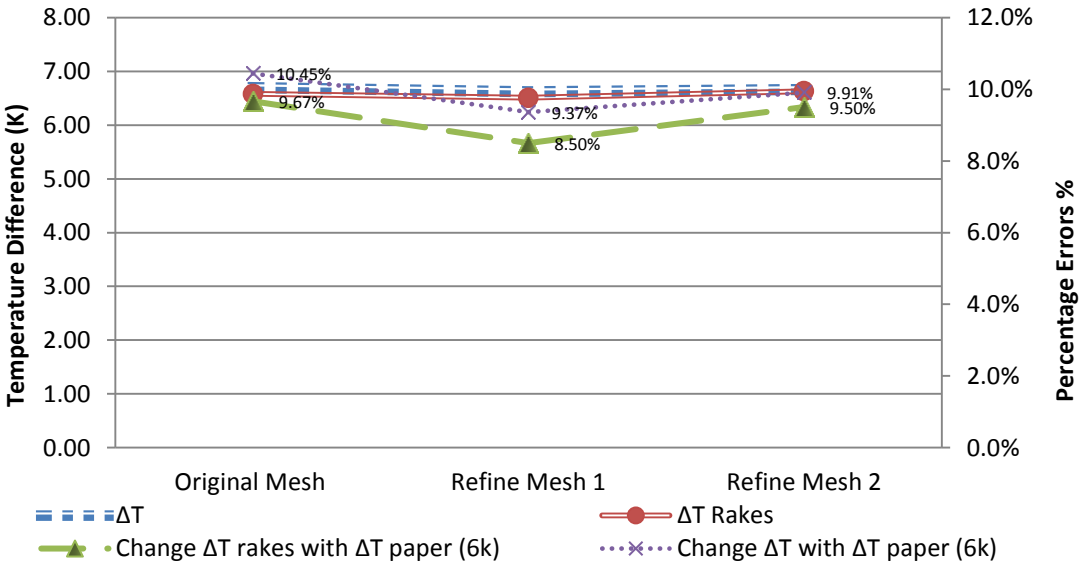

Figure 4.22: Comparison of ΔT in different meshes for Case two (velocity = 5.17 m/s) using SST k-ω with Ti = 289.305K, To = 293.02K compared with ΔT = 6K in the paper

Table 4.2: The comparison of ΔT in different meshes for case one and two using SST k-ω model with Ti = 289.305K

ORIGINAL MESH						
Cases	**Velocities (m/s)**	**ΔT paper (K) (Bhamjee et al. 2012)**	**ΔT (K)**	**Change with paper (Bhamjee et al. 2012)**	**ΔT Rakes (K)**	**Change with paper (Bhamjee et al. 2012)**
1	**5.22**	**7.00**	**7.68**	8.85%	**7.55**	7.86%
2	**5.17**	**6.00**	**6.70**	10.45%	**6.58**	9.67%
REFINED MESH 1						
Cases	**Velocities (m/s)**	**ΔT paper (K) (Bhamjee et al. 2012)**	**ΔT (K)**	**Change with paper (Bhamjee et al. 2012)**	**ΔT Rakes (K)**	**Change with paper (Bhamjee et al. 2012)**
1	**5.22**	**7.00**	**7.43**	6.14%	**7.32**	4.57%
2	**5.17**	**6.00**	**6.62**	9.37%	**6.51**	8.50%
REFINED MESH 2						
Cases	**Velocities (m/s)**	**ΔT paper (K) (Bhamjee et al. 2012)**	**ΔT (K)**	**Change with paper (Bhamjee et al. 2012)**	**ΔT Rakes (K)**	**Change with paper (Bhamjee et al. 2012)**
1	**5.22**	**7.00**	**7.49**	7.00%	**7.44**	6.29%
2	**5.17**	**6.00**	**6.66**	9.91%	**6.63**	9.50%

4.5.8 SST k-ω EXCLUSIVE VALIDATION

Figure 4.23 and Figure 4.24 stress a slightly rise of the differences between the temperatures at the inlet and outlet, for original surfaces of both cases one and two, from the original mesh to the second refinement where $T_{in} = 288.15$K, $T_{out} = 323.15$K. The mean difference between the temperatures of case one is 29.92K and it is 30.02K for case two. However, they show slightly varied calculated values of the differences between the temperatures at the inlet and outlet, for the rake lines of both scenarios one and two, at different magnitudes of the mesh for typical temperature inputs. The mean differences between the temperatures are 28.65K and 28.69K for higher and lower velocities, respectively. Overall, observations from both simulations of different inlet and outlet temperatures inputs employing SST k-ω turbulence model are similar and can demonstrate the model resistance to multiple temperature conditions. Furthermore, the trivial percentage errors between the results at the original and rake lines can prove the

failing influence of mesh complexity in both cases (one and two). The mean percentage error between the calculated values, at original and rake lines, of scenario one is 4.26 per cent and it is 4.41 per cent for scenario two.

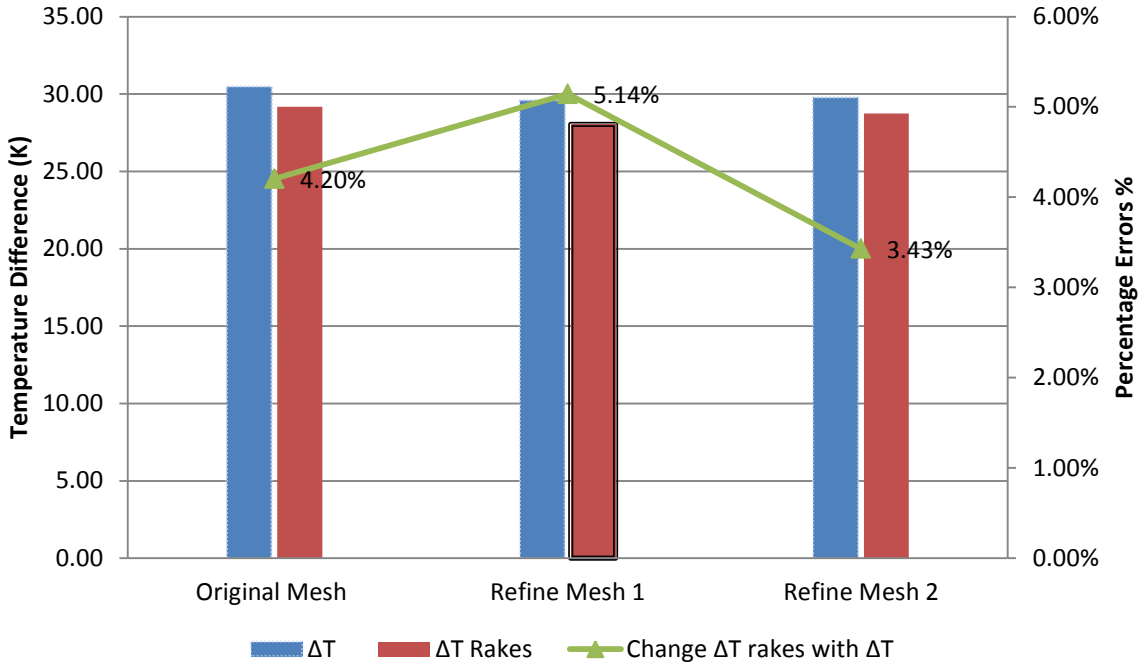

Figure 4.23: Comparison of ΔT in different meshes for Case One (velocity = 5.22 m/s) using SST k-ω with Ti = 288.15K, To = 323.15K

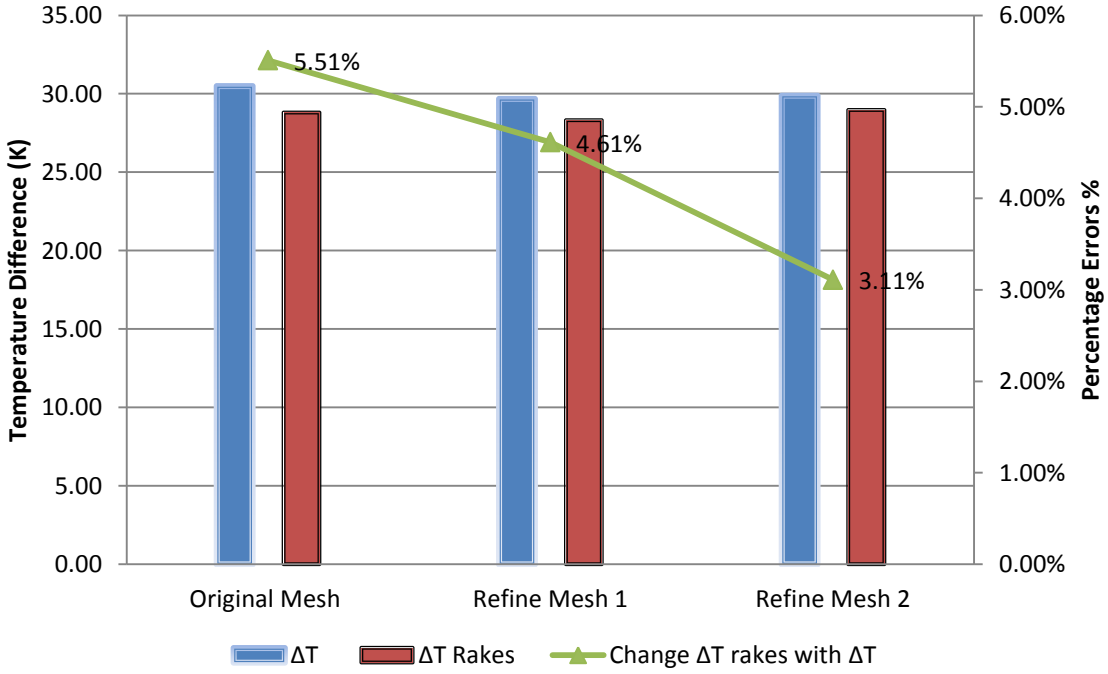

Figure 4.24 : Comparison of ΔT in different meshes for Case two (velocity= 5.17 m/s) using SST k-ω with Ti = 288.15K, To = 323.15K

The more temperature condition refinements applied, the more accurate SST k-ω model can be realized. Figure 4.25 and Figure Figure 4.26 demonstrate the failing influence of varied temperature improvements on SST k-ω model performance when $T_{in} = 286$K, $T_{out} = 306$K. The simulation for each case, one and two, produced gradually raised differences between the inlet and outlet temperatures for original surfaces from the original mesh to the second refinement. The mean difference between the temperatures of case one is 17.28K and it is 17.58K for case two. On the other hand, the trends of case one and case two for the rake lines are uneven. The simulation produced varied differences between the inlet and outlet temperatures at the mesh volumes. However, it can be noticed that the values from both surfaces are relatively similar. The mean differences between the temperatures are 16.83K and 17.06K for case one and case two, respectively.

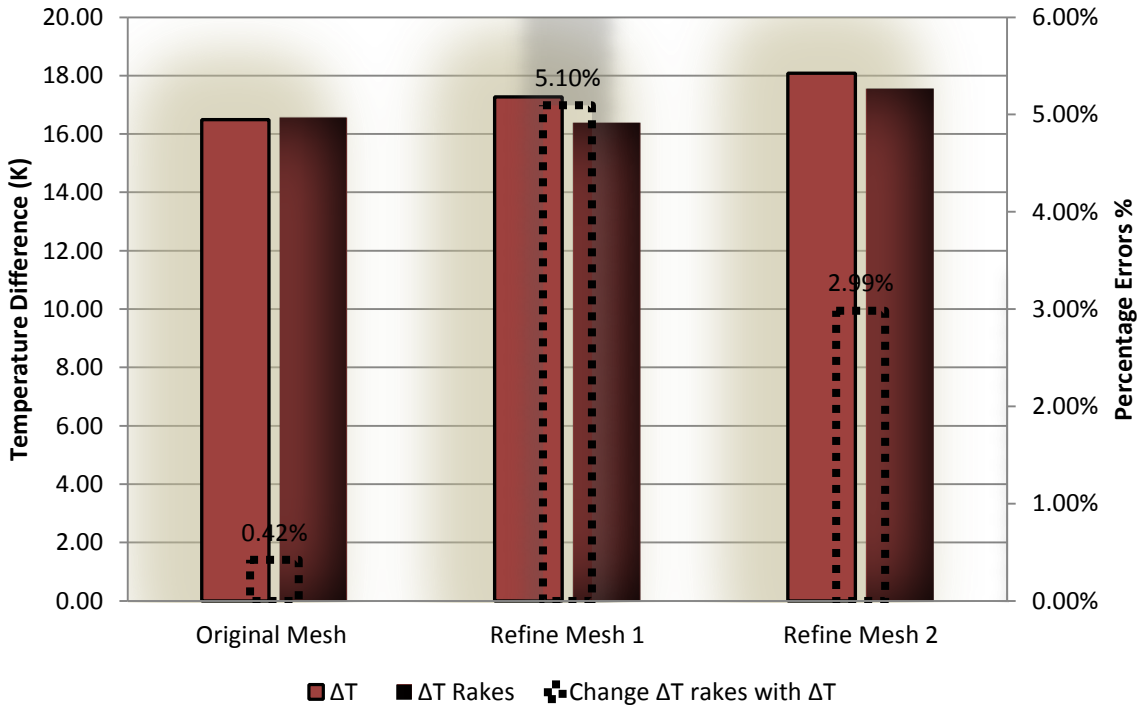

Figure 4.25: Comparison of ΔT in different meshes for Case One (velocity=5.22 m/s) using SST k-ω with Ti = Ti = 286, To = 306 (K)

Generally, even though the simulation produced different trends of values for original and rake lines, it shows the reliability of SST k-ω model performance for temperature variations. Also, it can be observed that the simulation is not mesh dependant since the

percentage errors between the calculated values for original and rake lines are considerably small in both scenarios. The mean percentage error between these values for case one is 2.84 per cent and it is 3.75 per cent for case two.

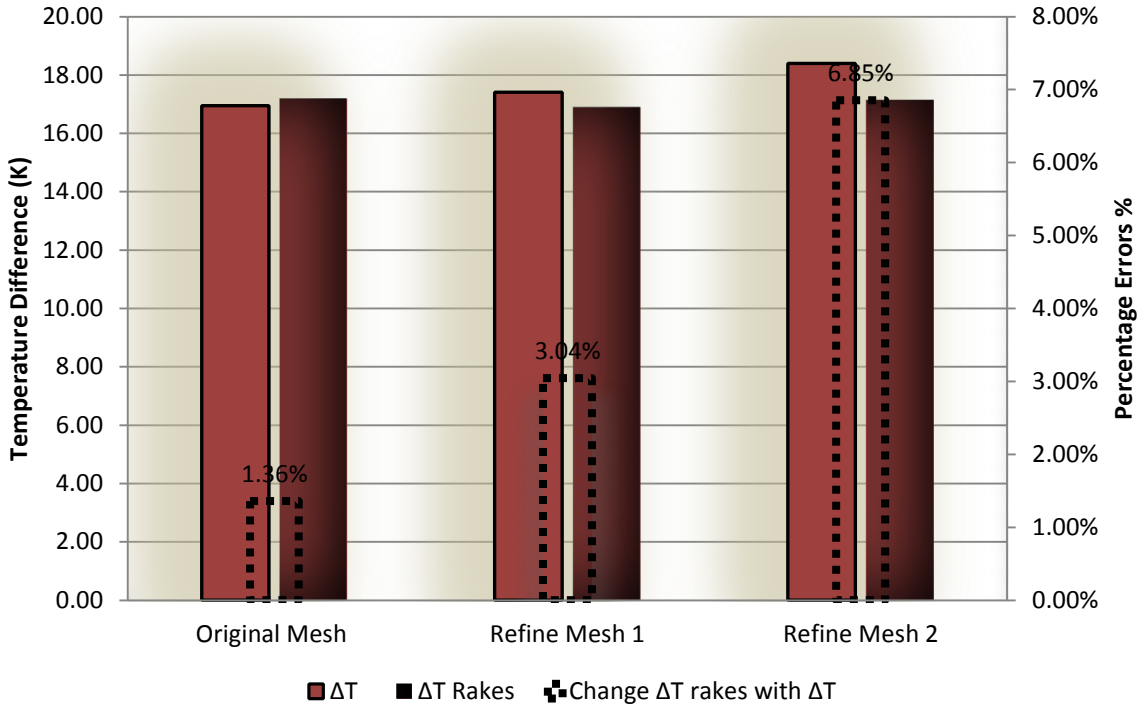

Figure 4.26: Comparison of ΔT in different meshes for Case two (velocity= 5.17 m/s) using SST k-ω with Ti = Ti = 286, To = 306 (K)

4.5.9 EMPLOYING SST TRANSITION TURBULENCE MODEL

This section underlines a comparison analysis between the variations of the inlet and outlet temperatures predicted in (Bhamjee et al. 2012) inside a cavity of a supply air window using SST k-ω turbulence model for case one (v=5.22 m/s) and case two (v=5.17 m/s) and those variations quantified in this simulation employing SST Transition turbulence model for different mesh patterns considering both cases. The inlet temperature was 289.305K for both simulations. The percentage changes between the two predictions were specified for each case. Furthermore, the section discusses an exclusive validation to more ascertain the reliability of SST Transition turbulence model performance. Typical parameters of supply air window model were used at three different mesh patterns for original and rake lines considering the two cases with two

inlet and outlet temperature refinements. In addition, the percentage differences were plotted between the results obtained for original and rake lines.

4.5.10 RESULTS AND DISCUSSION

Relatively comparable variations of the inlet and outlet temperatures calculated for the original and rake lines of the cases one and two, at three different mesh patterns when applying SST transition turbulence model, are shown in

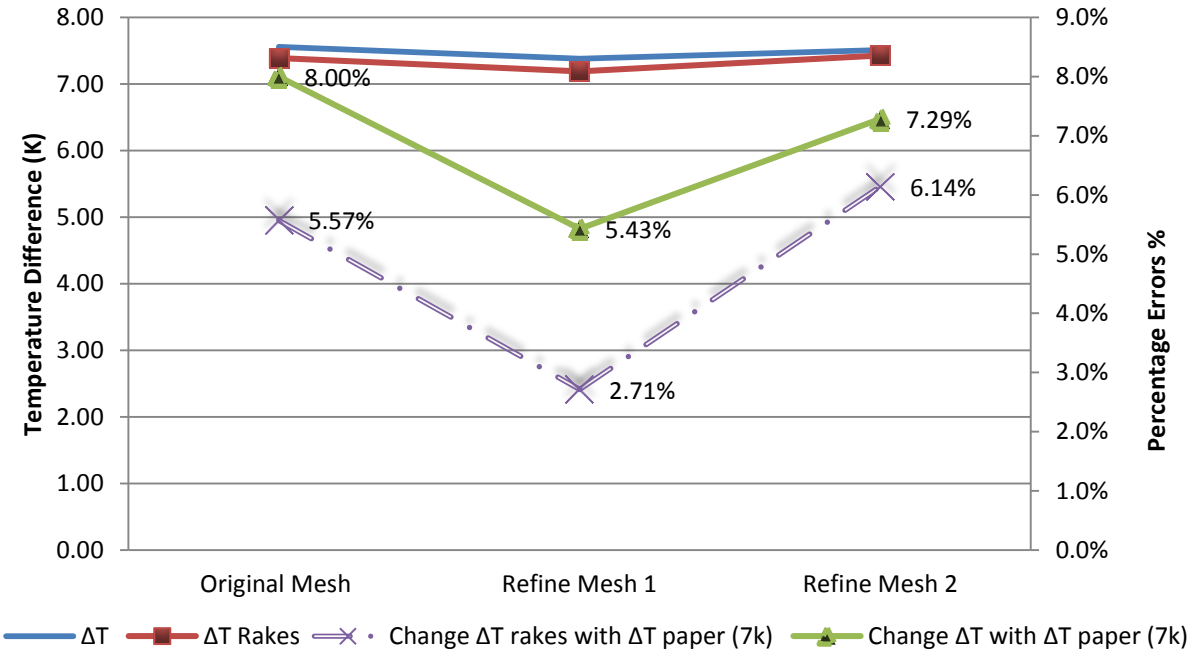

Figure 4.27 and Figure 4.28, respectively. Case one values indicates that the accuracy of SST k-ω and SST transition turbulence models are identical as the percentage change found between the results of each model do not exceed 10 per cent where the average of original line changes is 6.9 per cent, and it is 4.81 per cent for the rake lines. However, theses averages increase slightly under the case two, as shown in Figure 4.28 where 9.55 per cent of average changes for the original lines and 7.33 per cent of average errors for the rake lines, though, they are still considered as acceptable.

The two figures substantiate the success of obtaining an agreement between the predictions of both, the simulation and the literature where negligible percentage changes can be noticed between the two results. Overall, the validation analysis can reveal important aspects: no effect can be observed with mesh complexity for simulation

with SST Transition model; the rake patterns have negligible impact on the temperatures; Based on the outputs of the paper, the two turbulence models (SST Transition and SST k-ω) quantify similar values for typical inputs since the average variations of the inlet and outlet temperatures produced by the latter are 7.34K and 6.45K for case one and two, respectively. The comparison of ΔT in different meshes for case one and two are tabulated in Table 4.3.

Table 4.3 : The comparison of ΔT in different meshes for case one and two using SST transition model with Ti = 289.305K

ORIGINAL MESH						
Cases	**Velocities (m/s)**	**ΔT paper (K) (Bhamjee et al. 2012)**	**ΔT (K)**	**Change with paper (Bhamjee et al. 2012)**	**ΔT Rakes (K)**	**Change with paper (Bhamjee et al. 2012)**
1	**5.22**	**7.00**	**7.56**	8.00%	**7.39**	5.57%
2	**5.17**	**6.00**	**6.64**	9.64%	**6.52**	7.98%
REFINED MESH 1						
Cases	**Velocities (m/s)**	**ΔT paper (K) (Bhamjee et al. 2012)**	**ΔT (K)**	**Change with paper (Bhamjee et al. 2012)**	**ΔT Rakes (K)**	**Change with paper (Bhamjee et al. 2012)**
1	**5.22**	**7.00**	**7.38**	5.43%	**7.19**	2.71%
2	**5.17**	**6.00**	**6.57**	9.50%	**6.41**	6.83%
REFINED MESH 2						
Cases	**Velocities (m/s)**	**ΔT paper (K) (Bhamjee et al. 2012)**	**ΔT (K)**	**Change with paper (Bhamjee et al. 2012)**	**ΔT Rakes (K)**	**Change with paper (Bhamjee et al. 2012)**
1	**5.22**	**7.00**	**7.51**	7.29%	**7.43**	6.14%
2	**5.17**	**6.00**	**6.57**	9.50%	**6.43**	7.17%

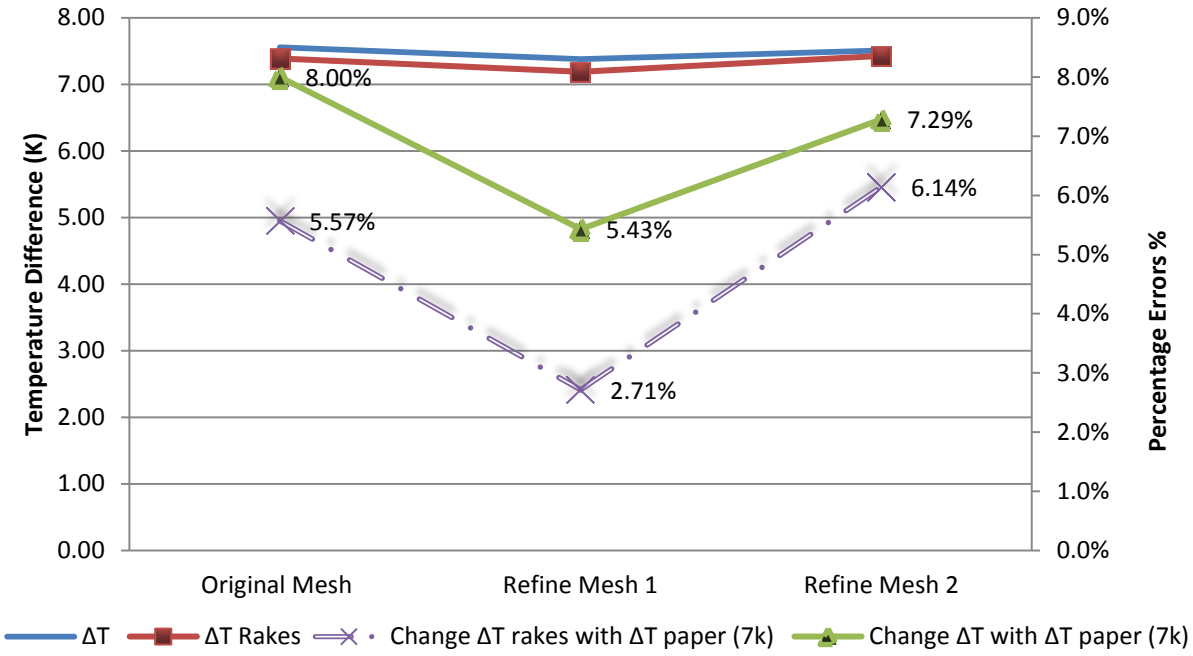

Figure 4.27: Comparison of ΔT in different meshes for Case One (velocity=5.22 m/s) using Transition SST with Ti = 289.305K compared with ΔT = 7K in the paper

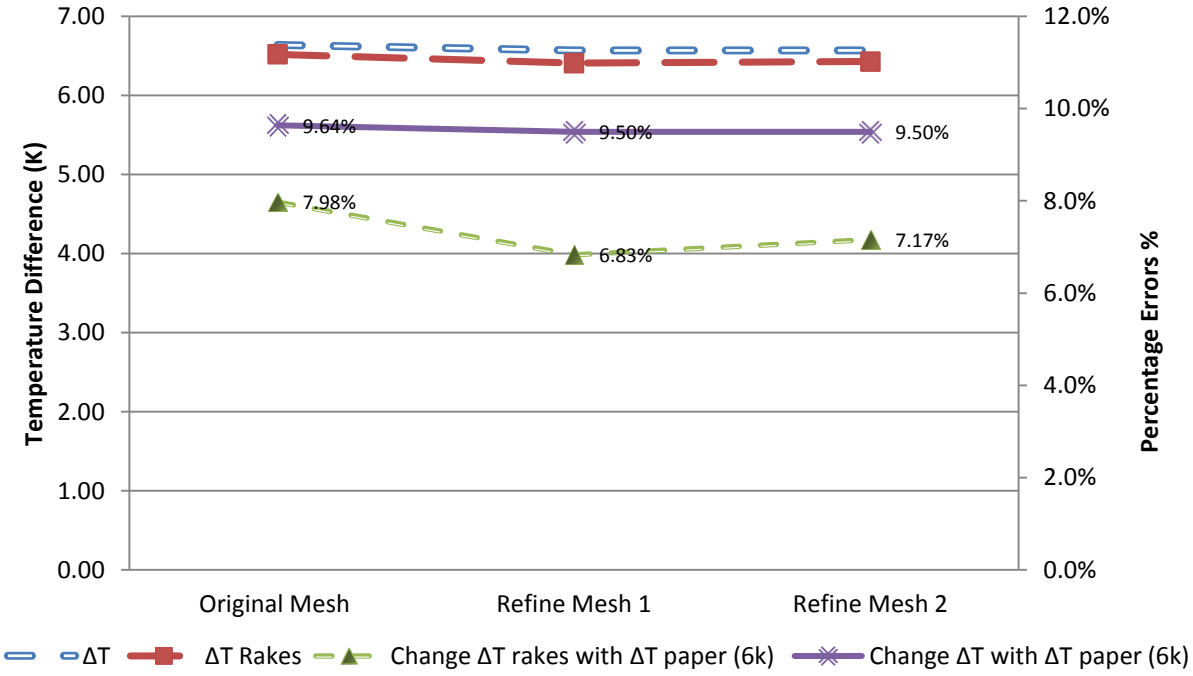

Figure 4.28: Comparison of ΔT in different meshes for Case two (velocity= 5.17 m/s) using Transition SST with Ti = 289.305K compared with ΔT = 6K in the paper

4.5.11 SST TRANSITION EXCLUSIVE VALIDATION

Figure 4.29 submits a proof of a negligible influence of the temperature condition refinements on SST Transition turbulence model performance. It shows minor percentage changes between values at original and rake lines for each mesh volume when $T_{in} = 288.15$K, $T_{out} = 323.15$K. The average percentage change between values at original surfaces is 4.66 per cent. It can also be shown that Figure 4.29 possesses similar trends for the variations of the inlet and outlet temperatures at the original and rake lines for case one. Indeed, both surfaces patterns offer gradually raised variations values from the original mesh to the second refinement. The average variance of the inlet and outlet temperatures are 29.04K and 27.72K at the original and rake lines, respectively. However, it appears that relatively similar variations of the inlet and outlet temperatures can be shown in Figure 4.30 at the original and rake lines with trivial raise from the original mesh to the second refinement for case two meaning that this figure also confirms the negligible impact of the same temperature condition on SST Transition turbulence model performance. The average variance of the inlet and outlet temperatures for the original surfaces is 30.61K and it is 29.71K for the rake lines. The average percentage change between the variations of the inlet and outlet temperatures for both surface patterns is 2.93 per cent.

By looking at the outputs of the inlet (286k) and the outlet (306k) temperatures for case one and two, it can be additionally confirmed that SST Transition turbulence model is capable to be applied for different temperature conditions. Indeed, in Figure 4.31 and Figure 4.32 similar characteristics can be obtained to those obtained from the previous figures. It seems that the variations of the inlet and outlet temperatures for the original surfaces of case one and two are relatively constant, yet negligible raise can be observed for each mesh volume. The average variance of the inlet and outlet temperatures for original surfaces is 17.49K of case one and it is 17.58K of case two.

On the other hand, both cases (higher and lower velocities) possess different trends of the inlet and outlet temperatures for the rake lines for each mesh pattern. From case one, the variations of the inlet and outlet temperatures are varied with an average of

16.91K whilst case two offer extremely minor raise of the variations of the inlet and outlet temperatures starting from the original mesh to the second refinement with an average of 17.27k. Generally, the percentage changes are yet trivial for both cases. It is 3.35 per cent between the predictions, for original and rake lines, of case one and it is 1.98 per cent of case two.

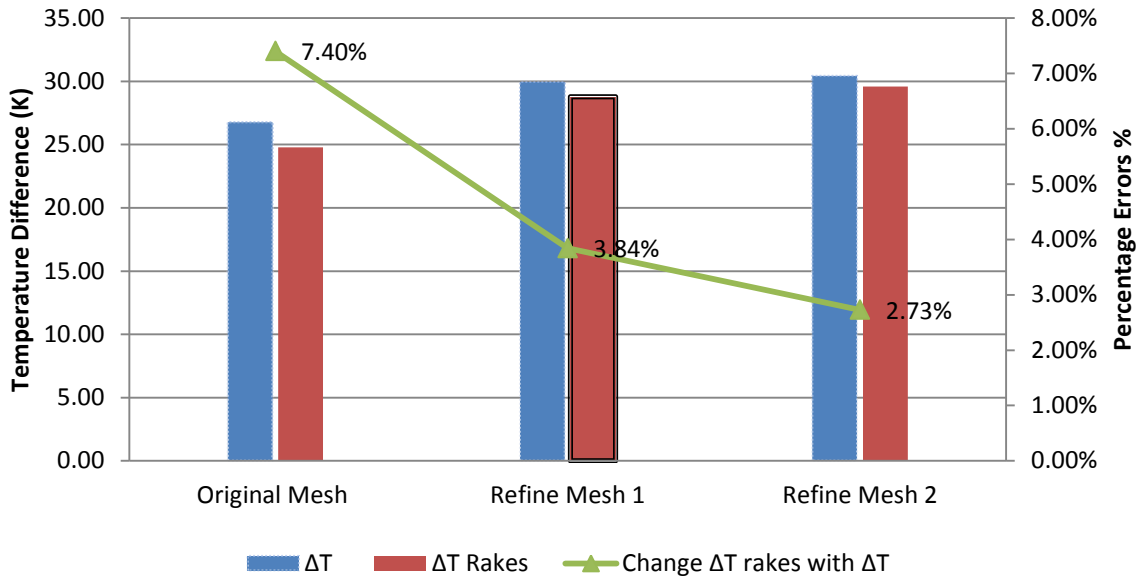

Figure 4.29: Comparison of ΔT in different meshes for Case One (velocity=5.22 m/s) using Transition SST with Ti = 288.15, To = 323.15 (K)

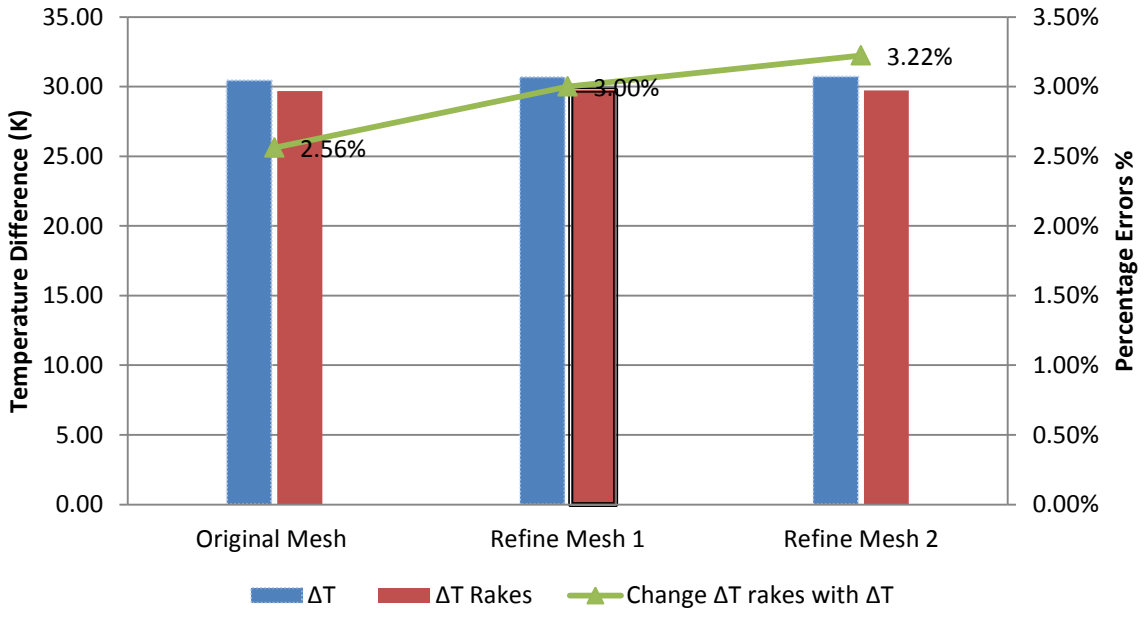

Figure 4.30: Comparison of ΔT in different meshes for Case two (velocity= 5.17 m/s) using Transition SST with Ti = 288.15, To = 323.15 (K)

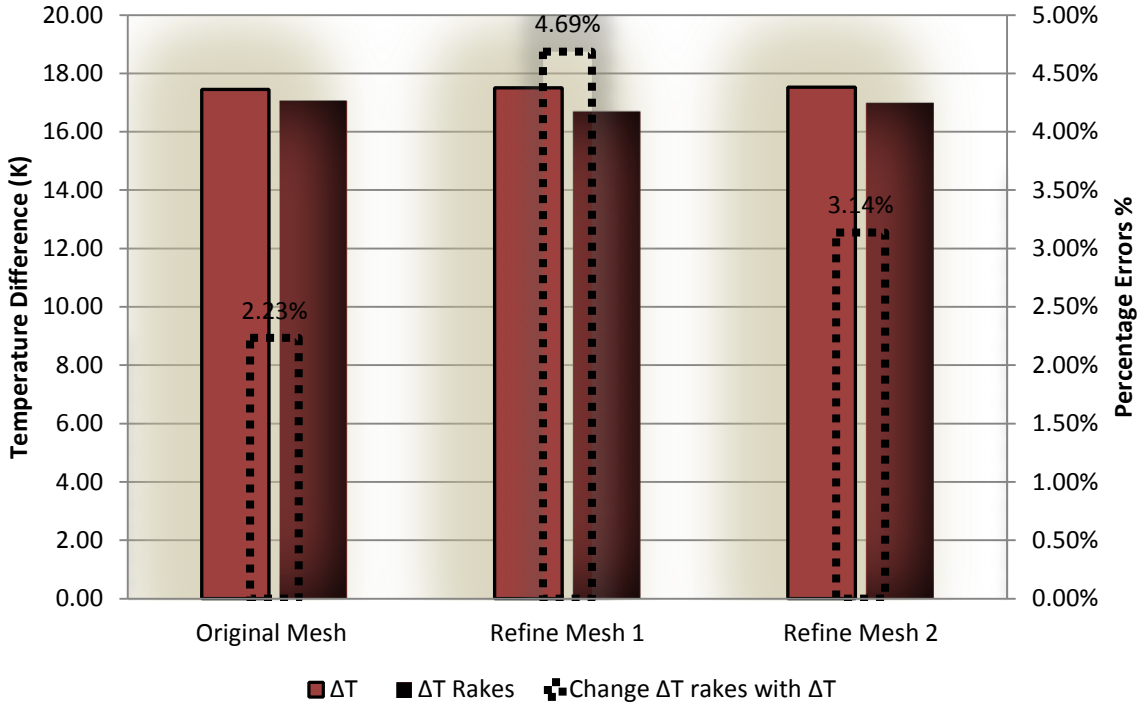

Figure 4.31: Comparison of ΔT in different meshes for Case One (velocity= 5.22 m/s) using Transition SST with Ti = 286K, To = 306K

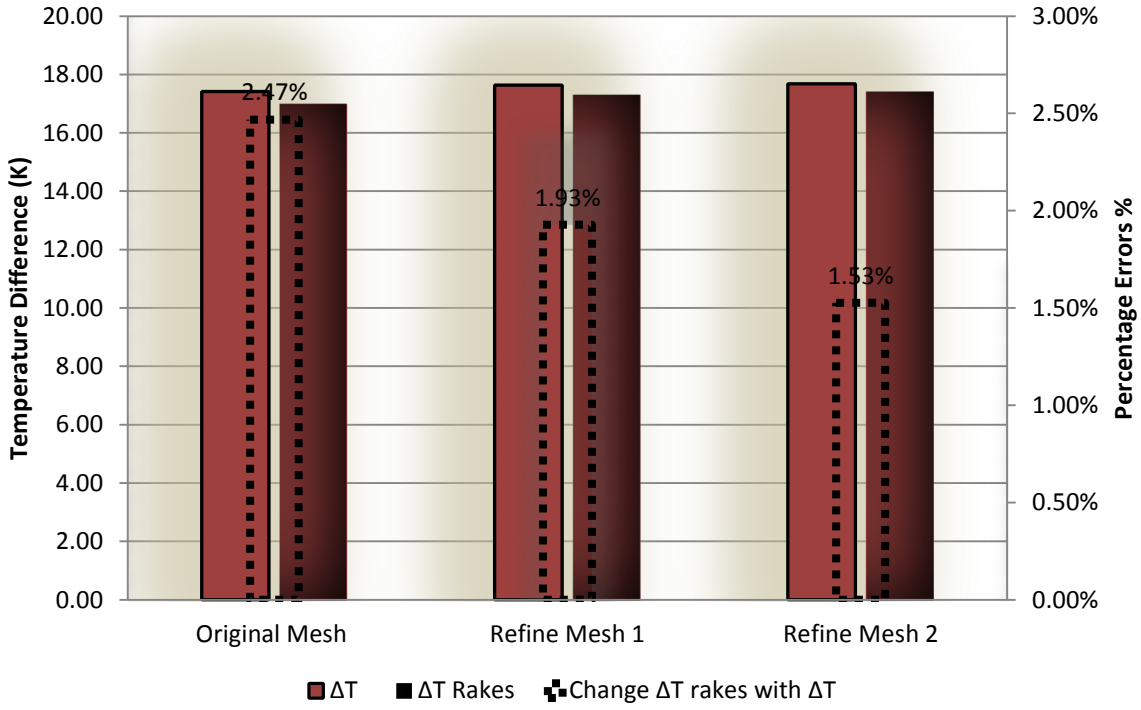

Figure 4.32: Comparison of ΔT in different meshes for Case Two (velocity= 5.17 m/s) using Transition SST with Ti = Ti = 286K, To = 306K

4.5.12 MEASUREMENT CALIBRATION

A further validation analysis was carried out to verify the quality of the outlet temperature measurements of the supply air window empirical model in (Bhamjee et al. 2012). In this section the percentage differences between those measurements and outlet temperature values of a typical two-dimensional supply air window simulation model are highlighted. Measurements were taken at three points within the outlet using a thermocouple each. The enhanced wall treatment with k-ε turbulence model (the most common used turbulence model) (ANSYS 2009) was employed to quantify the values of the outlet for the window model. The inlet (286k) and the outlet (306k) temperature condition used were identical to the conditions in the paper. The effect of different turbulence models performance was evaluated in terms of SST k-ω and SST Transition turbulence models.

4.5.13 RESULTS AND DISCUSSION

Figure 4.33 shows the accuracy of turbulence model performance for numerical evaluation. It can be seen that the agreement between measurements and predicted values is achieved. Similar relationship between the two outlet temperature plots can also be clear. The maximum outlet measured temperature is 27.1°C and it is 29.8°C from the simulation. Small percentage differences between both values are clearly observed with an average of 7 per cent meaning that the turbulence model is validated and the measurements are calibrated.

More validation clues can be found with applying several turbulence models to approve models' accuracy in calibrating the measurements. Figure 4.34 and Figure 4.35 assure a stable level of a percentage difference between measured and predicted outlet temperatures when employing different CFD turbulence models. Both plots offer negligible percentage differences with an average of 8 per cent for SST k-ω outputs and of 1.77 per cent for SST Transition results. The maximum outlet temperatures predicted by SST k-ω model is 30.85°C and it is 31.02°C for SST Transition model.

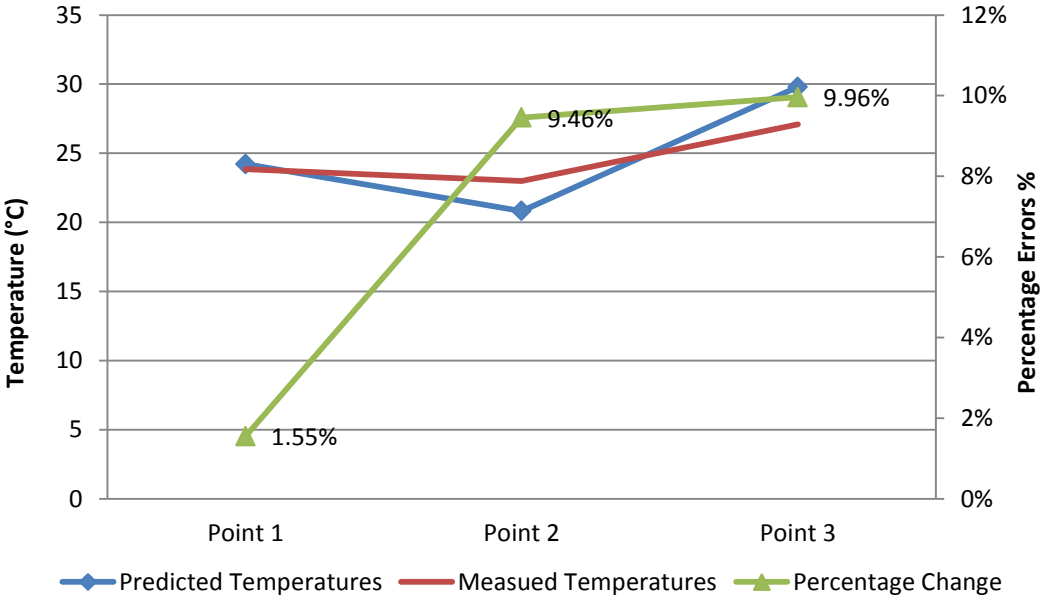

Figure 4.33: Comparison of outlet temperature predicted by k-ε turbulence model with enhanced wall treatment

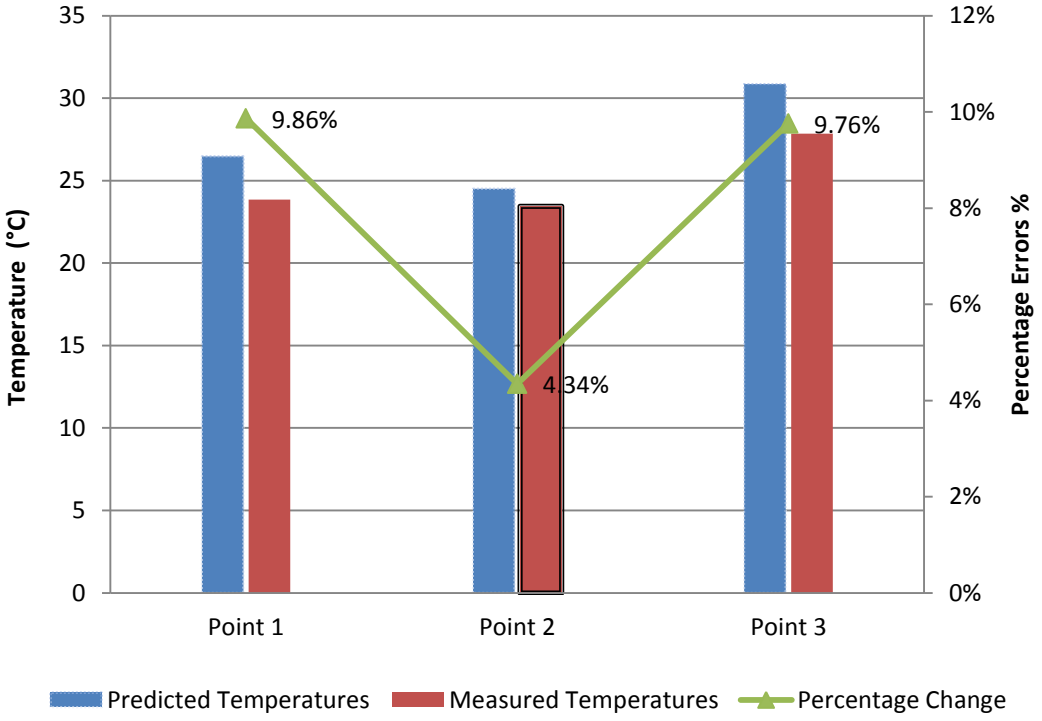

Figure 4.34: Comparison of outlet temperature predicted by SST k-ω turbulence model with enhanced wall treatment

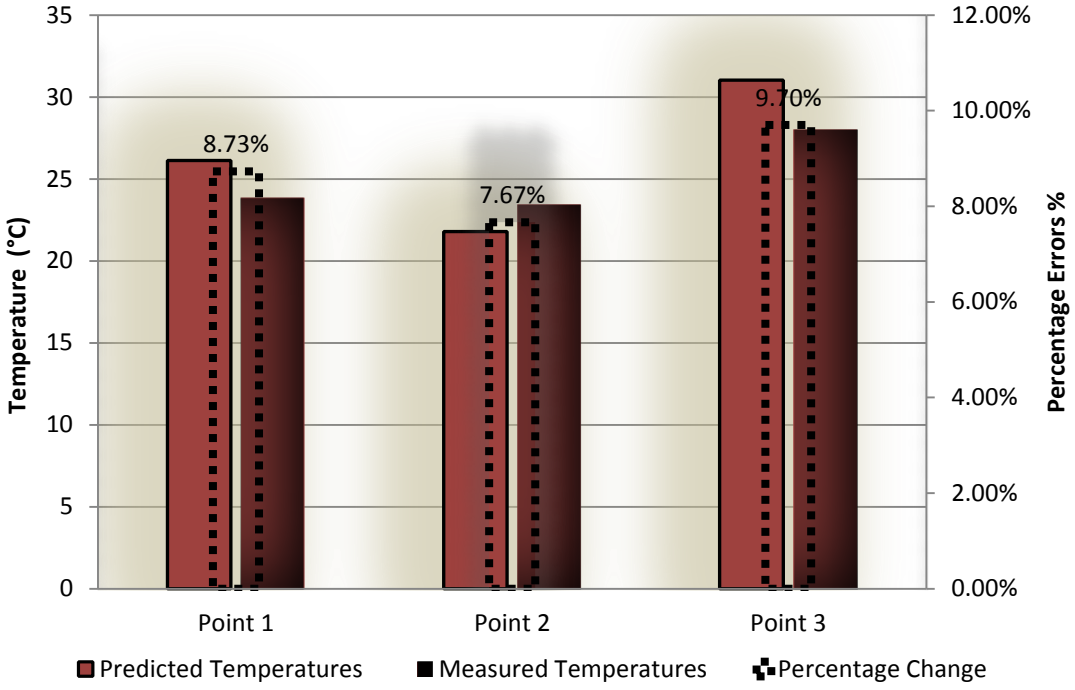

Figure 4.35: Comparison of outlet temperature predicted by SST Transition turbulence model with enhanced wall treatment

4.6 SUMMARY

The effect of varying operating and climatic conditions has been captured to prove the suitability of CFD turbulence models in order to determine the suitable model for dependable results and also for efficient simulation stability in terms of air temperatures at the outlet of a supply air window (fan-induced) empirical and computational model investigated in (Bhamjee et al. 2012). Numerically, it has been found that the representation of outlet temperatures by k-ε with enhanced wall treatment, SST k-ω and SST Transition turbulence models were in agreement comparing to the illustration of SST k-ω in (Bhamjee et al. 2012). Furthermore, they all simultaneously plotted consistent predictions. The errors found between the predictions, of simulation and literature, were considered as acceptable as they fall below the maximum limit, 10 per cent. However, these percentage changes may be attributed to several reasons where each one may have contributed apart in the formation of the differences: identifying velocities instead of using the inlet and outlet pressure due to the presence of volumetric flow rate and mass flow rate in the paper; and steady state instead of transient model was a neglected factor in the validation.

Despite, these turbulence models have achieved satisfied agreement between their estimations when they were exposed to multiple weather and computational circumstances, reasonable agreement empirically has been obtained between measurements and the predictions of turbulence models. Furthermore, the verification results have demonstrated exceptional aspects: results of several turbulence models have been consistent for investigating the supply air window demonstrating potentials under different environments and solution patterns; measurements and turbulence models are feasible tools. In summary, it can be concluded that all mentioned turbulence models are suitable for use to predict heat transfer for a given type of module of building component.

At this stage, the CFD tools have been validated to be applied for thermal and ventilation analysis proposed for this study. Thus, the next chapter will continue the validation analysis for daylighting tools.

CHAPTER 5 DAYLIGHTING

Daylight is a means to effective use of sustainable energy as it can displace artificial lighting of buildings. Building envelopes must contribute in feeding effectively and efficiently the interior spaces by natural illumination since the daylight is the preferred form of illumination in buildings (Al-Sallal 2007). Daylight can further afford building occupants an interaction with the outside environment. Despite the energy saving that daylight can account for, it is liable for the costs of specific glazing systems that passes through to allow daylight and maintain the interior thermally acceptable and glare proofed. Thus, for effective daylighting techniques, the following must be achieved:

- Optimal fenestration, plan shape, internal finishes and partition layout.
- Minimum heat loss through the glazing system.
- Unwanted solar gains protection.
- Responsive electric lights to the daylighting.

Figure 5.1 presents typical distribution of energy use for buildings such as offices, schools, and other industrial facilities.

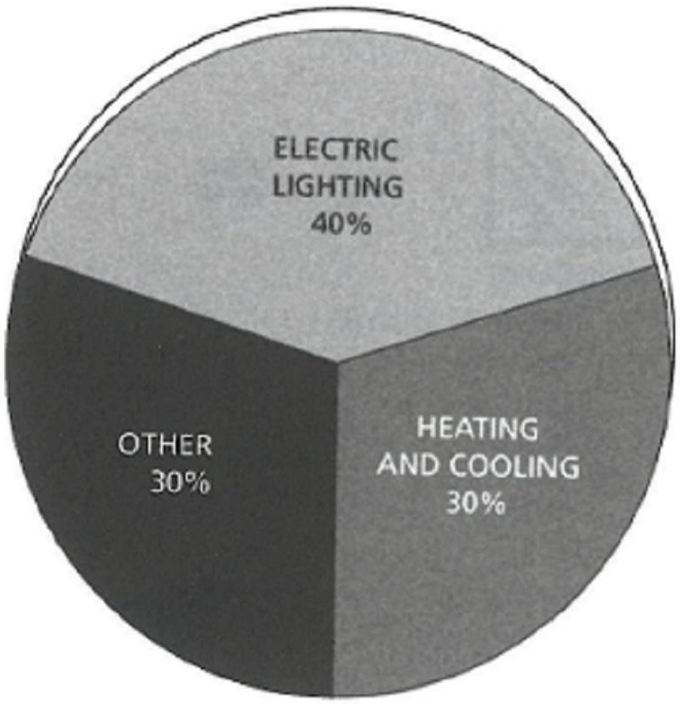

Figure 5.1: Breakdown of typical energy consumption for buildings such as offices, schools, and other industrial facilities (reproduced from (Lechner 2014))

Moreover, and more specifically, remarkable saving potentials from daylighting can be acquired when, firstly, electric lighting is controlled separately and it is responsive to daylight availability under the control of central system and secondly, daylight illumination is desirable to artificial illumination in some spaces (Lechner 2014). Table 5.1 indicates typical energy use of electric lighting and potential savings from daylighting.

Table 5.1: Breakdown of energy consumption by different buildings types and estimated saving from daylighting (Hall 2008)

Building type	**Proportion of total primary energy used for lighting (%)**	**Estimated saving from the uptake of a daylight strategy (%)**
Multi-residential	40	Small
Offices	30-50	20-40
Shops	90	Small
Education	22	10-30
Health	20-30	10-20
Factories	15	10-20

It appears from the Figure that offices can ascertain the highest potential savings from daylight due to the simplicity of installing control systems (Hall 2008).

5.1.1 STANDARD SKY MODELS

The variation of the daylight is dependent on the time of the day, weather conditions and atmospheric pollution. A common standard sky models have been proposed for daylight professionals to precisely quantify the amount of daylight reaching from the outside environment to an inside space.

Clear blue sky. The sunlight design requires this kind of sky model. It is designated for cooling seasons in the UK or countries where hot climate dominates. Whereas the most predominant weather condition in the UK is overcast, daylighting design is performed under the overcast sky model (Lechner 2014).

Uniform overcast sky. This is the model that is feasible for a heavily overcast sky. As the name implies, the nature of its appearance is equally bright from each direction as it produces a uniform luminance (Lechner 2014).

5.1.2 ILLUMINATION AND THE DAYLIGHT FACTOR

The determination of the quantity and quality of a daylighting design for the architect is essentially attributed to modelling, weather through actual- or simulation-based analyse (Lechner 2014). However, it is difficult to describe the absolute quantities of the daylight entering the room, thus, the daylight factor can estimate the amount of daylight at a particular point in a room. The daylight factor is the proportion of the daylight illumination that reaches an indoor point on an overcast day. The daylight assessment can be carried out under the effect of overcast sky at any time of the year or day including the worst daylight condition, the winter overcast sky (Lechner 2014). Table 5.2 offers typical minimum required daylight factor for different kinds of spaces. When the daylight factor exceeds the required amount listed in the Figure, most of the year will be extremely predominated with daylight. A well-lit space possesses a daylight factor above 5 with little need for electric lighting for visually poor spots. Essential electric lightings are required when daylight is less than 4 (Lechner 2014). The daylight factor can be calculated at a particular point on the room as follows (Lechner 2014):

$$DF = (Ei/Eo)\ 100 \quad 5.1$$

Where DF is daylight factor (%), Ei is illuminance due to daylight at a reference point on the indoors working plane (lux); Eo is simultaneous outdoor illuminance on a horizontal plane from an unobstructed hemisphere of overcast sky (lux).

Table 5.2: Typical minimum required daylight factor (Lechner 2014)

Type of Space	Daylight factor
Art studios, galleries	4-6
Factories, laboratories	3-5
Offices, classrooms, gymnasiums, Kitchens	2
Lobbies, lounges, living rooms, churches	1
Corridors, bedrooms	0.5

In theory, the daylight factor decreases towards the north of the planet, thus, the average indoor illumination can possibly be calculated from overcast skies and with available daylight factor and latitude by multiplying the illumination for different

latitudes, presented in Table 5.3, by the daylight factor. Modelling analyses often discuss the alternative designs and determine the most suitable for allowing preferable daylight. However, the actual outdoor lighting is time-dependent, as a consequence, it is impossible to consider comparison with footcandle (lux) measurements, but it is possible with daylight factor. Furthermore, the daylight factor remains constant in comparison to the changes of illumination between the indoor and outdoor for any given design under the impact of overcast skies (Lechner 2014).

Table 5.3: Average illumination from overcast skies (Lechner 2014)

North Latitude (degrees)	Illumination	
	Footcadles	Lux
46	700	7000
42	750	7500
38	800	8000
34	850	8500
30	900	9000

5.1.3 BASIC DAYLIGHTING STRATEGIES

Acquiring optimal daylight is primarily subject to lighting geometry and colour of finishes (Lechner 2014). Thus, it is essential to apply most or even all of both aspects' strategies to achieve a visually accepted day-lit interior, and they are as follow (Lechner 2014):

- **Orientation**. Since the most consistent sunlight in the north hemisphere comes from the south direction throughout the day and the year, daylight can be the most preferable from the south orientation of a building. During the heating seasons the interiors of a building might be thermally tolerable thanks to this constant sunlight coming from the south. As such, sun-control devices are required. However, north direction can be a source of consistent light which qualifies as a second choice for orientation. During the cooling season this direction might even be favourable to the south due to its lower light. East and west are the worst orientations due to the extremely poor sunlight they receive during the day and it reaches its maximum in the summer which causes overheating.

- **Lighting through the roof**. Horizontal openings usually are advantageous for two reasons. First, they dominate wide class of interior with uniform illumination. Second, the quantity of light that they receive is much more than the vertical openings. Though, two problems are concomitant with vertical openings: the possibility of overheating during the summer is greater than in winter due to the summer intensity of light; their shading is difficult. Therefore, considering vertical glazing on the roof with different designs can eliminate the problems. They can be in the form of clerestory windows, monitors, or sawtooth arrangements Figure 5.2.

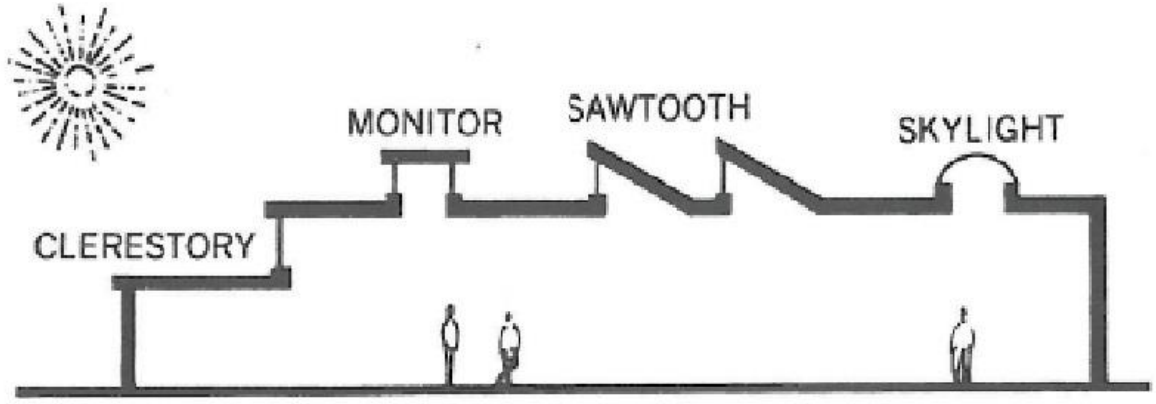

Figure 5.2: The various possibilities for overhead openings for daylighting (reproduced from (Lechner 2014))

- **Form**. Several building components are dependants on the form of a building such as the quantity of windows on each orientation, the quantity of skylights or clerestories on the roof, and the daylighting allowance due to the floor area. In general, windows can be responsible for daylighting a 9m perimeter zone fully for 4.5m and partially for the other 4.5m.
- **Space planning**. Open space planning can attach a great significance to the interior daylighting. Acoustical and visual privacies can be furnished with glass partitions and venetian blinds or translucent materials, respectively, whilst daylight is still allowed. Alternatively, partitions are preferably placed above the eye level.
- **Colour.** In order to reflect more light into the interior and the building as well, applying light colour to both indoors and the outdoors is a great option. For

instance, light-coloured facades are accountable for elevating the availability of daylighting at the lower floors and the sidewalks. Other building components such as the interiors can further diffuse the lights along the reflection, thus, dark shadows, glare, and excessive brightness ratios can be suppressed.

- **View and daylighting.** High and low windows are advantageous for excellent daylighting and view, respectively. Though, less daylight can be transmitted through the view glazing, heat gain and glare are controlled.

5.1.4 DAYLIGHTING ASSESSMENT AND SIMULATION TOOLS

The science is holistically overwhelmed by the phenomena of space lighting such as movement, reflection from specular and diffusing surfaces of multiple colours. Computer tools are capable of adapting the large amount of natural light data to be processed. They rather can predict the interaction between the light and daylight from the aspects of size, location orientation of windows, room dimensions, glazing system lighting transmission factors and surface reflectance and colour. Through a geometry model, the computer estimates the daylight entry and distribution within various points inside the room. The computer predictions, then, translated into contours of daylight factor or three dimensional rendered images that show the interior variations of daylight.

Several computer-based daylighting analysis studies (Atif et al. 2003; Lee et al. 2006; Li et al. 2006), and field measurements (Li et al. 2001; Krarti et al. 2005; Chel et al. 2009; Chel et al. 2010) have concluded that considerable lighting energy savings are attributed to daylighting controls. As such, a realistic schema to assess daylighting potential is needed to provide informative values that can be a source for evaluation the illuminance or daylight factor predictions for any building in the design stage. In the last decades, the utilization of daylighting computer simulation tools has been the key interest of most building professionals (Reinhart et al. 2006). Tools such as DOE-2 (Winkelmann et al. 1993), EnergyPlus, TRNSYS (Klein et al. 2004), and ECOTECT (Marsh 1996). These comprehensive sustainable design tools provide estimations for

illuminance levels and daylight factors externally and internally with reduced computational efforts (Seo et al. 2011). However, these tools are not properly suited for providing alternatives for daylighting design and analysis unless they are coupled with hybrid tools such as ESP-r with Radiance and ECOTECT with DAYSIM (Reinhart et al. 2000).

5.2 VALIDATION

In this validation, it is aimed to demonstrate the capability of the proposed system, which generates electricity and thermal energy, to control the daylight. As a consequence, evaluation of different techniques and strategies for the (STBIPV/T) system need to be performed using a computer simulation program to estimate the impact of the outdoor and indoor illuminance levels and daylight factors for dynamic daylighting exploitation. In so doing, a rigorous validation should be implemented to examine effectiveness and accuracy of the daylighting simulation algorithm, expected to be used in this context, by calibrating its outputs first, against different simulation tools' outputs considering the same input specifications for both, and second, against empirical measurements from the literature.

Thus, an elaborate validation analyses have been implemented into ECOTECT computer algorithm to examine its reliability in the daylighting performance of the prospective airflow window unit. ECOTECT results will be then compared against the results of different daylighting studies, brought from relevant literature, using different simulation tools such as daysim/radiance, troplux, radiance and BC/LC, and some empirical measurements. Daylight factor and illuminance levels were the principle quantities that taken into account for comparison between the tools since the amount of daylight entering a room can be best described by these proportions (Lechner 2014).

5.2.1 ECOTECT AGAINST DAYSIM/RADIANCE AND TROPLUX (case one)

A comparison of daylight factor estimated by ECOTECT was carried out with calculated daylight factor by Ramos et al. (2010) using Daysim/Radiance and Troplux. The simulations were implemented for two different rooms: one square (5m x 5m x 3m) and one deep rectangular (5m x 10m x 3m) as shown in Figure 5.3. These models have a window to wall ratio (WWR) of 50 per cent with the window in south facing façade in order to reduce the entrance of direct light in the environment. In the windows, the use of 3mm clear glass with a visible transmittance of 0.88 was considered. The models have white walls and ceilings with a reflectance of 0.85 and a beige floor with a reflectance of 0.6. In all of the simulations, the work surface was considered to be at a height of 0.75m. For each model, the daylight factor was calculated for five points assigned inside the room, aligned with the centre of the window enabling the program to response with increasing distance between the points analysed and the window. Sky conditions were overcast sky for all simulations. The comparison of the daylight factor for the two room models demonstrated by ECOTECT, Daysim/Radiance and Troplux programmes are depicted below.

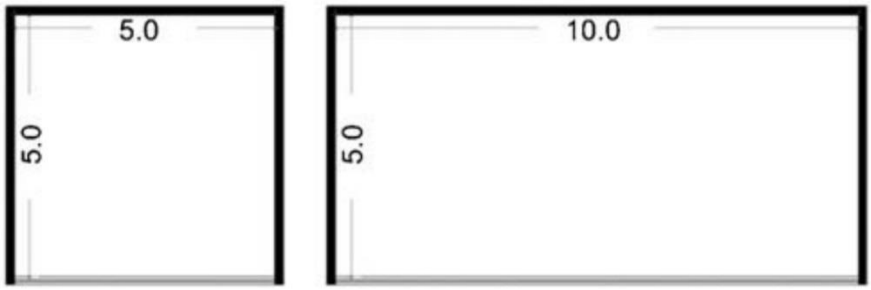

Figure 5.3: Dimension of the models studies reproduced from (Ramos et al. 2010)

Figure 5.4: Location of the points in the rooms for analysis of the DF reproduced from (Ramos et al. 2010)

Figure 5.5 presents the behaviour of the daylight factor for the model (5m x 5m x 3m) revealed from each mentioned simulation tool and the absolute difference found individually between these packages. By looking at the daylight factor trends, it appears that each software have achieved the maximum level of the daylight factor at the closest point to the window ranging from 18 to 28% where the highest was achieved by ECOTECT, then Radiance and TropLux. However, all the measuring points are in good agreement and the absolute difference do not override 10 per cent.

Similarly, the daylight factor behaviour analysed for the model (5m x 10m x 3m) in Figure 5.6, express identical findings to the previous model where the maximum absolute difference, between the values of the sampling points under each simulation tool, is 10 per cent. Moreover, the largest daylight factor found was from ECOTECT, 21 per cent, and the tapers gradually with Daysim/Rdiance, 24 per cent, to become 17.5 per cent with TropLux.

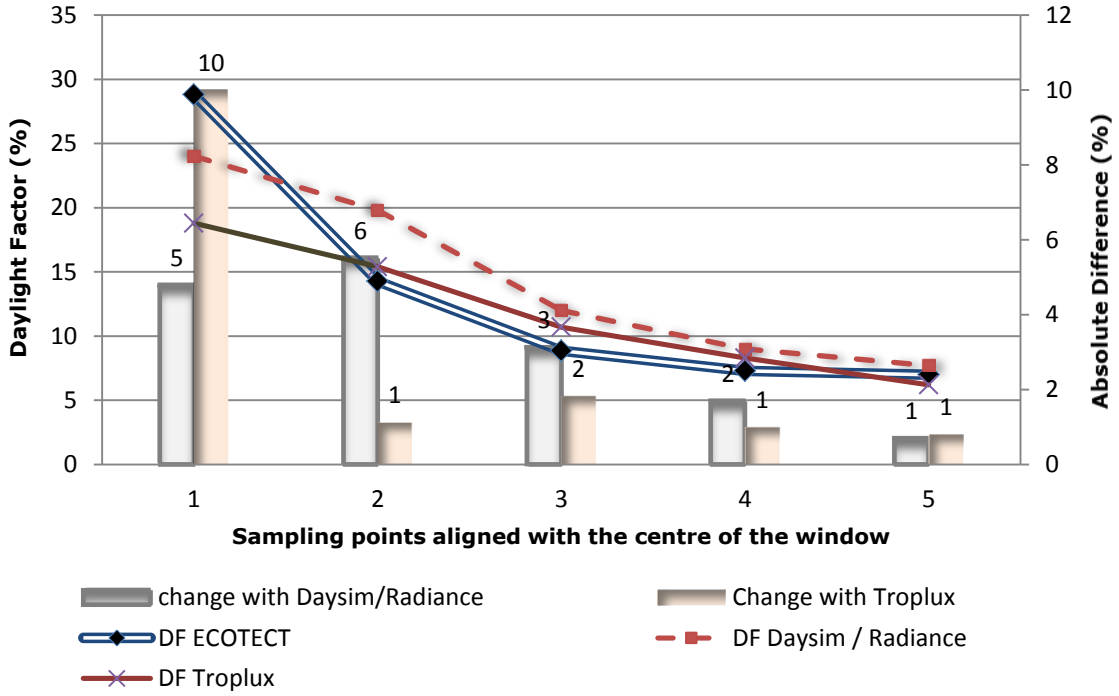

Figure 5.5 : Comparison of the daylight Factors for 5*5 [m] model

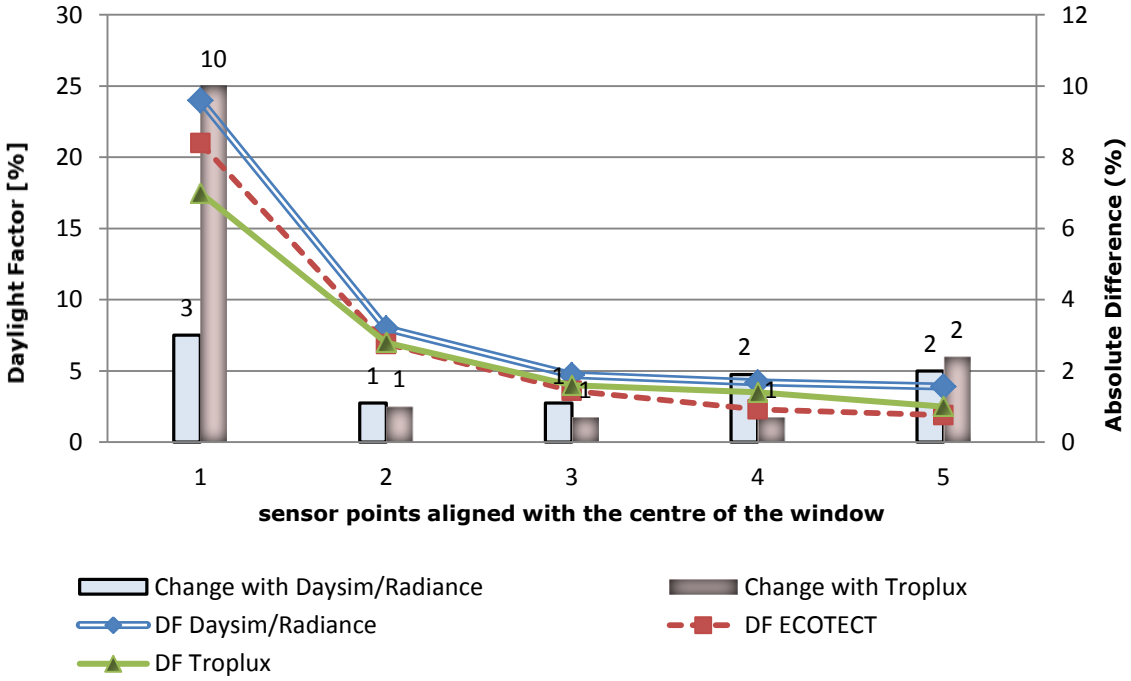

Figure 5.6 : Comparison of the daylight Factors for 5*10 [m] model

5.2.2 ECOTECT AGAINST EMPIRICAL MEASUREMENTS (case two)

In this section, the calculated daylight factor of ECOTECT was compared against physically measured data obtained from Zain-Ahmed (2000). Two base models were tested under an artificial sky. The floor area of each model was 30cm by 40cm and 30cm in height. Each model includes a south facing aperture of 16 cm by 8 cm in horizontal position and vertical position as model A and model B (shown in Figure 5.7), respectively, representing a full-scale window opening of 160cm by 80cm. In order to computationally exemplify these situations, the author has identified the building specifications. In the walls, the use of single layer brick 105 was considered with average reflectance of 0.8. Glazing was considered as single clear float glass, 4mm thick, solar absorptivity of 0.11 and optical transmissivity of 0.89. In both simulation models, eleven sampling points, oriented perpendicular to the centre of the window with interval of 0.25m, were considered for estimating the daylight factor at 0.8m height of work surface. Sky conditions were overcast.

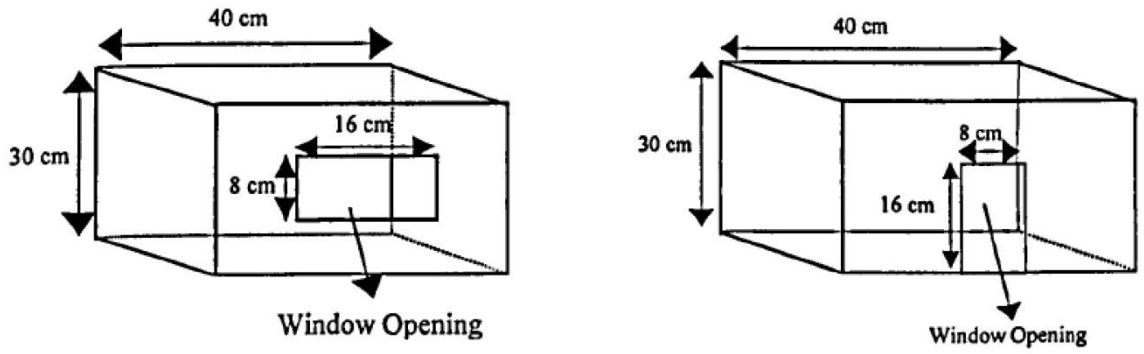

Figure 5.7: Model A (left) and model B (right) reproduced from (Zain-Ahmed 2000)

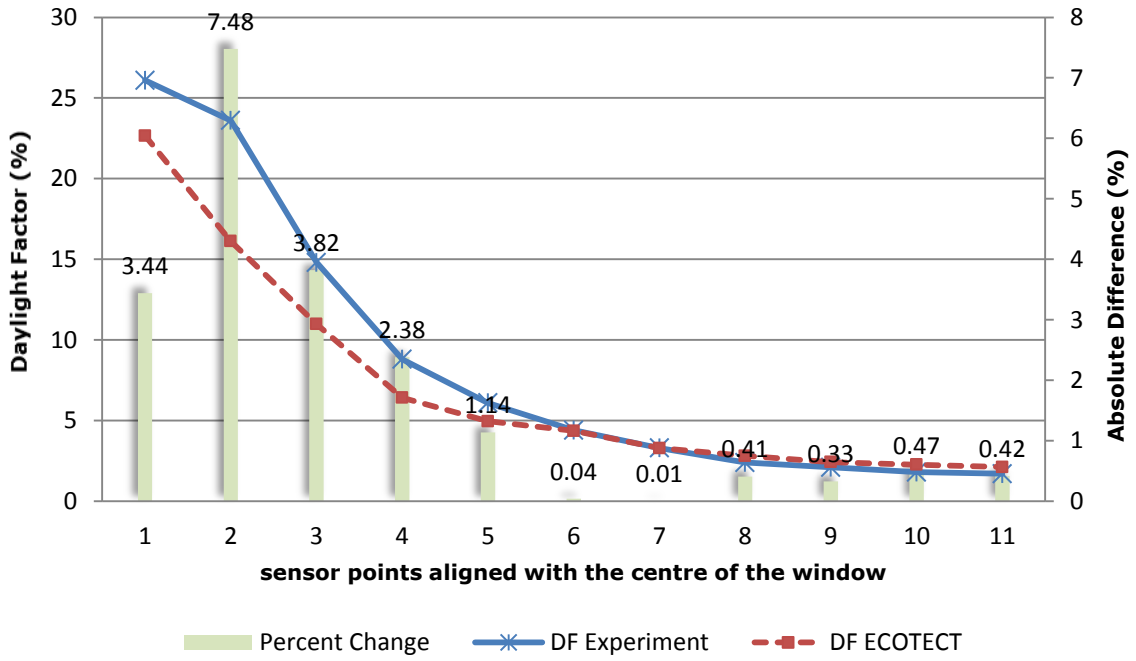

Figure 5.8: Comparison of the daylight Factors for model A

Figure 5.8 encompasses the two trends of daylight factor predicted by ECOTECT and measured by the experimental model A. The absolute change calculated and shows that ECOTECT results are slightly different (larger) from the measurements for five points starting at the point where the light enters. However, daylight factor values taper gradually and become almost equal for the remaining points as the distance increases from the centre of the window and the absolute difference is below 8 per cent for all the assigned points with an average of 1.81 per cent. Likewise, the measured and computed daylight factor by experimental model B and ECOTECT are presented in Figure 5.9 along with the absolute change between the values. It can be

observed that the difference between the two trends is slight at all points. Even though, ECOTCT results are not quite similar with the experimental results, they show the same trends of daylight factor of being high at the nearest point to the window and gradually becoming lower into the back of the room. The average change found between the predicted and empirical values is 2 per cent where the maximum value is 9 per cent, which is acceptable.

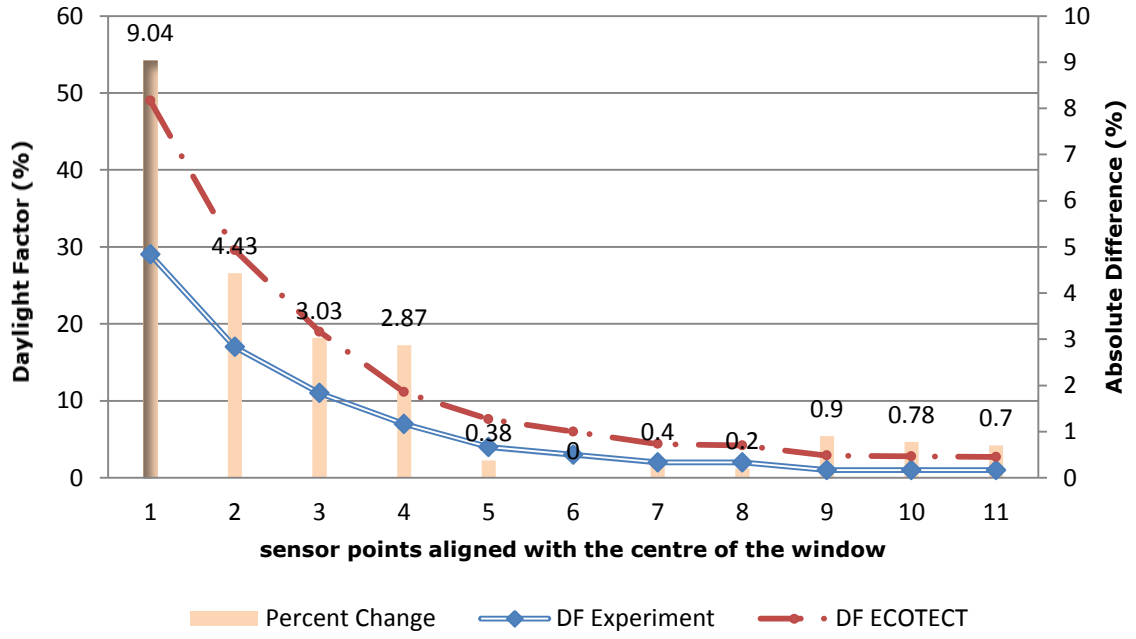

Figure 5.9: Comparison of the daylight Factors for model B

5.2.3 ECOTECT AGAINST RADIANCE AND BuildingCalc/LightCalc (BC/LC) (case three)

ECOTECT was compared against two daylighting simulation tools comparing the estimations of daylight factor and illuminance levels with outputs computed by Hviid et al. (2008). The computations were carried out for a (6m x 4m x 3m) with a south facing window. The window is 1.6m in height and 2m in width with overhang shading panel that is above the window by 0.1m extends horizontally along the wall by 4m with length of 0.4m, shown in Figure 5.10. The validation was carried out for the window with three different cases: clear double glazing with low-E coating case, blind lowered case and screen lowered case. The applied glazing was double with low-E coating with light transmittance of 0.782 (transmissivity=0.852). Blind was slat with

slat width of 0.08m, distance of 0.072m, and thickness of 0.5mm. Overhang shading panel was considered only with lowered blind case. Verosol Silver screen was applied with light transmittance of 0.0354. The diffuse reflectance varies between 0.7, 0.8, 0.3, 0.215, 0.2 and 0.096 for walls, ceiling, floor, glazing, Albedo and slat, respectively. The calculations were implemented at 6m distance from the window represented in eleven points in alignment with the centre of the window for every half meter. All cases run under the overcast sky conditions.

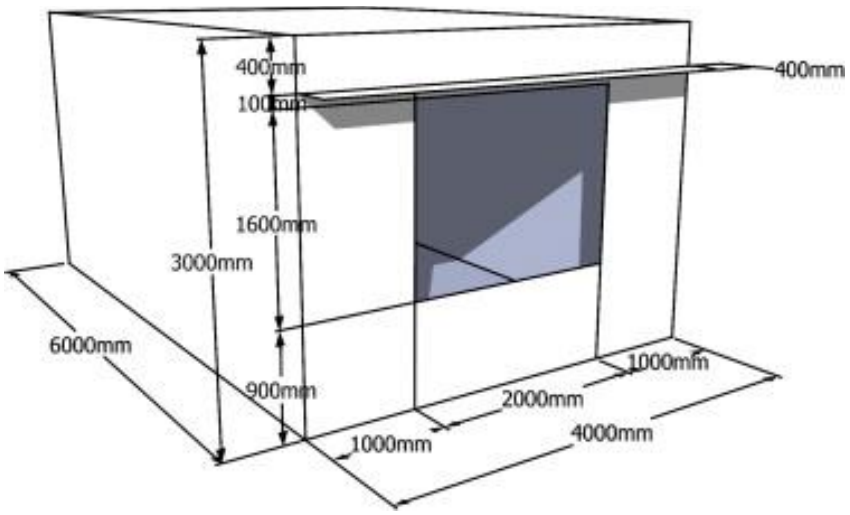

Figure 5.10: Dimensions of the validated room reproduced from (Hviid et al. 2008)

Figure 5.11 displays the comparison of computed daylight factor by ECOTECT with the one calculated by Radiance and BC/LC and the absolute error found between these tools and ECOTECT for clear double glazing with low-E coating case. It can be observed that the difference between the results from all programmes are slight as they appear in similar trend that starts higher, at the point that is the nearest to the window, and decreases gradually to become lower at the last point, the farthest from the window. The highest value obtained for the daylight factor was from ECOTECT, 23.14 per cent, whilst Radiance and BC/LC revealed consequent smaller values, 22.5 and 20.7 per cent, respectively. Though, the absolute changes are negligible as they range between 0 and 3 per cent with an average of one per cent.

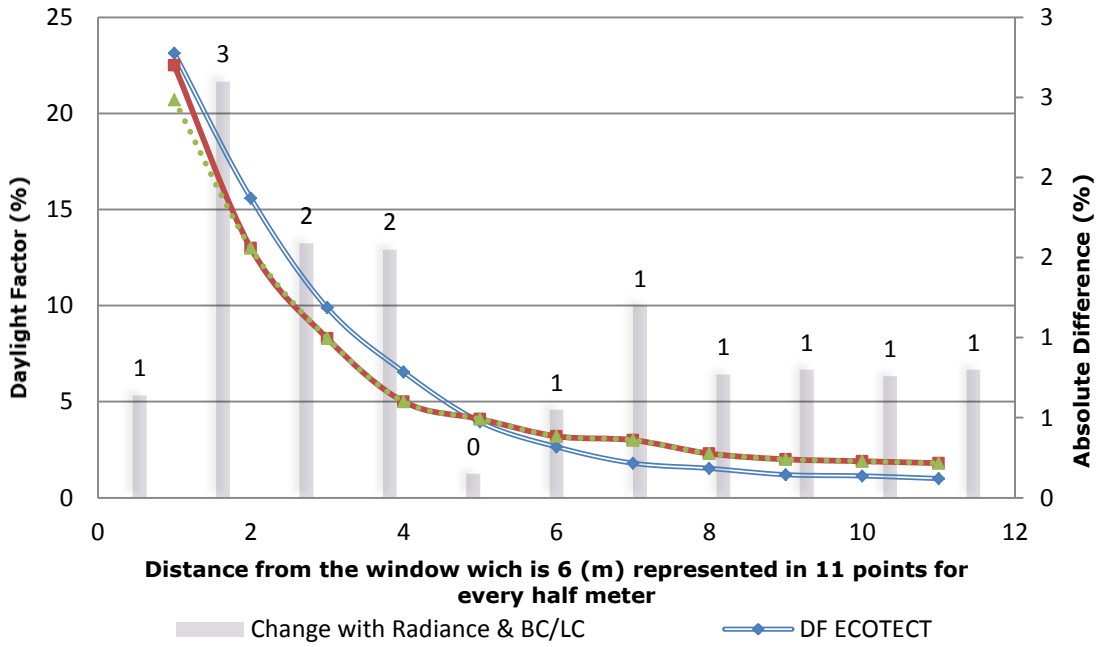

Figure 5.11: Daylight factor from CIE standard overcast sky model and a clear double glazing with Low-E coating

In contrast, Figure 5.12 shows the illuminance level outputs by ECOTECT, Radiance and BC/LC with major percentage change between ECOTECT and the other software for the blind lowered case which elevates up to 76 per cent. The estimations derived by ECOTECT show that the illuminance level distribution is quite lower than the illuminance trends produced by Radiance and BC/LC where the average illuminance from ECOTECT is 316.32Lux whilst it is 485.73Lux from Radiance and 420Lux from BC/LC. The average percentage difference between the ECOTECT values and the values obtained from the literature is 42 per cent which is unacceptable.

Similarly, Figure 5.13 depicts the comparison of illuminance levels produced by ECOTECT, Radiance and BC/LC with significant percentage difference calculated between the ECOTECT and the other tools for screen lowered case. The chart indicates that no agreement achieved between the estimations and the Radiance and BC/LC trends as the average change is 44 per cent, unacceptable, where the average illuminance of ECOTECT is 46.35Lux, of Radiance and BC/LC is 138.27Lux.

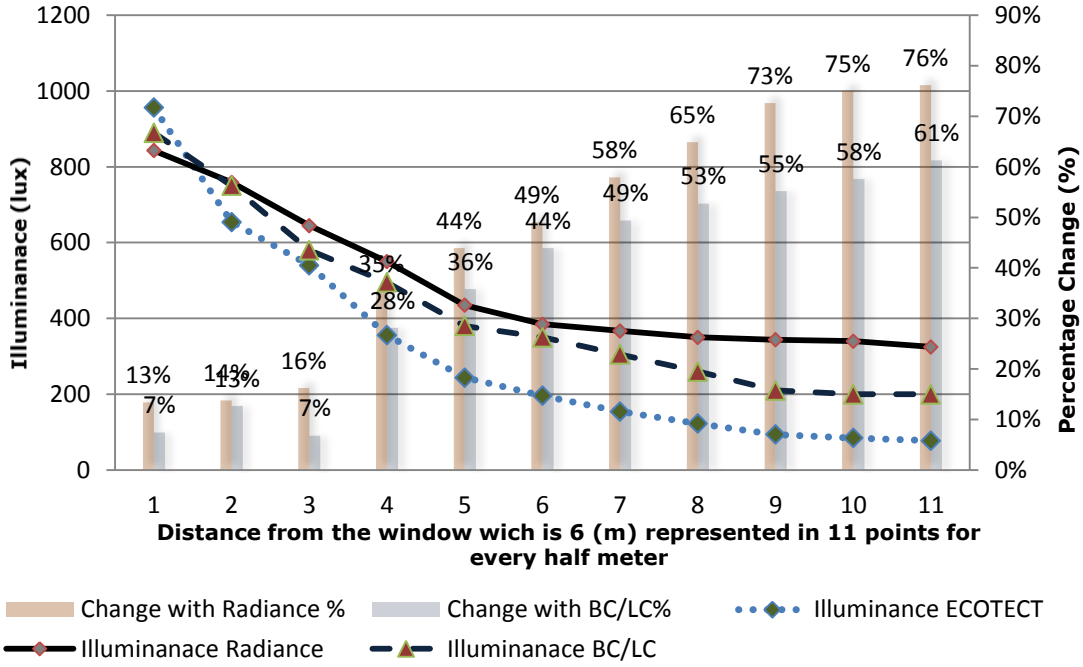

Figure 5.12: Comparison with blind lowered case

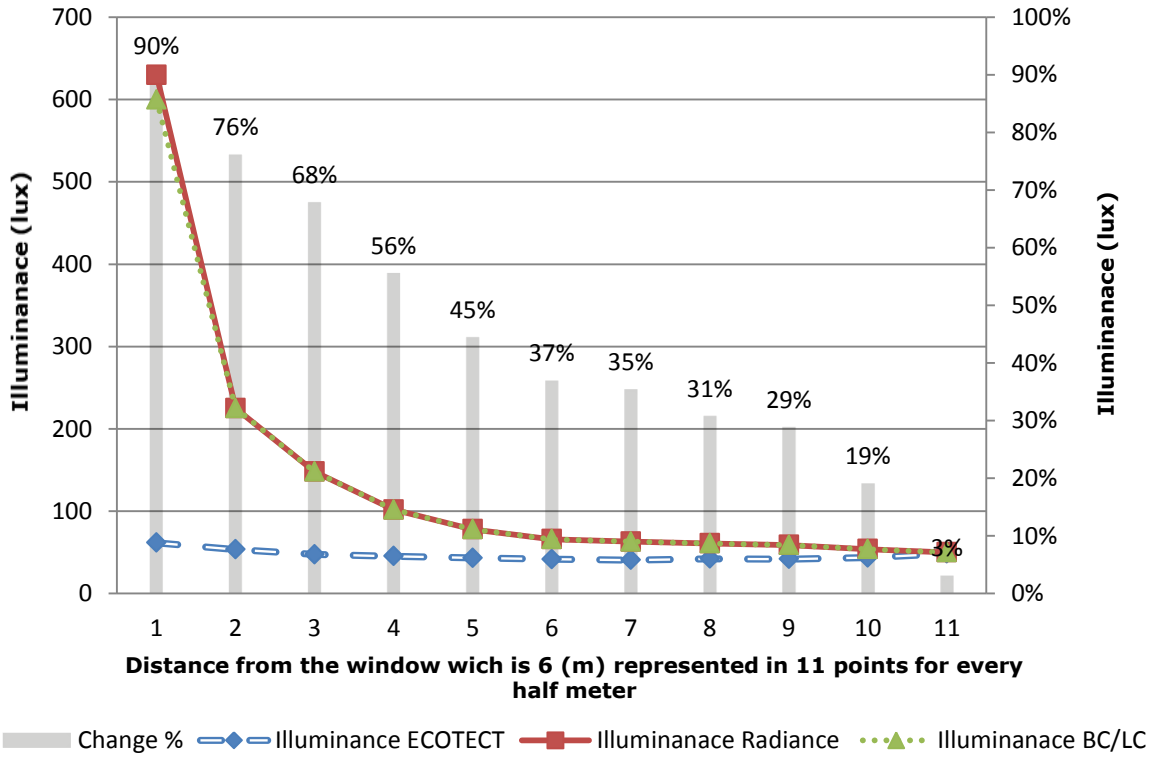

Figure 5.13: Comparison with screen lowered case

5.3 SUMMARY

From what has been discussed previously on the comparison of daylight factors and illuminance levels described by ECOTECT, in the cases one, two and three, and compared to those obtained by different daylighting simulation tools and experimental models extensively for multiple room designs, ECOTECT demonstrated excellent performance in predicting accurate daylight factors as they found to be comparable to those obtained in relevant literature. In contrast, the accuracy of estimated illuminance levels of ECOTECT was limited since they differed significantly from other software predictions and empirical calculations. Consequently, for a required accuracy of daylight factor evaluation, ECOTECT is recommended whereas it can't be so for estimating illuminance level. Overall, ECOTECT is a reliable scheme to assess daylighting potential for a given building model.

Having completed the validation analysis required for the computer tools that will be used for the study; next chapter will give an exhaustive investigation for setting up the simulation model for the proposed window system.

CHAPTER 6 THE PROPOSED SIMULATION MODEL SET UP

Since the configuration of the photovoltaic airflow window proposed in this research combines a double-pane unit on the inside and an outer PV glass pane separated by an air cavity where air is driven by pressure differential from outside to the inside, and vice versa through upper and bottom openings, each property figure was chosen as an optimum value according to previous studies in relevant literature and best practice guides.

6.1 AIR LAYERS WIDTHS

From Congress (2008), Aydın (2006), Hollands et al. (2001), and Aydin (2000), considerable energy savings can be achieved in the energy losses through the double-paned windows with optimum thickness of the air layer between the window glass membranes. According to Southall et al. (2000), Gosselin et al. (2008c), McEvoy et al. (2000), Gosselin et al. (2008b), and McEvoy et al. (2003), cavity width in the range of 10mm – 15mm can contribute in producing an adequate U-value and air outlet temperature. However, The Building Energy Simulation Test (BESTEST) purposely keep geometric and material specifications purely possible to avoid potential opportunity for input errors, therefore, it suggests properties for a conventional window with single and standard double-pane unit with different conditions of shading included generally in a similar base-case building. The zone consists of two classical windows with sealed double panes with a 13mm interpane air layer. As a result, 13mm was identified for the width of air layer of the window.

PV module should be properly ventilated to avoid overheating of the PV panel for great efficiency. Thus, careful attention must be paid when determining the width of the air open path behind it (Gan 2009b). Moreover, great potential can be attained from an accurate width of open air cavity to reduce the window U-value (McEvoy et al. 2000; Gan 2010a). Several research papers (Barakat 1987; Moshfegh et al. 1998; McEvoy et al. 2003) included remarkable dedicated efforts on analysing the effect of the air channel behind the PV module with various cavity widths. However, some

studies restricted the attempts on finding the optimum value for the gap width (McEvoy et al. 2000; Gan 2010a). According to Gan (2009a), the optimum air thickness for an open cavity is between 140mm and 160mm whilst Stapleton et al. (2005) recommends 150mm as an optimum air gap width to keep the PV module well ventilated. As a result, the open air channel width was chosen as 150mm.

6.2 AIR QUALITY AND VENTILATION FOR WORKPLACES

Offices are the most prominent commercial building type, thus, an office space area was chosen for the simulation to serve as the classical example of commercial buildings. For general terms, workplaces require fresh air driven from an area outside. Inside a space, freshness must be achieved through the removal of warm and/or humid air by sufficient air movement and without being blown with cold air. Additional ventilation may be required upon any phenomenon occurred within the workplace such as fumes, dusts, vapours, or heat. Furthermore, an involvement of mechanical ventilation may be presented to provide adequate ventilation along with windows and other openings of the facility (CIBSE 2006).

CIBSE guide A: environmental design sets out a general rule for supplying fresh air that the rate should not fall below 5 and 8 litre per second per occupant. Though, this will be a function of other factors including floor area per occupant, equipment used, process performed within the space, and whether the work is intense. More specifically, The British Council for Offices guide (BCO) (Offices 2009) recommendation, for offices, is $10\mathrm{m}^2$ per person to be used for identifying the functional criteria for floor occupancy density with an outdoor air rate of 12L/s per person. Therefore, and by considering an office apace allocated for two people, the floor area will be $10*2=20\mathrm{m}^2$. Height was 2.8m as standard from BCO.

6.3 DAYLIGHTING

Cherished daylight and controlled sunlight are often critical factors for an occupant's visual perception of a space. They rather enhance the appearance of a space (Carmody et al. 2004; Offices 2009). Thus, the allowable area of window must be

thoughtfully specified depending on the building types and application. Generally, energy performance in a building is partially a function of a window area or window-to-wall ratio (WWR). Window area plays a major role in determining the building's level of cooling, heating and lighting. It further extends to the natural environment in terms of access to daylighting, ventilation and outside views. The window-to-wall ratio is identified by dividing the building's total glazed area by its exterior envelope wall area. As per The American Society of Heating, Refrigerating and Air Conditioning Engineers, 40 per cent of the gross above-grade wall area is an optimum standard for office workplace window area. Furthermore, since the orientation has a significant effect on daylight illuminance levels in a perimeter space, window orientation was determined. According to Carmody et al. (2004) and BESTEST, the south-oriented perimeter spaces are preferred for providing noticeable daylight. Consequently, the window was directed to the south with an area of $5\mathrm{m}^2$ which represents the 25 per cent of the $20\mathrm{m}^2$ office floor area.

The Building Energy Simulation Test (BESTEST) purposely keep geometric and material specifications purely possible to avoid potential opportunity for input errors, therefore, it suggests properties for a conventional window with single and standard double-pane unit with different conditions of shading included generally in a similar base-case building. The zone consists of two classical windows with sealed double panes with a 13mm interpane air layer. Windows are positioned at the south wall occupying an area of 25 per cent of the floor area.

Likewise, the simulation of the airflow window module properties, including the perimeter space, could be specified based on the work of relevant literature such as Bhamjee (2012) and McEvoy et al. (2003) or The Building Energy Simulation Test (BESTEST) standards (Judkoff et al. 1995; Neymark et al. 2002). To put all these values in perspective, all properties employed for the airflow window initial simulation were tabulated below, Table 6.1.

Table 6.1 : CFD module characteristics

Configuration	Description
Space	Office room
Shape	Rectangular
Height	2.8m
People	2 persons with 10m^2 per person
Occupancy Schedule	From 5:00a.m. to 7:00p.m., 5 days per week
Ventilation	12L/s per person
Orientation	South direction
Sealed air layer thickness	13mm
Open air cavity width	150mm
Window to floor ratio	25% of floor area

6.4 HEAT TRANSFER

Heat can be transferred from the outdoor environment to the interior space by radiation and convection where the former involves interchange with other surfaces and the latter with air/surface interface. Radiation and convection are identified by a radiative heat transfer coefficient and a convective heat transfer coefficient h_r and h_c, respectively. The radiative heat transfer coefficient is generally attributed to the temperatures of elements interchange the radiation and it can be calculated by (CIBSE 2006): $h_r = 4\ \sigma\ T_s^3$. However, the convective heat transfer coefficient is a function of several parameters: The variation of the temperature between the surface and the air; the surface roughness; the air velocity; heat flow direction. Air flow occurrence complicates heat transfer process, yet, convective heat transfer coefficient for wind flow can be approximately estimated by the following equation (CIBSE 2006):

$$\boldsymbol{h_c} = 4 + 4_{\boldsymbol{v}} \qquad 6.1$$

Where h_c is the convective heat transfer coefficient $(\mathrm{W/m^2k})$ and v is the air velocity (m/s) that must be 1m/s or more.

An emissivity factor, $\boldsymbol{E}$, of each surface is simultaneously combined with h_r during the heat transmission and they produce internal and external surface resistances. These can be predicted by (CIBSE 2006):

For internal surface resistance:

$$\boldsymbol{R_{si}} = \frac{\mathbf{1}}{{}^{\mathbf{6}}/_{\mathbf{5}}\, \boldsymbol{E\, h_r + h_c}} \qquad 6.2$$

and for external surface resistance:

$$\boldsymbol{R_{se}} = \frac{\mathbf{1}}{\boldsymbol{E\, h_r + h_c}} \qquad 6.3$$

where $\mathrm{R_{si}}$ is the internal surface resistance and $\mathrm{R_{se}}$ is the external surface resistance. For the preliminary simulation, the aim is obtaining the predictions of the surface temperatures, thus, heat flux must be specified in the computation inputs. However, heat flux is exempt from identification for walls and roof since they are assumed to be insulated. Air velocity magnitude is one of the imperative factors – convective heat transfer depends on – requires to be crucially defined at the inlet represented in the modelled prototype of the office room. It can be determined by the volumetric flow rate, Q, and the area of the inlet, A, This can be expressed as: $\nu = \frac{\mathrm{Q}}{\mathrm{A}}$, where ν is the air velocity. For fully developed flows, it is appropriate to choose turbulence intensity and hydraulic diameter as specification method for both, inlet and outlet (Fluent 2009). The hydraulic diameter D_H, can be calculated as following:

$$\boldsymbol{D_H} = 2\,\mathrm{a\,b} \,/\, (\mathrm{a+b}) \qquad 6.4$$

where a is the width of the duct and b is the height of the duct.

The turbulence intensity, I, is the statistical measure of the various velocity patterns, $\boldsymbol{u}`$, to the mean flow velocity, u_{avg}. To estimate a fully-developed duct flow turbulent level, the following formula can be employed:

$$I = \frac{\boldsymbol{u}`}{\boldsymbol{u_{avg}}} = 0.16\, (\boldsymbol{R_{e_{D_H}}})^{-\mathbf{1}/\mathbf{8}} \qquad 6.5$$

However, it is sufficient to represent the fully-developed flow in a range of 5-10 per cent turbulence (Fluent 2009). Consequently, and in analogy with Bhamjee et al. (2012), turbulence intensity was defined as 10 per cent. The gravity state was

activated during the operation with the gravitational constant of $g = 9.81\ m/s^2$ positioned at the negative y-axis.

6.5 THERMAL PROPERTIES OF THE AIRFLOW WINDOW ELEMENTS

The properties of PV modules normally are customised based on the PV cells and the spacing between them inside the PV panel which contains three layers: glass/PV/glass (Petter Jelle et al. 2012). For this simulation, the PV cells applied were amorphous silicon semi-transparent cells. The double glazing behind the PV panel is a standard unit with clear glass and sealed air layer. To put these in perspective, the thermal properties of the various layers are listed in Table 6.2.

Table 6.2 : Thermal Properties of the Airflow Window

Material	Left side wall			Air path	Right side wall		
	Glass	PV	Glass		Glass	Air	Glass
Reflectivity	0.12	0.1	0.12		0.12		0.12
Absorptivity	0.08	0.4	0.08		0.08		0.08
Transmissivity	0.8	0.45	0.8		0.8		0.8
Electricty power		0.05					
Density (kg/m^3)	2500	2500	2500		2500	1	2500
Capacity (J/K)	1000	1000	1000		1000	1000	1000
Width (m)	0.004	0.0045	0.004	0.15	0.004	0.013	0.004

6.6 CFD SOLVER SET UP

Due to the straightforward features of the three-dimensional geometry of the office room, models were calculated with steady-state for the reasons of the constraints of time availability and the computational resources. ANSYS Fluent offers two solver technologies: pressure-based and density-based algorithms where both are sufficient for a broad class of flows, yet, each one features an exclusive use. Traditionally, incompressible and mildly compressible flows have been computed with the pressure-based solver whereas high-speed compressible flows were originally predicted with the density-based track. The pressure-based approach was employed since the flow inside the model is incompressible. Moreover, the pressure-based solver allows solving the problem in either segregated or coupled techniques. The segregated algorithm

provides two types of step-by-step procedures for steady-state calculation flows: SIMPLE and SIMPLEC where the former was chosen for pressure-velocity coupling.

Gradient and pressure discretization scheme were treated with the Last squares Cell based and the standard scheme, respectively, since they are applicable to the model operating condition and as advised by (Fluent 2009). For quad/hex mesher, the second order upwind discretization scheme is the best suitable solver; however, the first order upwind approach is yet acceptable. Generally, it is appropriate to consider applying the first-order scheme for adequate convergence unless the case requires the second-order algorithm then starting with the latter is preferably considered for the first few iterations and switching to the first-order solver afterwards unless otherwise no difficulties were encountered, then continuing with the second-order manner is possible.

The default under-relaxation factors set by (Fluent 2009) are effective for a wide range of problems; they were kept as default. However, in the event of any difficulties of reaching the convergence; gradually decreasing and increasing are prudently deemed for momentum and pressure, respectively. This alteration process is restricted down to 0.2 for the momentum and up to 0.7 for the pressure. The default under-relaxation factors are listed in Table 6.3. The residual for the equations were limited to $<10^{-3}$ except for the energy equation was fixed to $<10^{-6}$ as per (Fluent 2009).

Table 6.3 : CFD model under-relaxation factor

Under-relaxation factors	Value
Pressure	0.3 (maximum 0.7)
Density	1
Body forces	1
Momentum	0.7 (maximum 0.2)
Turbulent kinetic energy	0.8
Specific dissipation rate	0.8
Turbulent viscosity	1
Energy	1

6.7 LONDON WEATHER DATA

The London weather data, solar irradiance and air temperature, were derived from the CIBSE guide A, the environmental design. The solar irradiance values are the daily and hourly mean irradiance as beam and diffuse on vertical and horizontal surfaces whilst the air temperature values are provided in the hourly basis. The solar irradiance and air temperature, of the cold season of the city of London, employed in the computational model are of the day of the 29th of January and for the cooling season the data applied are for the month of June and day of 21st. The time for daily variation is considered for the period of the day time, 5:00 am-7:00 pm o'clock. However, the solar irradiance and the air temperature applied for winter and summer steady state simulation analyses were the highest values during the day time that occur at the noon time in order to demonstrate the maximum performance of the system. Table 6.4 represents the solar irradiance and air temperature values for both seasons.

Table 6.4: Solar irradiance and air temperature values of both seasons.

Cooling Season			**Heating Season**		
Jun 21st	**G (W/m^2)**	**T air °C**	**Jan 29th**	**G (W/m^2)**	**T air °C**
05h	62.16	16.80	05h	0	0.70
06h	91.52	18.50	06h	0	0.70
07h	107.53	20.10	07h	0	1.80
08h	210.21	21.50	08h	18.3	2.30
09h	342.32	22.70	09h	300.09	3.70
10h	448.98	23.60	10h	523.18	4.70
11h	516.95	24.40	11h	656.16	5.50
12h	538.62	24.50	12h	707.36	5.90
13h	511.66	24.40	13h	678.58	5.80
14h	438.96	24.20	14h	568.99	5.30
15h	328.76	23.50	15h	372.94	4.30
16h	194.93	22.50	16h	24.52	3.70
17h	106.16	19.30	17h	0	3.30
18h	89.22	17.90	18h	0	3.00
19h	57.52	16.80	19h	0	2.70

6.8 CALCULATION OF THE HEAT FLUX

The heat flux through the airflow window system can be calculated for the PV panel, glass panes, and the floor primarily based on the thermal properties of the system using the following equations (CIBSE 2006):

$$\mathcal{Q}_P = (G\,\alpha_P)(R_{se}/R_{si} + R_{se}) \quad 6.6$$

$$\mathcal{Q}_{ge} = [(\tau_P)\,\alpha_{ge}]/2 \quad 6.7$$

$$\mathcal{Q}_{gi} = [(\tau_P)\,(\alpha_{ge})]\,\alpha_{gi}/2 \quad 6.8$$

$$\mathcal{Q}_{\mathrm{f}} = (G\ \tau_P\ \tau_{ge}\,\tau_{gi}\ A_{\mathrm{w}})/\,A_{\mathrm{f}} \quad 6.9$$

where:

$\mathcal{Q}_P$ is the PV panel heat flux (W/m^2), G is the solar irradiance (W/m^2), α_P is the PV panel absorptivity, R_{se} is the external surface resistance (K.W^{-1}), R_{si} is the internal surface resistance (K.W^{-1}), $\mathcal{Q}_{ge}$ is the outer glass heat flux (W/m^2), α_{ge} is the outer glass absorptivity, $\mathcal{Q}_{gi}$ is the inner glass heat flux (W/m^2), α_{gi} is the inner glass absorptivity, $\mathcal{Q}_{\mathrm{f}}$ is the floor heat flux (W/m^2), τ_{ge} is the outer glass transmissivity, τ_{gi} is the inner glass transmissivity, A_{w} is the window area (m^2), A_{f} is the floor area (m^2).

The heat flux of the PV panel will be the largest value since it is exposed directly to the solar irradiance where its absorptivity and transmissivity determine the heat fluxes of the other surfaces, external and internal glass panes and the floor. The process of the heat transfer that occurs at the PV panel surface is a complex nature which is dependent on several phenomena such as differences between air and surface temperature where the emissivity of the PV panel can be combined with the radiative and convective coefficients to give the external and internal surface resistances. Due to the complex nature of heat transfer process, the internal and external surface resistances were simply obtained independently from temperature differences between radiating surfaces, surface roughness, and differences between surface and air temperatures, as recommended in (CIBSE 2006), as 0.13 and 0.06K.W^{-1}, respectively.

Part of the incident solar irradiance is absorbed by the PV panel and the rest transmits to the outer glass pane that is placed directly behind the PV panel where air can flow in between. Part of that transmitted solar irradiance is absorbed by the outer glass and again the rest transmits to the inner glass pane that is located directly behind the outer pane. Thus, the amount of absorbed solar irradiance by both outer and inner glass panes is divided by two parts to identify the heat flux of each side for each pane.

It is obvious that the heat flux of each surface is influenced by the transmissivity factor of the surface in front. However, the floor heat flux is attributed to the transmissivity factor of each of the PV panel, and outer and inner glass panes as well as the window and floor areas. Consequently, it is an essential figure in specifying the heat ought to be removed from the inside space. Thus, inlet area and air velocity are dependent on the heat flux of the floor due to the solar radiations and to the internal heat gains, e.g. occupants, artificial lighting, and computers.

6.9 CALCULATION OF AIR VELOCITY

For the winter condition, the air velocity passing through the airflow window into the inside space to the outlet that can be calculated using the mass balance equation which is as follows:

$$\boldsymbol{q} = \dot{m}\ C_P\ \Delta T \qquad 6.10$$

where:

$\boldsymbol{q}$ is the heat transfer rate (W), $\dot{m}$ is the mass flow rate (kg/s), C_P is the specific heat (J/ (kg k)), ΔT is the difference between the inlet and the outlet temperature (k).

High air velocity contributes to producing low inside space temperature, and conversely the increase of internal temperature could be a result of low air velocity. Since the outside temperature that will be applied for the heating season simulation is 5.9^0C, the difference between the inside and the outside temperature must be minimally 15 in order to achieve the thermally accepted inside area for which its temperature varies between 20 and 25^0C. Thus, an assumed air velocity of 0.35 m/s was considered to run an initial simulation to find out what type of temperature performance can produce. Then, it revealed that the difference between the inlet temperature and the outlet temperature was 11, therefore, the temperature needs to be increased 3 degrees to achieve the thermal comfort level. Thus, the above mentioned equation reveals that the air velocity of 0.25m/s can achieve the required temperature difference based on $\boldsymbol{q}$ = 90W. If the heat gains are much less, a minimum ventilation rate (e.g 10L/s-person) will be used for simulation.

However, for the cooling season, the air velocity calculation was obtained differently. According to what have been stated above regarding the air velocity attribution to the inside environment temperature as well as the flow rate that falls between 20 and 30L/s-person which is considered as an adequate and it is a function of the air velocity. As a consequence, the inlet air velocity must be higher to attain higher flow rate and thus, the velocity will be preliminarily assumed as 0.5m/s (double velocity used for winter).

6.10 CALCULATION OF THE AREA OF INLET AND OUTLET

The area of inlet of heating dominating season will be compatible with the area of the air flow opening since the essential method of the air flow during the winter period is supply mode that circulates the accumulated heat through the gap to the inside space. As such, the area of inlet is 0.42m^2 as 0.15m depth and 2.8m width. However, the area of the opening that allows air into the inside space relays on the required mass flow rate which is 0.02kg/s as discussed in the description chapter. Thus, assuming the inlet air velocity as 1m/s and using the following equation:

$$A = \frac{\dot{m}}{\nu \rho} \tag{6.11}$$

where:

A is the area of inlet (m^2), $\dot{m}$ is the mass flow rate (kg/s), ν is the air velocity (m/s), ρ is the density of air (kg/m^3).

The area of inlet equals to 0.02m^2 whereas the area of the outlet will be identical to the inlet area with a different shape located at bottom of the back of the room. The position and the size of the outlet allow the heated air to circulate inside the space and to maintain it thermally comfortable. In contrast, for the summer season, the area of inlet will be treated differently and calculated primarily based on the amount of heat that needs to be vented to the outside environment through the air channel located behind the PV panel using the following equation:

$$A = \frac{Q_{\mathrm{f}}}{(C_P\ \rho\ \Delta T\ \ \nu\ )} \qquad 6.12$$

where:

Q_{f} is the total floor heat (W), A is the area of inlet (m^2), C_P is the specific heat (J/kg K), ρ is the density of air (kg/m^3), ΔT is the difference between the inlet and the outlet temperature (k), ν is the air velocity (m/s).

The floor heat represents the amount of the undesirable heat whilst the difference between the inlet and the outlet temperature is the difference between inlet air temperature and the maximum thermally accepted inside temperature which is 25^0C. Once the area of inlet is recognised, the adequate flow rate can then be introduced by the following equation:

$$\dot{m} = A\ \rho\ \nu \qquad 6.13$$

The exhaust mode of the window during the cooling dominating season that vents out the accumulated heat inside the space to the outside environment through the gap opening, between the PV panel and the double glazing unit, will necessitates the outlet dimensions at least to be identical to the dimension of the air channel opening. Figure 6.1 and Figure 6.2 illustrate the air flow through the office room and the inlet and outlet positions as well as the occupied zone for the winter and the summer conditions, respectively.

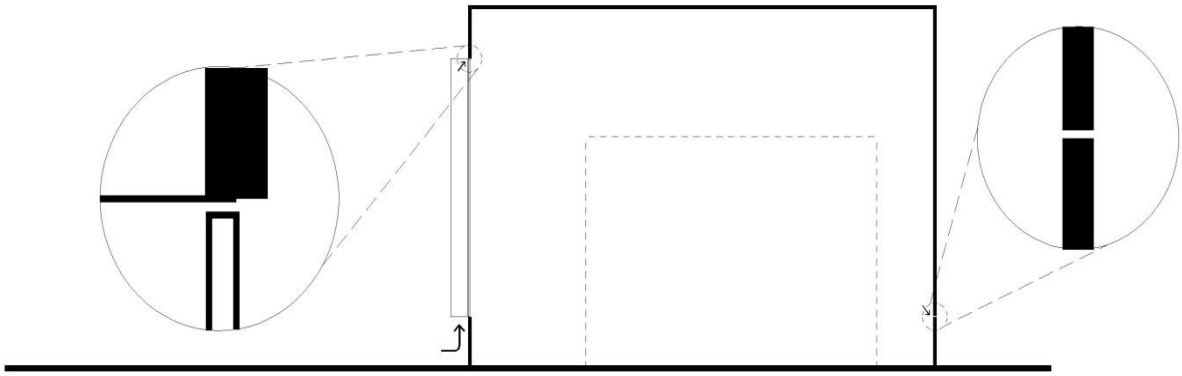

Figure 6.1: The supply mode of the winter season

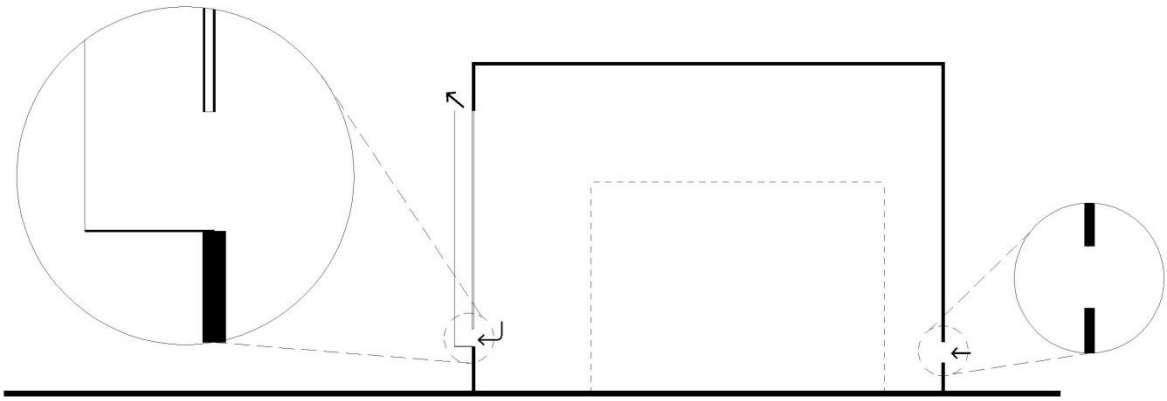

Figure 6.2: The exhaust mode of the summer season

6.11 PV TRANSPARENCY RATIOS

The optical characteristics of the PV panel are represented with its transparency ratios where the proportion of daylight is shared comfortably in the interior lighting level providing natural light and mitigating the energy consumption of artificial lights. There are only few references in the literature where the PV transparency levels and its effect on thermal and visual comfort have been numerically investigated (Vartiainen et al. 2000; De Boer et al. 2001; Miyazaki et al. 2005; Chow et al. 2007; Chow et al. 2009c; Han et al. 2009; Chen et al. 2012; Lu et al. 2013). Most of these studies discussed the ratio in the range of 10-60 per cent. De Boer et al. (2001) assigned the transparency of 25 per cent as a threshold and found that the 15 per cent is the optimum transparent level, though, Chen et al. (2012) revealed that 26.9 per cent is the PV transparent ratio that can optimally achieve energy saving and daylighting comfort inside the space.

In contrary, the investigation of Chow et al. (2007) indicated that the range of 45-55 per cent PV transmittance can do justice to the electricity saving and visual comfort. The same was true with 40 per cent PV transmittance level from Miyazaki et al. (2005). Thus, visual and thermal analyses will be performed under the effect of the PV transparencies of 0.15, 0.2, 0.25, 0.3, and 0.35 to find the optimal transparent level for the PV window unit during the summer and winter. The transparency will be limited to that range due to the fact that higher transparent values can excessively increase the direct solar contribution, and simultaneously decrease the indirect contribution through the absorption of solar radiation by the PV cells (De Boer et al. 2001).

6.12 SUMMARY

This chapter has incorporated and provided clear justification for all dimensions, parameters and inputs to be employed for the proposed simulation model. It predicated on the most recent published work and best practice guide. Thus, next chapter will proceed for the analysis and design optimization for the window unit under the effect of winter conditions.

CHAPTER 7 ANALYSIS AND DESIGN OPTIMISATION FOR WINTER SEASON

7.1 INTRODUCTION

Having completed the setup of the specifications for the airflow window CFD model, this chapter presents a CFD analysis for the airflow window system under the effect of mechanical force only, buoyancy force only, and the combination of both forces considering the winter weather condition for the city of London. Furthermore, daylighting studies are included for various PV transparent degrees. Generally, the chapter offers optimisation of the system and design for energy efficiency and adequate level of thermal and visual comfort when applied to an office building.

Three attempts of simulation have been carried out first for mechanical ventilation only, second for buoyancy ventilation only, and then for combined mechanical and buoyancy force to identify the effect of the buoyant flow on the performance of the airflow window when providing thermal comfort and adequate ventilation rate. For the mechanical force and combined forces simulations, a fan speed of 0.25m/s was used as a base air velocity for airflow window at a window height of 2m and width of 0.15m.

7.1.1 MECHANICAL VENTILATION ONLY

Under fan-driven mechanical ventilation, cool ambient air flowed into the office space from the opening of the airflow window at the bottom flowed across the top opening through the inside space to the outside space through the outlet aperture at the back of the room as seen from Figure 7.1. The flow direction of incoming air can maintain the space properly ventilated where air is circulating widely over the inside environment. Even though the incoming air jet is slightly attached to the room surface due to the Conada effect, the air velocity is relatively high inside the space more specifically inside the area of the occupied zone that is dominated with 3m/s air

velocity which considered as uncomfortable. The force rather has elevated the velocity at the outlet to 5.15m/s with a flow rate of 55L/s.

Figure 7.2 shows the predicted temperature distribution inside the office room under fan-induced mechanical ventilation. The cool ambient air flowed from the window openings picking up the accumulated heat between the cavities into the inside space providing the indoor environment with air that maintains it thermally comfortable with a predominant temperature of 22 ^{0}C and 20^{0}C at the outlet.

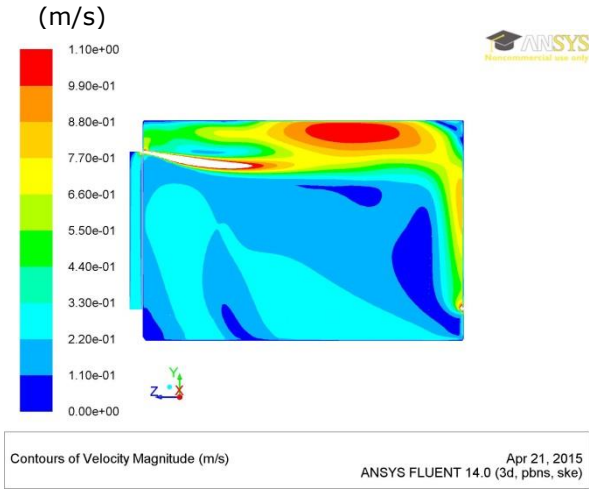

Figure 7.1: Air flow Pattern

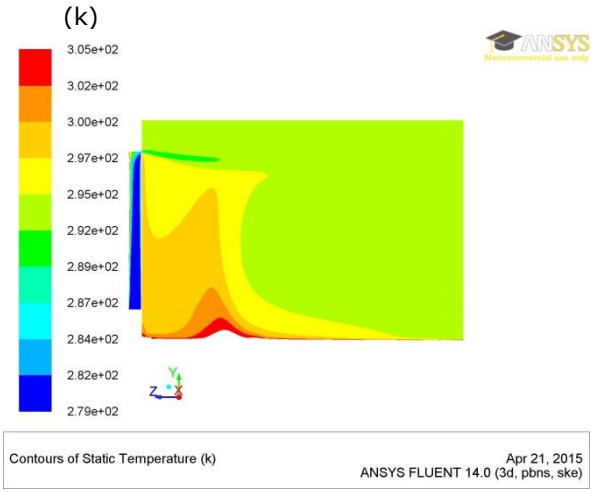

Figure 7.2: Temperature distribution

7.1.2 BUOYANCY VENTILATION ONLY

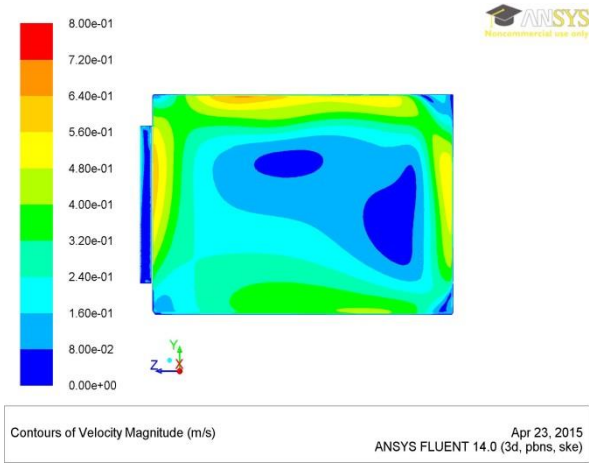

Figure 7.3: Air flow Pattern

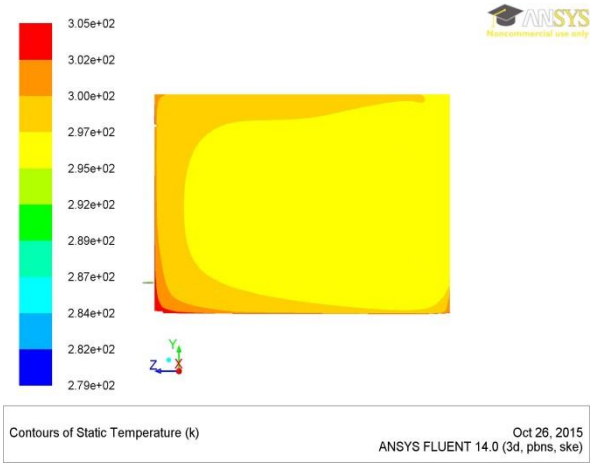

Figure 7.4: Temperature distribution

The changing pattern of air velocity behaviour under buoyancy-driven ventilation is shown in Figure 7.3. Due to the buoyancy effect only, cool ambient air flowed into the office space from the opening of the airflow window at the bottom flowed across the top opening through the inside space to the outside the space through the outlet aperture at the back of the room. The incoming air was flowing along the roof and walls with an air velocity ranging between 0.3 and 0.6m/s. Thus, the air movement around the inside space is relatively poor with predominant air velocity ranging between 0 and 0.2m/s which the latter represents the velocity at the outlet.

Figure 7.4 presents the variation of temperature performance inside the office space due to buoyancy-induced ventilation. It can be noticed that, the accumulated heat between the cavities is impeded from being supplied to the inside environment causing overheating for the PV panel, with quite unrealistic temperature degree leaving the room with thermally unaccepted condition with an average temperature of 28^0C.

7.1.3 COMBINED MECHANICAL AND BUOYANCY VENTILATION EFFECTS

The air flow patterns in the office space under both fan speed and buoyancy forces are shown in Figure 7.5. It can be noticed that the air movement is circulating slightly faster inside the space than it flowed under the mechanical force only due to the buoyancy force of cool incoming air which spreads the indoor air refreshing the office room before it flows to the outdoor environment along the surface with the assistance of the mechanical force, though, the dominated air velocity varies between 1 and 3m/s with a mass flow rate at the outlet of 55L/s.

The predicted temperature distribution under the combined forces of mechanical and buoyancy is given in Figure 7.6. It can be seen that the addition of the buoyancy force to the fan speed force made negligible difference in distributing heat throughout the indoor environment where the heat in the left bottom of the space was cooled down slightly as a function of the opposite effect of the buoyancy that dropped the air on

the floor vertically along the back (cool) glass pane to circulate more heat than it moved in the case of mechanical force only, however, the predominant indoor air temperature is still thermally comfortable with 22^{0}C.

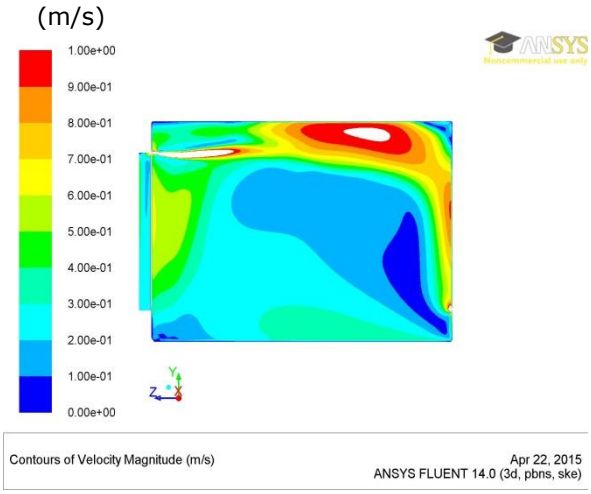

Figure 7.5: Air flow Pattern

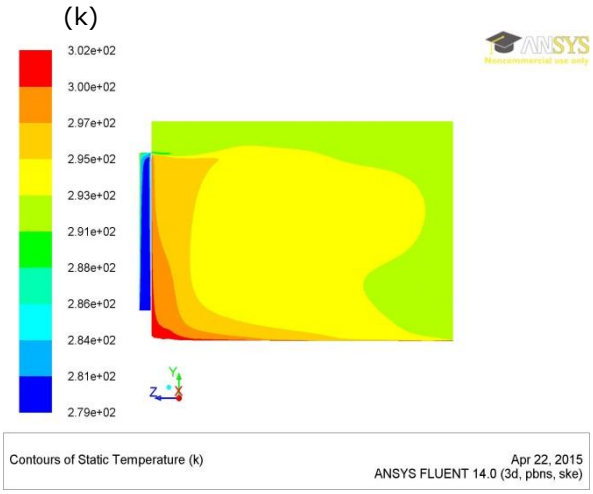

Figure 7.6: Temperature distribution

7.2 COMPARSION OF VENTILATION FORCES

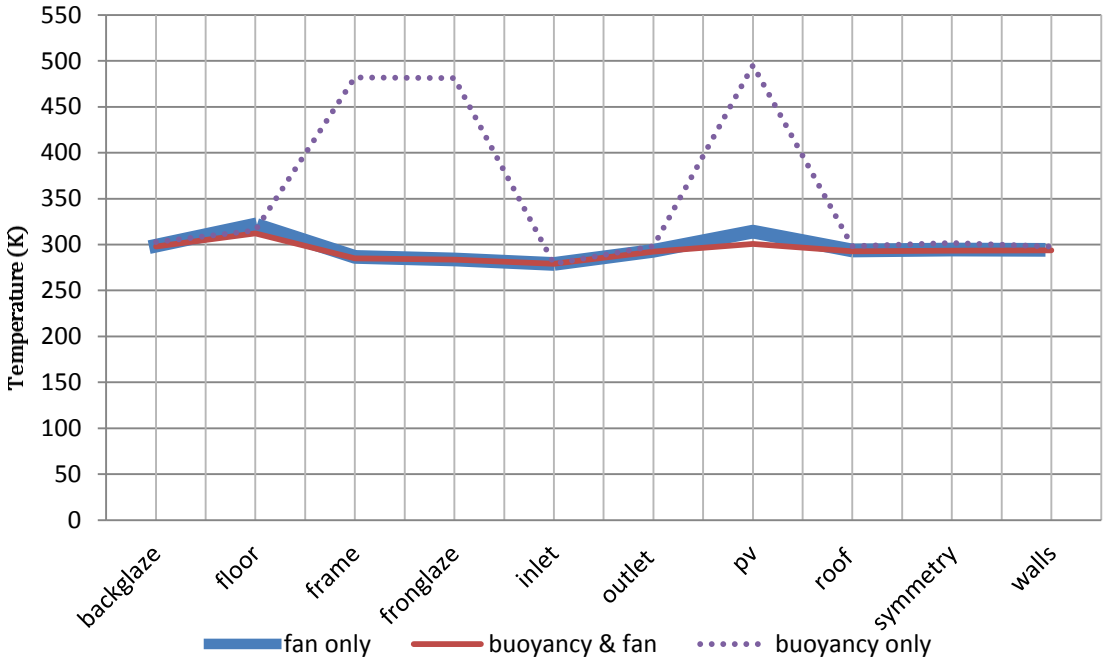

Figure 7.7: The magnitude of the temperature values for fan force only, the combination of buoyancy and fan forces, and buoyancy force only

The magnitude of the temperature behaviour according to the effect of each ventilation force is shown in Figure 7.7. It presents the average value of the temperature distribution for each component. It can be seen that the mechanical-

induced ventilation and the combination of both mechanical and buoyancy ventilation force are relatively similar in terms of their temperature performance. However, the buoyancy-induced ventilation alone presented a different temperature pattern even though similarities can be noticed from some components such as the floor, back glaze, and the outlet. The increase in the temperature values due to the buoyancy force effect is much more from the other forces. Furthermore, the temperatures are elevated to a point of overheating meaning that the buoyancy-induced ventilation, for this design, is incapable of air movement inside the space to achieve the required level of thermal comfort.

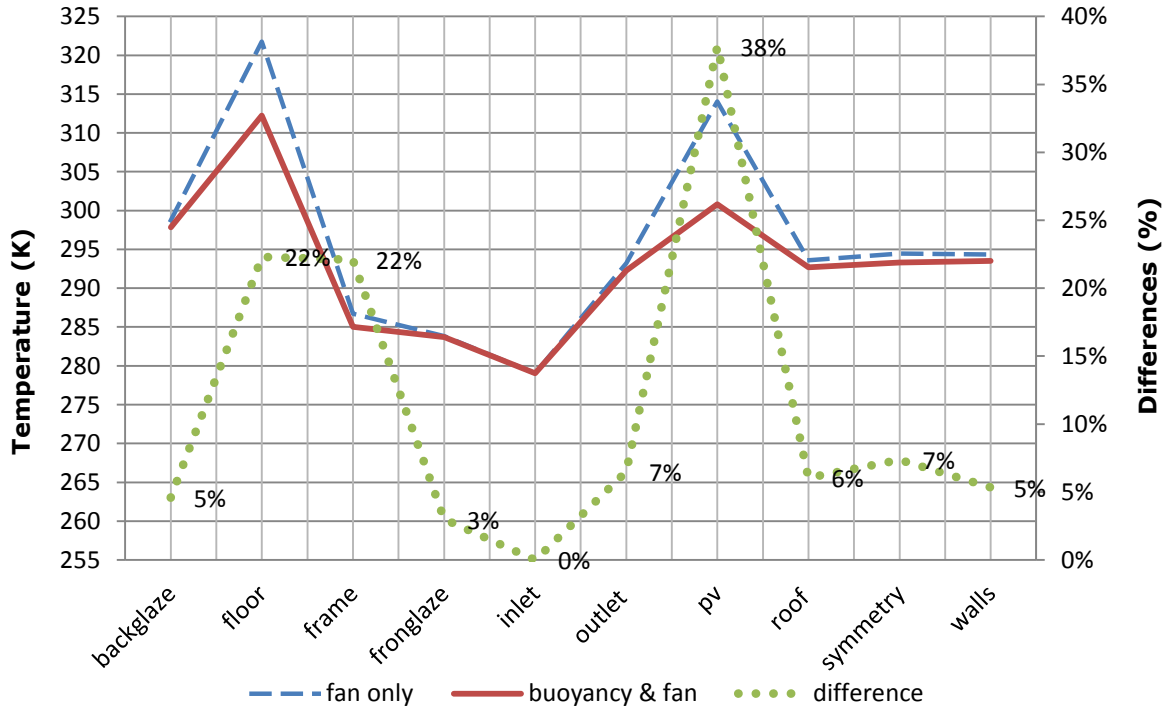

Figure 7.8: The magnitude of the temperature values for fan force only, the combination of buoyancy and fan forces, and the average differences

Figure 7.8 shows the magnitude of the temperature patterns of the boundaries due to the mechanical ventilation force and the combination of mechanical and buoyancy ventilation forces as well as the percentage differences found between these values individually for each element. Differences that ranging between 0 and 7% can be seen from the figure above between the two temperature performance of both ventilation forces for most of the elements except three that are floor, front glaze, and PV where the changes were significant and escalated up to 22, 22, and 38 per cent,

respectively. These changes reveal higher temperature values from the mechanical force only than the integration of both mechanical and buoyancy ventilation processes. This can be translated as overheating possibility when applying the mechanical ventilation force only for the airflow window whereas the combination of both forces can satisfy the required thermal level of the space.

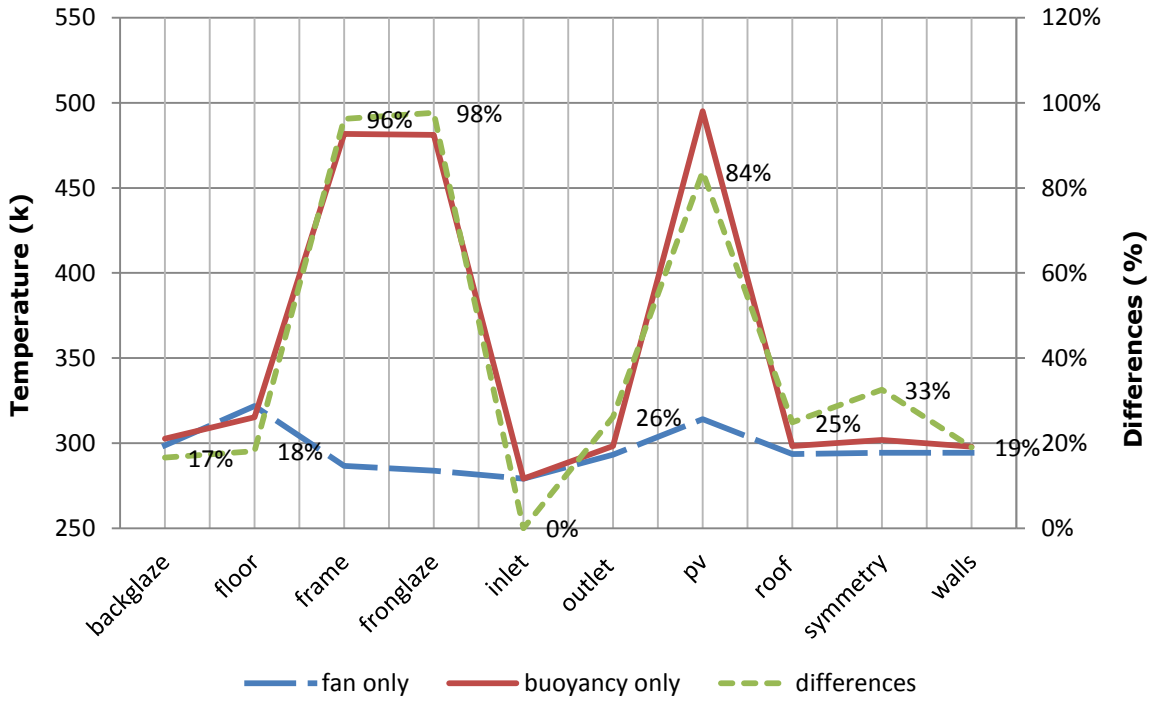

Figure 7.9: The magnitude of the temperature values for fan force only, buoyancy force only, and the average differences

The trends of the temperature behaviours of the boundaries as a function of the mechanical and the buoyancy ventilation forces as well as the percentage differences found between these values individually for each element are presented in Figure 7.9. It can be observed that the effect of the buoyancy force alone leads to much higher temperature than that produced under the effect of the fan force. The same is true with the temperature performance issued under the impact of buoyancy force only and the integration of mechanical and buoyancy ventilation forces as shown in Figure 7.10. From both figures, it appears that the temperature performance of mechanical ventilation force and of its integration with the buoyancy force is feasible to provide adequate thermal level that the buoyancy ventilation force only is incapable of where considerable differences are found from the behaviours of the other forces.

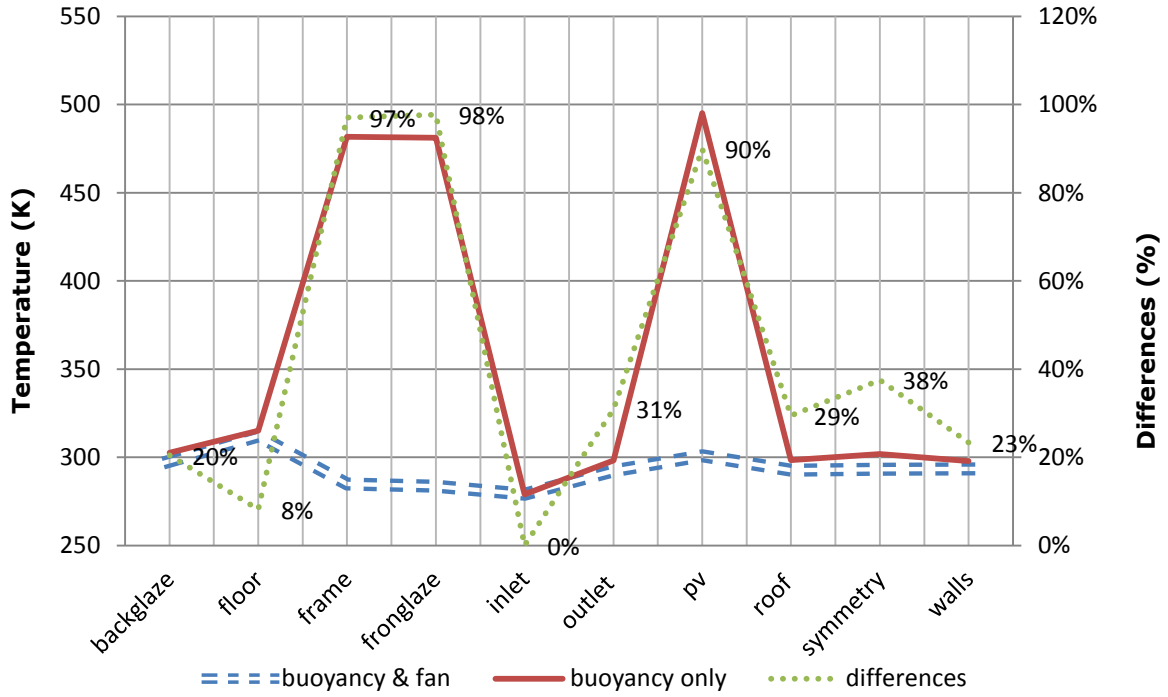

Figure 7.10: The magnitude of the temperature values for the combination of buoyancy and fan forces, buoyancy force only, and the average differences

The temperature values for the symmetry plane, along a horizontal rake that extends from the window to the bottom of the back of the room, due to the effect of each ventilation force: buoyancy-induced flow, the integration of buoyancy- and mechanical-induced flow, and the mechanical-induced flow are shown in Figure 7.11. It can be observed that there is a large gap between the trend of the temperature behaviour due to the effect of buoyancy flow and the trends of the temperature performance due to the impact of the mechanical flow and to its integration with the buoyancy flow. However, the average temperatures, along the rake, under their effects all fell within the thermal comfort level with 24^0C for the buoyancy force, 22^0C for the mechanical force, and 20^0C for the integration of both ventilation forces. The high temperature values appear near to the window where they exceed 25^0C with each ventilation force whilst the back of the space is thermally acceptable with each ventilation flow as well.

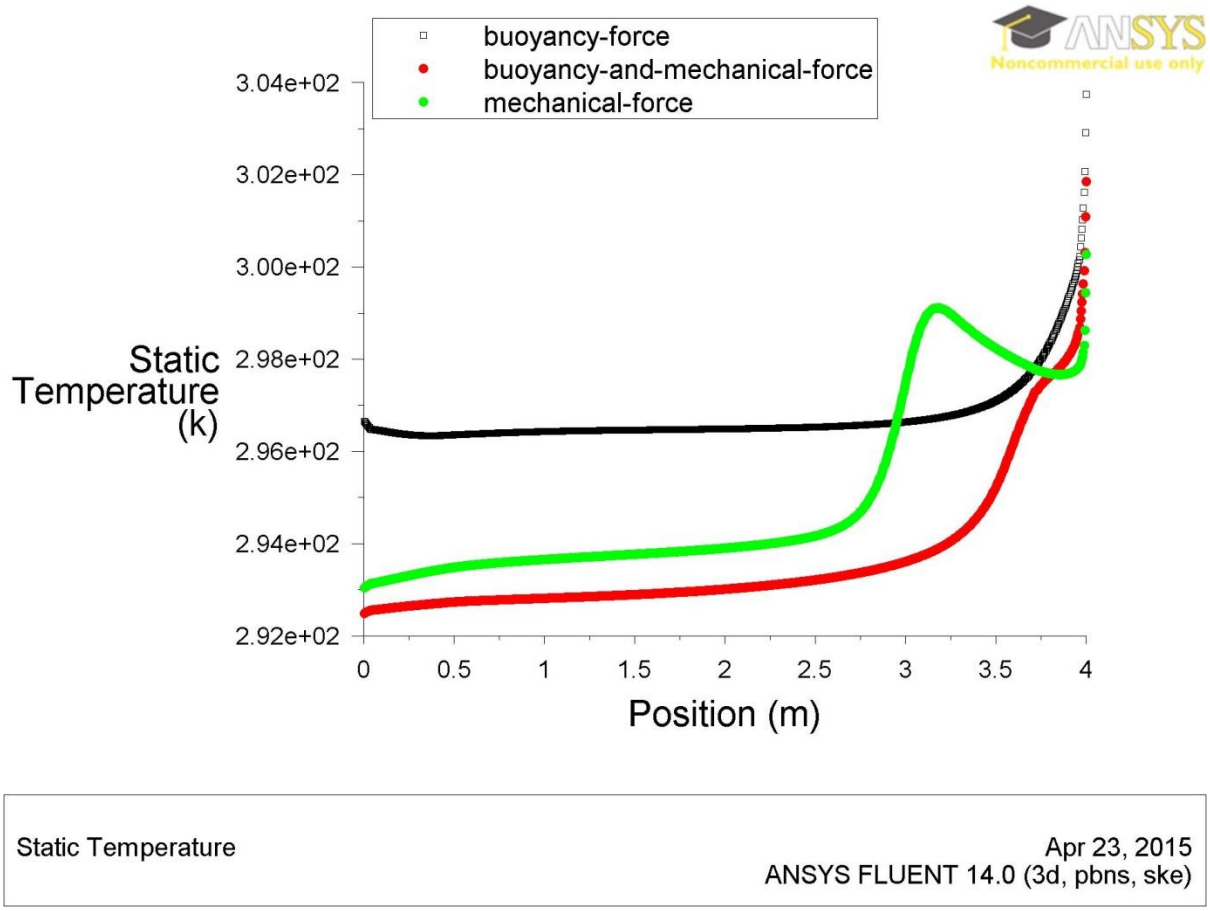

Figure 7.11: Symmetry plane temperatures under the effect of each ventilation force

Predicting air flow and temperature distribution inside an office space, for two occupants, equipped with an airflow window due to the mechanical- and buoyancy-driven ventilation has confirmed that the addition of the buoyancy force would contribute in slight increase in air flow to spread the heat around the indoor space warming it to be thermally accepted. Indeed, the buoyancy force can assist the mechanical force for adequate indoor environment during the heating seasons. Though, different PV transparency levels must be investigated to achieve the most optimal thermal level from the most suitable driving flow.

7.3 EFFECT OF PV TRANSPARENCY LEVELS

Since the combined force for driving the flow is appropriate as revealed in the conclusion above, an occupied zone was considered for the model for more analysis to reach the adequate thermally tolerable zone under different PV transparency levels. The occupied zone was specified as 0.5m from any wall and 1m from the window with a height of 1.8m where normally the occupants reside the volume of air is confined by specific horizontal and vertical planes (Institution 2014). The zone is represented by two horizontal and three vertical planes where the formers are the head and foot planes and the latters are the front, back, and the side planes. Under each PV transparency the temperature was calculated for each plane and the average temperature of the zone. Each plane was assigned a rake to identify its temperature. Figure 7.12 illustrates the occupied zone within the model. The variations of the predicted temperatures inside the occupied zone under the effect of the heat passing through PV panel with different transparencies of 0.15, 0.2, 0.25, 0.3, and 0.35 was plotted for each plane of the zone. Figure 7.13 presents the rake position of each plane in the zone and Table 7.1 shows the PV properties under different transparency degrees during the winter season.

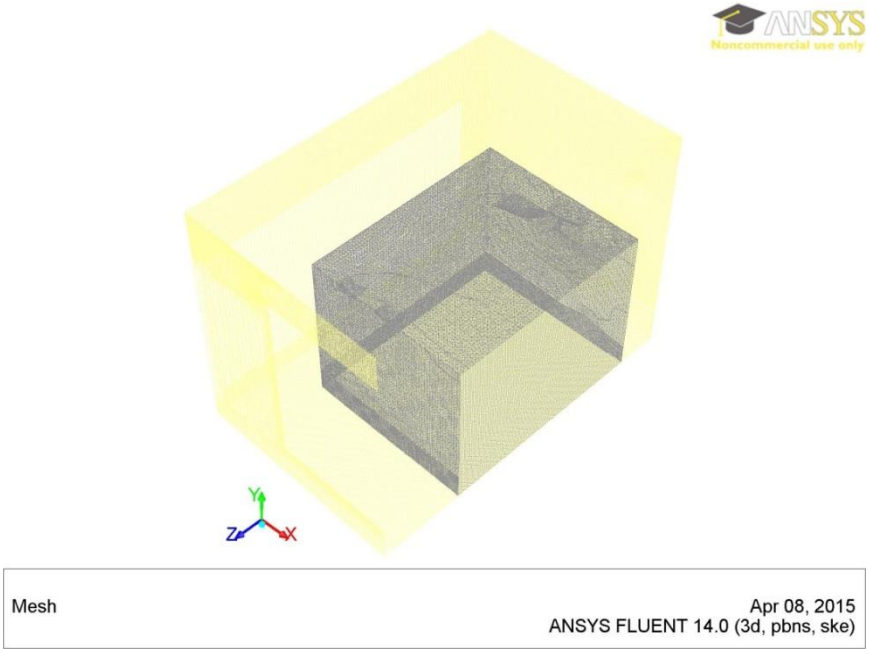

Figure 7.12: The occupied zone within the model space

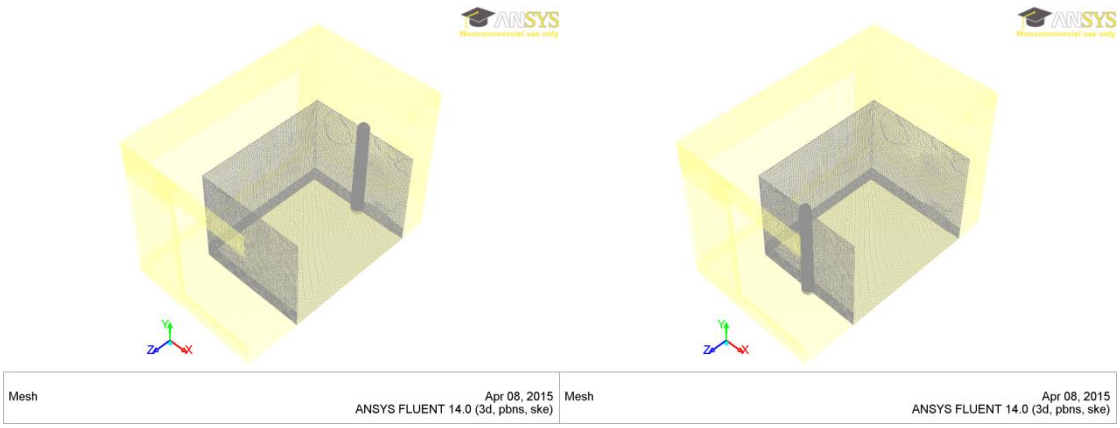

(a): Back plane rake (b): Front plane rake

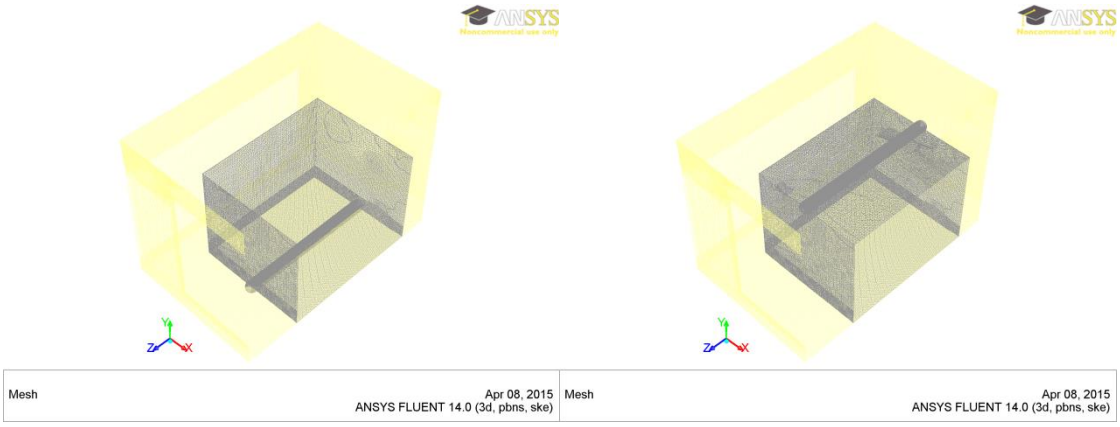

(c): Foot plane rake (d): Head plane rake

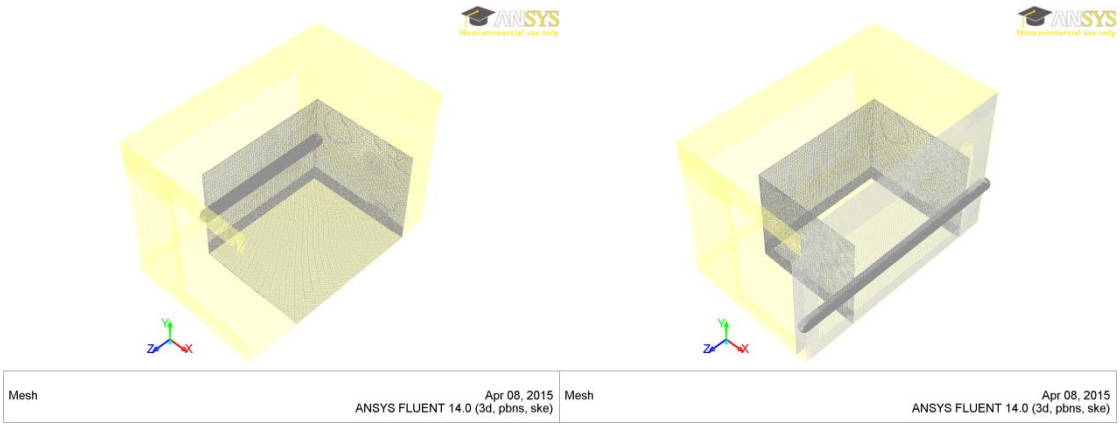

(e): Sidewall plane rake (f): Symmetry plane rake

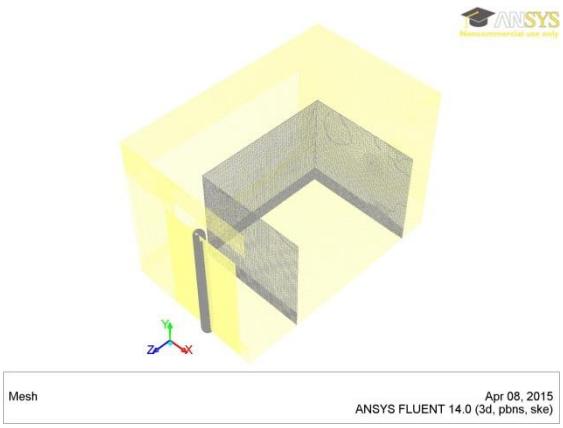

(g): PV plane rake

Figure 7.13: Rake position

Table 7.1: PV Characteristics under different transparency levels

PV	Transparency Levels				
	0.15	**0.2**	**0.25**	**0.3**	**0.35**
Heat Flux (W/m^2)	158.45	147.13	135.81	124.50	113.18
Reflectivity	0.1	0.1	0.1	0.1	0.1
Absorptivity	0.7	0.65	0.6	0.55	0.5
Transmissivity	0.15	0.2	0.25	0.3	0.35
Electricity conversion efficiency	0.05	0.05	0.05	0.5	0.05
Conductivity (W/m k)[1]	169.79	169.79	169.79	169.79	169.79
Density (kg/m^3)[1]	8330	8330	8330	8330	8330
Heat capacity (J/K)[1]	1677	1677	1677	1677	1677
Width (m)	0.0125	0.0125	0.0125	0.0125	0.0125

7.3.1 PV TRANSPARENCY LEVEL OF 0.15

Figure 7.14 shows the temperature distribution for the back and front planes vertically along the space height. It can be observed that the temperature of the front plane is slightly higher than the back one due to its direct exposure of the window with a highest temperature approximately of 33.37^{0}C and the lowest temperature of 20.42^{0}C whereas the peak temperature of the back plane is approximately 28.98^{0}C and the minimum is 19.88^{0}C. Thus, the temperature of vertical depth of the space is thermally acceptable for the occupants in most of the space.

[1] Material properties of STPV material (Wah et al. 2005)

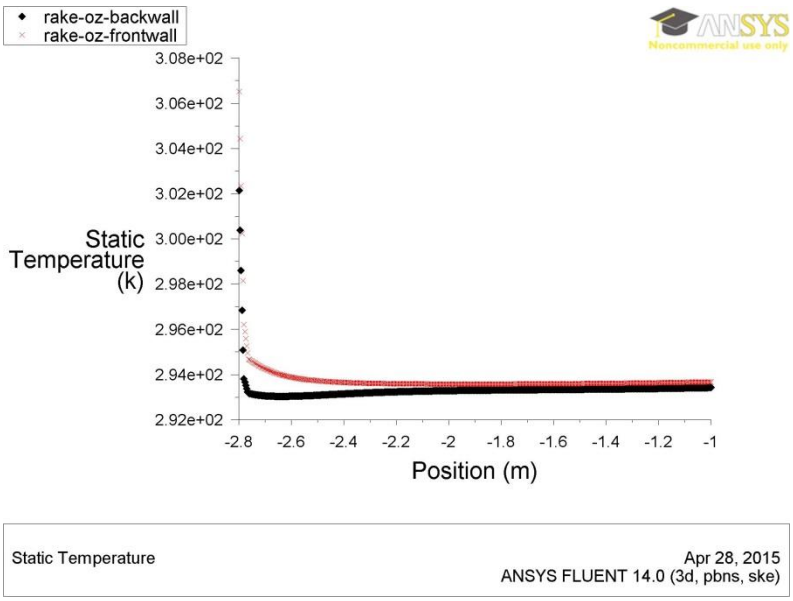

Figure 7.14: Front and back plane temperatures under 0.15 PV transparency level

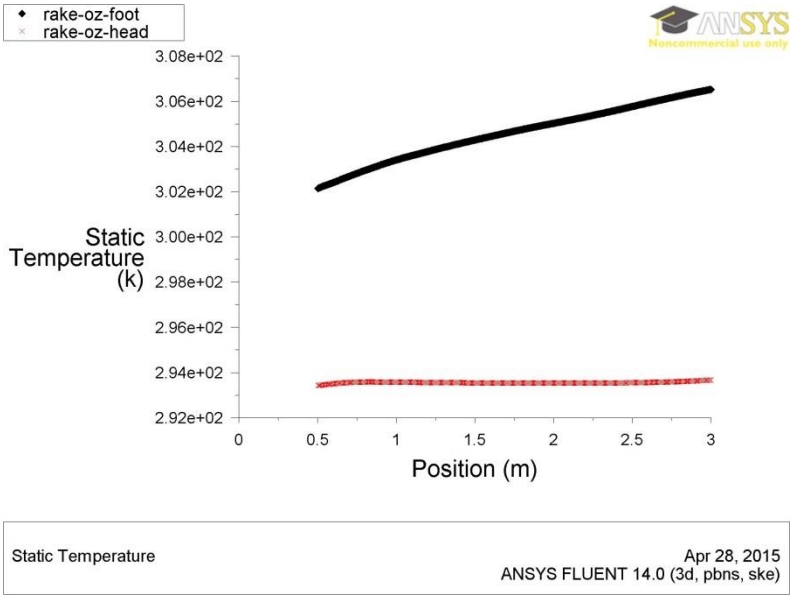

Figure 7.15: Head and foot plane temperatures under 0.15 PV transparency level

Figure 7.15 shows the temperature distribution for the head and foot planes horizontally along the model width. The temperature of the foot plane is higher than the head plane since the former is directly absorbing the heat from the floor with a highest temperature around 33.37^{0}C and the lowest temperature of 28.98^{0}C whilst the maximum temperature of the head plane is approximately 20.51^{0}C and the minimum is 20.26^{0}C. Thus, the temperature of horizontal depth of the room is comfortable at head level.

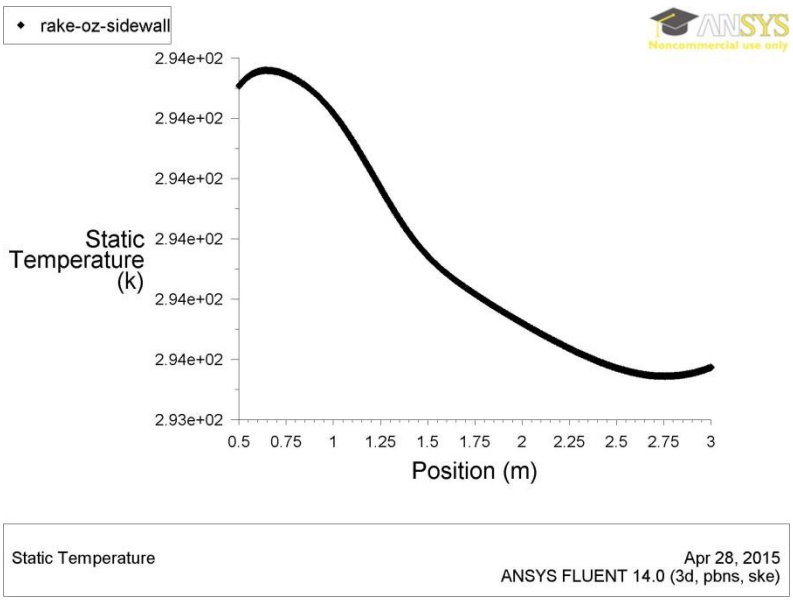

Figure 7.16: Side wall plane temperatures under 0.15 PV transparency level

Figure 7.16 shows the thermally accepted temperature distribution for the sidewall plane horizontally along the model width where the temperature of the side wall plane varies between 20^0C and 21^0C temperature value from the nearest point to the window to the back of the occupied zone.

7.3.2 PV TRANSPARENCY LEVEL OF 0.2

The results given in Figure 7.17 represent the temperature distribution for the back and front planes vertically as a function of the space height. For the lowest point of the occupied zone, the temperature of the front plane is relatively higher than the temperature of the back one since it receives direct solar radiation from the window with an approximate temperature of 24.55^0C and 17.98^0C for the highest point of the zone whereas the peak temperature of the back plane is approximately 21.52^0C and the minimum is 17.55^0C.

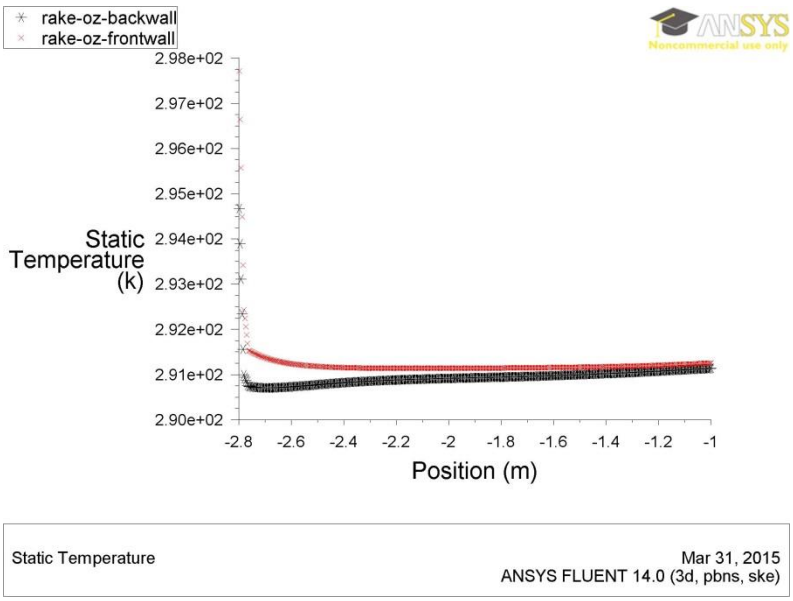

Figure 7.17: Front and back plane temperatures under 0.2 PV transparency level

Figure 7.18 shows the temperature distribution for the head and foot planes horizontally as a function of the zone width. The temperature of the foot plane is in its highest at the nearest point to the window an approximate temperature of 24.55^{0}C and the lowest temperature of 21.52^{0}C at the farthest point from the window whilst the maximum temperature of the head plane is approximately 18.1^{0}C and the minimum is 17.98^{0}C. Thus, the temperature of horizontal and vertical depth of the room can bring the space into a thermally adequate level for the occupants. In contrary, both points of the sidewall plane, the nearest and the farthest from the window along the zone width, are roughly restricted to an approximate temperature value of 18^{0}C as shown in Figure 7.19.

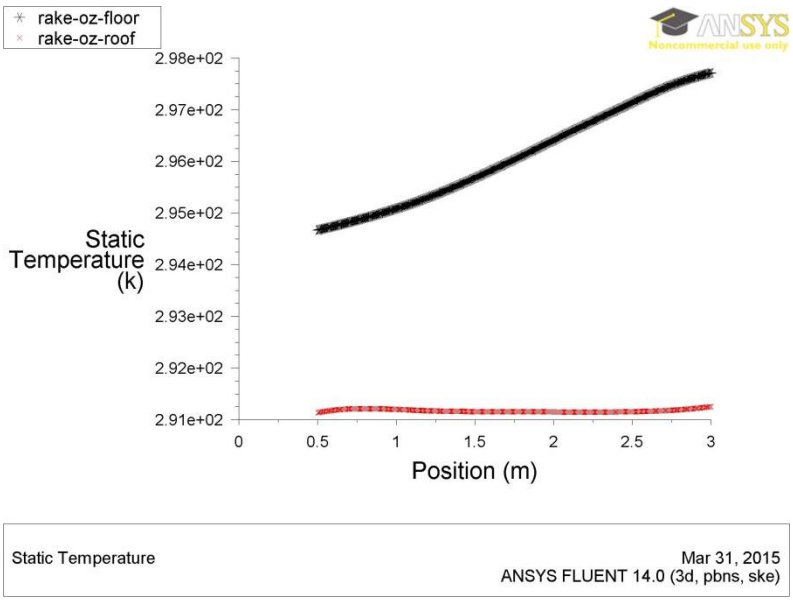

Figure 7.18: head and foot plane temperatures under 0.2 PV transparency level

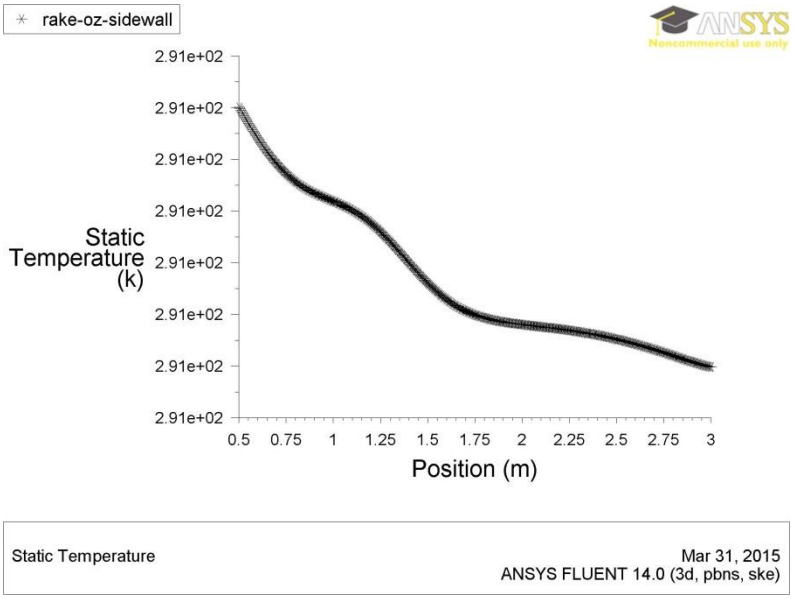

Figure 7.19: Side wall plane temperatures under 0.2 PV transparency level

7.3.3 PV TRANSPARENCY LEVEL OF 0.25

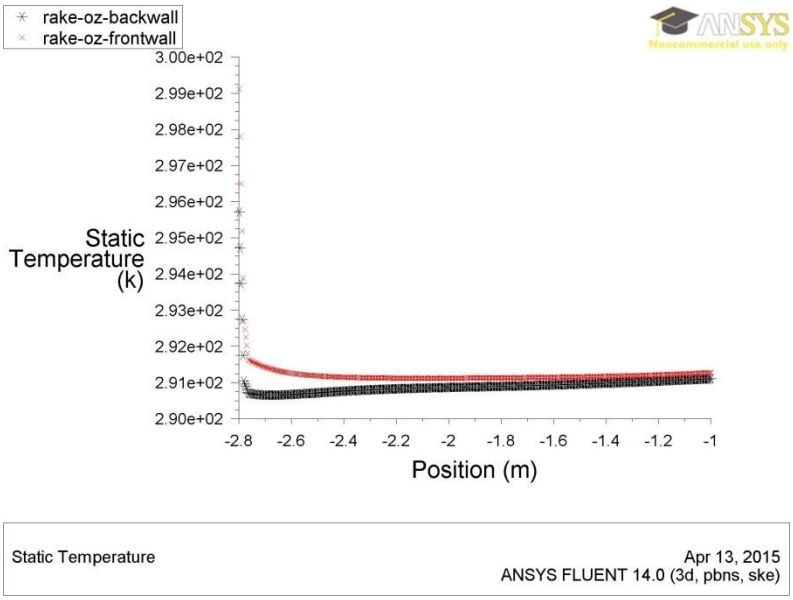

Figure 7.20: Front and back plane temperatures under 0.25 PV transparency level

The temperature distribution for the back and front planes vertically along the space height is presented in Figure 7.20. Being close to the window, the temperature of the front plane is slightly higher than the back one. However, the temperatures of both planes are thermally adequate that falls into the range between 17.5-25.95^{0}C with a highest temperature approximately of 25.95^{0}C and the minimum temperature of 17.97^{0}C for the front plane and the highest of 22.56^{0}C and the minimum is 17.5^{0}C for the back plane.

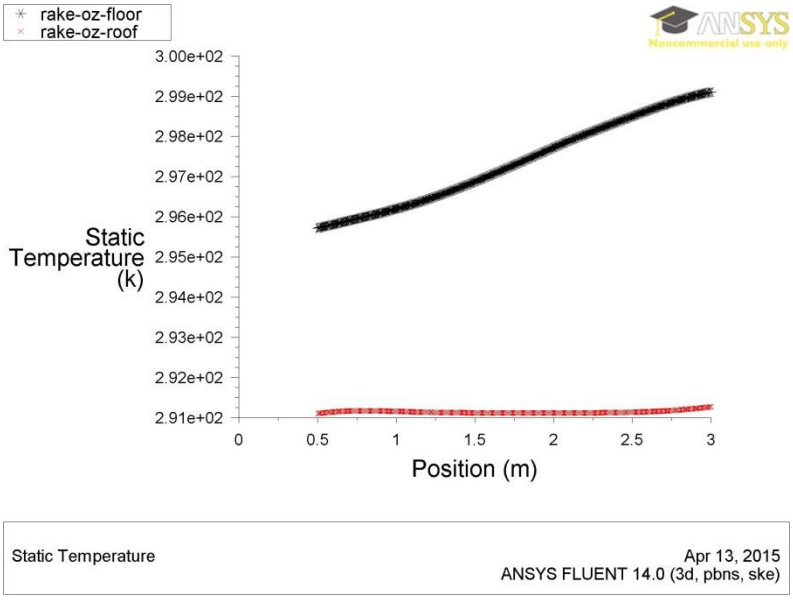

Figure 7.21: head and foot plane temperatures under 0.25 PV transparency level

The temperature distribution for the head and foot planes horizontally along the room depth is shown in Figure 7.21. The temperature of the foot plane is higher than the head plane with a maximum temperature of 25.95^{0}C and the minimum temperature of 22.56^{0}C whereas the highest temperature of the head plane is approximately 18.12^{0}C and the minimum is 17.94^{0}C. Thus, the occupied zone planes achieve the required thermal comfort inside the space.

The temperature distribution for the side wall plane horizontally along the space width is shown in Figure 7.22. It shows that from the nearest point to the window to the back of the occupied zone the temperature of the side wall plane is restricted to a value of approximately 18^{0}C.

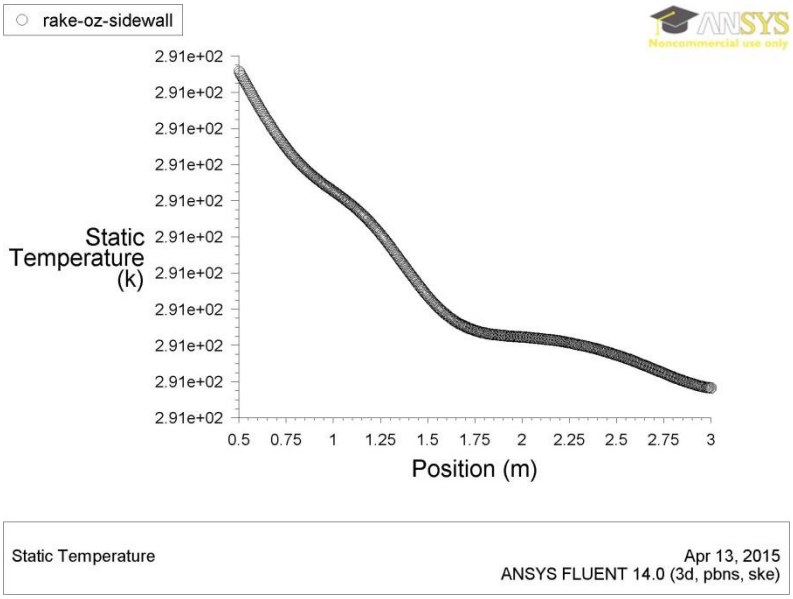

Figure 7.22: Side wall plane temperatures under 0.25 PV transparency level

7.3.4 PV TRANSPARENCY LEVEL OF 0.3

Figure 7.23 compares the temperature predictions of the front and the back planes of the occupied zone vertically from their bottom to their top. A slight deviation between the two temperatures can be noticed since the front plane is being close to the window which allows excessive solar radiation to be received. However, the temperatures of the back plane are thermally adequate as they fall into the range between 17.45-23.58^{0}C whilst they do into the range of 17.98-27.26 for the front plane which consider as partially overheated and mostly comfortable.

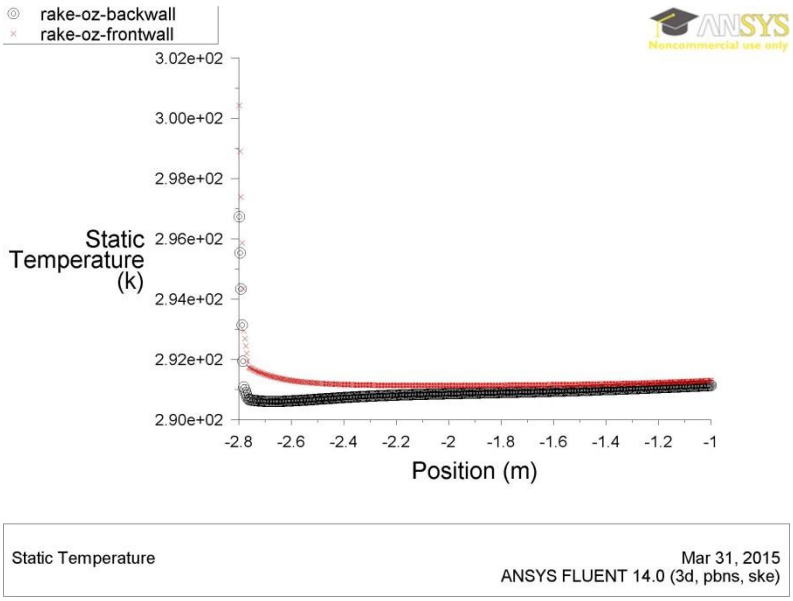

Figure 7.23: Front and back plane temperatures under 0.3 PV transparency level

Figure 7.24 compares the temperature performance for the head and foot planes horizontally from the back offset to the window offset that represents the occupied zone. It can be seen that the temperatures of the foot plane relatively deviate from the head temperatures with a difference of 9^0C. This can be explained by the fact that foot plane is absorbing most of the incident solar radiation coming from the window causing the plane to be excessively heated with temperatures range of 23.58-27.26^{0}C. Though, the head plane is still left cold with temperatures ranging in 17.96-18.14^{0}C.

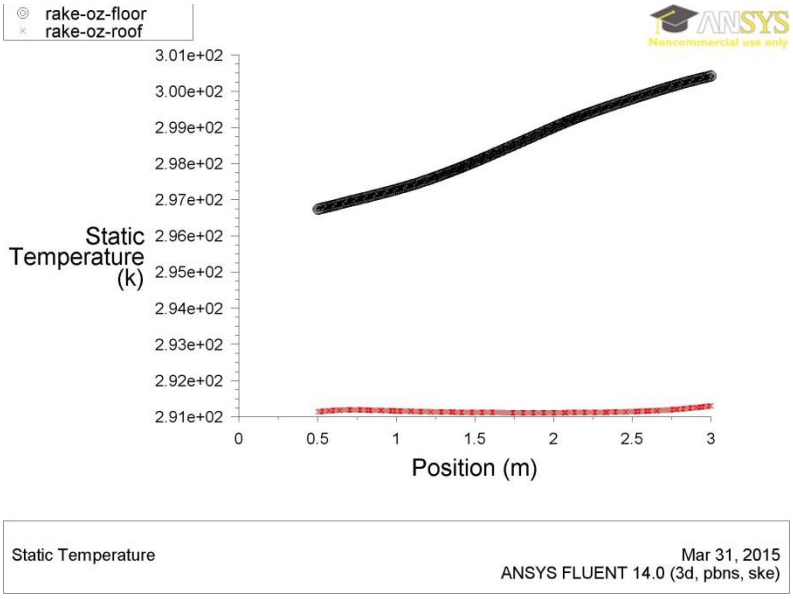

Figure 7.24: Head and foot plane temperatures under 0.3 PV transparency level

The temperature distribution for the side wall plane horizontally along the space width is shown in Figure 7.25. It shows that from the nearest point to the window to the back of the occupied zone the temperature of the side wall plane is ranging between temperature values of 17.95^{0}C and 18.04^{0}C.

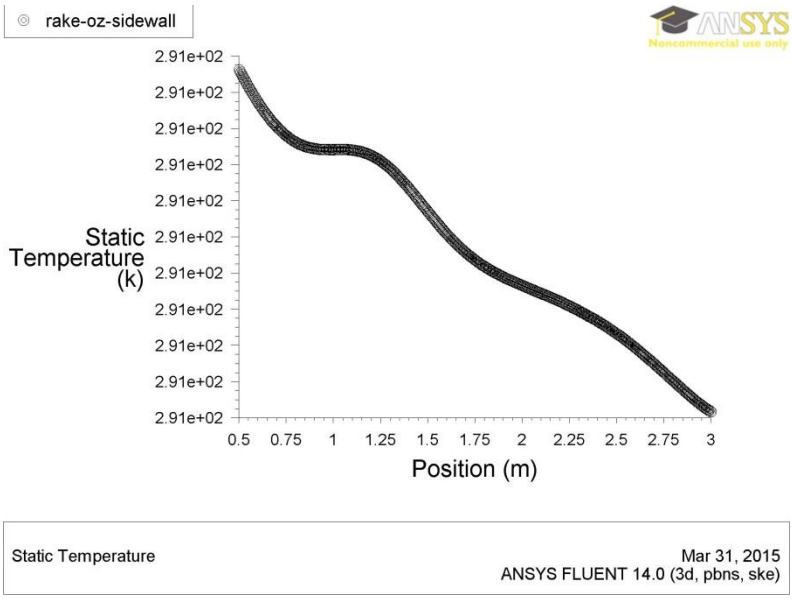

Figure 7.25: Side wall plane temperatures under 0.3 PV transparency level

7.3.5 PV TRANSPARENCY LEVEL OF 0.35

The temperature distribution for the back and front planes vertically along the space height is presented in Figure 7.26. The direct expose to the window and the high level of PV transparency has increased the temperature of the front and the back planes where the front plane temperature is relatively higher than the back plane as both temperature magnitudes range between 17.97-29.06^{0}C with a highest temperature approximately of 29.06^{0}C and the lowest temperature of 18.65^{0}C for the front plane and the maximum of 24.01^{0}C and the minimum is 17.97^{0}C for the back plane.

The same is true for the temperature distribution of the head and foot planes horizontally along the room depth shown in Figure 7.27 where the temperature of the foot plane is higher than the temperatures of the head plane with a maximum temperature of 29.06^{0}C and the minimum temperature of 24.01^{0}C whereas the highest temperature of the head plane is approximately 18.69^{0}C and the minimum is 18.59^{0}C due to the buoyancy effect on the floor and the insulation of the head.

However, the temperature of horizontal width of the room is ranging from 18.59-29.06^{0}C and it is regarded for occupants as thermally uncomfortable. Figure 7.28 shows the temperature magnitude for the sidewall plane horizontally along the space width. It can be observed that from the nearest point to the window to the back of the occupied zone the temperature of the sidewall plane is roughly constant to 18.9^{0}C. The maximum and the minimum temperature values for each plane of the occupied zone under the impact of each PV transmittance were tabulated below in Table 7.2 for comparison.

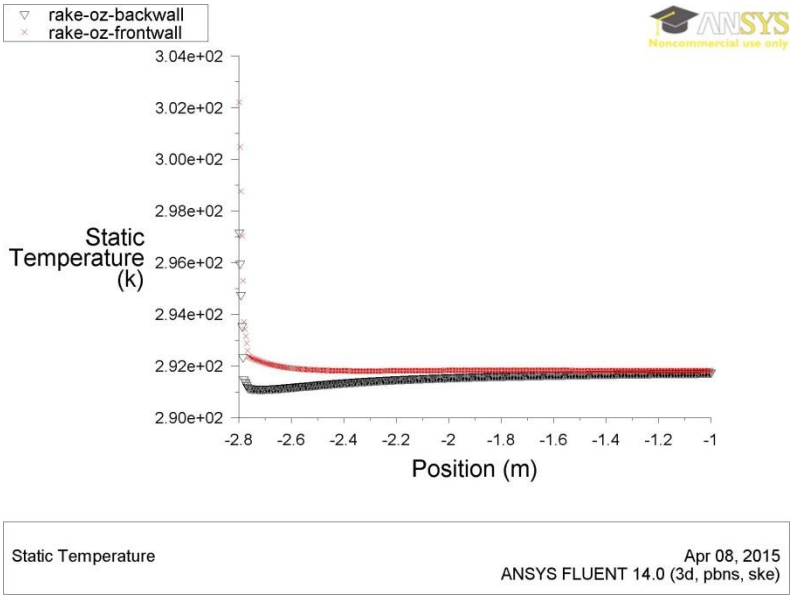

Figure 7.26: Front and back plane temperatures under 0.35 PV transparency level

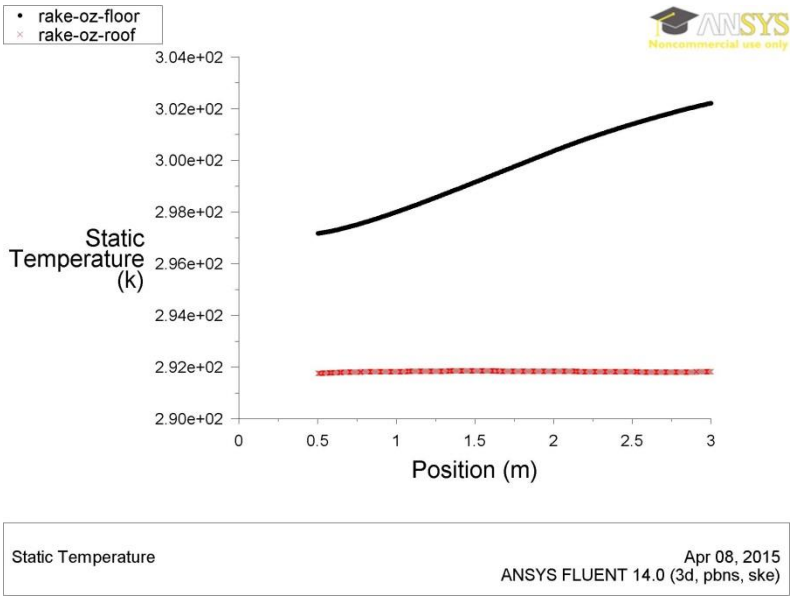

Figure 7.27: Head and foot plane temperatures under 0.35 PV transparency level

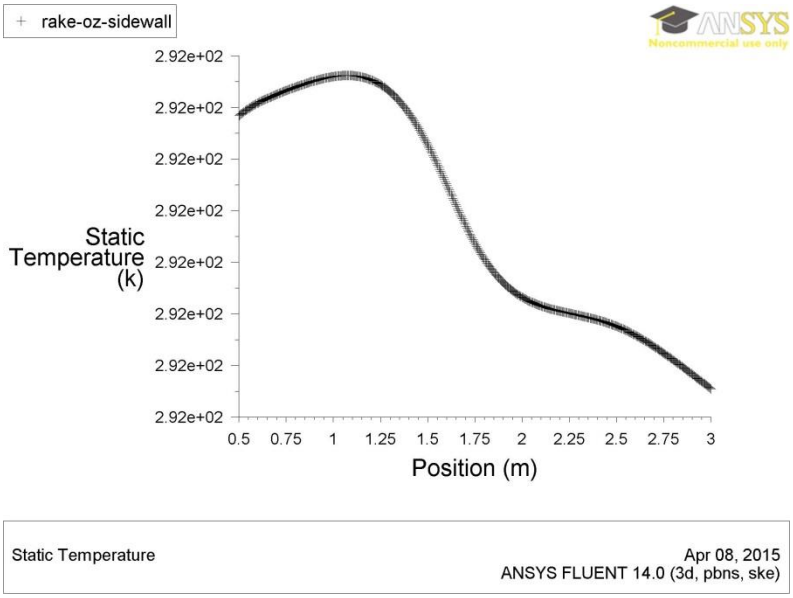

Figure 7.28: Sidewall plane temperatures under 0.35 PV transparency level

Table 7.2: Maximum and minimum temperatures of the occupied zone planes under different PV transparency levels due to the heating season

Transparency Levels	Occupied Zone Planes									
	Front plane		Back plane		Foot plane		Head plane		Sidewall plane	
	min	max	min	max	min	max	min	max	min	max
0.15	20	33	20	29	29	33	20	21	20	20
0.2	**18**	**25**	**18**	**22**	**22**	**25**	**18**	**18**	**18**	**18**
0.25	18	26	18	23	23	26	18	18	18	18
0.3	18	27	17	24	24	27	18	18	18	18
0.35	19	29	18	24	24	29	19	19	19	19

7.4 COMPARISON BETWEEN DIFFERENT PV TRANSPARENT LEVELS

Figure 7.29 offers temperature distributions for the symmetry plane of the five PV transparent degrees: 0.15, 0.2, 0.25, 0.3 and 0.35. It can be seen that 0.15 transparency level is the only one that does not bring the interior space into the thermally accepted quality without additional heat input where the temperature distributions of the symmetry plane, under its effect, range between 17^0C and 19^0C horizontally as a function of the space width. However, the other degrees of PV transparency can achieve the required standard with temperature values that range between 20^0C and 21^0C. The transparent values of 0.2 and 0.25 offer relatively similar

temperature performance inside the space represented for the symmetry plane with a minimum temperature of 17^{0}C for the farthest point from the window to 20^{0}C for the nearest pint from the window, for both transparency degrees, horizontally along the room width. Likewise, the temperature distributions for the symmetry plane under the impact of 0.3 and 0.35 PV transparencies can satisfy the required thermal level as a minimum of 17^{0}C and 18^{0}C for 0.3 and 0.35, respectively, at the back wall of the room and 21^{0}C as a maximum for both transparencies for the front wall of the space where the solar radiations are allowed.

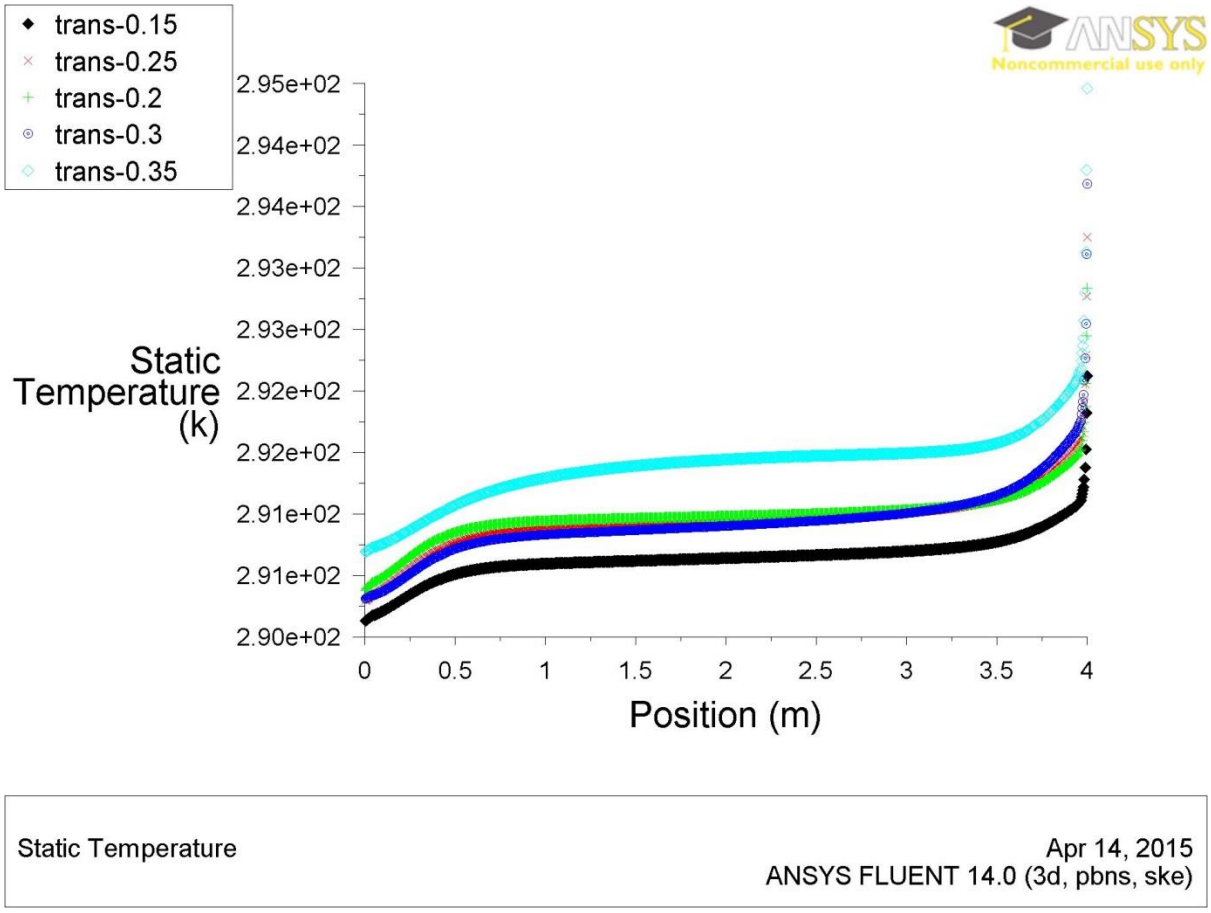

Figure 7.29: Symmetry plane temperatures under the effect of each PV transparent level

7.5 PV PANEL ELECTRIC ANALYSIS

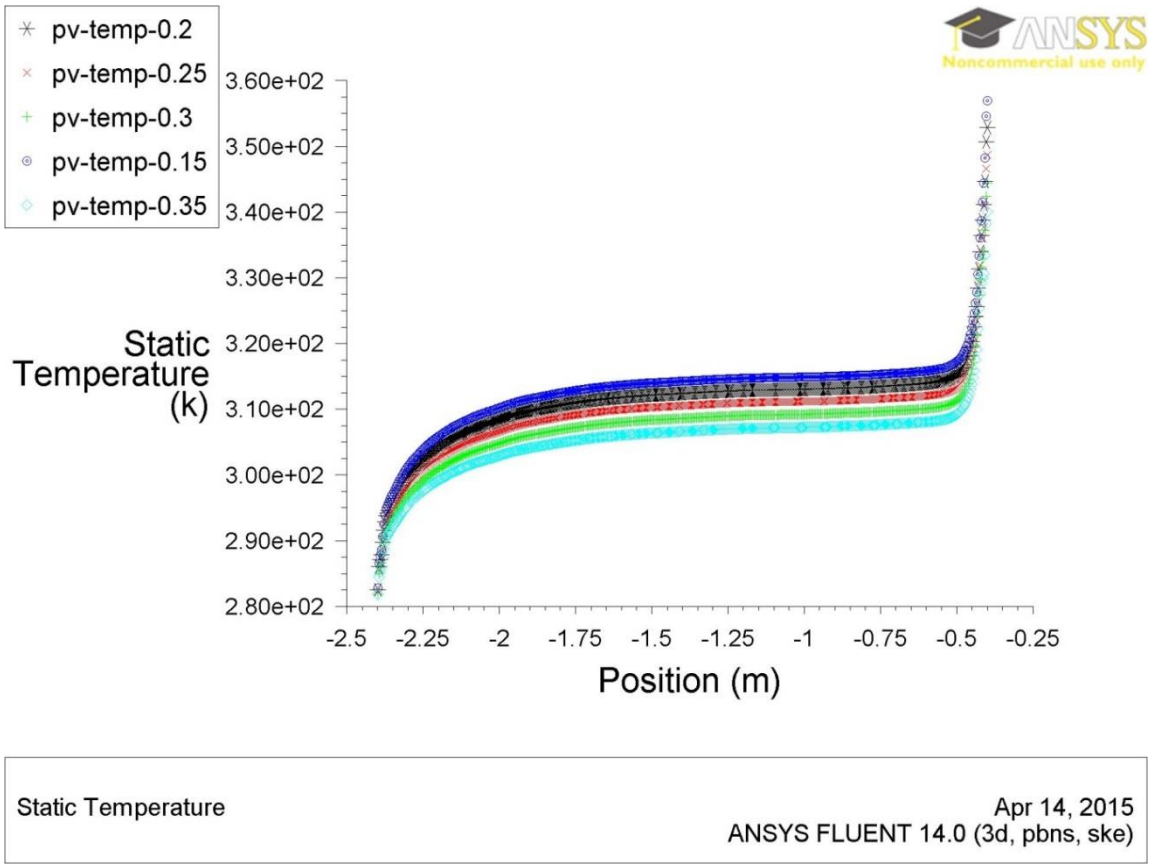

Figure 7.30: average PV temperatures under the effect of each transparent level

Since the necessity of performing PV electric analysis is pivotal as concluded previously, a rake was created in the centre of the panel along the vertical depth in order to predict the PV temperature with each transparent value. The electric performance of a PV is dependent on both cell temperature and solar radiation. Figure 7.30 presents the temperatures along the rake, from the bottom to the top of the panel, under the effect of each transmittance. It can be seen that the less transparent value is employed, the higher PV temperature is gained and the lower interior temperature is attained and vice versa. That is interpreted as high transparent level allows more heat to pass across the panel to the inside space whilst the low transparent value enables the PV panel to absorb most of the heat transferring through the panel.

7.5.1 POWER GENERATION MODEL

An amorphous silicon solar cell type PV single panel was accounted in the PV system proposed in this study due to its semi-transparency for the application to windows and overall façade. It is rather has been developed, by Sanyo Electric Co., Ltd, to a high level of efficiency and transparency and it is called the see-through a-Si solar cell (Takeoka et al. 1993). It is well known that most of the solar radiation absorbed by a photovoltaic panel is a factor of increasing the module temperature. Thus, a reduction in the power output of the solar cell is related to the transmittance of the solar cell (Takeoka et al. 1993). Calculation models and important parameters on power generation will be discussed for the PV cells efficiency calculation. For a semi-transparent PV cells efficiency calculation the model used in Miyazaki et al. (2005) is given by the following equation:

$$P = G\,\eta\left\{1 - K\,(T_c - 25)\right\} \qquad 7.1$$

It calculates the electricity output, P, from the electricity conversion efficiency, η, the temperature coefficient of power output, K, the solar cell temperature, T_c, and the solar cell radiation, G.

Since the calculation pf the PV electricity output corresponds to material and optical properties of the semi-transparent PV panel, a review of the literature has been done to obtain the most appropriate parameters of for the calculation. Parameters such as the transmittance of the clear glass layer is given by the photovoltaic manufacture and it was used in Miyazaki et al. (2005) and Wah et al. (2005) as 0.774. However, the temperature coefficient of power prediction varies based on the type of the PV, and it is listed in (Evans 1981) and since the assumed PV model is amorphous silicon single glass, the coefficient used was $0.0025^{0}C^{-1}$, and it was used in Yamawaki et al. (2001) and Wah et al. (2005). For the rest of the parameters, they were assumed and discussed previously according to the study aims and objectives

The effect of each transmittance value on the PV panel temperature and the output of electricity have been translated into average temperatures, as a function of the panel height along a centred rake, and amount of electric generation, Table 7.3, to find out the most suitable transmittance criteria that enable the PV cells to work efficiently. From the Table 7.3, it appears that each PV transparent degree is able to maintain the PV temperature as moderated with averages that don not exceed 30^0C in winter which is reasonable for PV efficiency. However, the more transparent the PV is the less solar radiation the PV can absorb and the lower PV temperature will be.

It can be drawn that the PV panel, under the effect of the 0.35 transparency level, can function efficiently since this transparent value allows most of the heat transfer through the panel and maintain its cells with low temperature which in turn increase the PV efficiency level, however, the amount of heat that pass through can excessively increase the interior temperature and minimize the electricity generation of the PV cells that essentially rely on the solar absorption. Thus, considering the daylighting analysis will be a crucial step for determining the most suitable PV transparent level for the airflow window during the heating season.

Table 7.3: Average PV temperatures under different transparency levels and electricity output

	PV power parameters, temperature, and electricity output				
τ_p	**0.15**	**0.2**	**0.25**	**0.3**	**0.35**
A_p	4.76	4.48	4.2	3.92	3.64
$G_P$winter	158.45	147.13	135.81	124.5	113.18
$G_P$summer	120.65	112.03	103.42	94.8	86.18
α_p	0.7	0.65	0.6	0.55	0.5
Average PV temperature winter (^{0}C)	**29**	**28**	**26**	**25**	**24**
Average PV temperature summer (^{0}C)	**45**	**44**	**43**	**42**	**41**
Electricity output winter(W/m^2)	7.84	7.30	6.77	6.23	5.67
Electricity output summer(W/m^2)	5.72	5.32	4.93	4.53	4.13

7.6 PV PANEL DAYLIGHTING ANALYSIS

The necessity for the daylighting analysis has urged to utilize a computer tool that can demonstrate each transparent value implications on the PV panel and the interior space. ECOTECT was applied to estimate the indoor illuminanace levels and daylight

factors and capture the impact of each transparent degree of the PV panel when equipped with the airflow window for the office space. A model was created inside ECOTECT, shown in Figure 7.31, and the daylight factors were predicted as an initial design parameter under each transparency (0.15, 0.2, 0.25, 0.3, and 0.35) for points that aligned with the centre of the window along the space width. The average daylight factor required for general office space is 2 per cent as minimum value (CIBSE 2006), however, the average daylight factor can also be calculated as follows:

$$D = 0.1\,P \qquad 7.2$$

where:

D = Daylight factor

P = Percentage glazing to floor area

As such, the average daylight factor for the interior space of the office model is estimated to be: $D = 2.8\%$

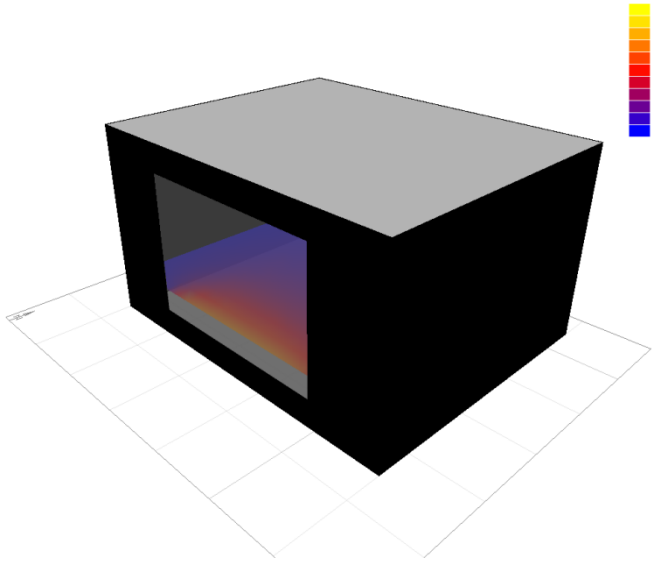

Figure 7.31: Office space model inside ECOTECT

7.7 PV PANEL TRANSPARENCIES DAYLIGHTING EFFECT

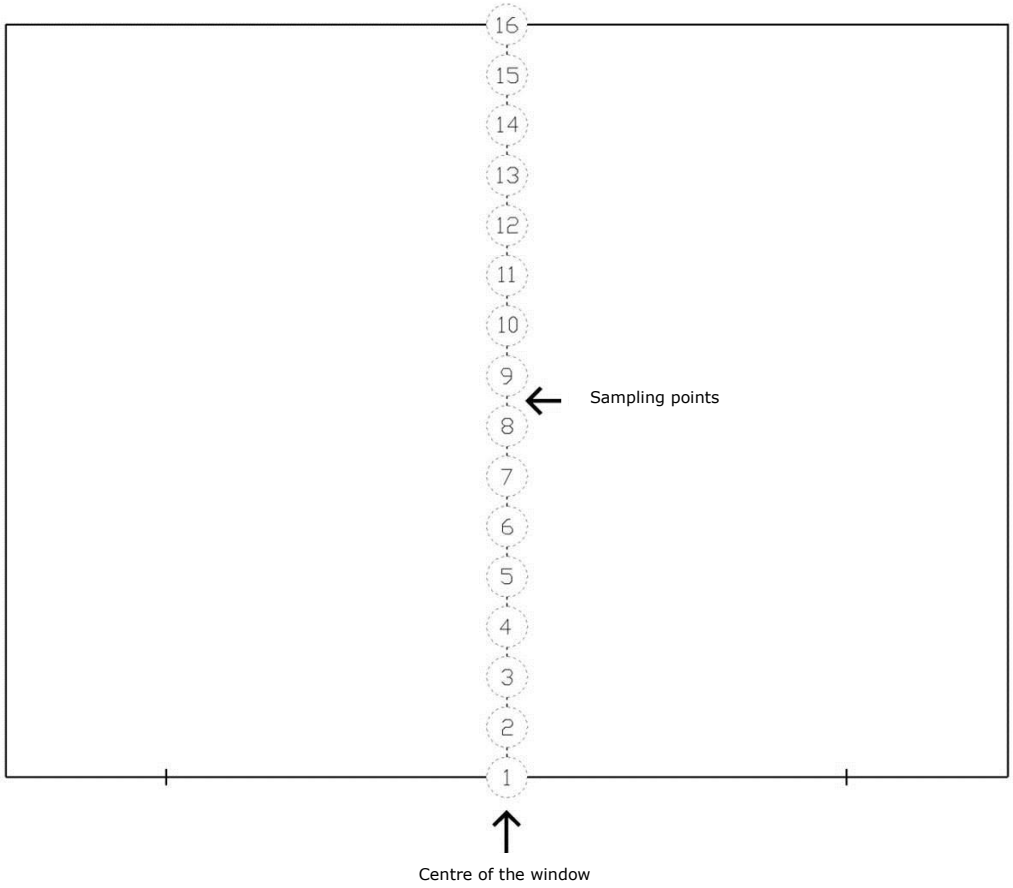

Figure 7.32: Sampling points along the depth of the room aligned with the centre of the window

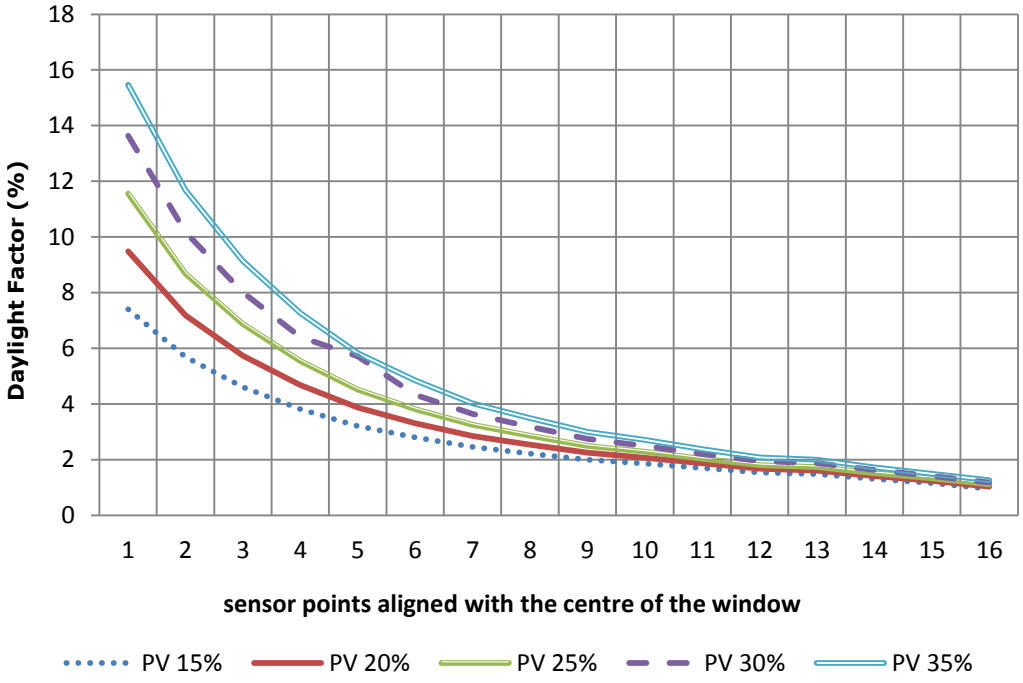

Figure 7.33: Comparison of the daylight Factors for different PV transparency levels

Table 7.4: Daylight Factor Predictions of Different Transparencies

PV transparency level (%)	15	20	25	30	35
Sampling Points	**Daylight factor (%)**				
1	7.41	9.49	11.56	13.64	15.72
2	5.69	7.19	8.68	10.18	11.68
3	4.61	5.74	6.88	8.01	9.14
4	3.82	4.68	5.54	6.41	7.27
5	3.21	3.87	4.52	5.71	5.83
6	2.80	3.31	3.82	4.34	4.85
7	2.46	2.85	3.25	3.64	4.03
8	2.22	2.54	2.86	3.18	3.50
9	2.00	2.25	2.50	2.75	3.00
10	1.86	2.07	2.29	2.5	2.71
11	1.70	1.87	2.04	2.21	2.38
12	1.54	1.68	1.81	1.95	2.08
13	1.48	1.61	1.74	1.87	2.00
14	1.31	1.42	1.52	1.63	1.73
15	1.16	1.24	1.33	1.42	1.50
16	0.95	1.03	1.11	1.19	1.27
Daylight factor average (%)	**1.96**	**2.29**	**2.62**	**2.95**	**3.28**

The sampling points were defined along the depth of the room and aligned with the centre of the window with an interval of 0.25m, presented in Figure 7.32, in order to read the daylight factors of the interior space under the effect of each transparent level. The behaviour of the daylight factors of each transparent degree is shown in Figure 7.33. It appears that similar trends of daylight factors of each transparency are produced demonstrating a maximum value from the nearest point to the window, where the solar incidence is transferred, with a gradual decrease to the far end of the room. However, the daylight factors of each value are different, as listed in Table 7.4, where the higher transparent value is applied; the higher daylight factors are attained. The most suitable transparent degree is the one that meets the minimum required daylight factor for the space. The average daylight factor for the values 0.15, 0.2, 0.25, 0.3, and 0.35 are 1.96 per cent, 2.29 per cent, 2.62 per cent, 2.92 per cent, and 3.28 per cent respectively.

As a consequence, all of the transparencies are in compliance with the required average daylight factors since they produced more than the minimum required value except the 0.15 degree which its performance is below the standard; yet, the 0.2 and 0.25 degrees are the most suited levels because they combine both comfortable visual and thermal aspects.

7.8 SUMMARY

An occupied zone was defined within the model interior to attain idealised results for the collective buoyancy and mechanical driving forces employing variable PV transparencies to carefully ensure a thermally accepted area for the occupants. From what has been illustrated above, each PV transparency supplied the interior space with different amount of heat that kept the occupied zone either thermally suitable or overheated. The PV transparency of 0.2 was the only degree that satisfied the required level of thermal comfort; yet, the 0.25 transmittance has attained similar thermal performance with one temperature degree above the thermal standard. However, overheating was prominent with the rest of the transmittance values inside the space. Thus, daylighting and thermal analyses essentially needed to be performed for the PV panel with each transparent value to identify the most suitable transparent degree for the room interior that combines thermal and visual comfort.

Therefore, visual and thermal analyses were performed for the PV panel under the effect of five different degrees of transparencies: 0.15, 0.2, 0.25, 0.3, and 0.35 in order to distinguish the transmittance that achieves the optimum comfort of visual and thermal level for the interior space and maintain the PV sheet in a moderate temperature for an efficient performance. The previous discussion reveals that each level of transparency can be either thermally comfortable or uncomfortable to the room occupants providing the interior with different temperature degrees that reach up to 29^0C. Though, the PV cells can function effectively with the PV transparent values of 0.15, 0.2, and 0.25 since they reach up to 29^0C with the lower transparent degree of 0.15 and decrease gradually with higher levels. However, the transparent

levels of 0.2 and 0.25 are distinguished with maintaining the inside environment visually and thermally comfortable for the occupants as they achieve more than the minimum requirements of the daylight factors for the office room, two per cent whereas the 0.15 transparent value leaves the interior slightly lit. Thus, for the time of simulation (noon time) the degrees of 0.2 and 0.25 transparency are the appropriate transparent levels to be specified for the PV panel that encompasses the features of optimising the PV performance, and guaranteeing the space occupants visual and thermal comfort and most commensurate of all, the PV transmittance of 0.2 is ideal as it allows the PV to generate greater electric power. It must be taken into account that the optimum PV levels found will function only for the design provided, however, the other PV transparencies are applicable if design alteration was considered and the diffuser of the space was directed the air to the occupants.

Having fulfilled the optimization of the system according to the winter season, next chapter will proceed for the analysis and design optimization under the effect of summer conditions.

CHAPTER 8 ANALYSIS AND DESIGN OPTIMISATION FOR SUMMER SEASON

8.1 INTRODUCTION

This chapter continues the CFD analysis for the airflow window unit with identical procedure of the previous chapter except that it predicates on the summer weather conditions to find the most suitable driving force and PV transparency level for summer cooling period.

Three ventilation forces: mechanical ventilation only, buoyancy ventilation only, and combined mechanical and buoyancy force, have been implemented to distinguish the most appropriate ventilation force for the airflow window unit during the cooling season for achieving thermal comfort and adequate ventilation rate. For the mechanical force and the combination of both forces, a fan speed of 0.5m/s was used as a base air velocity for airflow window at a window height of 2m and thickness of 0.15m.

8.1.1 MECHANICAL VENTILATION ONLY

Figure 8.1 shows the mechanical ventilation force effect on the air velocity magnitude inside the space during the summer season. The moderated ambient air, with a degree of 24^0C, flowed into the room from the aperture at the bottom of the back wall of the room forming an air movement throughout the interior and flowing to the outside through the opening of the window unit at the bottom of its cavities. It can be noticed that adequate air movement is achieved inside the space with a predominant air velocity of 0.2m/s and a flow rate of 76.5L/s. Furthermore, the speed of the air flow is increasing gradually, between the window cavities, and contributes in the removal of the accumulated heat, behind the PV panel, that may hinder its efficiency.

Likewise, Figure 8.2 presents the mechanical-driven ventilation flow impact on the temperature distributions throughout the office model the office simulation model. It can be seen that the incoming air flow temperature of 24^0C through the inlet opening

at the back wall moves the heat from the floor and elevates the interior temperature to an accepted degree of thermal comfort, 25^{0}C. However, it increases gradually behind the PV panel, but it is still suitable for maintaining the panel efficient.

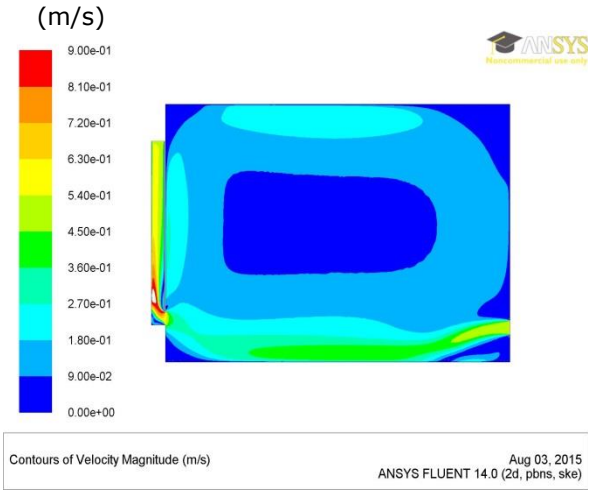

Figure 8.1 :Air flow Pattern

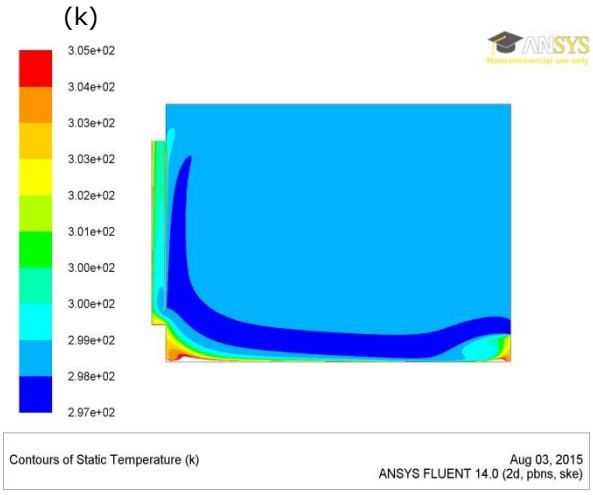

Figure 8.2: Temperature distribution

8.1.2 BUOYANCY VENTILATION ONLY

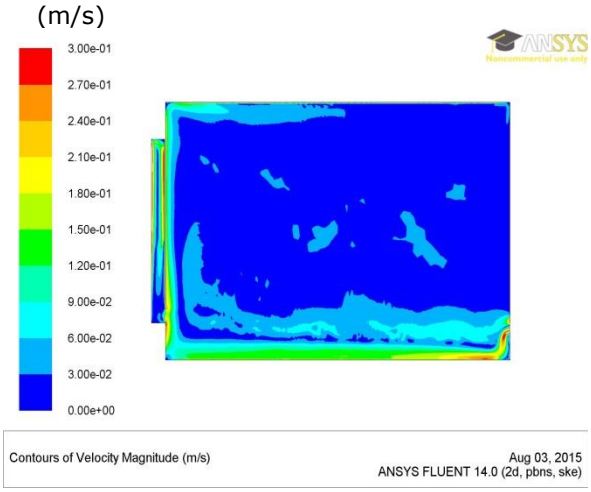

Figure 8.3: Air flow Pattern

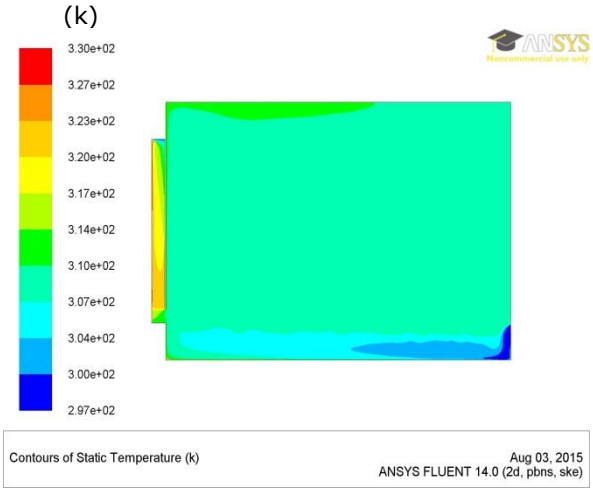

Figure 8.4: Temperature distribution

The air flow pattern of the office model is shown in Figure 8.3 due to the effect of buoyancy ventilation force alone. It is indicated from the figure that the air flow forms a mess up flow magnitude throughout the inside environment. Furthermore, it appears that the force is incapable of driving the flow properly to circulate the air inside the space and vent out the accumulated heat between the window cavities. The same can be observed from the Figure 8.4 that presents the temperature estimations

for the model interior where overheating is dominating the space and behind the PV panel that is impeded from efficient performance.

8.1.3 COMBINED MECHANICAL AND BUOYANCY VENTILATION EFFECTS

The attribution of combining both mechanical and buoyancy driving flows to the air flow pattern inside the office model interior is shown in Figure 8.5. The figure indicates that the air is effective to the occupants' environment throughout the interior with a dominated velocity of 0.15m/s and a flow rate of 79.08L/s. The velocity even becomes faster between the cavities, behind the PV panel, in which the accumulated heat is vented out through the window unit opening at the bottom and grants the PV cells to work efficiently.

Similarly, the induction of collective mechanical and buoyant ventilation flows into the temperature distributions inside the office interior is presented in Figure 8.6. It appears that occupants can feel neutral inside the space which is dominated with a temperature of 25^{0}C, and even it is still effective for the PV cells efficiency where a gradual increase occurs, up to 32^{0}C, between the cavities of the window system. However, and due the addition of the buoyancy force, a gradual temperature increase appears on the top of the space where the temperature escalates to 27^{0}C.

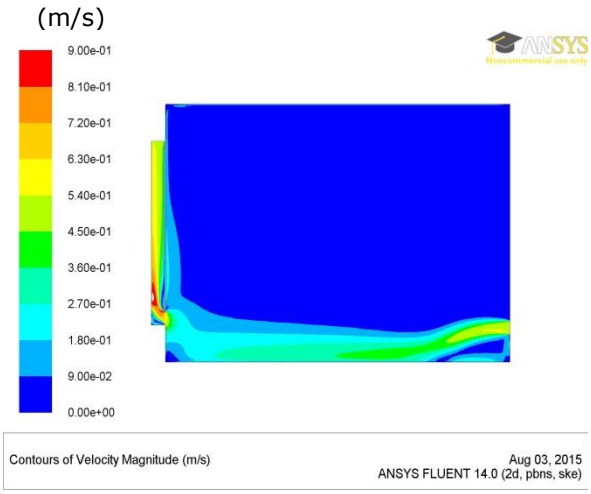

Figure 8.5: Air flow Pattern

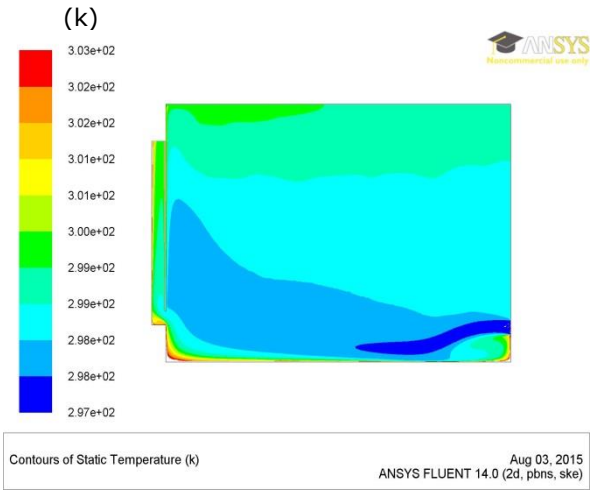

Figure 8.6: Temperature distribution

8.2 COMPARSION OF VENTILATION FORCES

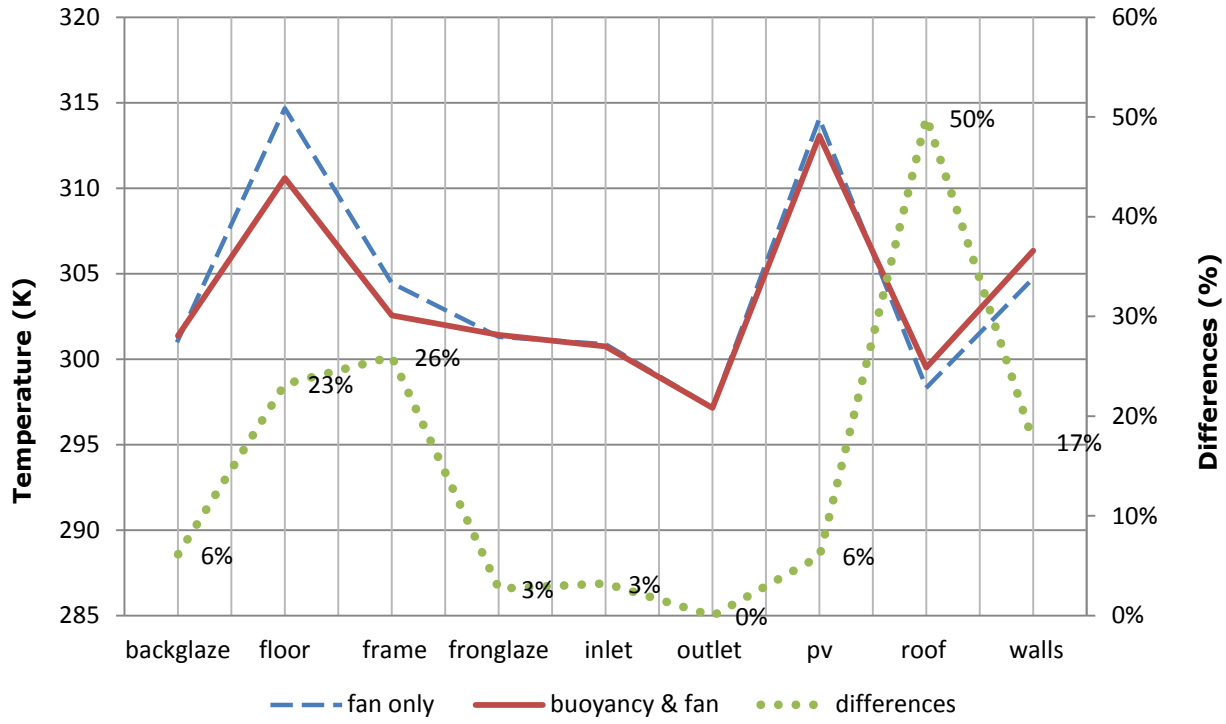

Figure 8.7: The magnitude of the temperature values for fan force only and the combination of buoyancy and fan forces.

The prediction of the mean temperature values of each element of the office model are presented twice in Figure 8.7, first for the attribution of the mechanical-induced ventilation flow, and the second for the attribution of both, mechanical and buoyant, ventilation flows. Furthermore, the percentage errors between those estimations individually for each component are calculated. It is obvious from the figure that both temperature performances are extremely identical except over the floor element where the mechanical ventilation force deviates slightly and the temperature increases with two per cent higher than the temperature under the impact of the combined forces, mechanical and buoyancy, whilst the roof component temperature deviates significantly, under the effect of both forces, and escalates with 50 per cent higher. This can be construed as negative effect, on the indoor flow behaviour, of the buoyancy where it opposes the fan-driven flow and move the indoor heated air, on the floor, upwards to the roof and increases its temperature whilst cools down the

temperature of the floor. Thus, possible overheating on the roof is expected when employing both mechanical and buoyant ventilation forces.

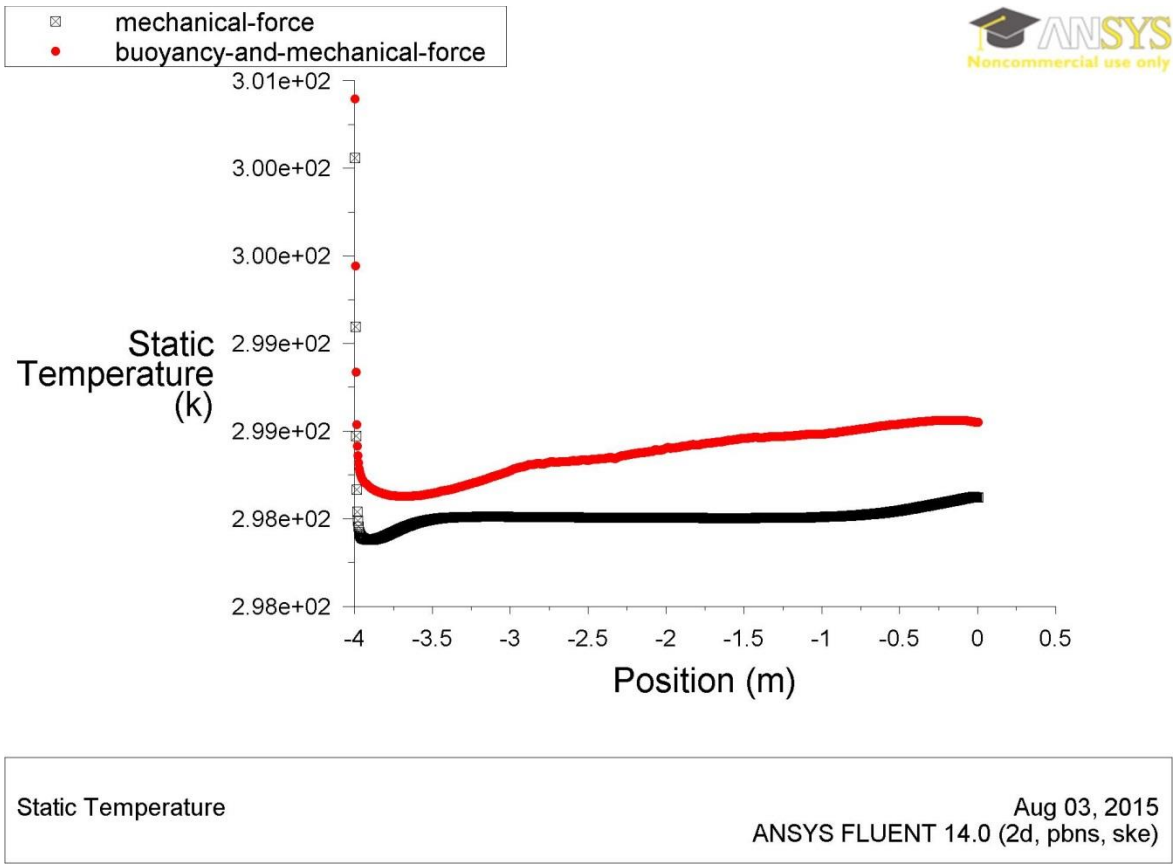

Figure 8.8: Centred rake temperatures under the effect of each ventilation force

Figure 8.8 shows the predicted temperatures for the centred rake that extends horizontally along the model from the window to the back wall across the centre of the occupied zone due to the impact of both attempts of ventilation forces: collective buoyant and mechanical flows, and mechanical flow only. It is indicated from the two temperature trends that both attempts reveal slightly similar performance with negligible differences. It can be perceived as either of attempts can bring the temperature performance inside the interior environment to a comfort level. However, considering the mechanical ventilation force alone can rather optimise the temperature behaviour since it offers lower temperature values near the window and the roof where they become higher with the combined ventilation forces.

The airflow window unit temperature performance under combined buoyant and mechanical ventilation forces during the cooling season inside an office room resided

by two individuals has revealed optimum performance in comparison to other ventilation flows: mechanical only and buoyancy only. Despite applying the combined mechanical and buoyant ventilation forces can drive the air flow to a level that the occupants can feel thermally neutral, the mechanical force alone can be more effective to the comfort level. However, different PV transparencies must be analysed to find out the optimised window system criteria for thermal comfort under the summer conditions.

8.3 EFFECT OF PV TRANSPARENCY LEVELS

The mechanical ventilation force has been shown to be adequate for analysis that optimises the temperature performance of the space under optimum PV transparency level. Thus, the same occupied zone was specified as 0.5m from any wall and 1m from the window with a height of 1.8m where normally the occupants reside, the volume of air is confined by specific horizontal and vertical rakes. The representation of the zone is identified by four rakes (because of the change of model from three into two dimensional since the former has consumed excessive time, due to the limited computational domain used, and it was found there is no difference between the results of each model in Pasut et al. (2012)) as head, foot, back wall, and front wall. Figure 8.9 illustrates the occupied zone within the model and Figure 8.10 presents the centred rake across the occupied zone. Under each PV transparency the area weighted average temperature was calculated for each rake. The variations of the predicted temperatures inside the occupied zone under the effect of the heat passing through PV panel with different transparencies of 0.15, 0.2, 0.25, 0.3, and 0.35 was plotted for each rake of the zone. Table 8.1 shows the PV properties under different transparency degrees during the summer season.

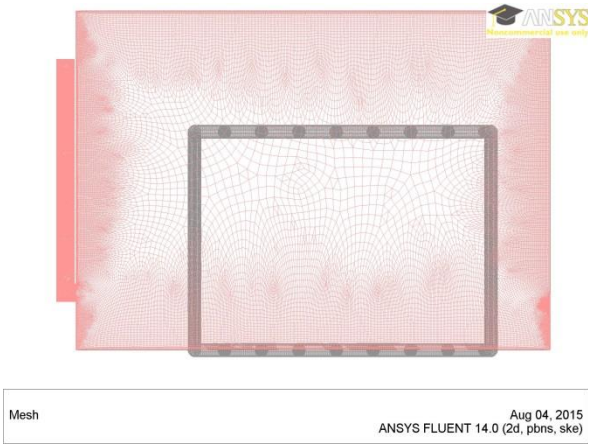

Figure 8.9: The occupied zone within the model space

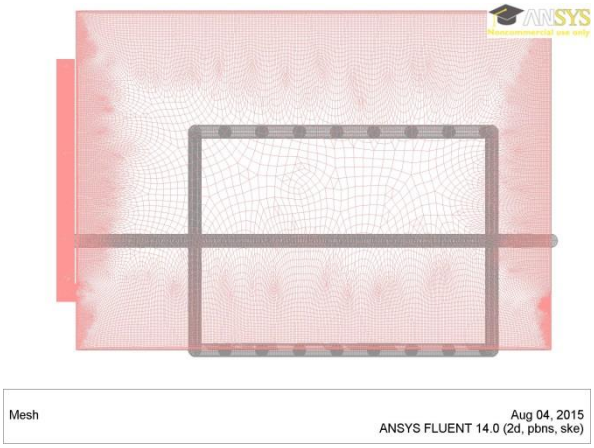

Figure 8.10: The occupied zone within the model space and the middle rake across the zone

Table 8.1: PV Characteristics under different transparency levels for summer season

	Transparency Levels				
PV	**0.15**	**0.2**	**0.25**	**0.3**	**0.35**
Heat Flux (W/m^2)	120.65	112.03	103.42	94.80	86.18
Reflectivity	0.1	0.1	0.1	0.1	0.1
Absorptivity	0.7	0.65	0.6	0.55	0.5
Transmissivity	0.15	0.2	0.25	0.3	0.35
Electricty conversion efficiency	0.05	0.05	0.05	0.5	0.05
Conductivity (W/m k)[2]	169.79	169.79	169.79	169.79	169.79
Density (kg/m^3)[2]	8330	8330	8330	8330	8330
Heat capacity (J/K)[2]	1677	1677	1677	1677	1677
Width (m)	0.0125	0.0125	0.0125	0.0125	0.0125

8.3.1 PV TRANSPARENCY LEVEL OF 0.15

Figure 8.11 shows the estimated temperature performance due to the effect of mechanical ventilation force alone and the PV transparency level of 0.15 during the cooling season. It can be observed that the heat comes from the outside environment through the inlet at the bottom opening in the back of the room with a temperature degree of 24^{0}C and increase inside the space by one degree to dominate the interior with a thermally tolerable temperature degree of 25^{0}C.

[2] Material properties of STPV material (Wah et al. 2005)

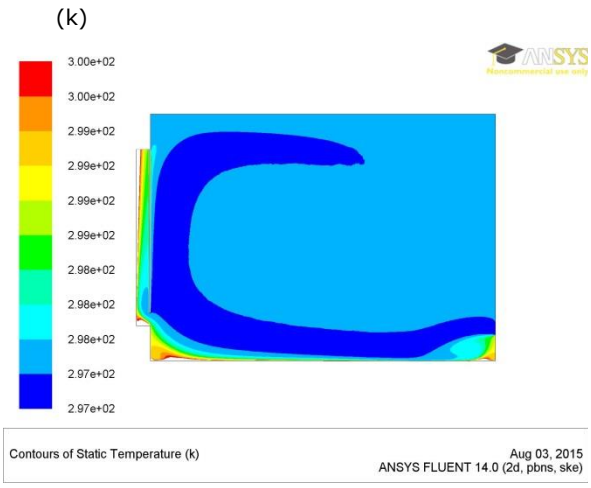

Figure 8.11: Temperature distribution

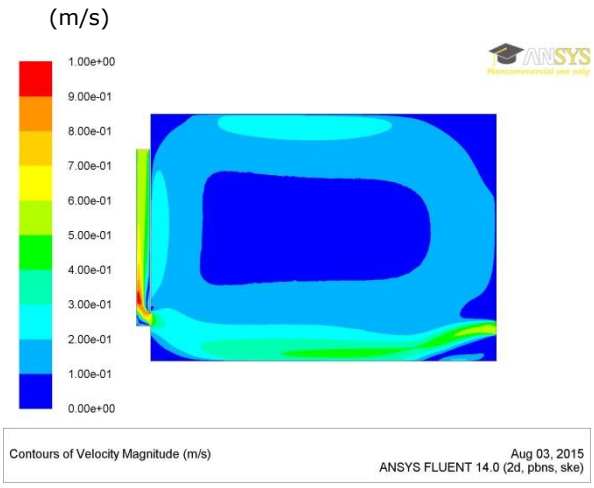

Figure 8.12: Air flow pattern

The air velocity magnitude inside the office space as a function of mechanical-driven flow is presented in Figure 8.12. It shows that the air comes into the inside space through the aperture at the bottom of the back wall of the room with an air velocity of 0.5m/s and decreases gradually until it reaches the window unit opening at the top and increases again gradually to vent out the accumulated heat between the cavities leaving the PV panel in a moderate temperature that enable it to work efficiently. However, the air movement inside the room is circulating adequately throughout the space with a predominant velocity in the range of 0.1-0.4m/s.

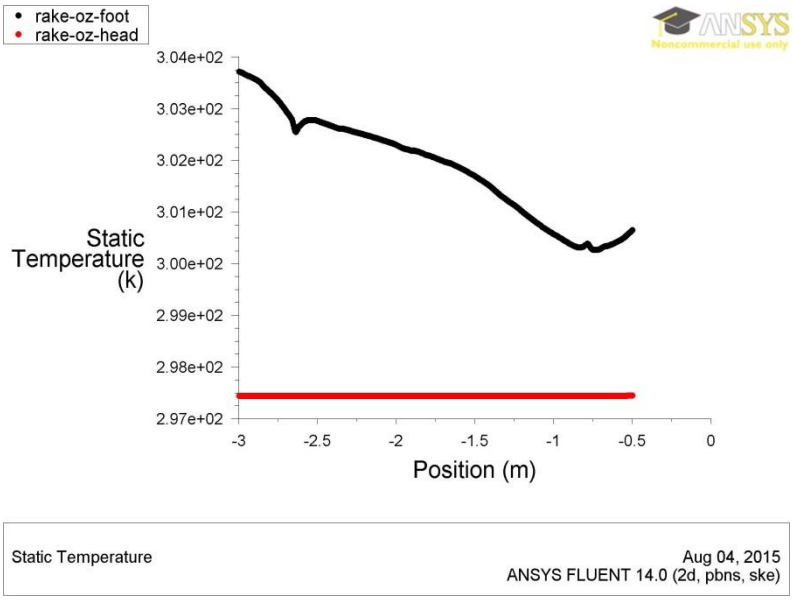

Figure 8.13: Head and foot rake temperatures under PV transparency level of 0.15

Figure 8.13 shows the temperature distribution for the foot and the head rakes horizontally along the occupied zone width. It can be seen that the temperature of the

foot rake is higher than the back one due to its absorption of the sun radiation incidents directly from the window with a maximum temperature approximately of 31^0C and the lowest temperature of 27^0C whereas the peak and the minimum temperatures of the head rake are approximately constant to the degree of 24.29^0C. Thus, the PV transparency level of 0.15 offers thermally accepted environment for the occupants for the horizontal depth of the space where the temperatures range from 24.29-31^0C and an average temperature of the foot rake of 24^0C.

Similarly, the temperature performance for the front wall and the back wall rakes, as presented in Figure 8.14, is thermally uncomfortable for the occupants along the vertical height of the space where the temperature of the vertical depth of the room is ranging from 24 and 31^0C. The temperature of the front wall rake is higher than that of the back wall rake due to the direct exposure to the sun radiation coming from the window that increases its temperature to the maximum of 31^0C and a minimum temperature of 24.22^0C whilst the peak temperature of the back wall rake is 27.5^0C and the lowest temperature is 24^0C. However, the average temperature for both rakes offer comfortable thermal condition with a degree of 24.29^0C.

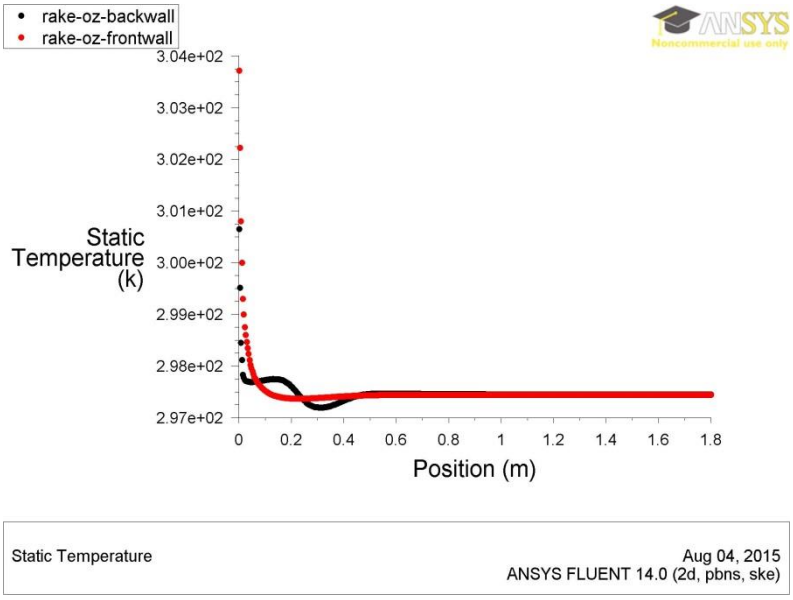

Figure 8.14: Front and back rake temperatures under PV transparency level of 0.15

8.3.2 PV TRANSPARENCY LEVEL OF 0.2

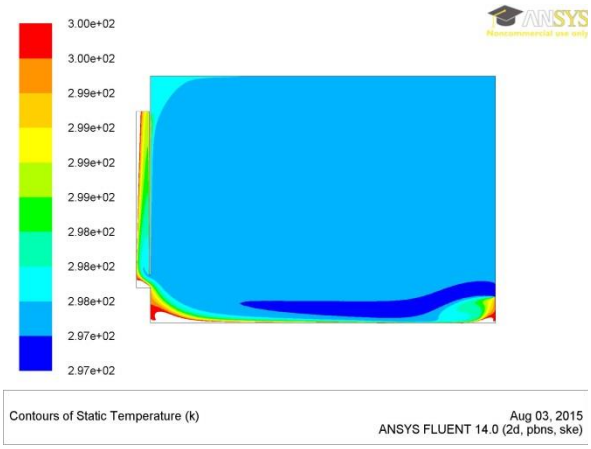

Figure 8.15: Temperature distribution

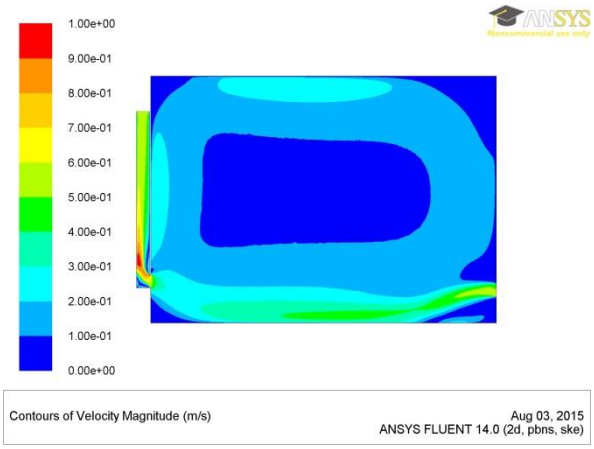

Figure 8.16: Air flow pattern

The predicted temperature behaviour as a function of both mechanical-induced ventilation flow and the PV transparency level of 0.2 during the summer season is presented in Figure 8.15. It can be noticed that the inlet temperature of 24^{0}C at the bottom opening of the back of the room increases one degree throughout the room to become 25^{0}C which is a thermally comfortable temperature for the occupants. However, it increases gradually between the window cavities behind the PV panel to reach up to 27^{0}C that maintains the panel working efficiently.

Figure 8.16 shows the air velocity performance inside the office space due to the effect of mechanical flow and the PV transparency level of 0.20 under the effect of the summer conditions. It can be seen that the air inlet velocity of 0.5m/s at the bottom opening of the back wall of the room decreases gradually whereas circulating throughout the inside space with predominant velocity that range between 0.1-0.4m/s and a flow rate of 76.55L/s. Though, it increases at the top opening of the window cavities to remove the accumulated heat behind the PV panel and maintains it in a moderated temperature level and draws the heat to the outside.

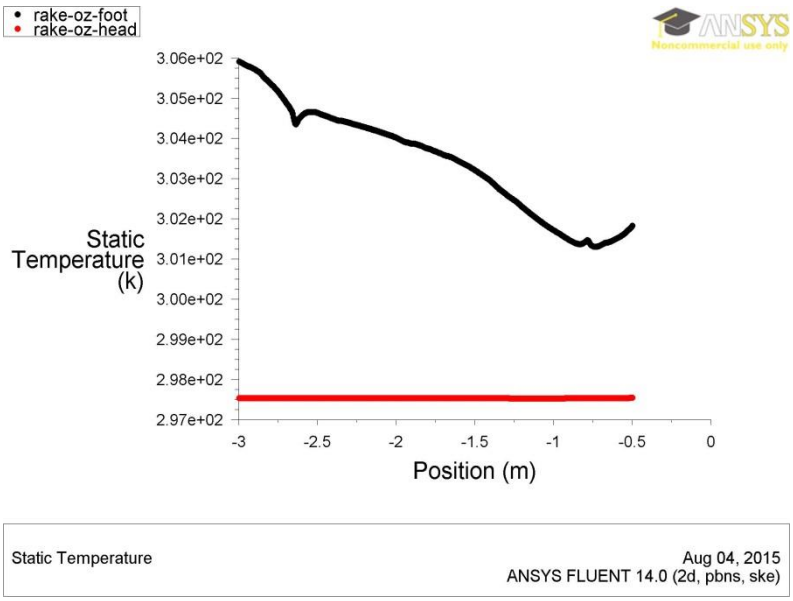

Figure 8.17: Head and foot rake temperatures under PV transparency level of 0.20

The estimated temperature behaviours of the foot and the head rakes horizontally along the occupied zone width are shown in Figure 8.17. It can be seen that the temperatures of the foot and head rakes fall in a range of 24.37-32.75^{0}C. The maximum temperature of the foot rake is 32.75^{0}C and the minimum is 28.15^{0}C whilst the temperature of the head rake is in a stable temperature of 24.37^{0}C. Therefore, the foot and the head elements under the PV transparency level of 0.2 is proper for the providing the required thermal level for the space.

Likewise, Figure 8.18 presents the temperature performance for the rakes of the front and the back walls along the vertical height of the occupied zone. The maximum temperature of the front wall rake is 32.75^{0}C and the minimum is 24.29^{0}C and the back wall rake temperature range between 24.05^{0}C and 28.67^{0}C. Consequently, the temperatures of the front and the back wall rakes fall in a range of 24.05–32.75^{0}C which exceeds the required level of thermal comfort within partial area. However, the average temperature of both the front and the back walls is 24.41^{0}C which is thermally accepted.

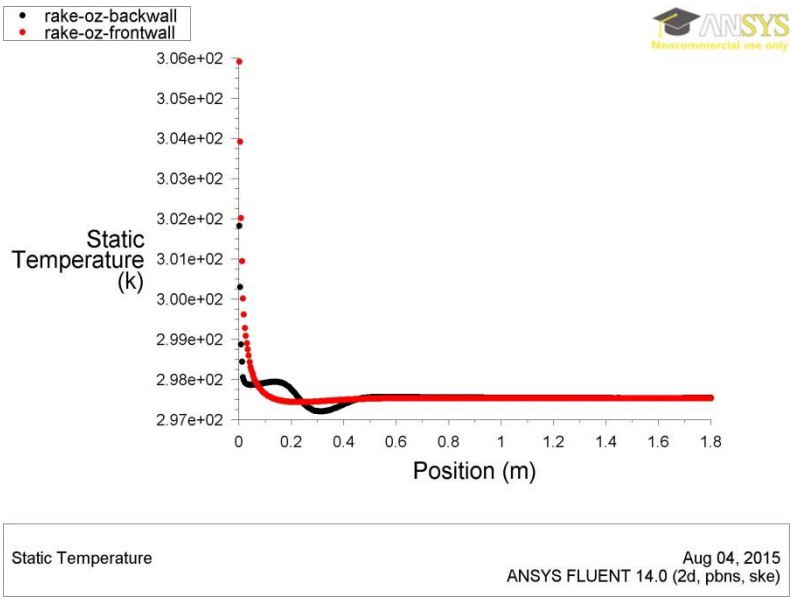

Figure 8.18: Front and back rake temperatures under PV transparency level of 0.20

8.3.3 PV TRANSPARENCY LEVEL OF 0.25

Figure 8.19 offers the predicted temperature trends under the impact of the PV transparency level of 0.25 and the mechanical air flow as a function of the cooling season conditions. The figure indicates that the predominant temperature of the interior environment is approximately 25^{0}C which is one degree higher than the inlet temperature of 24^{0}C at the bottom opening of the back of the room. Thus, the occupants can still feel thermally comfortable. However, gradual increment appears between the window cavities behind the PV panel to elevate up to 27^{0}C which is moderated for the panel.

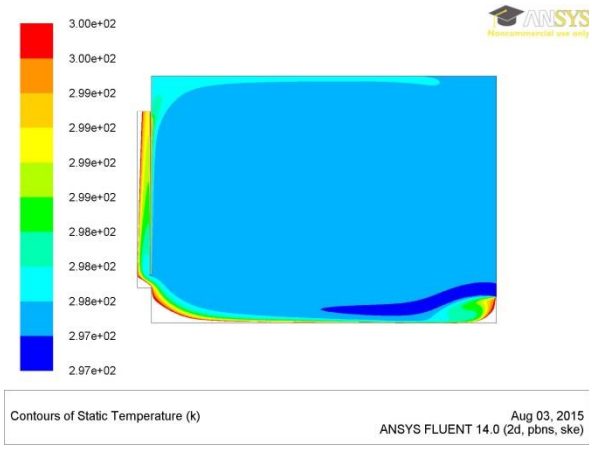

Figure 8.19: Temperature distribution

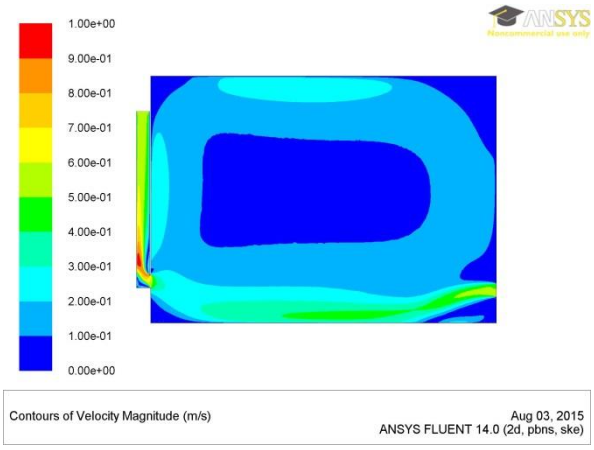

Figure 8.20: Air flow pattern

The air velocity magnitude inside the office space under the impact of the PV transparency level of 0.25 and of the combination of both ventilation forces, mechanical and buoyant, due to the effect of the cooling season conditions are shown in Figure 8.20. The figure indicates that a proper air movement inside the interior environment is circulating throughout the room with an air velocity varying between 0.1 and 0.4m/s, and a flow rate of 76.55L/s. However, air flows are attached to the floor, roof and behind the window unit with higher velocity that reaches up to 0.6m/s whereas the air velocity increases gradually at the top opening of the window and between its cavities venting out the accumulated heat behind the PV panel to the outside environment through the bottom aperture of the window cavities.

Figure 8.21 shows the predicted temperature trends horizontally along the occupied zone width for the foot and the head rakes. It is shown that the temperatures of the foot rake of the PV transparency level of 0.25 offer inadequate level of thermal comfort for the occupants. The foot rake temperatures decrease gradually from the nearest point to the window, from 34.94^{0}C to 29.18^{0}C at the farthest point from the window whilst the temperatures of the head rake is stable to a degree of 24.48^{0}C. Furthermore, the average temperature of the foot rake is 29^{0}C which is still considered improper.

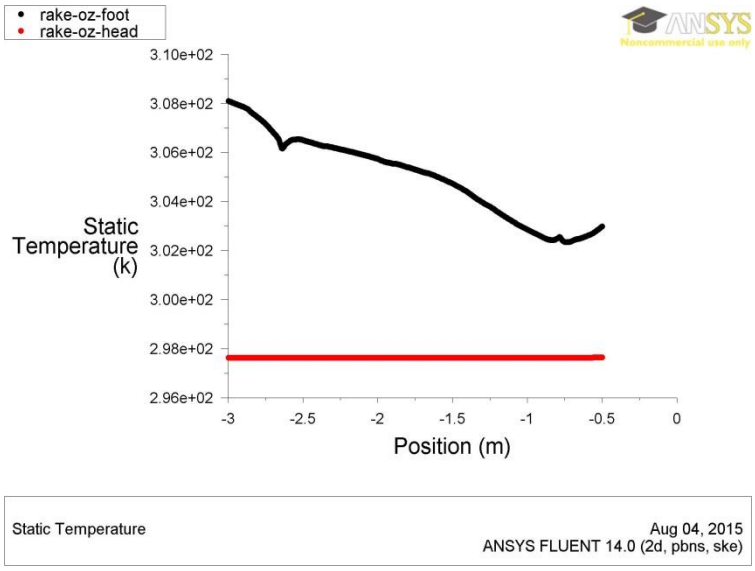

Figure 8.21: Head and foot rake temperatures under PV transparency level of 0.25

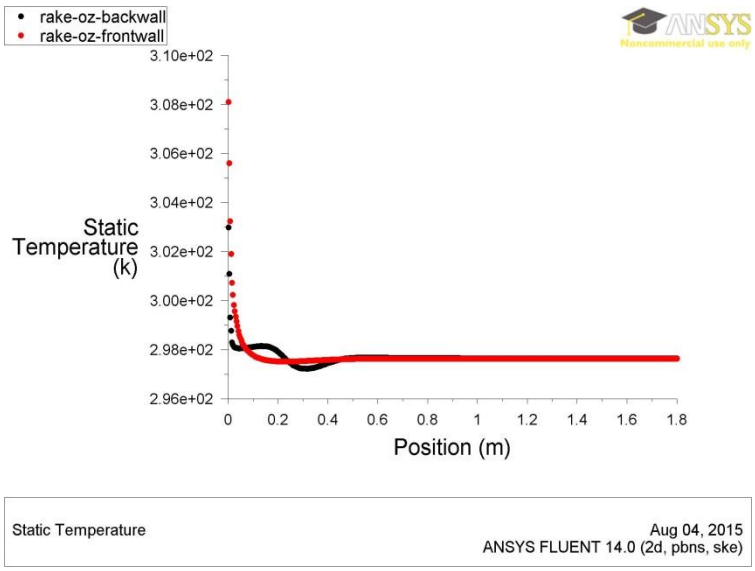

Figure 8.22: Front and back rake temperatures under PV transparency level of 0.25

The same is true from the Figure 8.22 indications. It offers the estimated temperature trends along the vertical height of the occupied zone for the rakes of the front and the back walls. The maximum temperature of the front wall rake is 34.94^{0}C and the minimum is 24.35^{0}C and the back wall rake temperatures range between 24.07^{0}C and 29.48^{0}C. Therefore, the temperatures of the front and the back walls rakes fall between in a range of 24.06–29.83^{0}C which overrides the required standard of thermal comfort, though, the average temperature of both the front and the back walls is 24.52^{0}C which is thermally adequate.

8.3.4 PV TRANSPARENCY LEVEL OF 0.3

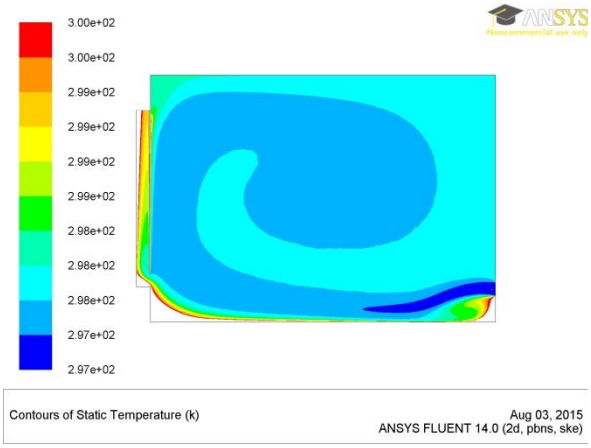

Figure 8.23: Temperature distribution

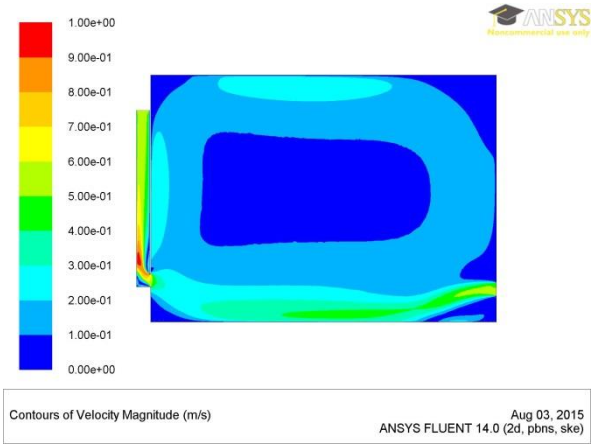

Figure 8.24: Air flow pattern

The estimated temperature behaviours due to the effect of the PV transparency level of 0.3 and the mechanical-induced air flow under the conditions of the summer season are shown in Figure 8.23. It can be observed that the difference between the inlet and the outlet temperature is around 3^0C. However, the temperature increment throughout the interior space is one degree higher than the inlet temperature of 24^0C at the bottom opening of the back of the room which is roughly 25^0C whereas the gradual temperature increase appears around the window unit and specifically behind the PV panel where the heat is accumulated.

Figure 8.24 presents the air flow pattern inside the office space as a function of the mechanical-driven air flow and the PV transparency level of 0.3 due to the conditions of the summer period. It can be noticed that the roof, the floor and the back of the window component come along with air flow that their velocities vary between 0.12 and 0.6m/s. However, the interior space is dominated with an adequate air movement with an air velocity ranging from 0.2 and 0.4m/s with a flow rate of 76.55L/s whilst the air velocity increases gradually at the top opening of the window and between its cavities removing out the accumulated heat behind the PV panel to the outside environment through the bottom aperture of the window unit.

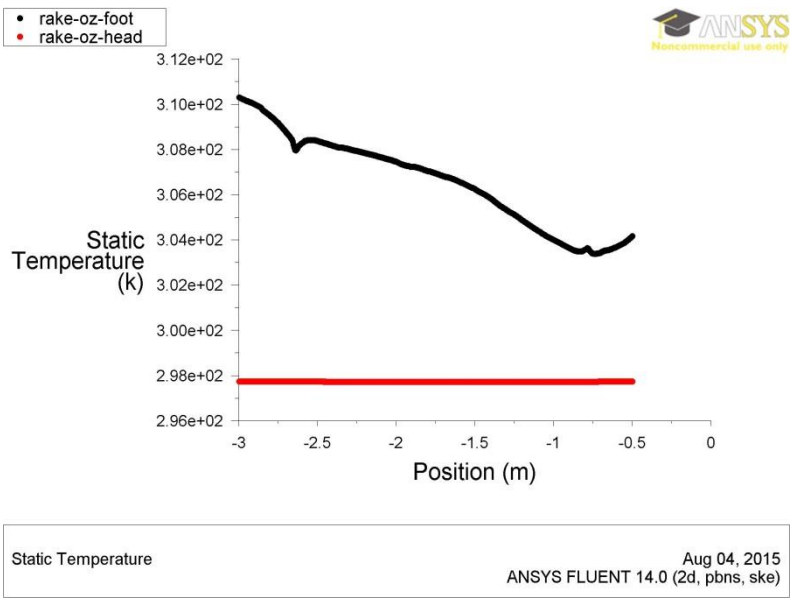

Figure 8.25: Head and foot rake temperatures under PV transparency level of 0.3

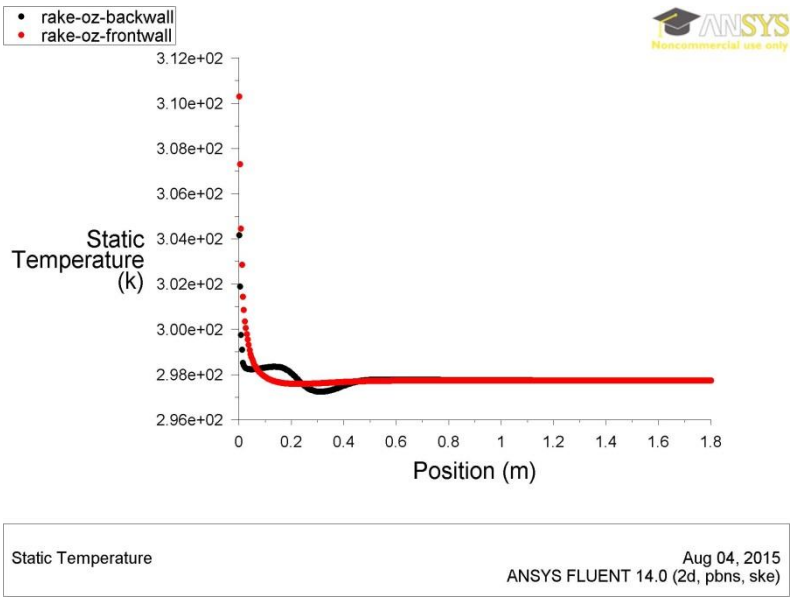

Figure 8.26: Front and back rake temperatures under PV transparency level of 0.3

The predicted temperature performance of the foot and the head rakes is illustrated horizontally in Figure 8.25 from the nearest point to the window to the farthest point from the window due to the impact of the PV transparency level of 0.3. It can be seen that high temperature values of the foot rake are offered with its highest of 37.13^{0}C and the lowest of 30.22^{0}C whereas the temperatures of the head rake are constant to 24.58^{0}C. Notwithstanding, the average temperature of the foot rake is low, 30^{0}C, it is still above the required level occupants thermal comfort. As a result, it is impossible to achieve the thermal level with the PV transparency level of 0.3 since it allows excessive heat into the interior space that overrides the required level thermal comfort. Likewise, the same can be drawn from Figure 8.26 that presents the estimated temperature pattern of the occupied zone from the bottom to the top for the rakes of the front and the back walls. The maximum temperature of the front wall rake is 37.13^{0}C and the minimum is 24.42^{0}C and the back wall rake temperatures range between 24.08^{0}C and 31^{0}C.

8.3.5 PV TRANSPARENCY LEVEL OF 0.35

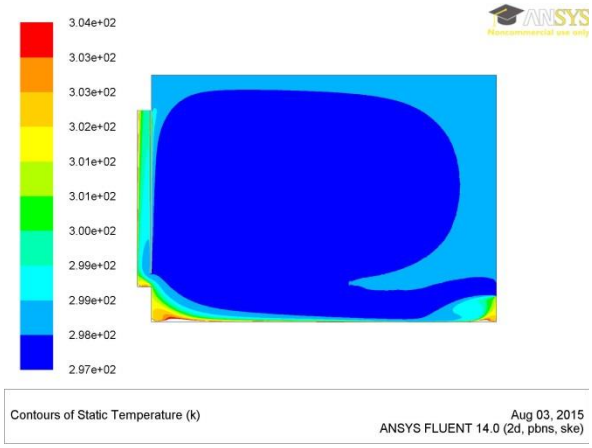

Figure 8.27: Temperature distribution

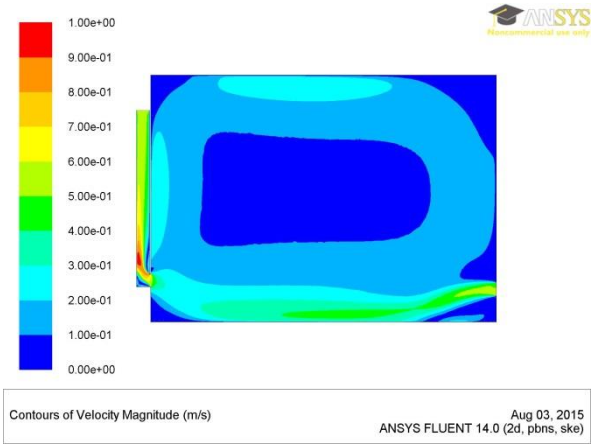

Figure 8.28: Air flow pattern

Figure 8.27 shows the predicted temperature pattern under the conditions of the summer season due to the impact of the mechanical-driven ventilation force and the PV transparency level of 0.35. It can be noticed that the overall thermal comfort is achieved throughout the interior space with a dominated degree of 25^0C, though, the increase of the temperature is occurring on the floor and around the window unit and specifically behind the PV panel within the window cavities.

The air velocity magnitude due to the conditions of the cooling period inside the office space as a function of the mechanical-induced ventilation flow and the PV transparency level of 0.35 is presented in Figure 8.28. It can be observed that the incoming air velocity from the opening at the bottom of the back wall is increasing gradually and forming air jets around the roof, the floor and around the window unit varying between 0.1 and 0.6m/s. However, the interior space is predominant with a proper air circulation that's velocity range from 0.1 and 0.4m/s with a flow rate of 76.55L/s. It can also be seen that the air velocity reaches up to 1m/s between the window cavities and behind the PV panel expelling out the accumulated heat behind to the outside environment through the bottom opening of the window cavities.

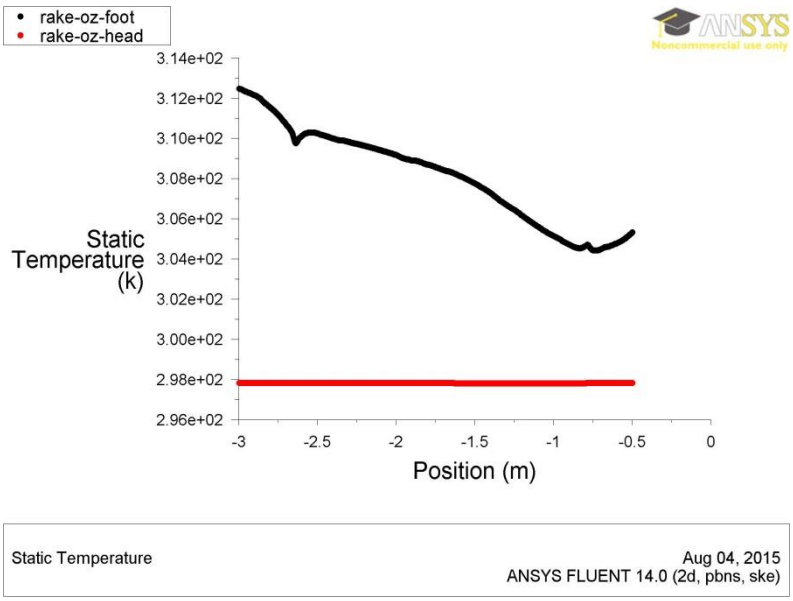

Figure 8.29: Head and foot rake temperatures under PV transparency level of 0.35

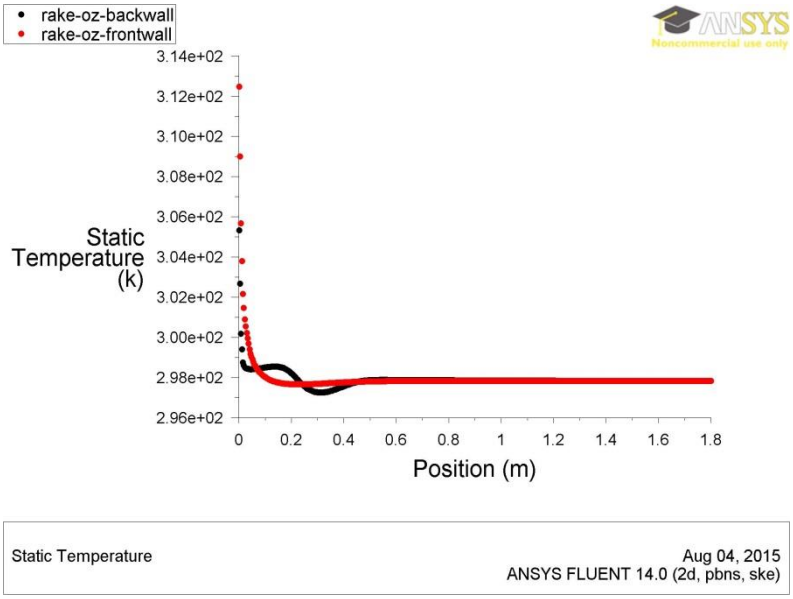

Figure 8.30: Front and back rake temperatures under PV transparency level of 0.35

The trends of estimated temperatures of the foot and the head rakes horizontally along the occupied zone width are shown in Figure 8.29 as a function of the PV transparency level of 0.35. It is indicated that the transparent level allows high volume of heat that increases the temperature of the foot rake to a maximum of 39.32^{0}C and to a minimum of 31.26^{0}C, though, stability appears on the temperature value of the head rake as 24.65^{0}C. As a result, it is impossible to acquire thermal comfort with the PV transparency level of 0.35. Similarly, the same can be concluded from the predicted trends of the temperature values vertically along of the occupied

zone height for the rakes of the front and the back walls as shown in Figure 8.30. The front wall rake temperature elevated to the peak value of 39.32^{0}C and a minimum of 24.5^{0}C and the maximum temperature value of the back wall is 32.16^{0}C and the minimum is 24^{0}C and. For comparison, the maximum and the minimum temperature values were tabulated as well as the averages of the occupied zone rakes under the effect of each PV transparency level due to the cooling season. Table 8.2 shows the maximum and minimum temperature as well as the averages of the occupied zone rakes under different PV transparency levels due to the cooling season.

Table 8.2: Maximum and minimum temperature as well as the averages of the occupied zone rakes under different PV transparency levels due to the cooling season

Transparency Levels	**Occupied Zone Rakes**									
	Front rake			**Back rake**		**Foot rake**			**Head rake**	
	min	max	ave	min	max	min	max	ave	min	max
0.15	**24**	**31**	**24**	**24**	**27**	**27**	**31**	**27**	**24**	**24**
0.20	24	33	24	24	28	28	33	28	24	24
0.25	24	35	25	24	29	29	35	29	24	24
0.30	24	37	25	24	31	30	37	30	25	25
0.35	25	39	25	24	32	31	39	31	25	25

8.4 COMPARISON BETWEEN DIFFERENT PV TRANSPARENT LEVELS

The comparison between the different PV transparent degrees is presented in Figure 8.31 where the temperature values of a created centred rake horizontally along the model width through the middle of the occupied zone of each PV transparent level: 0.15, 0.2, 0.25, 0.3 and 0.35 are plotted. It can be observed that PV transmittance of 0.15 is the only level that satisfies the required thermal quality that appears on the temperature performance of the centred rake, as a function of its impact, with a maximum value of 25^{0}C and a minimum degree of 24^{0}C along the room width whilst the rest of the transparencies deteriorate, partially and entirely, the thermal comfort inside the space by elevating the temperature of their rakes above the accepted level, however, the average temperature of each rake, under each PV transparent degree, is within the thermal standard and ranging between 24^{0}C and 25^{0}C. Since the conditions

applied are for the cooling period, there is no need for gaining heat. Thus, the lower PV transmittance is applied, the more solar radiation is absorbed and the less heat, into inside environment, is allowed.

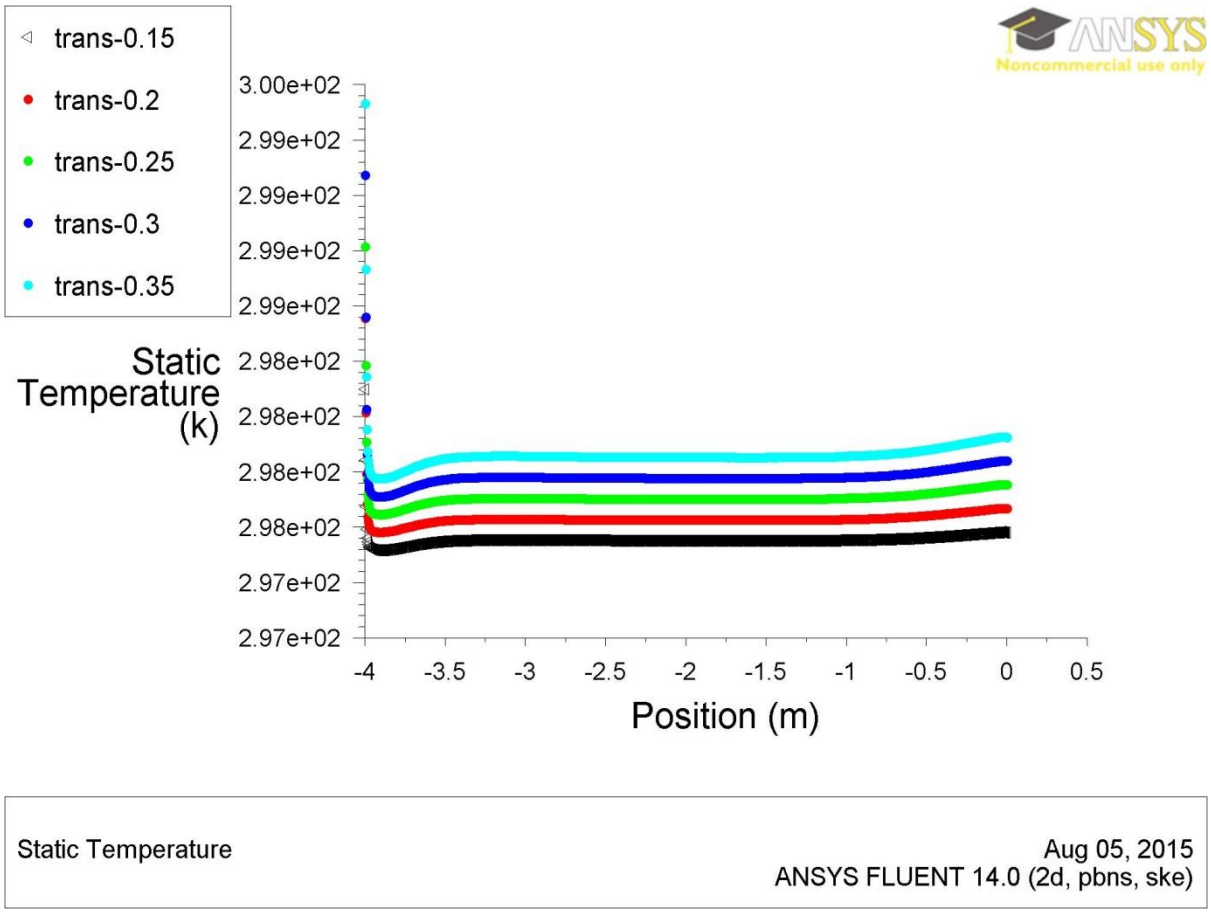

Figure 8.31: Centred rake temperatures under the effect of each PV transparent level

8.5 PV PANEL ELECTRIC ANALYSIS

Performing PV electric analysis is a necessity in order to optimise the PV efficiency with the most proper transparency level. Thus, a rake was created vertically along the PV panel boundary to estimate the PV temperature behaviour due to each transparent degree. The cell temperature and solar radiation are the key factors for the electric performance of a PV. Figure 8.32 illustrates the temperature values of the created rake from the lowest point at the panel, at the edge of the bottom window opening to the highest pint at the top, as a function of each transmittance.

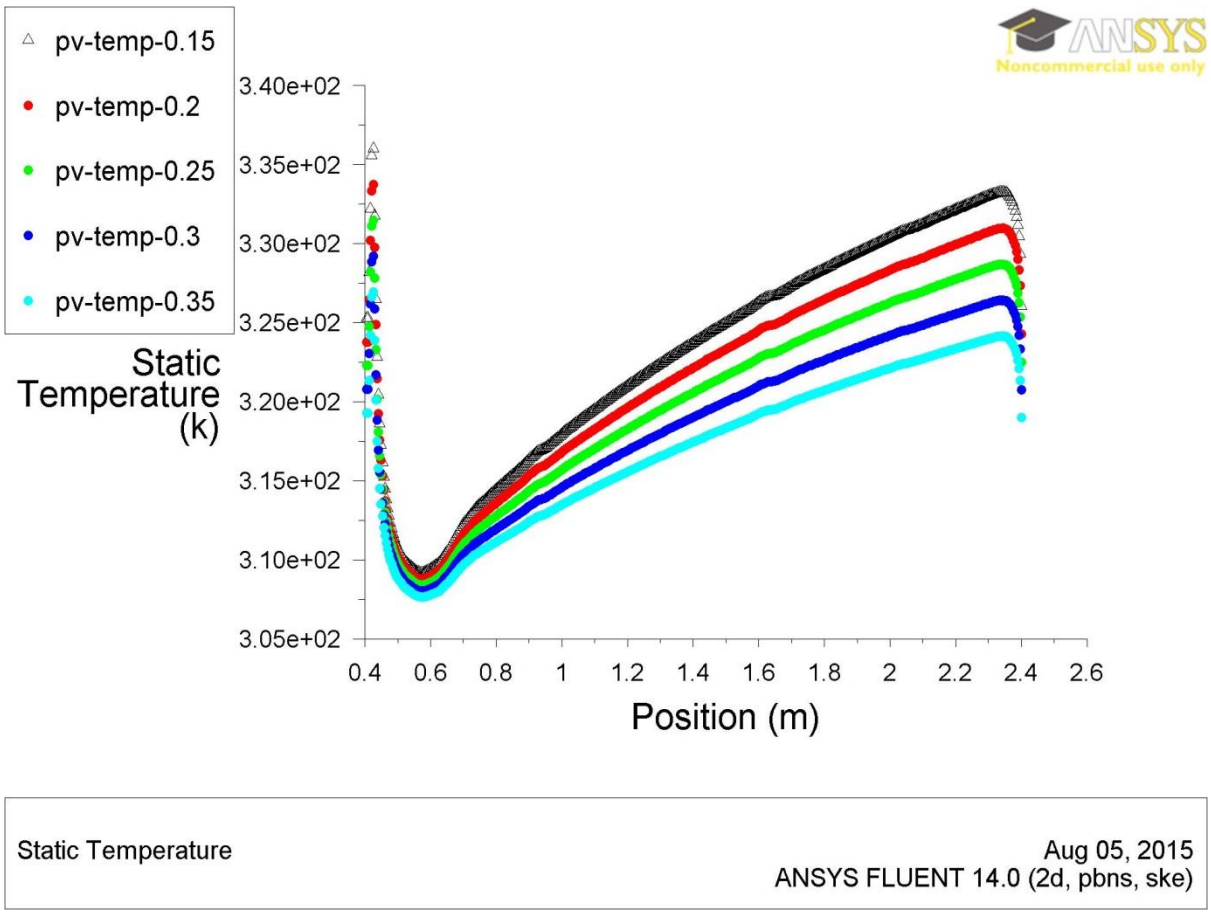

Figure 8.32: PV temperatures under the effect of each transparent level

The figure indicates that the absorption of the heat increases with low PV transparent level and thus less heat is gained inside the interior environment since the level of 0.15 has achieved the higher temperature values along the PV rake. The average temperature of the PV rake was obtained for each transmittance degree along with the PV power generation were tabulated in Table 7.3 to identify the most suitable transmittance level that satisfies the required PV cells standard of efficiency. The table indicates that the PV can generate electricity efficiently with each transmittance since each transparent level do not overrides the PV panel average temperatures above 45^0C which is still feasible. Though, during the cooling season the less heat gain is preferred, thus, the transmittance of 0.15 can balance between maintaining the PV cells efficiency and the amount of heat gaining into the inside space since this transparent value allows much less heat than the other transmittance levels and enables the PV panel to absorb much more solar radiations that maximize the electricity generation.

8.6 SUMMARY

In summary, an occupied zone, that ensures the occupants feels thermally neutral, was created within the model interior with rakes that represent the zone measures to predict the results and introduce the most adequate PV transparent level for the summer season under the combination of buoyancy- and mechanical-driven ventilation flows. The PV transparent degree of 0.15 was the sole level that achieved the preferred criteria of thermal comfort; however, the indication of the averages of the rest transmittance values appeared accepted, but it is still thermally uncomfortable where overheating was noticed, specifically, on the floor, around the window unit and between the cavities behind the PV panel. Therefore, PV electric analysis is crucial for a certain and optimum PV transmittance level for the summer season.

At this stage, the design optimization is complete for the window unit under each condition, winter and summer. Next chapter will investigate the impact of internal heat gains on thermal and ventilation performance of the system according to each season.

CHAPTER 9 IMPACT OF INTERNAL HEAT GAINS ON THERMAL AND VENTILATION PERFORMANCES OF AIRFLOW WINDOW

This chapter offers a more CFD analysis for the airflow window unit employing the optimum ventilation force found in the previous chapter, the combined buoyant and mechanical forces, considering the internal heat gains for both winter heating and summer cooling conditions of the city of London of the noon time. Furthermore, the chapter investigates the impact of internal heat resources on the flow rate and thermal performance and discusses the most suitable air velocity and ventilation rate for each PV transparency level of 0.15, 0.2, 0.25, 0.3, and 0.35. Based on the optimum PV level found for each season, the chapter will investigate the impact of transient treatment from the same aspects.

9.1 INTERNAL HEAT GAINS

Internal heat gain is the heat acquired within an interior environment in state of sensible and latent heat emitted from any source, such as human bodies, lighting, computers and office equipment, electric motors, appliances, and other domestic equipment. Offices internal heat gains are primarily emitted from the occupants, artificial lighting, and office equipment connected to the small power electrical distribution (CIBSE 2006). Thus, benchmark values of the office internal heat gains presented in (CIBSE 2006), Table 9.1, will be added to the floor heat flux for each simulation.

Table 9.1: Benchmark values of the office internal heat gains

Office use	Density of occupation/person.m^{-2}	Sensible heat gain/W.m^{-2}			Latent heat gain/ W.m^{-2}	
		People	Lighting	Equipment	People	Other
General	12	6.7	8-12	15	5	-
	16	5	8-12	12	4	-
City centre	6	13.5	8-12	25	10	-
	10	8	8-12	18	6	-

The internal heat gains from human body will be considered as sensible state since it is absorbed by the surrounding surfaces and stored in the material; however, latent

heat gain was not taken into account that is to be added to the moisture content of the air which is neglected in the simulations. Thus, and since the floor area is set as $10m^2$ for each people, the density of occupation will be $10/person.m^{-2}$ and the sensible heat gains for people, lighting, and equipment will be 8, 12, and 18, respectively, as total of $38W.m^{-2}$ that will be added to the floor heat flux of each simulation.

9.2 CALCULATION OF THE PARAMETERS (HEAT FLUX, AIR VELOCITY, AND FLOW RATE)

For each PV transmittance level, same heat fluxes, applied in the earlier chapter, were used for each component in the simulation analysis except the floor; its heat flux was loaded with the value of $38W.m^{-2}$, the internal heat gains. However, the air velocities were calculated using the equations provided previously for a preliminary simulation to find out to what extend the thermal comfort and the required ventilation rate could be attained, and then based on the temperature difference, the air velocity was recalculated and a simulation was performed. Table 9.2 and Table 9.3 represent the values applied for winter and summer simulation analyses.

Table 9.2: Sequential values applied for winter simulation

	Transparency Levels				
Parameters	**0.15**	**0.2**	**0.25**	**0.3**	**0.35**
Solar irradiance (W)	707.36	707.36	707.36	707.36	707.36
G floor(W.m-2)	19.014	25.35	31.69	38.03	44.37
G floor+38(W.m-2)	57.014	63.35	69.69	76.03	82.37
Actual flow rate (L/s)	**26**	**30**	**28**	**28**	**30**
Velocity (m/s)	0.15	0.16	0.18	0.2	0.21
Velocity 2nd attempt (m/s)	-	-	-	0.16	-
Actual velocity (m/s)	**0.17**	**0.19**	**0.18**	**0.18**	**0.19**

For each rake of the occupied zone as shown in Figure 9.1, the temperature distribution was plotted for the entire PV transparencies. They were specifically plotted for the front-wall rake, the back-wall rake, the foot rake, the head rake, and the middle rake across the zone as area weighted average temperature and velocity for both winter heating and summer cooling conditions. However, the air velocity

magnitude was represented as a contour image of air velocity pattern and as air velocity predictions along the middle rake extending across the model from the window to the back wall.

Table 9.3: Sequential values applied for summer simulation

	Transparency Levels				
Parameters	**0.15**	**0.2**	**0.25**	**0.3**	**0.35**
Solar irradiance (W)	538.62	538.62	538.62	538.62	538.62
G floor($W.m^{-2}$)	14.48	19.3	24.13	28.96	33.78
G floor+38($W.m^{-2}$)	52.48	57.3	62.13	66.96	71.78
Actual flow rate (L/s)	**66**	**73**	**81**	**86**	**94**
Velocity	0.52	0.57	0.62	0.66	0.71
Velocity 2nd attempt	0.45		-	-	
Actual velocity	**0.43**	**0.48**	**0.53**	**0.57**	**0.62**

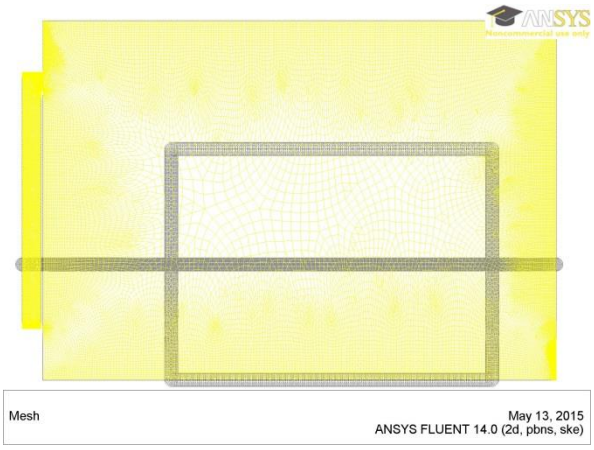

Figure 9.1: The occupied zone within the model space and the middle rake across the zone

9.3 IMPACT OF INTERNAL HEAT GAINS

The impact of internal heat gains was examined, during the heating and cooling season, through a comparison between the thermal performance resulting from each PV transparency level of each specified element of the occupied zone as well as the ventilation performance of the interior space. Furthermore, the PV panel efficiency was investigated with relevance to each PV transmittance and compared to assure that the optimum PV transparency is effective from all aspects.

9.3.1 TEMPERATURE PERFORMANCE FOR WINTER HEATING

Figure 9.2 presents the temperature estimations vertically along the front-wall of the occupied zone within the model space from the bottom to the top collectively for PV transparencies: 0.15, 0.2, 0.25, 0.3 and 0.35. The figure shows that the front-wall receives the highest heat volume when the PV level of 0.15 is applied and the heat decreases gradually with 0.3, 0.25, 0.35, and 0.2 degrees, respectively. It is obvious that the lower air velocity employed, the higher temperature is obtained where the lowest actual velocity that elevated the temperature trend to the highest scale was 0.17m/s for the PV transparency degree of 0.15. However, all the transparencies have achieved accepted level of thermal comfort along the front-wall of the zone with average temperatures of 24^0C for the PV transparencies of 0.15, 0.25, and 0.3 whilst 22^0C for 0.2 level and 23^0C for 0.35 level.

Likewise, the temperature distributions that are shown, vertically from the bottom to the top of the back-wall of the occupied zone, in Figure 9.3 for each PV transmittance value have introduced similar scales of the temperature trends of the PV transparency degrees to those estimated from the front-wall. The temperature values are even equal where the back-wall average temperature values are 24^0C for the PV transmittance level of 0.15 and 0.3 and 23^0C for the levels of 0.25 and 0.35 as well as 22^0C for the degree of 0.2.

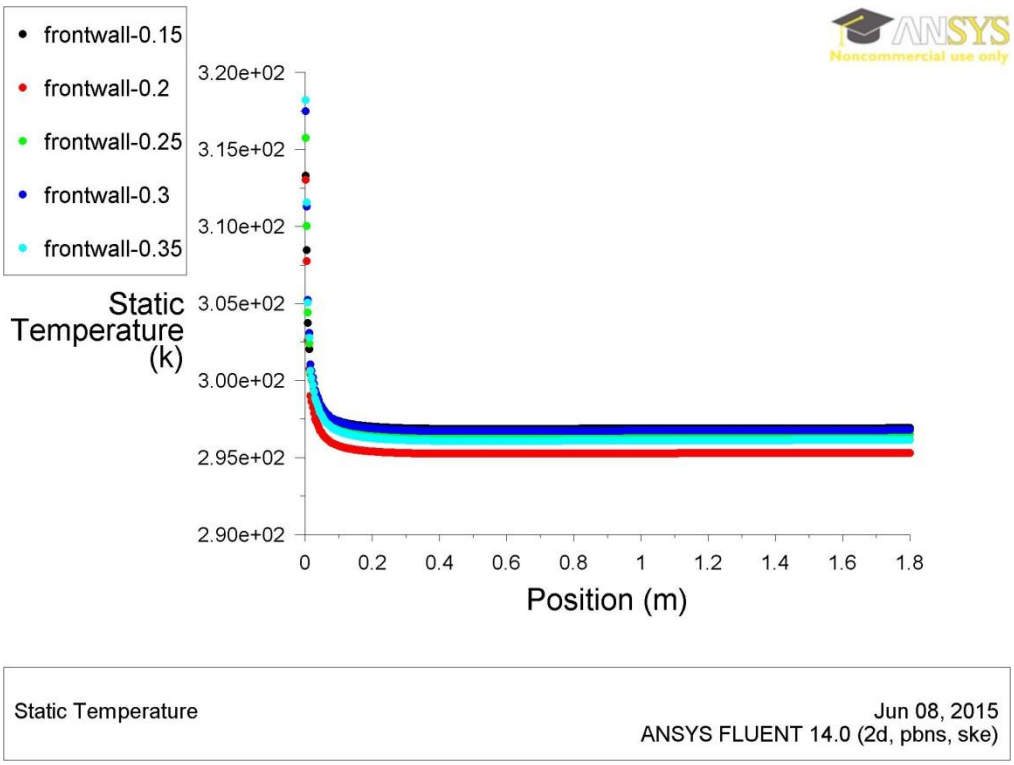

Figure 9.2: Front-wall temperature trends under the effect of each PV transparency level

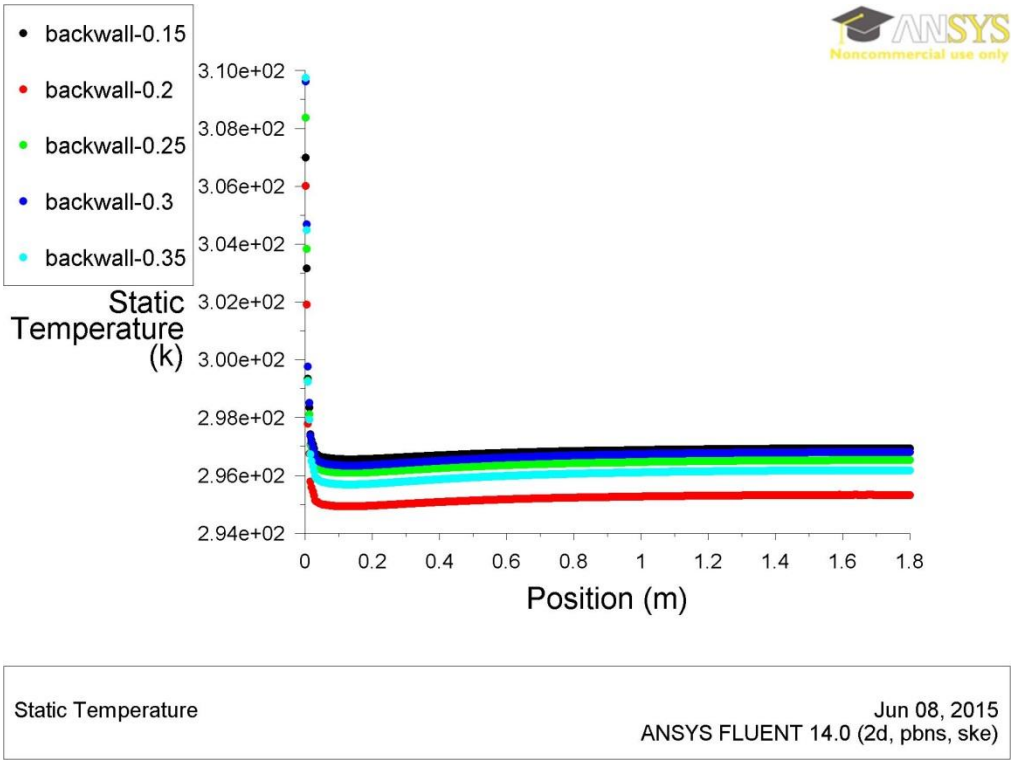

Figure 9.3: Back-wall temperature trends under the effect of each PV transparency level

The temperature trends of the occupied zone foot rakes that were introduced for the models of each PV transparency level are shown in Figure 9.4. The temperature patterns can reveal that the temperature of the foot area, when PV transparency of 0.35 was applied, can be increased to the largest scale with an average of 32^{0}C and the temperatures decrease gradually with the PV levels of 0.3, 0.25, 0.15, and 0.2 with temperature averages of 32^{0}C, 31^{0}C, 31^{0}C, and 30^{0}C, respectively. It is clear that the foot temperature is above the recommended comfort criteria, up to 25^{0}C for interior heating and up to 29^{0}C for floor heating (CIBSE 2006), level of comfort with each transmittance applied. However, the PV transparency degree of 0.2 can achieve the lowest temperature value. In contrary, the order of PV levels effectivity was altered with the temperature distributions of the head rakes presented in Figure 9.5 where the largest scale appeared for the PV levels of 0.15 and 0.3 with an average temperature of 24^{0}C whereas the head rake possessed an average of 23^{0}C with the degrees of 0.25 and 0.35 and 22^{0}C 0.2 PV level.

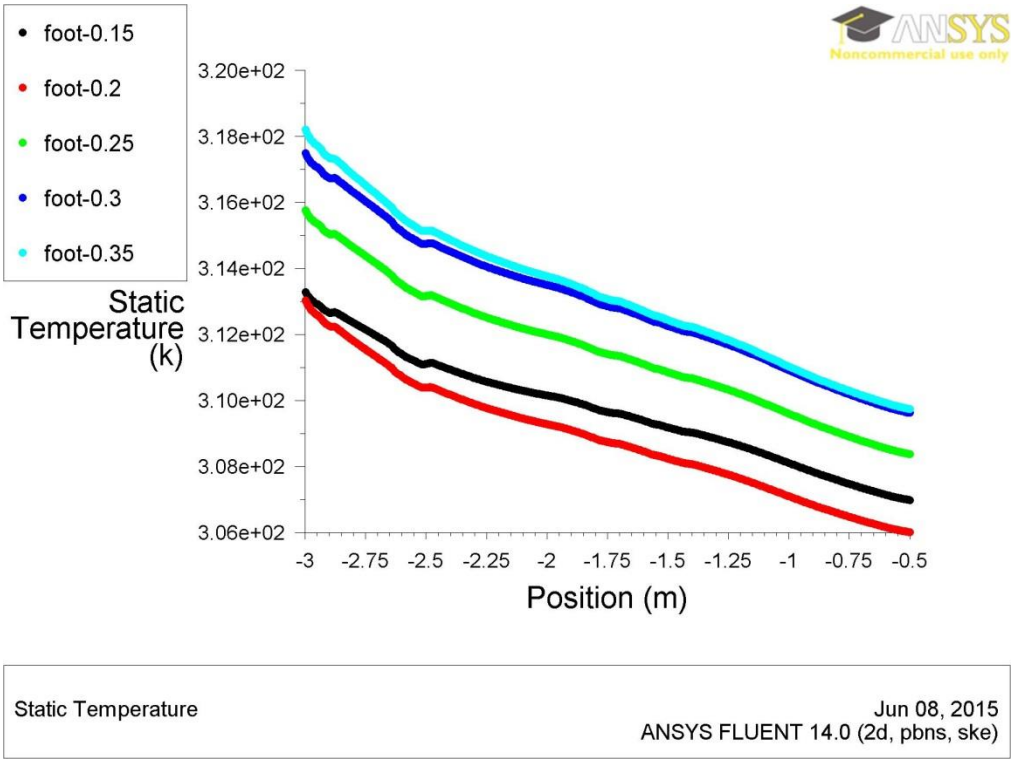

Figure 9.4: Foot temperature trends under the effect of each PV transparency level

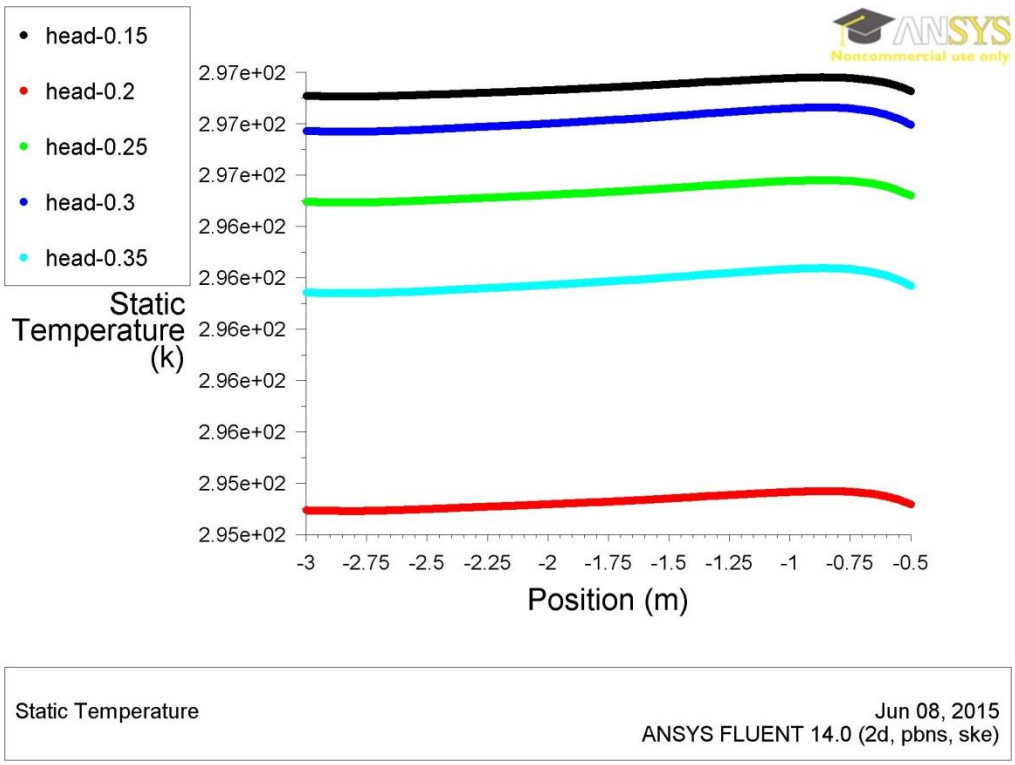

Figure 9.5: Head temperature trends under the effect of each PV transparency level

Figure 9.6 shows the temperature values of the middle rake that was created horizontally along the space width for each PV transparency degree. It can be noticed that the occupied zone can acquire thermal comfort with each PV level along the middle rake with average temperature values vary between 22^0C and 24^0C in a gradual sequence of 0.15, 0.3, 0.25, 0.35, and 0.2 from high to low. Though, the temperature values of the space exceed the standard level near the window with each PV level except the degree of 0.2 that its performance maintains the accepted level for the with a maximum temperature degree of 25^0C at the closest point to the window wall. Table 9.4 presents the average temperature values of each rake in the model under each PV transmittance level.

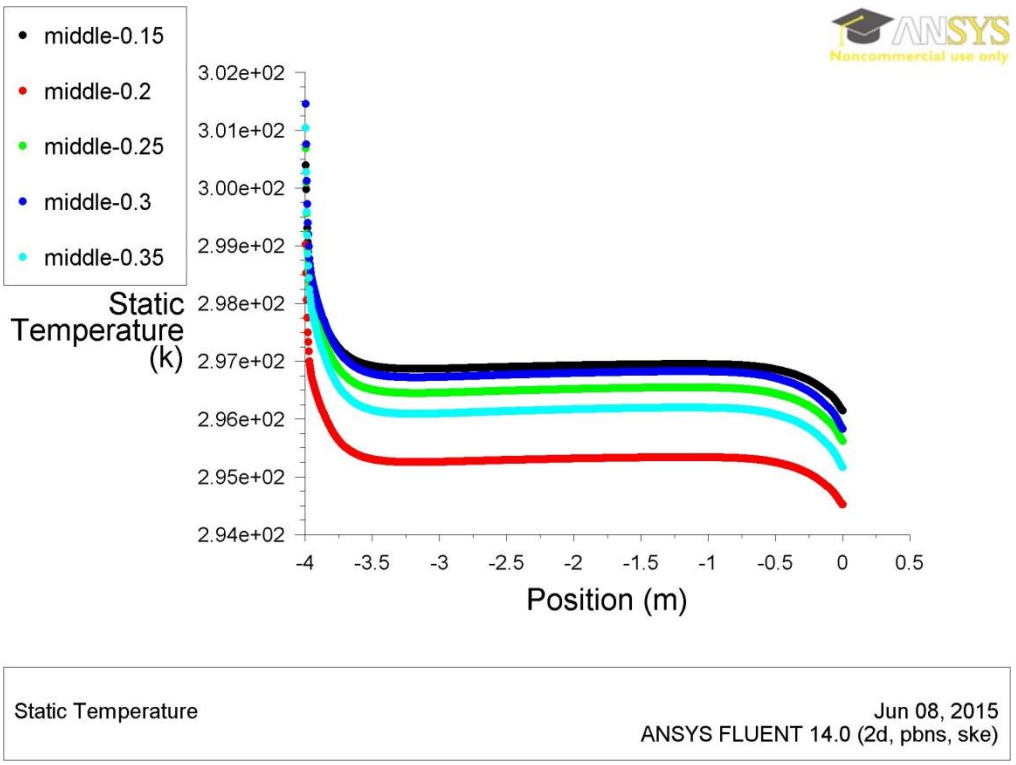

Figure 9.6: Middle rake temperature trends under the effect of each PV transparency level

Table 9.4: Average temperature values of each rake in the model under each PV transmittance level

	Occupied Zone Rakes				
Transparency Levels	**Front Rake**	**Back Rake**	**Foot Rake**	**Head Rake**	**Middle Rake**
0.15	24	24	31	24	24
0.2	**22**	**22**	**30**	**22**	**22**
0.25	24	23	31	23	23
0.3	24	24	32	24	24
0.35	23	23	32	23	23

9.3.2 VENTILATION PERFORMANCE FOR WINTER HEATING

Figure 9.7 (a, b, c, d, e and f) shows the air velocity performance, inside the office space, that were impacted with PV transparency levels of 0.15, 0.2, 0.25, 0.3, and 0.35, respectively. The figure denotes that the air movement can be convenient under each PV transmittance degree where optimum air inlet velocities were used for each PV level sequential simulation attempts. It can be further noticed that the predominant air velocities of the interior environment vary between 0.6 and 0.9m/s with different average flow rates of 26L/s for 0.15, 28L/s for 0.25 and 0.3, and 30L/s for 0.2 and 0.35.

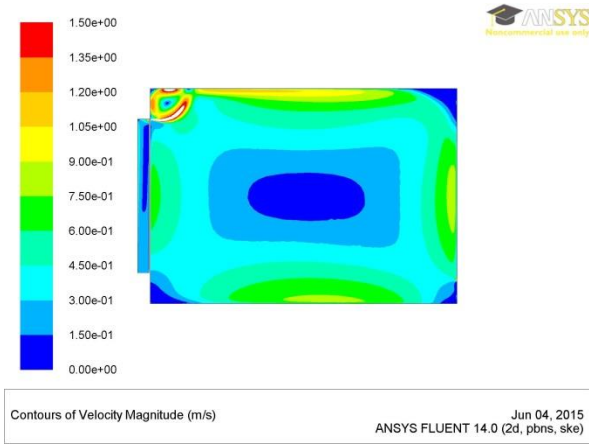

(a): Air flow pattern for PV transparency level of 0.15

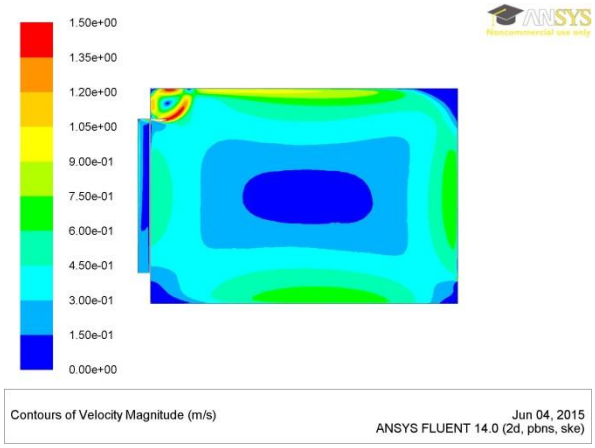

(b): Air flow pattern for PV transparency level of 0.2

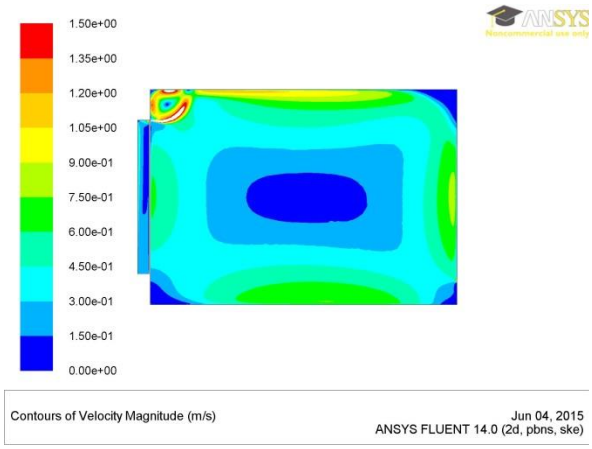

(c): Air flow pattern for PV transparency level of 0.25

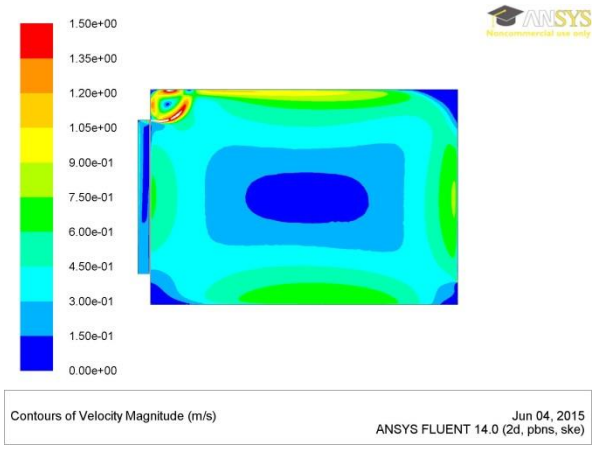

(d): Air flow pattern for PV transparency level of 0.3

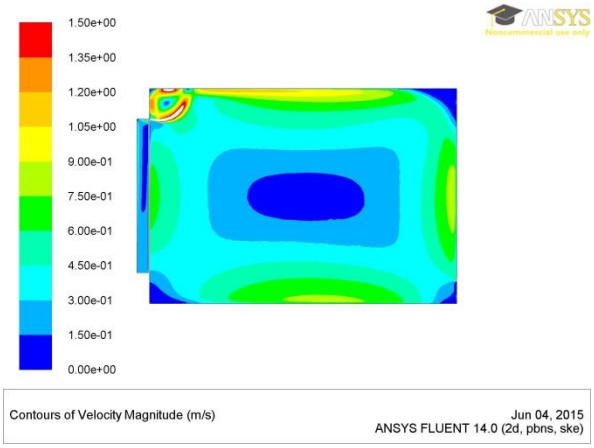

(e): Air flow pattern for PV transparency level of 0.35

Figure 9.7: Air flow pattern for different PV transparency levels

The air velocity magnitudes that were inputted to the five PV transparency degrees: 0.15, 0.2, 0.25, 0.3 and 0.35 and predicted along the middle rake are presented in Figure 9.8. Since the highest actual air velocity employed to the PV levels of 0.35 and 0.2, the ventilation performance were escalated to the highest scale under their effects. Though, relatively similar velocity trends can be seen from all the transparencies, due to the small differences between the applied velocities, with an average of 0.3m/s for each performance along the middle rake whilst it is 0.2m/s within the occupied zone. The air velocity inside the interior of the zone is dominated between 0.2 and 0.4m/s leaving the interior comfortably ventilated.

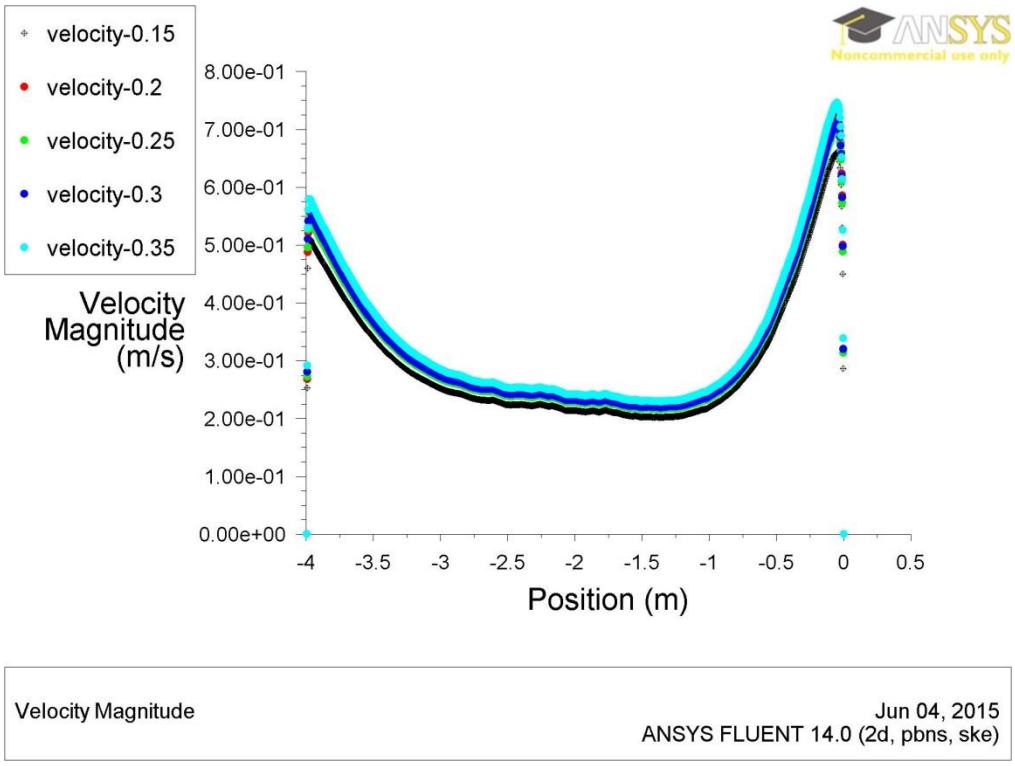

Figure 9.8: Air velocity trends under the effect of each PV transparency level

9.4 COMPARISON BETWEEN DIFFERENT PV TRANSPARENT LEVELS WITH AND WITHOUT INTERNAL HEAT GAINS

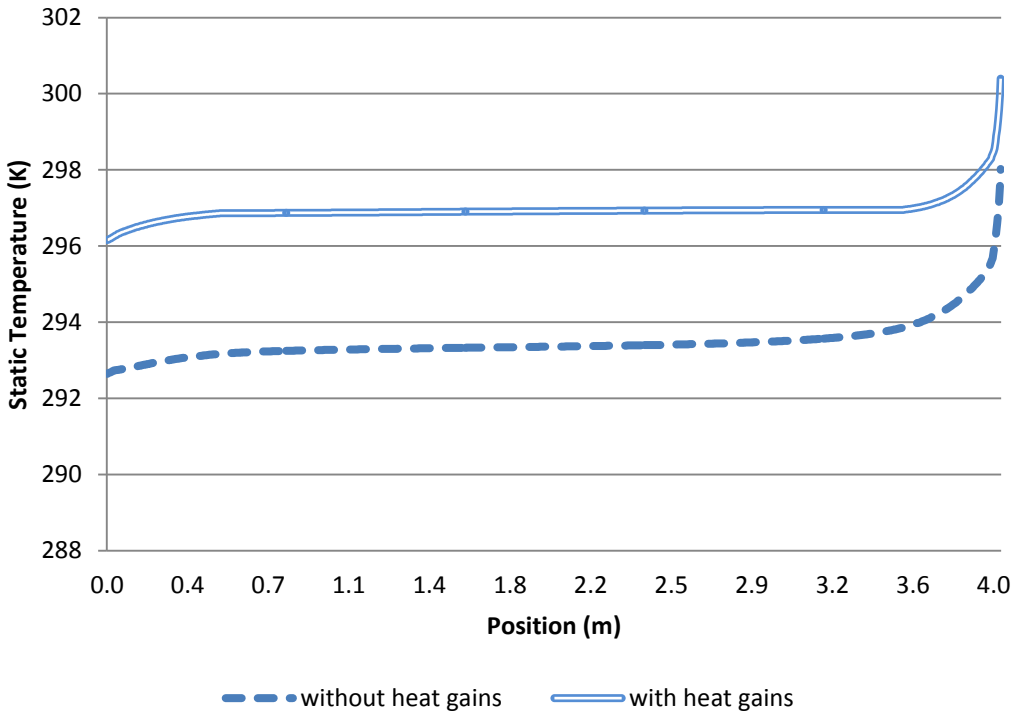

Figure 9.9: Middle rake temperature trends under the effect of PV transparency level of 0.15 with and without internal heat gains

The temperature distributions, along the rake extending from the window to the back of the room, that were traced to the PV transparency level of 0.15 with and without the internal heat gains are shown in Figure 9.9. It can be seen that effect of internal heat sources can occur to the temperature performance where the difference between the averages temperature of both cases were 4 degrees, however, the occupants can still feel comfortable inside the space whereas overheating appear near the window. Likewise, the addition of the heat sources, when inputted to the PV transparency level of 0.2, as presented in Figure 9.10, elevated the average temperature 3 degrees higher. Thus, thermal comfort became available for the occupants and throughout the interior space since the exclusion case of the heat sources revealed unaccepted low temperature performance with an average of 18^0C for the interior environment. It can be concluded that the PV transmittance of 0.2 is an optimum transparency level that offsets the occupants a thermally accepted interior during the winter conditions.

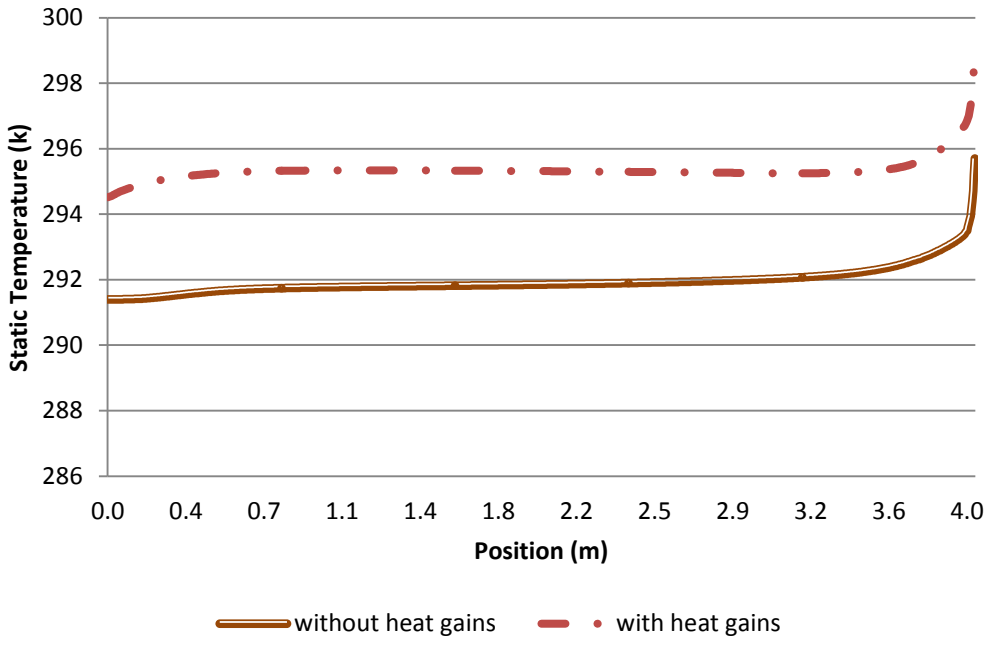

Figure 9.10: Middle rake temperature trends under the effect of PV transparency level of 0.2 with and without internal heat gains

9.5 TEMPERATURE PERFORMANCE FOR SUMMER COOLING

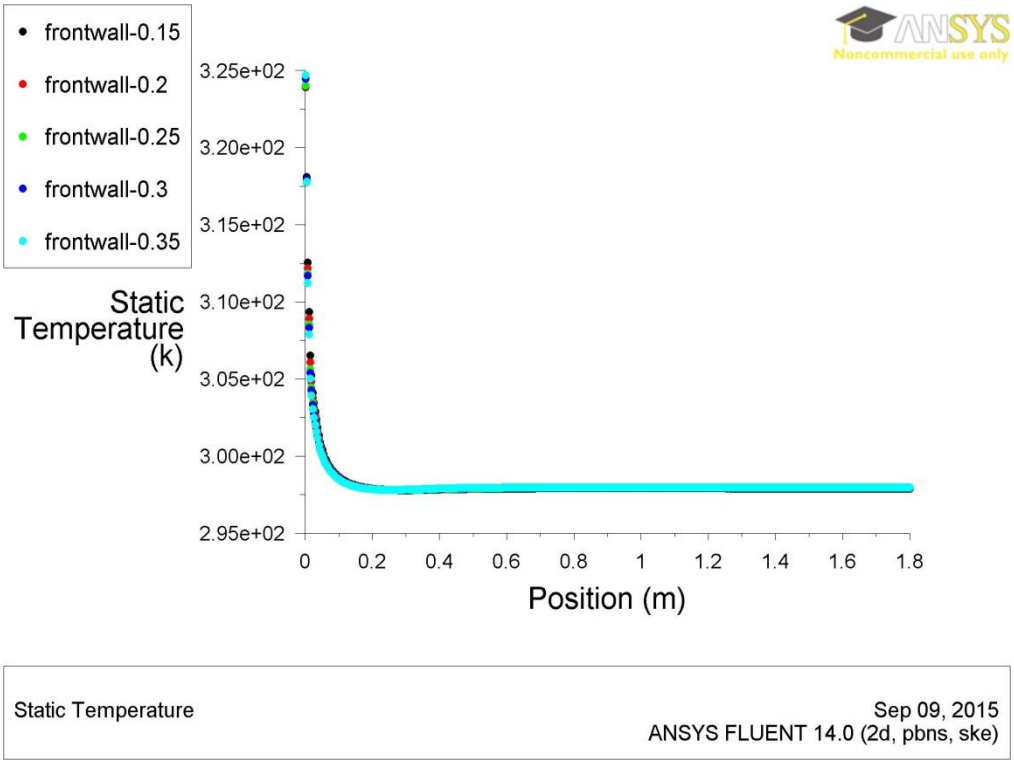

Figure 9.11: Front-wall temperature trends under the effect of each PV transparency level

The temperature trends revealed from the effect of each PV transparency level, 0.15, 0.2, 0.25, 0.3 and 0.35, and estimated vertically along the front-wall rake of the occupied zone within the office room are shown in Figure 9.11. The figure indicates

that the magnitude of heat was conveyed equally, from all PV levels, to the front wall where the average temperature for the front wall is 25^0C, under all transparencies, which is still within the required comfort standard. Similarly, Figure 9.12 presents the temperature patterns of back-wall rake under the impact of all PV transparencies and indicates that identical temperature scale was liberated to the back wall from each PV. Furthermore, the temperature trends of all transparencies appear slightly identical and constant along the wall except around the inlet area where a temperature decrease is obvious. The average temperature for the back rake varies 25^0C which is thermally comfortable.

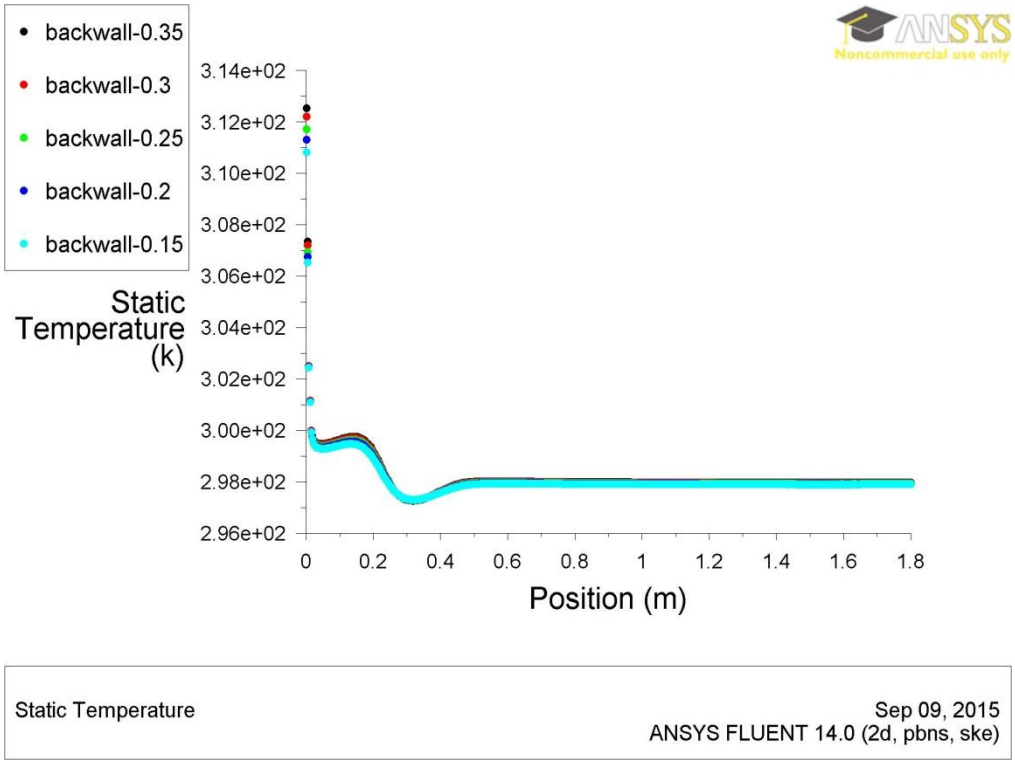

Figure 9.12: Back-wall temperature trends under the effect of each PV transparency level

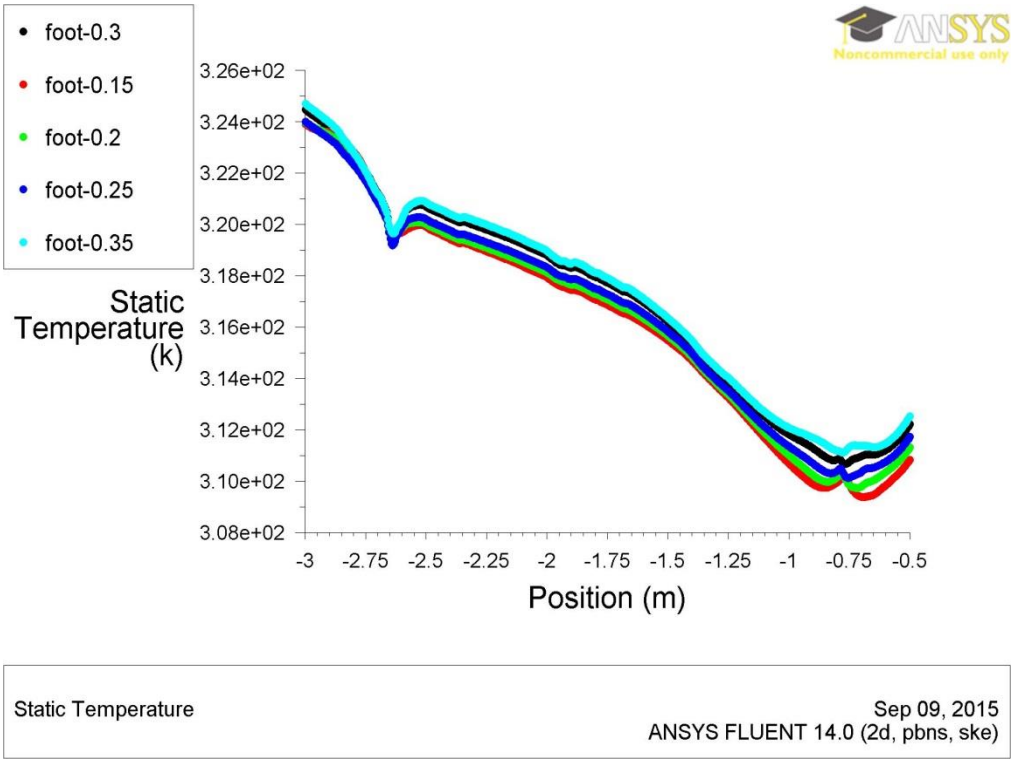

Figure 9.13: Foot temperature trends under the effect of each PV transparency level

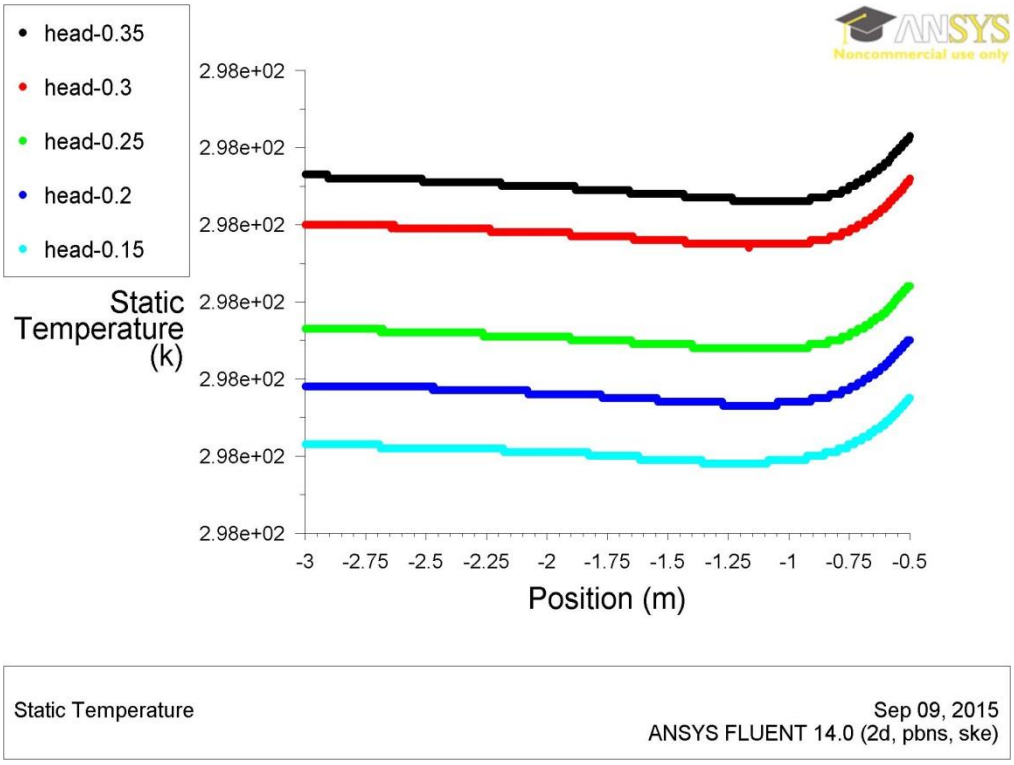

Figure 9.14: Head temperature trends under the effect of each PV transparency level

Figure 9.13 shows the temperature performance of the foot rakes that were created for the occupied zone as a function of the five PV transparency levels. It can be noticed that the foot area are the most effected when the PV transparency levels of 0.15 was applied with an average temperature of 37^0C, though, the volume of the heat was relatively similar when the other transparencies considered with trivial decrease. The overall average temperature for the foot from the other transparencies is 36^0C which is accounted as thermally uncomfortable. In contrary, Figure 9.14 offers constant temperature behaviours for the head rake with each PV transparency degree where the average temperature for each performance is 25^0C.

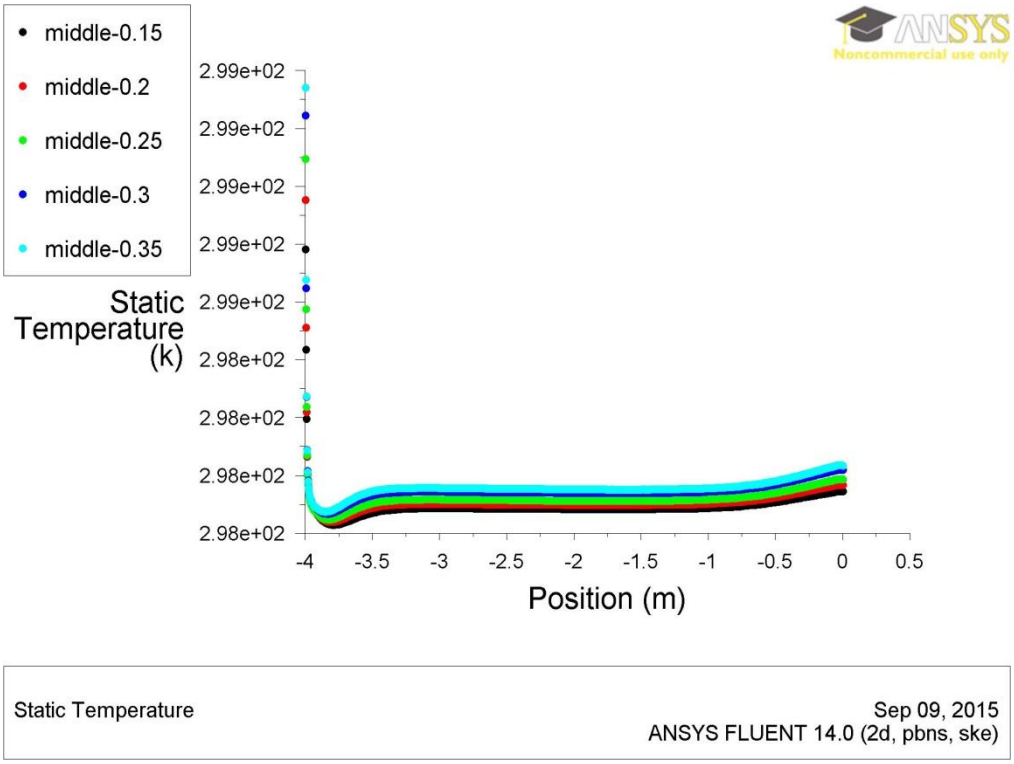

Figure 9.15: Middle rake temperature trends under the effect of each PV transparency level

The temperature predictions of the middle rake that was identified horizontally from the window to the back wall for each PV transparency level are shown in Figure 9.15. The figure indicates that identical temperature trends can be obtained when the PV transparency levels of 0.15, 0.2, 0.25, 0.3, and 0.35 were employed where the average temperature value is 25^0C which is the required thermal level. Table 9.5 presents the average temperature values of each rake in the model under each PV transmittance level.

Table 9.5: Average temperature values of each rake in the model under each PV transmittance level

Transparency Levels	Occupied Zone Rakes				
	Front Rake	Back Rake	Foot Rake	Head Rake	Middle Rake
0.15	**25**	**25**	**37**	**25**	**25**
0.2	25	25	36	25	25
0.25	25	25	36	25	25
0.3	25	25	36	25	25
0.35	25	25	36	25	25

9.5.1 VENTILATION PERFORMANCE FOR SUMMER COOLING

The air velocity magnitudes of the space interior are illustrated in Figure 9.16 (a, b, c, d, e and f). The figure includes the effect of each PV transparency level on the interior ventilation behaviour. It can be observed that the best air circulation can be achieved inside the office room when applying the PV level of 0.35, and that is traceable to the high velocity applied for this level as shown in Table 9.3. However, the air flow rate was extremely high, 94L/s, whilst it was acceptable, 66L/s, when the PV level of 0.15 employed where the air movement appeared relatively poor. The PV levels of 0.2, 0.25, and 0.3 had similar impact on the ventilation pattern where the air properly moved inside the space with air flow rate vary between 73L/s and 87L/s.

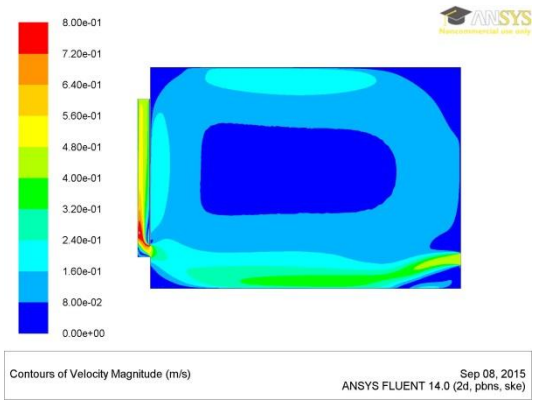

(a): Air flow pattern for PV transparency level of 0.15

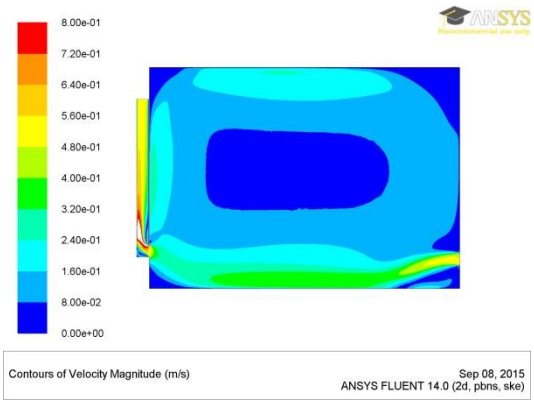

(b): Air flow pattern for PV transparency level of 0.2

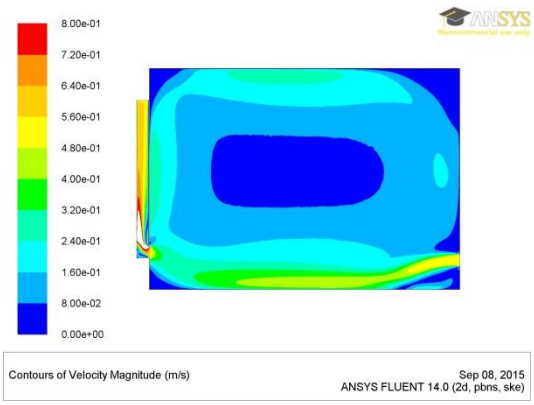

(d): Air flow pattern for PV transparency level of 0.25

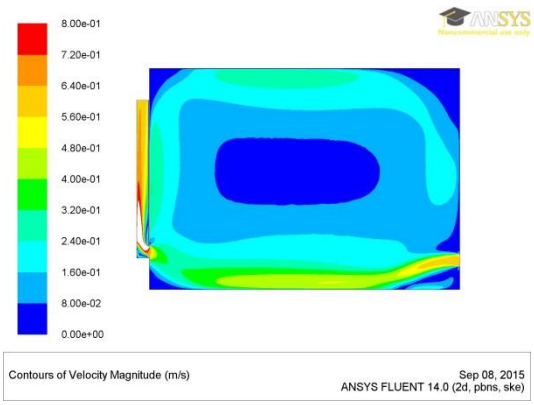

(e): Air flow pattern for PV transparency level of 0.3

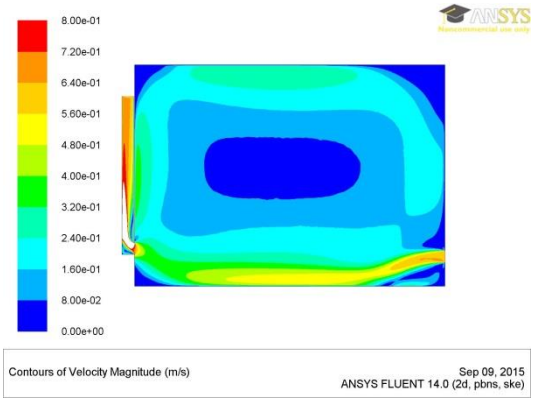

(f): Air flow pattern for PV transparency level of 0.35

Figure 9.16: Air flow pattern for different PV transparency levels

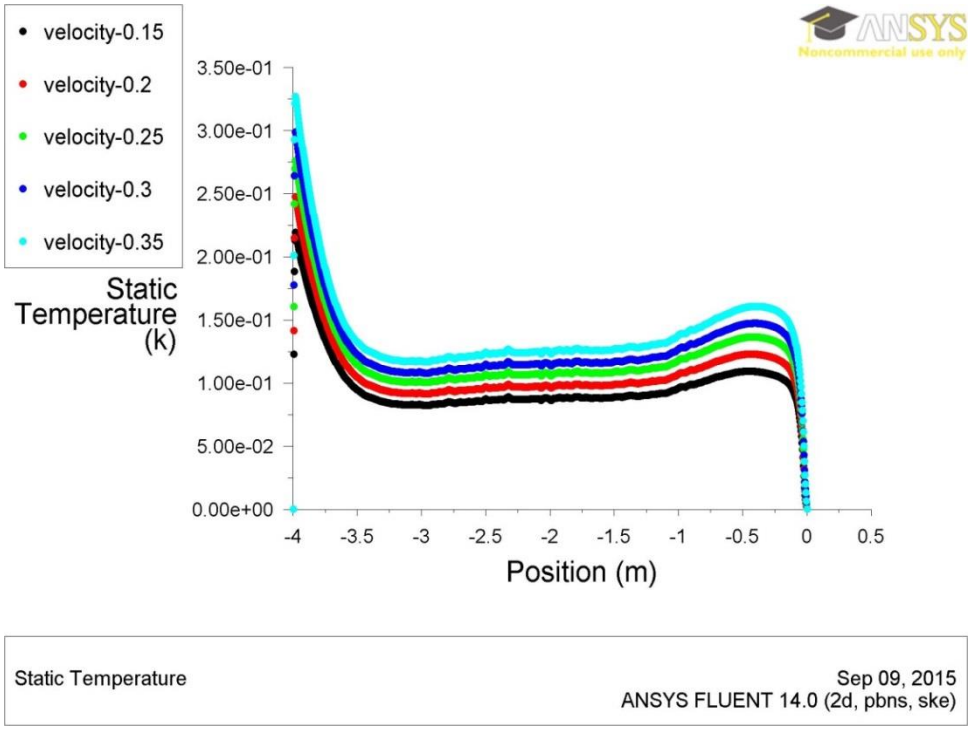

Figure 9.17: Air velocity trends under the effect of each PV transparency level

Figure 9.17 presents the impact of each PV transparency level on the ventilation performance as trends of the air velocity that was predicted along the middle rake of the room model. The figure denotes that various air velocity magnitudes were found from the five transparencies. This can be imputed to the fact that the consecutive simulations were aimed to achieve accepted air temperature under each PV level. Thus, the actual air velocities harnessed to the PV levels were slightly different and so did the velocity behaviours. The air velocity inside the interior environment is predominated with a pace varying between 0.09 and 0.14m/s.

9.6 COMPARISON BETWEEN DIFFERENT PV TRANSPARENT LEVELS WITH AND WITHOUT INTERNAL HEAT GAINS

Figure 9.18 shows the temperature estimations along the horizontal rake that extends across the room as imputed to the PV transparency level of 0.15 for both cases: with and without internal heat gains. It can be noticed that the addition of such heat sources can relatively escalate the air temperature inside the space to override the thermal required standard. However, increasing the air velocity, when considering internal heat gains, can bring the interior to the comfort plane with an acceptable elevated flow rate. In conclusion, the PV transparency level of 0.15 is optimal for the summer conditions.

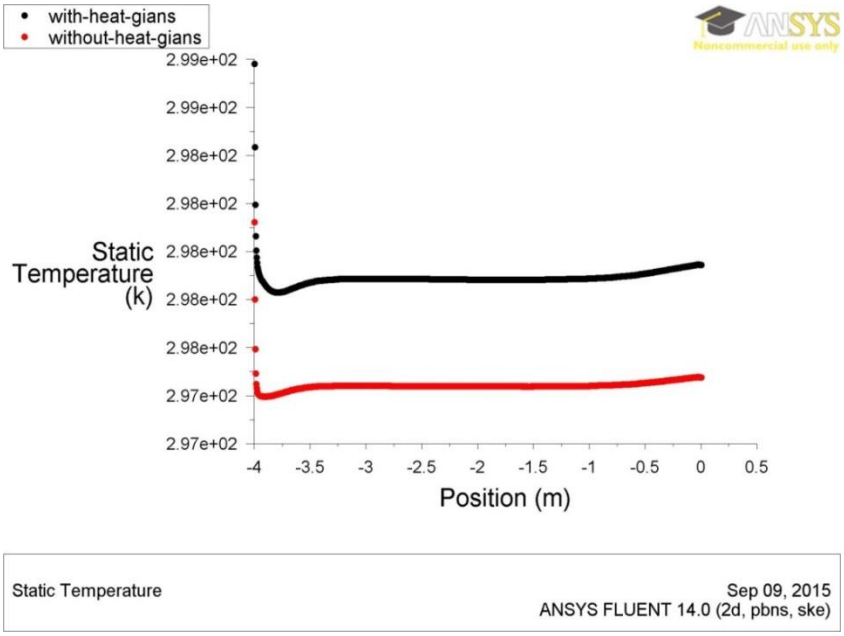

Figure 9.18: Middle rake temperature trends under the effect of PV transparency level of 0.15 with and without internal heat gains

9.7 SUMMARY

The values of internal heat gains emitted from the occupants, artificial lighting, and office equipment were added to the floor heat flux and the temperature and ventilation performance inside the space were predicted along the centre line (under the effect of PV transparency level of 20% for winter and 15% for summer) and compared to the estimations without the internal heat gains. This reveals that the thermal comfort is still acceptable with the addition of internal heat gains as it did not exceed the required thermal level in winter. However, in the summer, internal heat gains can relatively escalates the temperature around the window, but this can be sorted out with increased air velocity. Next chapter will investigate the effect of transient treatment on thermal and ventilation performances of the window unit.

CHAPTER 10 IMPACT OF TRANSIENT TREATMENT ON THERMAL AND VENTILATION PERFORMANCES OF AIRFLOW WINDOW

The effect of the time-dependant condition was investigated through a comparison between the thermal and ventilation performance of the transient and steady state conditions for the window unit under the impact of the solar radiation of each hour during the daytime in the season of winter and summer. The optimum PV transparency levels found in the previous analysis as well as the optimum ventilation force for each season were implemented. In addition, PV electric analysis were carried with relevance to each condition, steady and transient, as a result of each solar radiation since it constitutes a key element in PV function.

The transient flow modelling was performed through the calculation of the solar irradiance for each minute in the winter, from 8am to 4pm, and in the summer, from 5am to 7pm. Then, the solar radiation levels incident on each of the PV panel, the double glazing panes and the floor were calculated for both seasons according to the solar irradiance of each minute. Consequently, simulations were run, under transient solver, for each minute's inputs to estimate its thermal and ventilation impact on the interior space. The first minute was iterated until it is converged whilst the rest of the time 10 s time step was constantly assigned, as recommended in (Fluent 2009) for each minute to capture the prompt temperature change. Ultimately, the effects of variant solar radiations that can express different potentials, (18.3, 300.09, 523.18, 656.16 and 707.36G) for winter and (62.16, 107.53, 210.21, 448.98 and 538.62G) for summer, on the thermal and ventilation performance as well as PV efficiency under transient and steady state conditions were compared to depict the impact of transient operation.

10.1 WINTER HEATING

10.1.1 TEMPERATURE PERFORMANCE FOR WINTER HEATING

The temperature estimations of the thermal performance liberated from the solar radiation of 18.3W/m^2 for the transient and steady state conditions are presented in Figure 10.1. It can be observed that the solar radiation of 18.3W/m^2 can convey similar thermal behaviour for both conditions where the average temperature of the space under either condition is 6^{0}C. In contrary, Figure 10.2 shows different temperature performance when the solar radiation of 300.09W/m^2 was applied for each condition. The figure manifests that the thermal performance under the impact of steady state condition inside the space can be two degrees higher than the transient state performance. The average transient and steady temperatures of the interior are 9^{0}C and 11^{0}C, respectively. This difference might be attributed to the wide class of analysed data under the transient operation that ascertain numerically the actual thermal patterns.

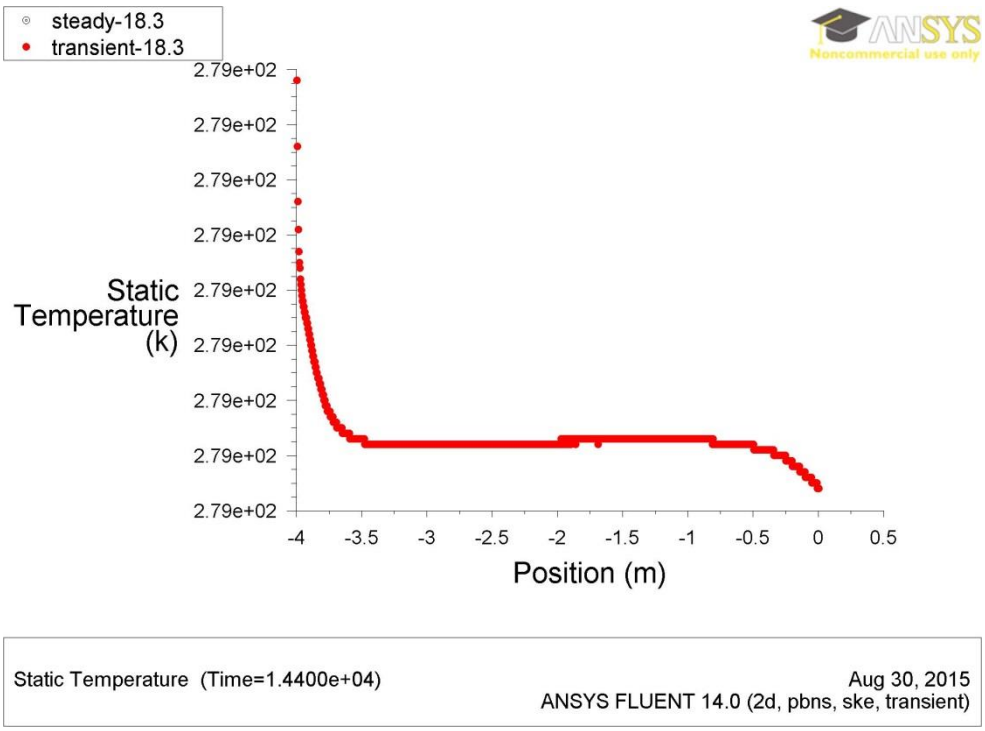

Figure 10.1: Temperature trends under the effect of solar radiation of 18.3W/m^2 for steady and transient state

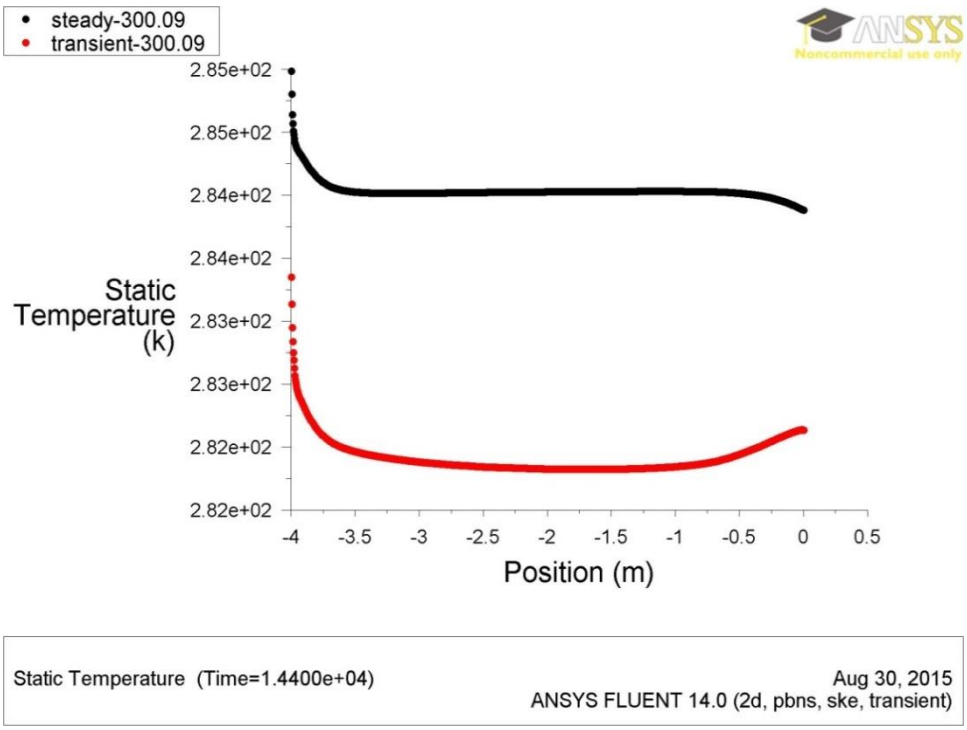

Figure 10.2: Temperature trends under the effect of solar radiation of 300.09W/m^2 for steady and transient state

Figure 10.3 shows the temperature patterns of the transient and steady state conditions when the solar radiation of 523.18W/m^2 was applied. It can be noticed that the heat that can be liberated from the mentioned solar radiation is higher under the steady state condition than the transient where the average temperature of the interior under the transient and the steady state conditions are 13^{0}C and 15^{0}C, respectively. Similarly, the same can be seen from the temperature predictions of both conditions when the solar radiation of 656.16W/m^2 was considered as shown in Figure 10.4. The inside space can possess more heat under the steady condition than it does under the transient regime revealing an average temperature of 17^{0}C which transcends the average of transient condition which is 16^{0}C. Furthermore, the representation of the steady and transient temperature trends according to the impact of the solar radiation of 707.36W/m^2 can be similar to the previous outcomes which are shown in Figure 10.5. The figure indicates that the interior temperature, under the steady state, is higher than the interior thermal performance under the transient state with an average temperature of 18^{0}C and 17^{0}C for the former and latter, respectively. Table 10.1 shows the Average temperature values of each condition under each solar radiation.

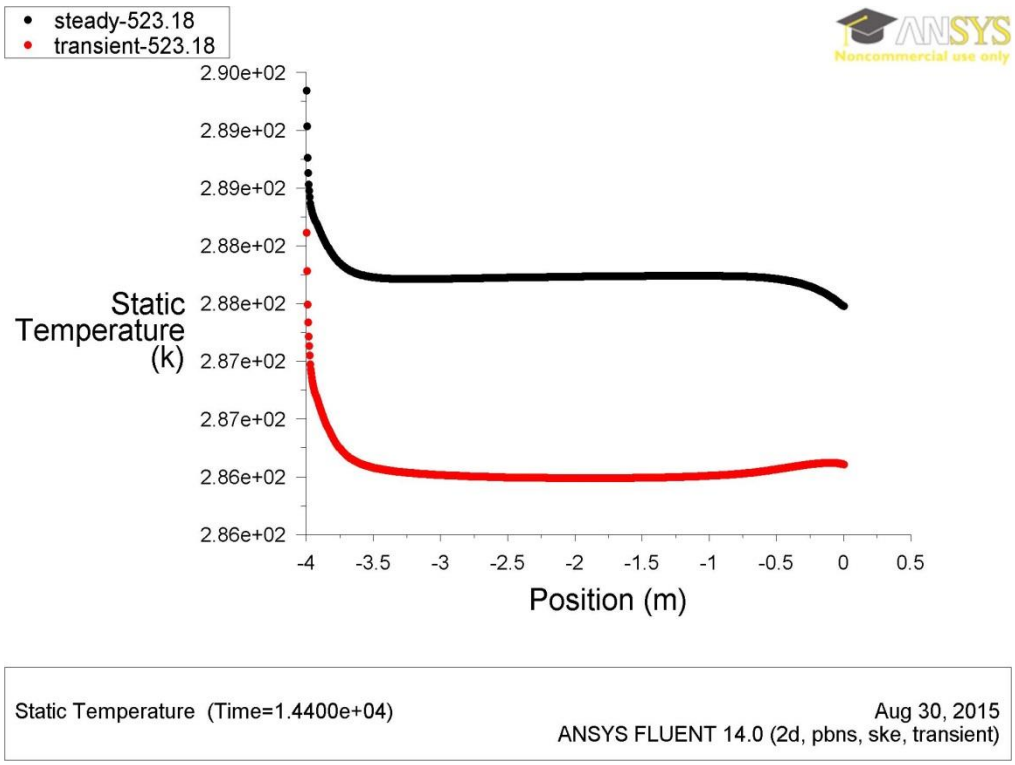

Figure 10.3: Temperature trends under the effect of solar radiation of 523.18W/m^2 for steady and transient state

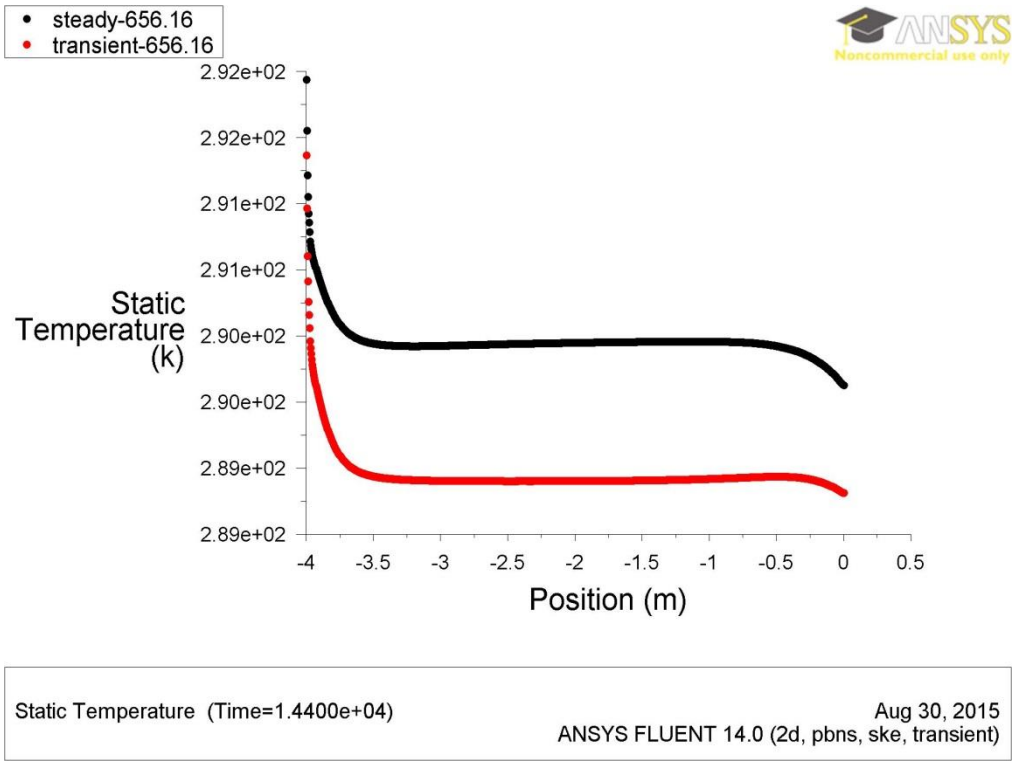

Figure 10.4: Temperature trends under the effect of solar radiation of 656.16W/m^2 for steady and transient state

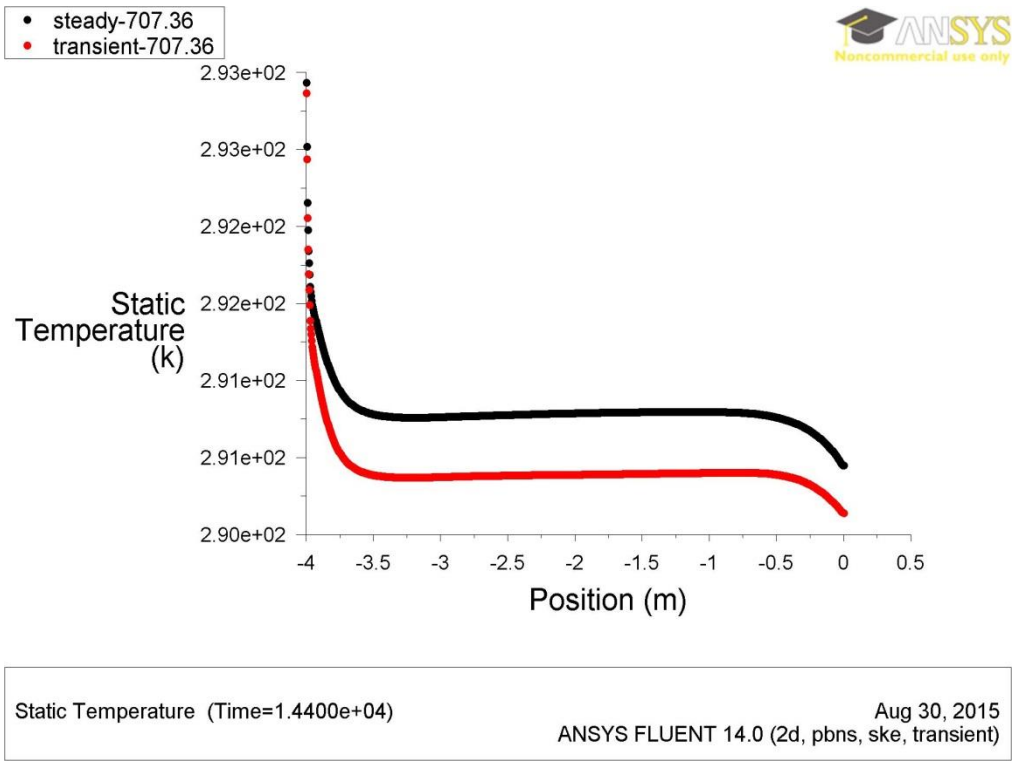

Figure 10.5: Temperature trends under the effect of solar radiation of 707.36W/m^2 for steady and transient state

Table 10.1: Average temperature values of each condition under each solar radiation of the winter season

	Solar Radiation W/m^2				
Conditions	**18.3**	**300.09**	**523.18**	**656.16**	**707.36**
Steady ^{0}C	6	11	15	17	18
Transient ^{0}C	6	9	13	16	17

10.1.2 VENTILATION PERFORMANCE FOR WINTER HEATING

The air flow performance, inside the office space, according to the impact of the solar radiations of 18.3, 300.09, 523.18, 656.16 and 707.36W/m^2 for the steady and transient conditions is presented in Figures 10.6-10.15, respectively. For the effect of the solar radiation of 18.3W/m^2, as shown in Figures 10.6 and 10.7, it can be seen that the air motion of the steady state is better than it circulates in transient state. The overwhelmed air velocity ranges between 0.15 and 0.45m/s with an average of 0.26m/s for the steady condition whilst it falls between 0.15 and 0.3m/s with an average of 0.15m/s for the transient. However, the air flow rate under each condition is 30L/s. Likewise; the same can be denoted from the Figures 10.8 and 10.9 for the impact of the solar radiation of 300.09 W/m^2. The domination of the air velocity, in the steady state, exceeds its peer in

the transient state where it ranges in the former between 0.15 and 0.45m/s and it falls between 0.15 and 0.3m/s in the latter condition with an average of 0.27m/s under the steady condition and 0.19m/s under the transient condition.

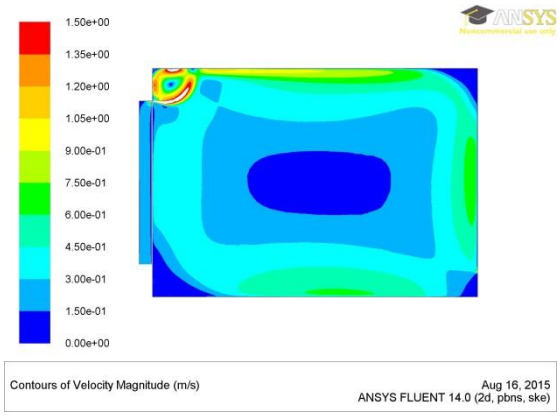

Figure 10.6: Air flow pattern for the solar radiation of 18.3W/m^2 of the steady condition

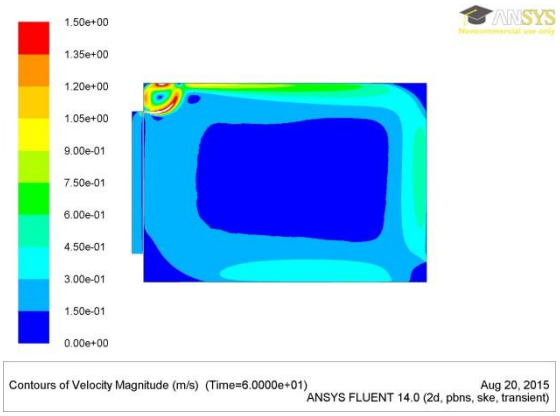

Figure 10.7: Air flow pattern for the solar radiation of 18.3W/m^2 of the transient condition

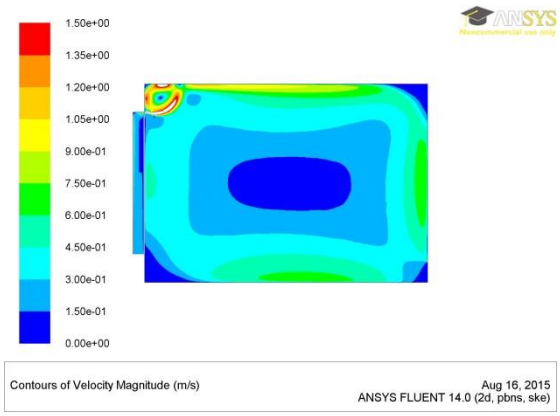

Figure 10.8: Air flow pattern for the solar radiation of 300.09W/m^2 of the steady condition

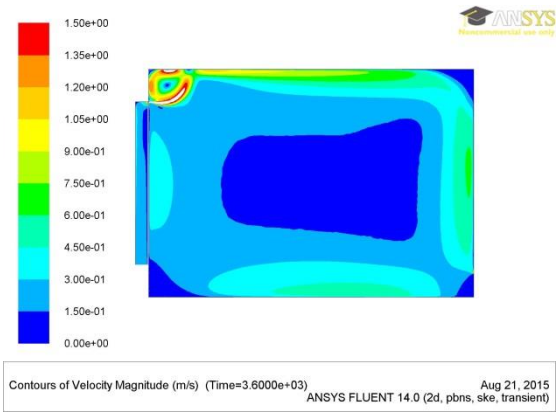

Figure 10.9: Air flow pattern for the solar radiation of 300.09W/m^2 of the transient condition

For the effect of the solar radiation of 523.18W/m^2, Figure 10.10 shows the ventilation performance under the steady condition and under the transient state the ventilation behaviour is presented in Figure 10.11. It can be noticed that the steady case offers adequate air movement than the transient does where the occupants can feel the air flow with a velocity that reaches up to 0.45m/s with an average of 0.28m/s whereas it decreases to 0.3m/s, when the transient operation is applied, with an average of 0.22m/s. Though, the air flow rate found under each case was 30L/s.

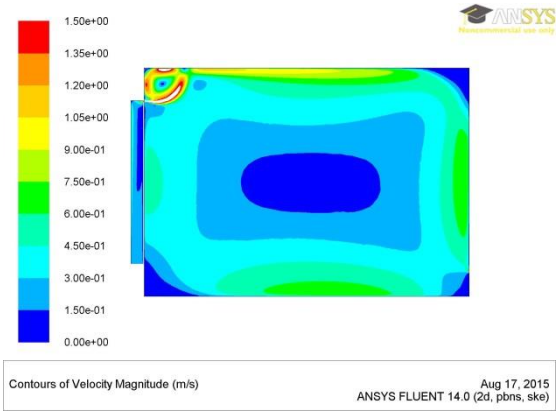

Figure 10.10: Air flow pattern for the solar radiation of 523.18W/m^2 of the steady condition

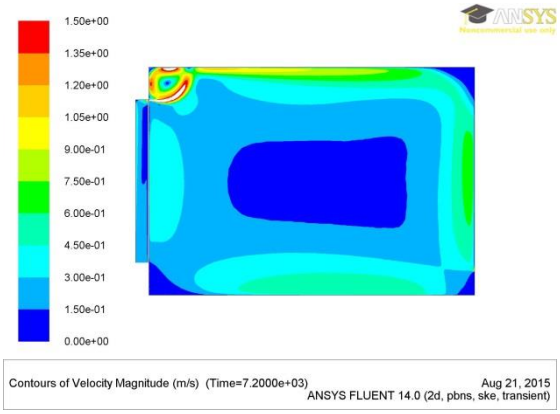

Figure 10.11: Air flow pattern for the solar radiation of 523.18W/m^2 of the transient condition

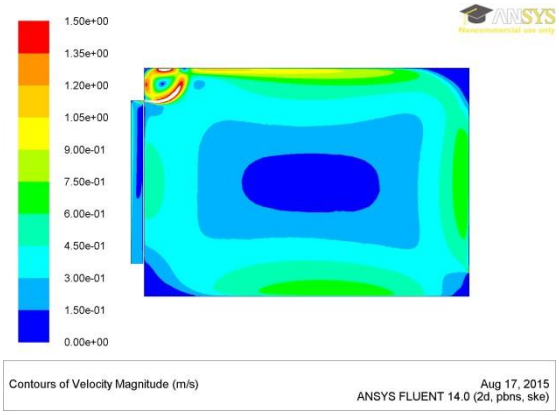

Figure 10.12: Air flow pattern for the solar radiation of 656.16W/m^2 of the steady condition

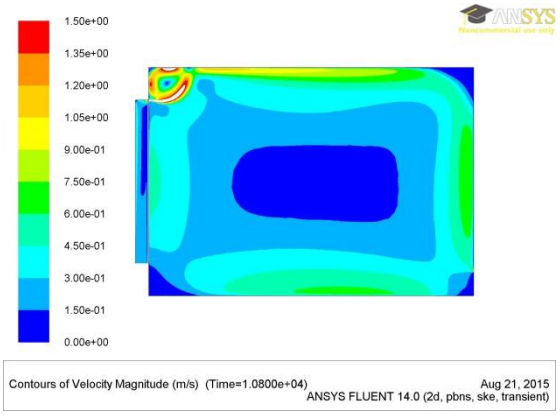

Figure 10.13: Air flow pattern for the solar radiation of 656.16W/m^2 of the transient condition

In contrary, the ventilation performance of the interior, for the steady (Figure 10.12) and transient (Figure 10.13) case when the solar radiation of 656.16W/m^2 was applied, was slightly comparable in air movement ranging in velocity between 0.15 and 0.45m/s and an average velocity of 0.29m/s for the steady state and of 0.24m/s for the transient state. The air flow rate obtained for each state was 30L/s. Similarly, the steady, as shown in Figure 10.14, and the transient, as presented in Figure 10.15, states have delivered slightly identical ventilation behaviour inside the space under the effect of the radiation of 707.36W/m^2 with appropriate air motion that predominantly circulates with a velocity of 0.45m/s. However, the average velocity of the steady condition was 0.29m/s, and it was 0.26m/s for the transient state. The air flow rate predicted for each condition was 30L/s. Table 10.2 presents the average air velocities of each condition under each solar radiation.

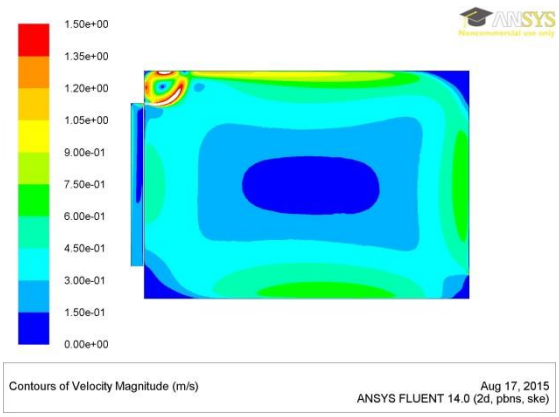

Figure 10.14: Air flow pattern for the solar radiation of 707.36W/m^2 of the steady condition

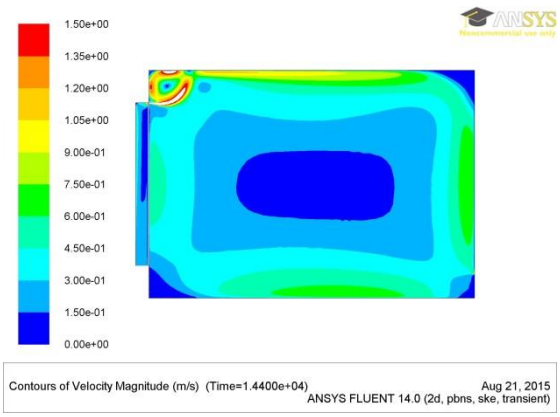

Figure 10.15: Air flow pattern for the solar radiation of 707.36W/m^2 of the transient condition

Table 10.2: Average air velocities of each condition under each solar radiation of the winter season

	Solar Radiation W/m^2				
Conditions	**18.3**	**300.09**	**523.18**	**656.16**	**707.36**
Steady m/s	0.26	0.27	0.28	0.29	0.29
Transient m/s	0.15	0.19	0.22	0.24	0.26

10.1.3 PV PANEL ELECTRIC ANALYSIS FOR WINTER HEATING

The temperature performance of the PV panel as a function of the solar radiation of 18.3W/m^2 for steady and transient state is shown in Figure 10.16. The diagram offers mostly congruent temperature estimations for each condition with an average temperature of 8^{0}C. However, the PV temperature predictions become slightly different when the solar radiation of 300.09W/m^2 was considered, as shown in Figure 10.17, with an average temperature for the steady performance of 25^{0}C and for the transient performance of 23^{0}C. Concerning the temperature values of behaviour that resultant from the rest of the solar radiations (523.18, 656.16, and 707.36W/m^2), illustrated in Figures 10.18, 10.19, and 10.20, respectively, the steady and the transient states composed identical PV temperature trends. The average temperature for each condition according to the solar value of 523.18W/m^2 was 32^{0}C and 36^{0}C for the value of 656.16W/m^2, and it was 37^{0}C for the value of 707.36W/m^2. Table 10.3 presents the average PV temperatures and electricity output resultant from different solar radiations for each condition.

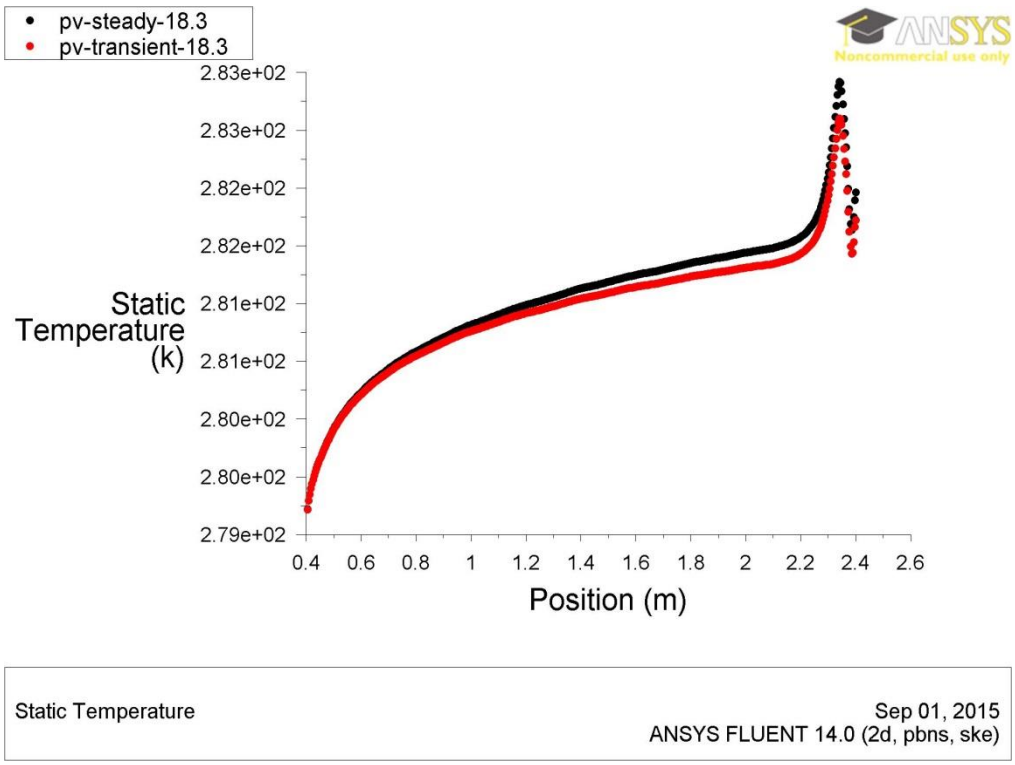

Figure 10.16:PV temperatures under the effect of the solar radiation of 18.3W/m^2

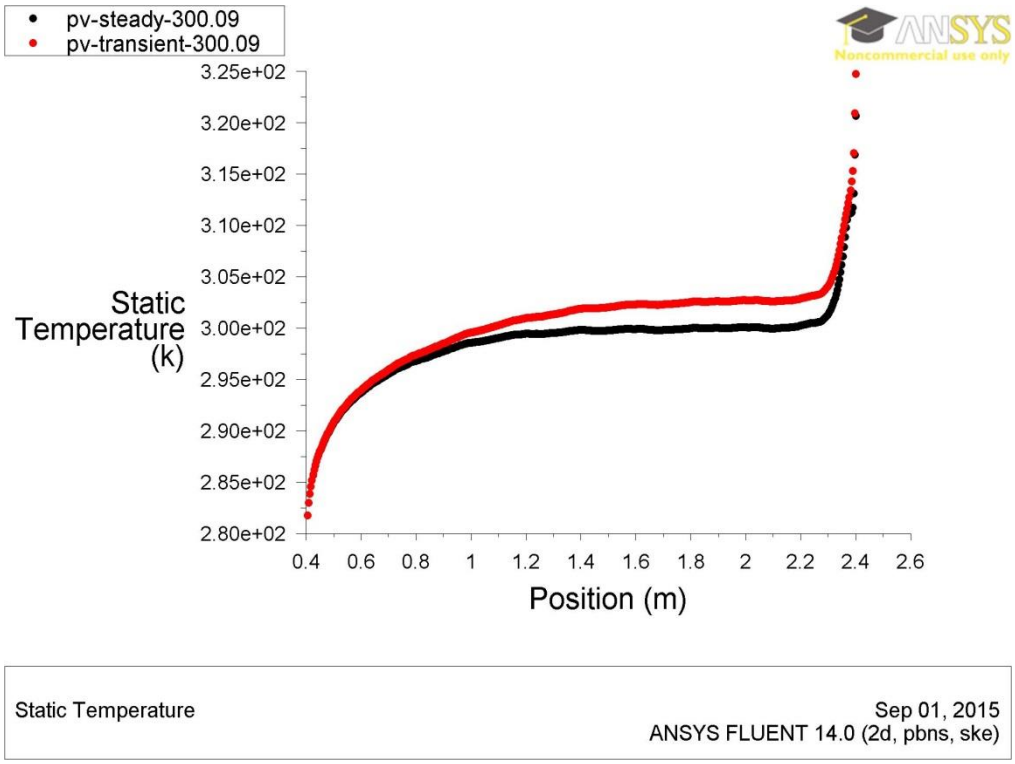

Figure 10.17:PV temperatures under the effect of the solar radiation of 300.09W/m^2

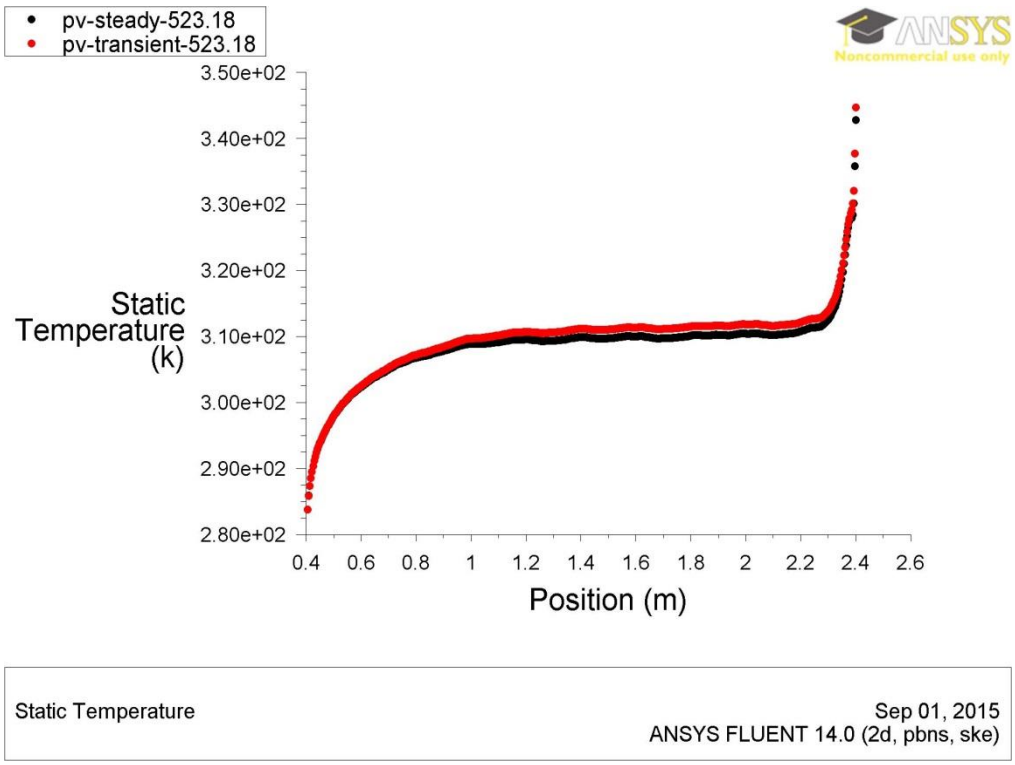

Figure 10.18:PV temperatures under the effect of the solar radiation of 523.18W/m^2

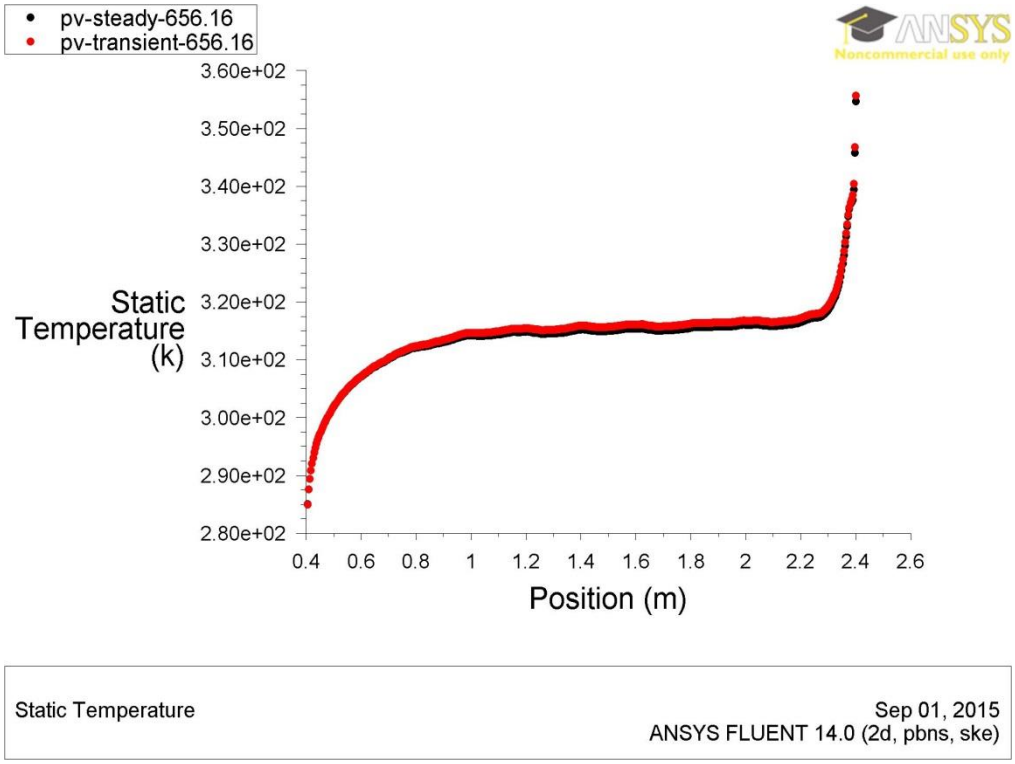

Figure 10.19:PV temperatures under the effect of the solar radiation of 656.16W/m^2

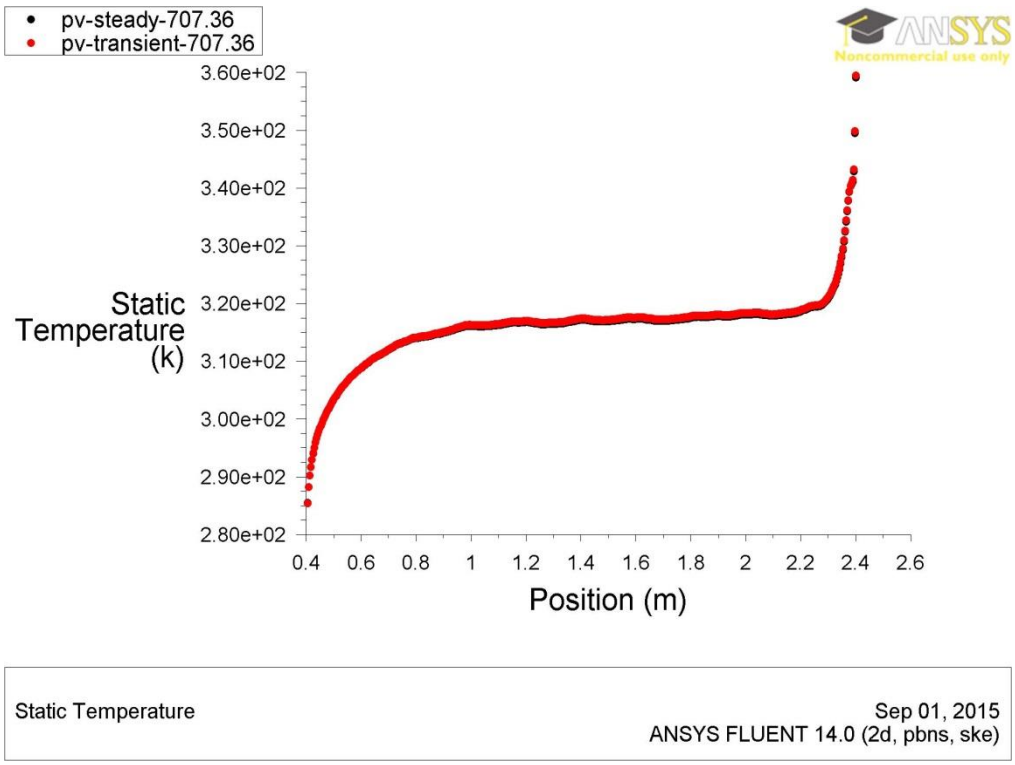

Figure 10.20: PV temperatures under the effect of the solar radiation of 707.36W/m^2

Table 10.3: Average PV panel temperature and electricity output of each condition under each solar radiation of the winter season

	$G_{(winter)}$ W/m^2				
	18.3	**300.09**	**523.18**	**656.16**	**707.36**
(Q_P)	**3.81**	**62.42**	**108.82**	**136.48**	**147.13**
Steady ^{0}C	8	25	32	36	37
Electricity output $_{winter}$(W/m^2)	**0.2**	**3.12**	**5.34**	**6.63**	**7.13**
Transient ^{0}C	8	23	32	36	37
Electricity output $_{winter}$(W/m^2)	**0.2**	**3.14**	**5.34**	**6.63**	**7.13**

10.2 SUMMER COOLING

10.2.1 TEMPERATURE PERFORMANCE FOR SUMMER COOLING

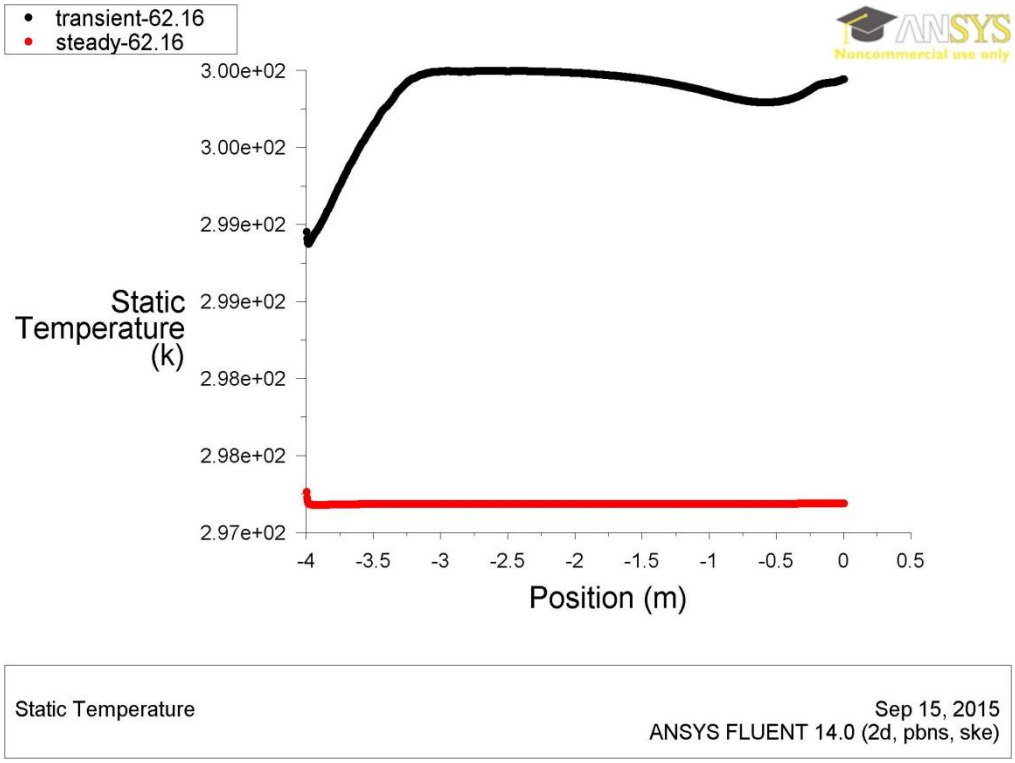

Figure 10.21 : Temperature trends under the effect of solar radiation of 62.16W/m^2 for steady and transient state

Conveyed thermal power, from the solar radiation of 62.16W/m2, into the room interior for the steady and transient state is represented by temperature value trends in Figure 10.21. The figure shows that different thermal performance is attained from transient and steady state condition where former case has escalated the temperature above the comfort level with an average of 27^{0}C whilst the latter case maintained the level to the required degree with an average temperature of 24^{0}C. Similarly, liberated thermal energy from the solar radiation of 107.53W/m2, as seen in Figure 10.22, formulates different temperature behaviour from the time-dependant and independent states. It can be observed that when involving time impact on the thermal performance, occupants can feel uncomfortable where the average temperature obtained is 27^{0}C, though, it is 24^{0}C and occupants can feel neutral when fixed time was applied.

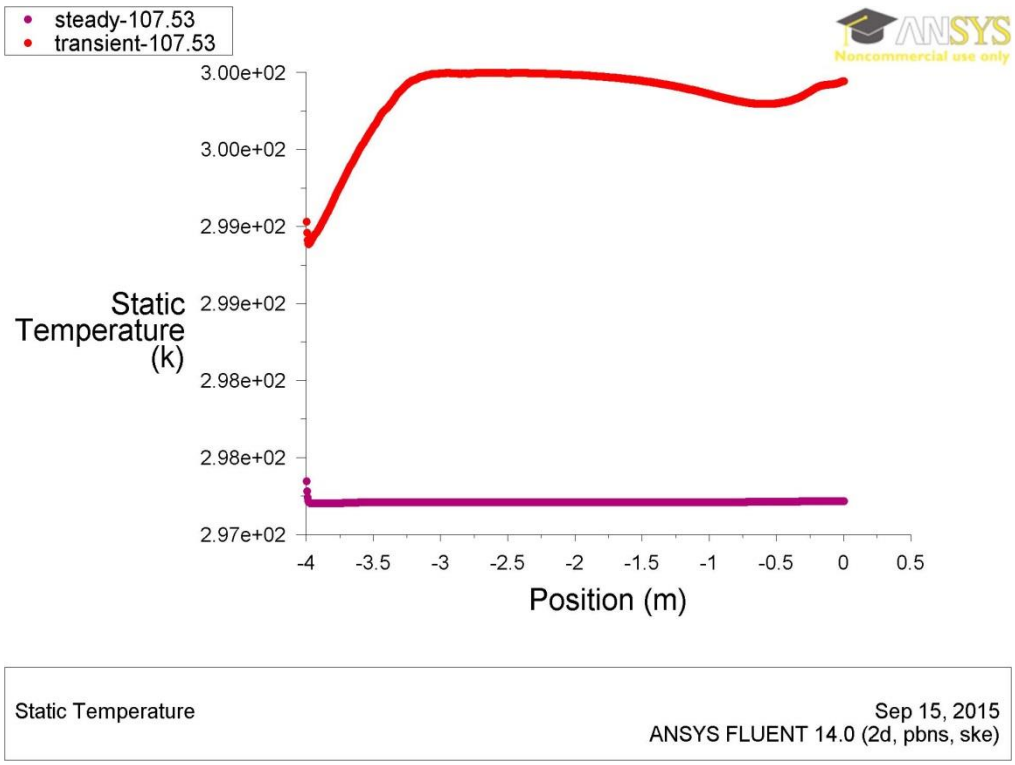

Figure 10.22 : Temperature trends under the effect of solar radiation of 107.53W/m^2 for steady and transient state

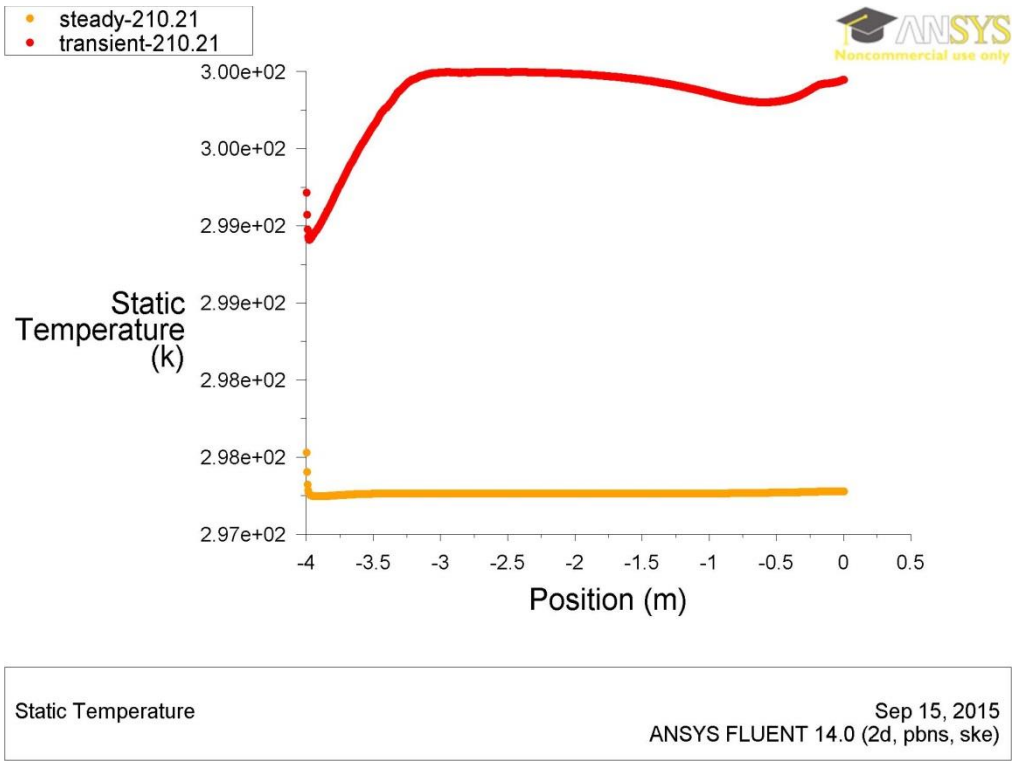

Figure 10.23 : Temperature trends under the effect of solar radiation of 210.21W/m2 for steady and transient state

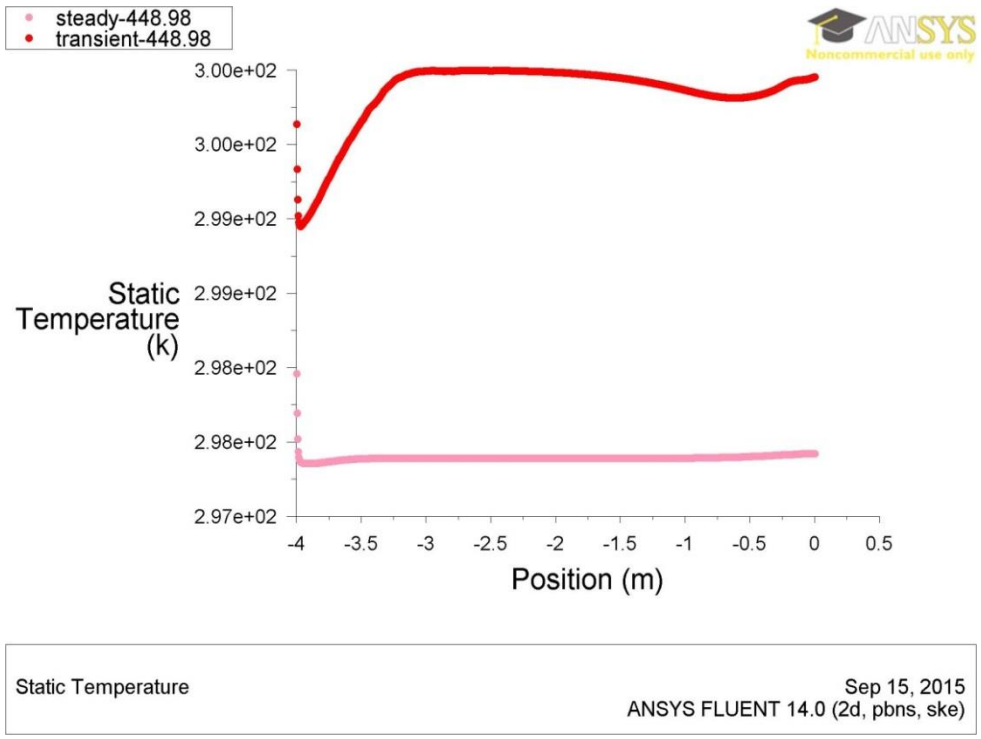

Figure 10.24 : Temperature trends under the effect of solar radiation of 448.98W/m2 for steady and transient state

The temperature performance of time-dependent and time-fixed conditions attributed to the solar radiation of 210.21W/m^2 is shown in Figure 10.23. It can be seen that the heat transferred into the space interior can be higher under the transient state than it is under the steady state where the average temperature of higher heat and the lower heat are 27^{0}C and 24^{0}C, respectively. Likewise, similar can be noticed from the temperature estimations of both conditions with imputation to the solar radiation of 448.98W/m^2 as presented in Figure 10.24. Indeed, occupants can be thermally uncomfortable under the transient state where the interior temperature overrode the comfort level with an average of 27^{0}C; however, they can be thermally neutral under the impact of fixed time condition with an average temperature of 24^{0}C. Moreover, the transient and the steady thermal outcomes of the solar radiation of 538.62W/m^2 can be even identical to the previous results which are illustrated in Figure 10.25. It can be seen that the two behaviours are various as high heat was evolved from the transient condition compare to the steady one giving an average temperature for the room interior of 27^{0}C, high, and 24^{0}C, low. Table 10.4 shows the Average temperature values of each condition under each solar radiation.

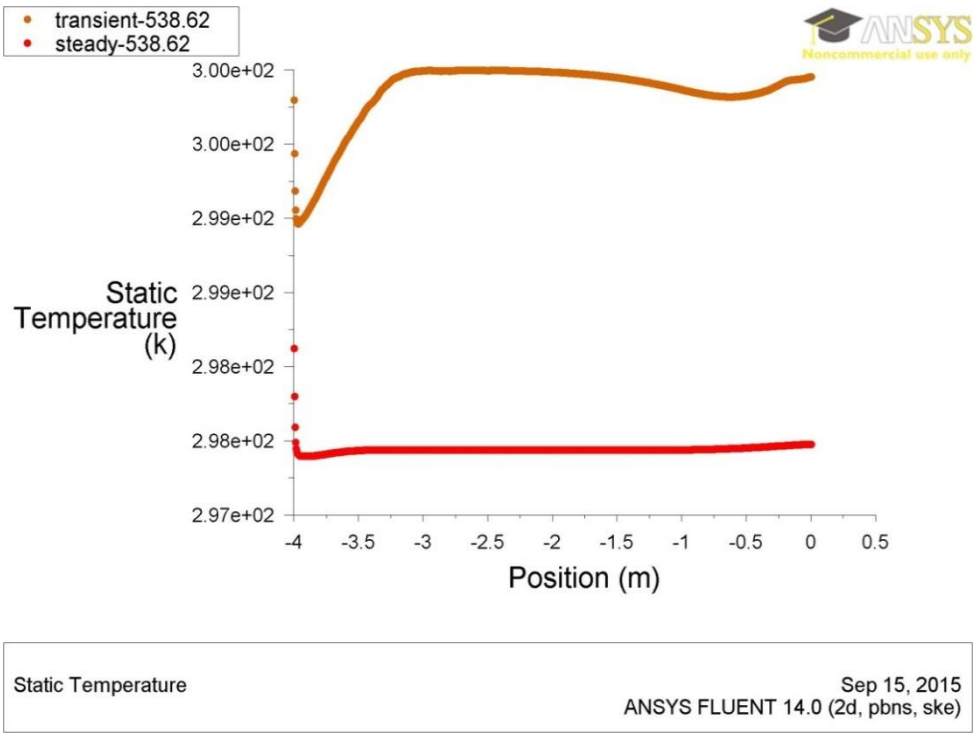

Figure 10.25 : Temperature trends under the effect of solar radiation of 538.62W/m2 for steady and transient state

Table 10.4 : Average PV panel temperature of each condition under each solar radiation of the summer season

	Solar Radiation W/m^2				
Conditions	**62.16**	**107.53**	**210.21**	**448.98**	**538.62**
Steady ^{0}C	24.03	24.05	24.11	24.24	24.28
Transient ^{0}C	26.69	26.69	26.69	26.69	26.70

10.2.2 VENTILATION PERFORMANCE FOR SUMMER COOLING

Figures 10.26-10.35 show the resultant air flow pattern, from the solar radiations of 62.16, 107.53, 210.21, 448.98 and 538.62W/m^2, respectively, of the room environment that is traced to time-induced and time-liberated conditions. The behaviour representation, Figures 10.26 and 10.27, of the solar radiation of 62.16W/m^2 shows that the steady state can demonstrate more proper air movement than the transient condition does. The dominant air velocity for the appropriate motion falls between 0.09 and 0.9m/s with an average of 0.25m/s whereas the inconvenient air circulation ranges between 0.05 and 0.5m/s with an average of 0.16m/s. However, the air flow rate under each condition is 77L/s. For the rest solar radiations, the prevailing condition is reflected in a recursive steady state and transient air flow, as seen in Figures 10.28-10.35, where the steady movement is higher than the transient one and the air circulates in a similar

rate, 77L/s. The average air velocities of each condition under each solar radiation are tabulated in Table 10.5.

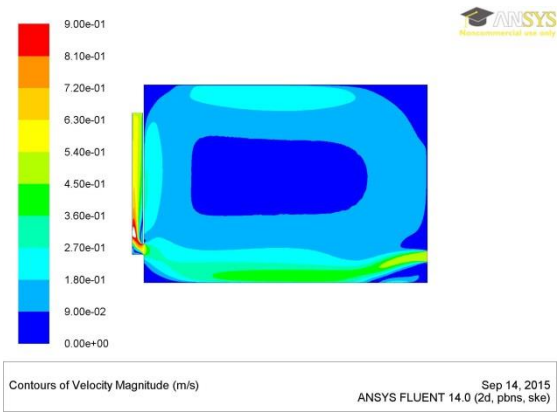

Figure 10.26 : Air flow pattern for the solar radiation of 62.16W/m^2 of the steady condition

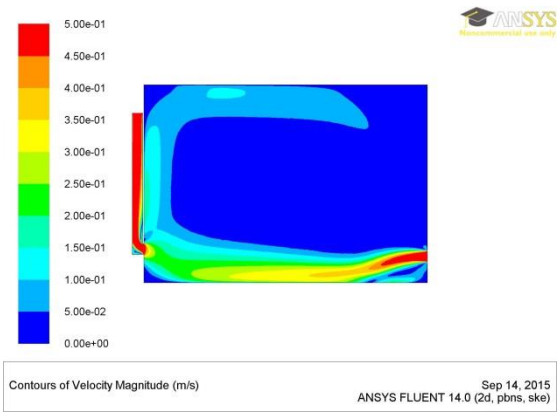

Figure 10.27: Air flow pattern for the solar radiation of 62.16W/m^2 of the transient condition

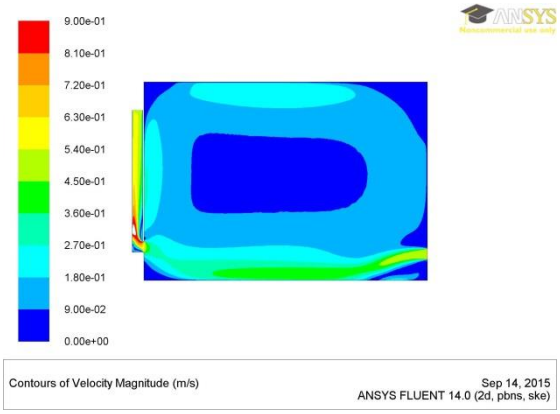

Figure 10.28: Air flow pattern for the solar radiation of 107.53W/m^2 of the steady condition

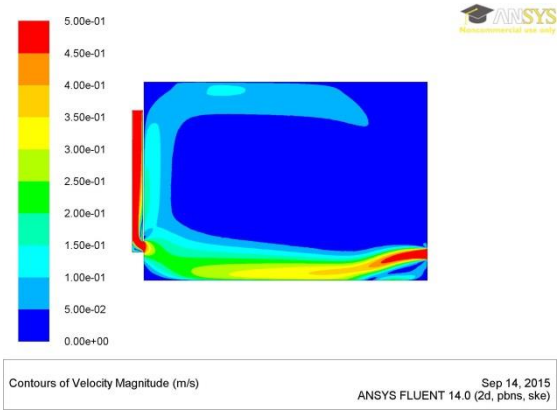

Figure 10.29: Air flow pattern for the solar radiation of 107.53W/m^2 of the transient condition

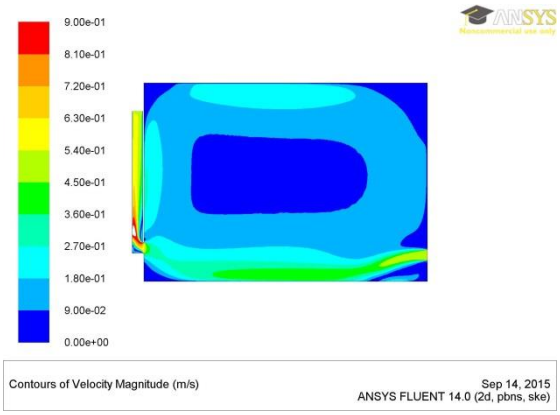

Figure 10.30: Air flow pattern for the solar radiation of 210.21W/m^2 of the steady condition

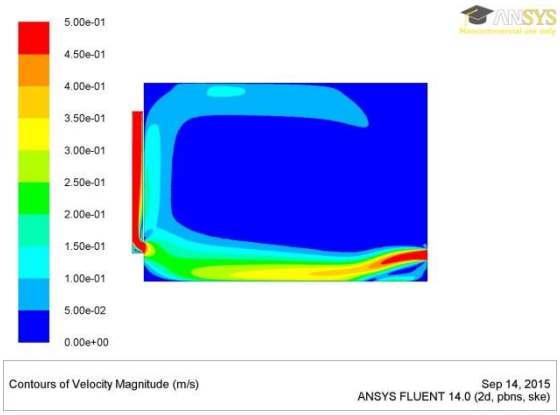

Figure 10.31: Air flow pattern for the solar radiation of 210.21W/m^2 of the transient condition

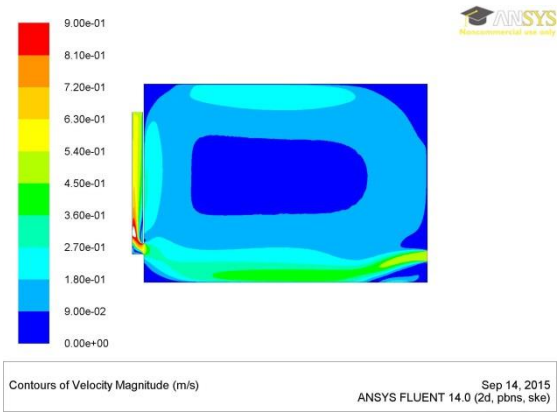

Figure 10.32: Air flow pattern for the solar radiation of 448.98W/m^2 of the steady condition

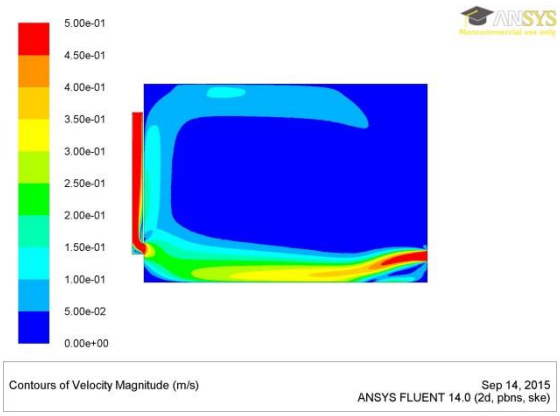

Figure 10.33: Air flow pattern for the solar radiation of 448.98W/m^2 of the transient condition

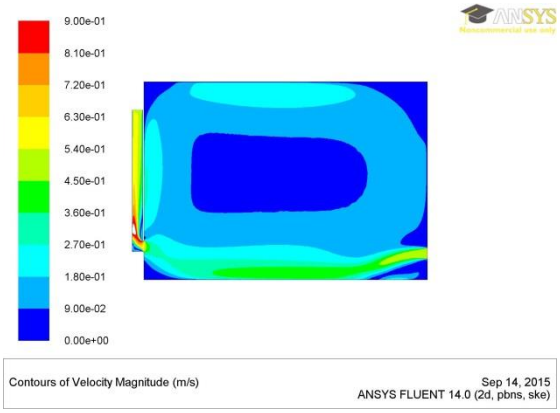

Figure 10.34: Air flow pattern for the solar radiation of 538.62W/m^2 of the steady condition

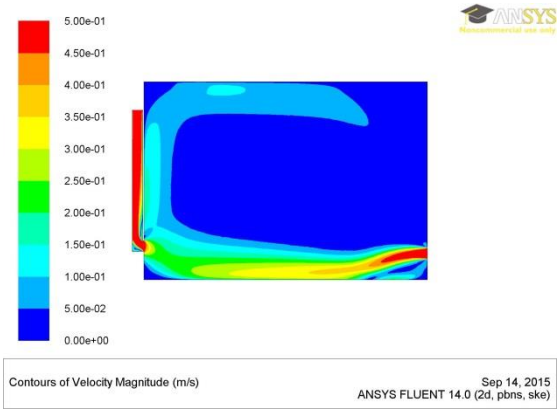

Figure 10.35: Air flow pattern for the solar radiation of 538.62W/m^2 of the transient condition

Table 10.5: Average air velocities of each condition under each solar radiation of the summer season

	Solar Radiation W/m^2				
Conditions	**62.16**	**107.53**	**210.21**	**448.98**	**538.62**
Steady m/s	0.25	0.25	0.25	0.25	0.25
Transient m/s	0.16	0.16	0.16	0.16	0.16

10.2.3 PV PANEL ELECTRIC ANALYSIS FOR SUMMER COOLING

Figure 10.36 shows the consequent PV panel temperature from the solar radiation of 62.16W/m2 as a function of time-dependant and time-independent conditions. It can be observed that the PV panel transient temperature transcends the panel steady temperature by two degrees, though; the PV can be efficient under each condition as its temperature remained tolerable with an average of 27^{0}C and 28^{0}C for the steady state and transient condition, respectively. Similarly, the solar radiation of 107.53 W/m2 plays identical effect on the transient and the steady PV thermal behaviour, as presented in Figure 10.37, by leaving two degrees difference between the two conditions with an

average of 28^{0}C, as steady, and 30^{0}C, as transient in spite that the PV efficiency continues as viable.

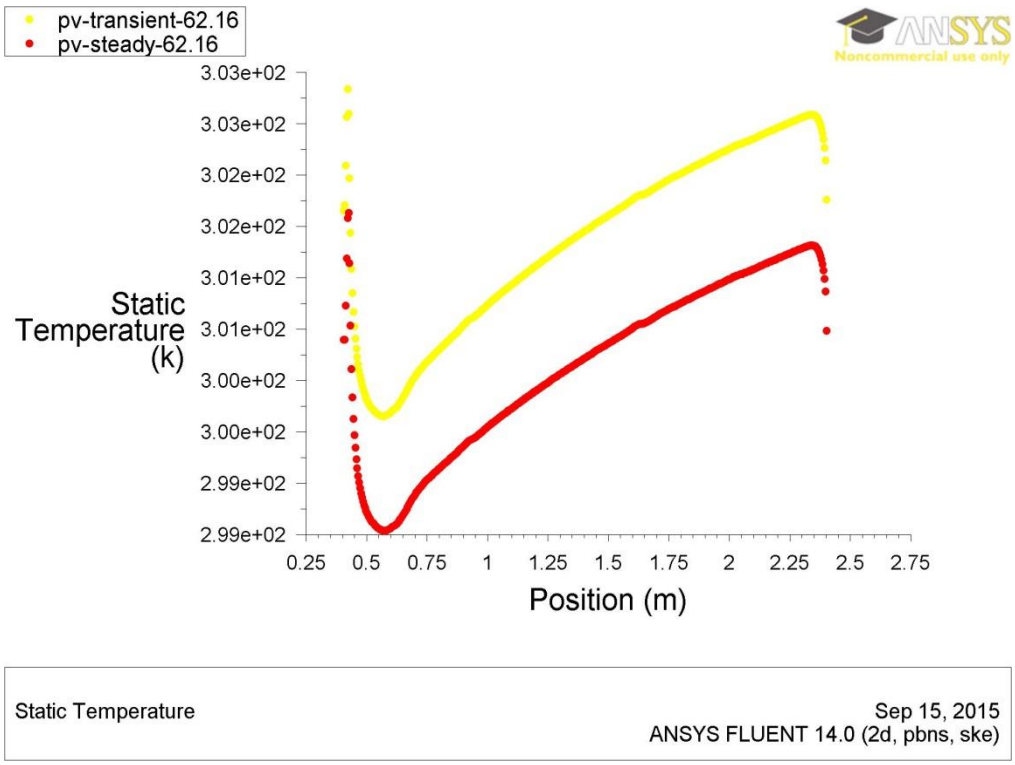

Figure 10.36: PV temperatures under the effect of the solar radiation of 62.16W/m^2

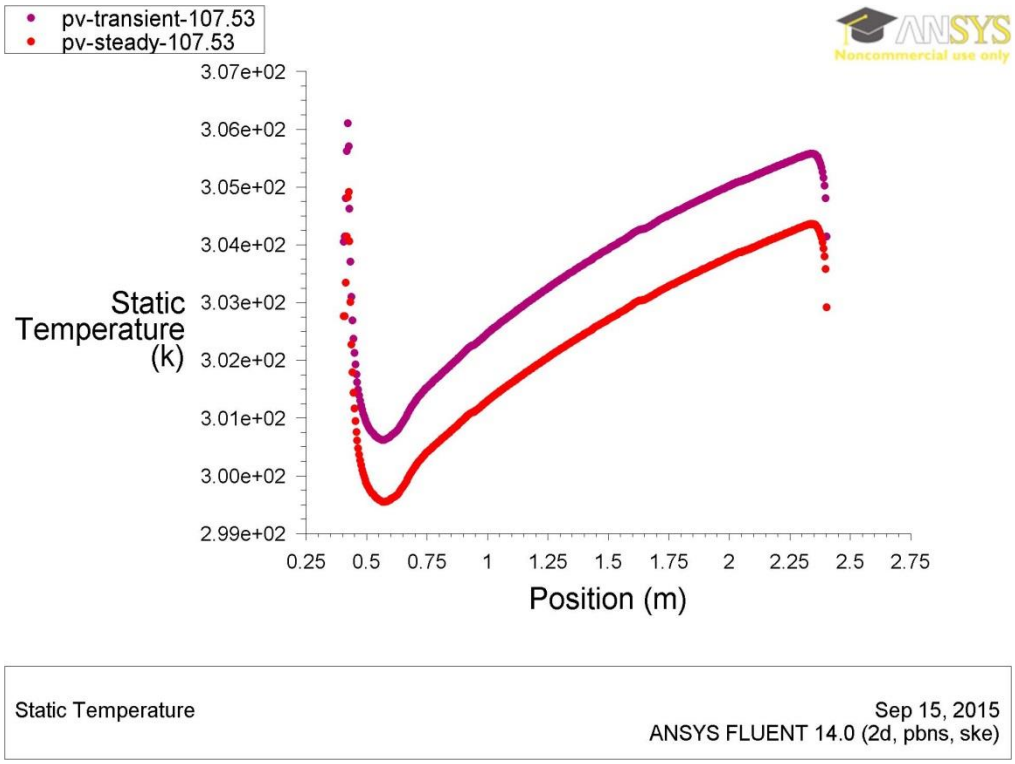

Figure 10.37: PV temperatures under the effect of the solar radiation of 107.53W/m^2

However, the more the solar radiation arises, the less the difference becomes between the PV panel transient and steady temperature as shown in the Figures 10.38, 10.39, and 10.40 for the solar radiations of 210.21, 448.98, and 538.62 W/m2, respectively, with an average temperatures of 33, 43, 46^{0}C acquired by the time-free condition and the time-induced state possessed averages of 34, 44, and 47^{0}C. This can be construed as the PV panel efficiency tumbles only with the highest solar radiation as its temperature transcended 45^{0}C which is the maximum for feasible power generation. Table 10.6 presents the average PV temperatures and electricity output resultant from different solar radiations for each condition.

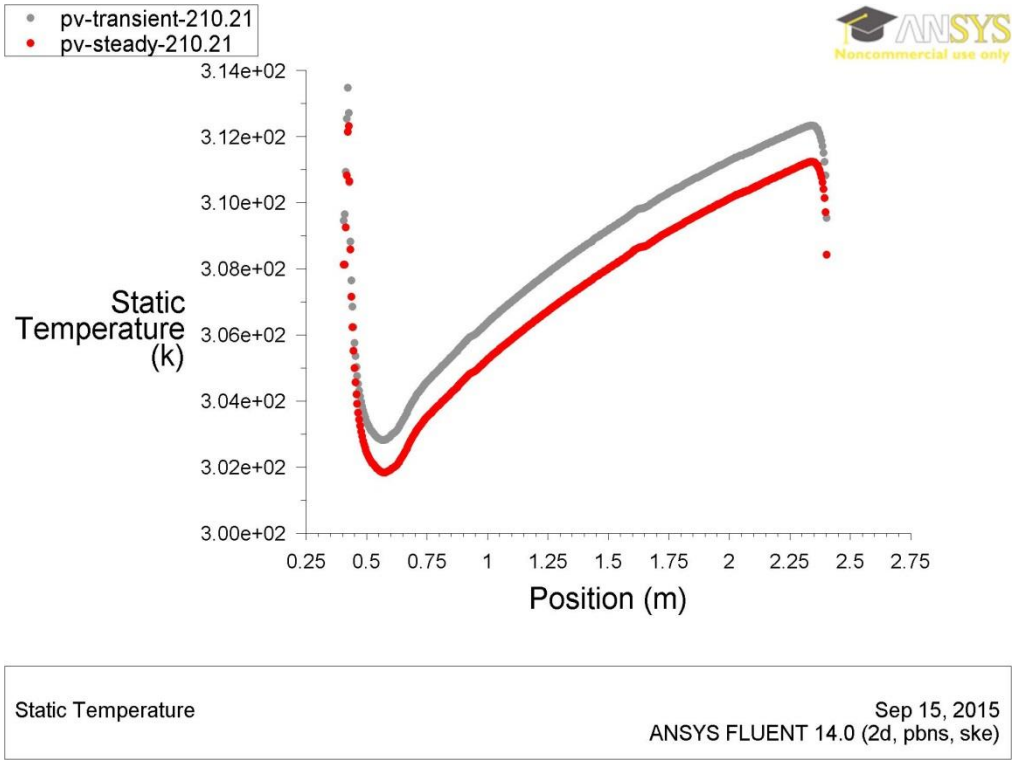

Figure 10.38: PV temperatures under the effect of the solar radiation of 210.21W/m^2

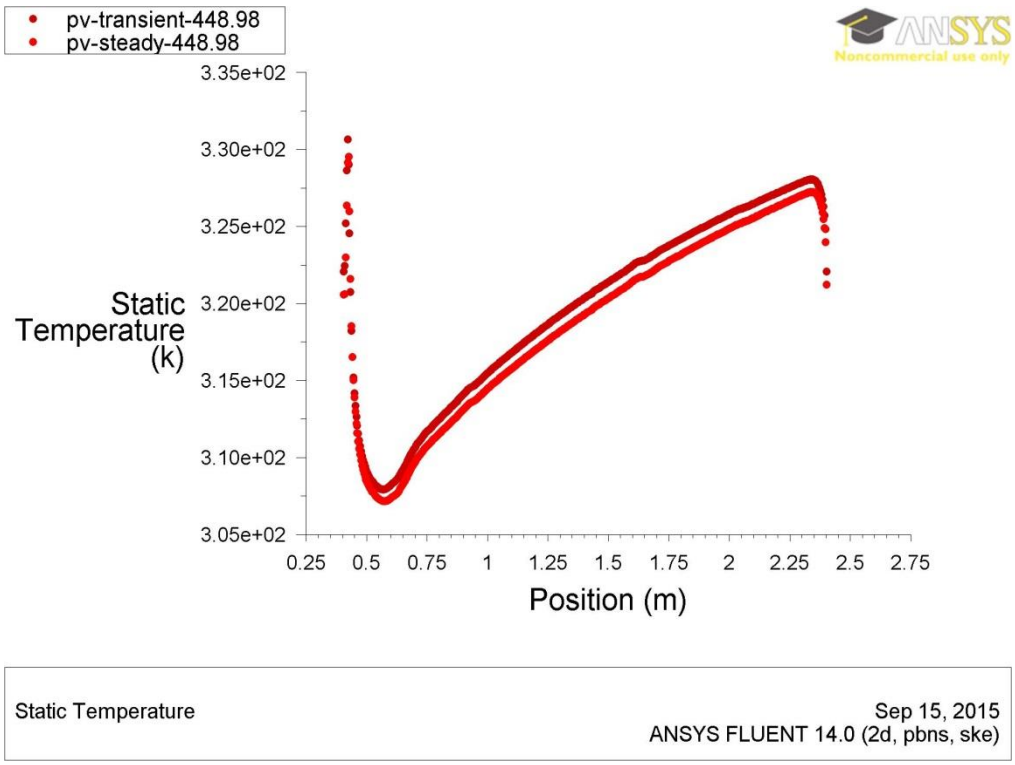

Figure 10.39: PV temperatures under the effect of the solar radiation of 448.98W/m^2

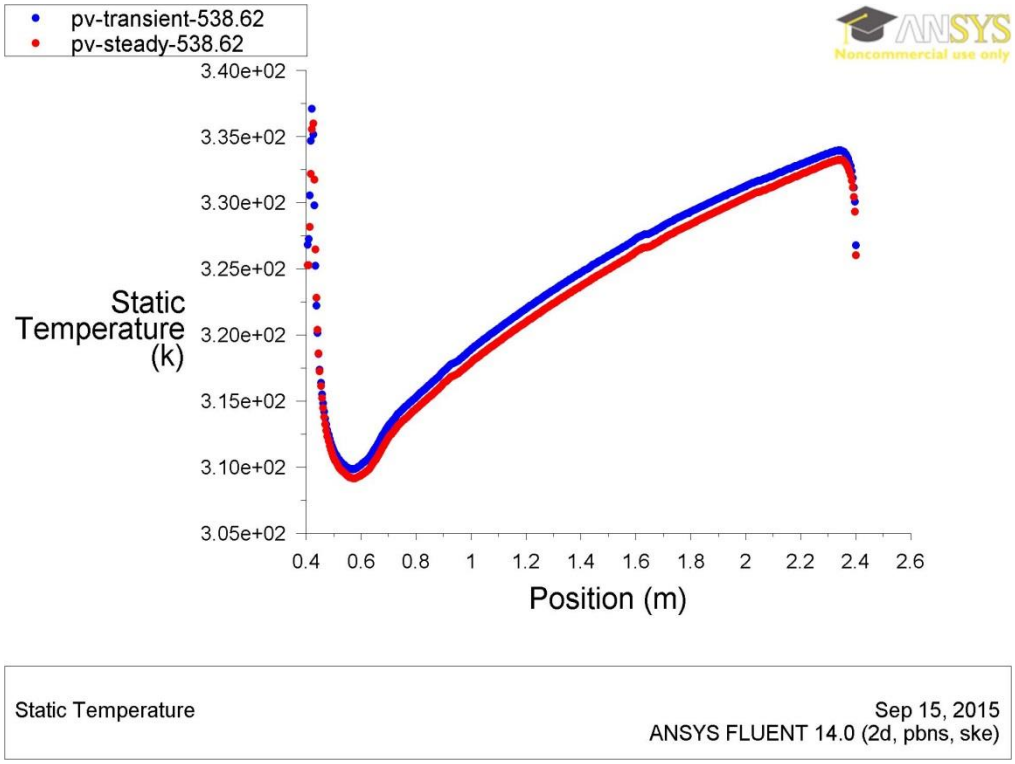

Figure 10.40: PV temperatures under the effect of the solar radiation of 538.62W/m^2

Table 10.6: Average PV panel temperature and electricity output of each condition under each solar radiation of the summer season

	$G_{(summer)}$ W/m²				
	62.16	**107.53**	**210.21**	**448.98**	**538.62**
(Q_P)	**13.92**	**24.09**	**47.09**	**100.57**	**120.65**
Steady ^{0}C	27	28	33	43	46
Electricity output $_{summer}$(W/m²)	**0.69**	**1.20**	**2.31**	**4.79**	**5.70**
Transient ^{0}C	28	30	34	44	47
Electricity output $_{summer}$(W/m²)	**0.69**	**1.20**	**2.30**	**4.78**	**5.69**

10.3 SUMMARY

The consequent thermal and ventilation behaviour of the transient and steady condition inside an office room was compared and investigated when the airflow window unit was exposed to gradual solar radiation of a typical daytime of the winter and summer seasons. The numerical simulation has shown that the difference between the thermal performance of the steady and the transient state decrease with the increase of the solar value. However, the overall difference is trivial where the steady-induced temperatures remain higher than those of transient. This is due to numerical errors (meshing, time steps used and the number of iterations) or because in the steady state operation, the sequential alteration of the solar radiation values was in hourly pattern whilst in the transient treatment the sequential move, between consecutive radiation values, was based in each minute until it reaches the following hour.

The study has further shown that the variation between the steady-and transient-induced ventilation performance offers similar scene of behaviour that the air motion inside the space, as a consequent of the steady state, possess higher air velocities than those resulting from the transient where the difference tapers gradually with relevance to increasing solar value. However, the air flow rate, 30L/s, is equal under each radiation in winter whilst in summer the ventilation performance presented constant values (due to the fixed mechanical speed applied since the ventilation force is fan-induced alone) for both conditions where the higher movement was revealed from the steady state condition despite the air flow rate under each condition was 77L/s.

For both seasons, steady state and transient treatment have no effect on the PV electricity output, as seen in the tables 10.3 and 10.6, and similar outputs can be obtained under the effect of each condition where the efficiency during the winter is higher than it is during the summer, due to the higher solar radiation of winter, and it can be dropped down around the noon time in the summer as the PV temperature exceeds 45^0C. Next chapter will conclude the study and highlight the most important findings and give recommendations.

CHAPTER 11 CONCLUSION AND RECOMMENDATIONS

11.1 INTRODUCTION

Previous studies have focused on an airflow window that encompasses two segments, a lower part which represents an opaque PV solar panel responsible for electricity generation, and an upper portion that accounts for daylighting and thermal authorization, as it consists of a ventilated double glazing unit. These studies concluded that the two parts should be unified as a single airflow window model for more robust performance.

This research study has outlined strategies for such an airflow window, composed of standard double glass panels on the inside and an outer semi-transparent PV glass sheet separated by interstitial cavity. This proposal provides the reasoning behind expanding the PV area to absorb more solar incidents, which releases potential extra power generation, and behind the use of see-through solar cells to produce an architecturally sleek façade and function as a daylighting component whilst alleviating the glare of solar radiation. The study explains that PV overheating can be minimised due to the ventilation phenomenon, and this system can work in the summer as an exhaust mode, and in winter as a supply mode. Previous to this, to the researcher's knowledge, no study had been carried out on the characteristics and various behaviours of the semi-transparent PV panel integrated with an airflow window.

The study was managed through computer modelling for the window system. This was installed in an office occupied by two people. The pre-set validation analyses were conducted in order to ascertain the dependability of the applied-prospective modules and informative results were obtained. First, CFD analyses were carried out individually for three ventilation forces: mechanical only, buoyancy only, and combined mechanical and buoyancy forces to gauge their effect on the thermal and ventilation performance and explore which is the most suitable for winter and summer. Then, considering the optimum driving force, the window unit underwent five rounds of CFD analysis with assorted PV transparency levels: 15, 20, 25, 30, and 35 per cent. Thereafter, the

thermal performance was depicted and investigated for each simulation and the optimum PV level was acquired for each condition. Ultimately, daylight penetration, through each PV transmittance, into the space was studied to underline that the level was thermally and visually effective. Furthermore, PV electric output was calculated under each level and season.

11.2 CONTRIBUTION

This study substantiates its contribution to the body of knowledge by developing the design of the airflow window for both winter and summer, to function as a sustainable cooling and heating segment through adopting dual air circulation modes, supply and exhaust. This study has presented a research methodology, the first half of which included validation analysis for some calculation models. The second half of this methodology referred to validation analysis for CFD models and ECOTECT based on comparison with data and results from relevant literature and benchmarks. It also described the initial FULENT set up and model dimension for analysing an office prototype when incorporating an airflow window integrated with a semi-transparent PV panel.

11.3 FINDINGS

The study revealed important findings and they are highlighted below:

- Thoughtful care should be exerted for cavity design, as it is an important element for air flow rate and heat transfer behaviour;
- Combined buoyancy and mechanical ventilation force can produce preferable indoor thermal and ventilation performance during the winter whilst the forced convection only is sufficient for the summer season; however, in reality, the buoyancy force cannot be neglected because it is always present and the recommendation for the cooling season as mechanical force alone is just to distinguish the buoyancy effect and their results just for the simulation purposes;
- Buoyancy alone is not sufficient for ventilation during both seasons;

- For the proposed design, PV transparency level of 20 per cent is thermally and visually effective during the heating season whilst 15 per cent can deliver a better performance for the cooling period; otherwise, the PV level should be compromised between 15 and 20% to be suitable for both seasons;
- Electricity output can reach its highest level with these optimum transparency levels;
- Other PV transparency degrees of 25, 30, and 35 can be practical under other operating conditions e.g. at higher ventilation rates;
- Time-variable conditions exhibited slight impact on the airflow window performance;
- PV electricity output remains efficient during the winter and drops down around midday in the summer.

11.4 LIMITATIONS

Although the research has adhered to its objectives, some unavoidable limitations were evident. First, due to the utilisation of the FLUENT software that requires a significant time period and great computational resources to iterate and calculate the most accurate predictions from the finest meshing used, the weather conditions applied were limited to the city of London's climate, as it is mild with no dry season in winter and warm summers. They were also limited to the solar values of one day in each season, a single design alternative for the window unit and to only one type of building. Second, the software validation analysis, performed at the early stage of the study to ascertain the reliability of the CFD code, has obviated the need for more experimental work. Finally, due to these limitations, it was difficult to reflect a wide class of findings; however, they are informative as a base for further studies.

11.5 FUTURE WORK

The proposed window unit was found to be effective. It combines the options of energy saving, electricity generation, cooling and heating load mitigation as well as daylighting allowance. However, further work is necessary to address the limitations experienced during the current study. Thus, recommendations for future areas of investigation should be given clearly. First, future research would consider using a more advanced computer with a high-level capacity that is so-called 'High Performance Computing' or 'Supercomputer' instead of relying on a general-purpose computer in order to minimise the considerable time demanded for simulation with the FLUENT software and to involve a larger scale of analysis. Second, it would be necessary to investigate the influence of different climate conditions such as desert weather (hot and dry) or tropical weather (hot and wet) on the performance of the proposed system. Hence, the applicability of the unit will be investigated in various locations, which would then release a broad range of findings that reflect views on alternative design criteria for the window unit.

Third, further work could seek to examine each alternative window design that suits its designated climate. It is also advised to cover the annual operation analysis for more realistic research and to demonstrate the design alterations for each cardinal direction (north, south, east and west) of a building and to prove the applicability of all PV transparency levels. Design modifications would involve an addition of a blind, low e-coating or any inflector window insulators that can tackle the window heat infiltration, high conductivity and solar radiation factors. Furthermore, a suggestion of a further study is to examine the thermal bridging that would be produced from the framing materials.

Moreover, future research would be comprehensive if optimising the design of the window component when it is integrated in other types of premises such as residential, educational and religious buildings or parking structures and storage. This will expand the chance of an effective use of the system. Finally, empirical investigations would be sought to validate the numerical analysis, which then provide insight into a scientific hypothesis.

11.6 CLOSURE

The study has provided instructive analysis of the photovoltaic airflow window using simulation models. It has added a critical piece of knowledge to the simulation of building façade components. The objectives of this study that were outlined at the commencement of this work have been fully fulfilled under the consideration of the stated scope and limitations. The study is hoped to facilitate the exploration of future research areas for sustainable buildings.

REFERENCES

Agrawal, B. and G. Tiwari (2010). "Optimizing the energy and exergy of building integrated photovoltaic thermal (BIPVT) systems under cold climatic conditions." Applied Energy **87**(2): 417-426.

Agrawal, B. and G. N. Tiwari (2011). "An Energy and Exergy Analysis of Building Integrated Photovoltaic Thermal Systems." Energy Sources Part A: Recovery, Utilization, and Environmental Effects(1556-7036, 1556-7036).

Aitken, D. (1981). "Use of air flow windows and blinds for building thermal control and for solar-assisted heating, cooling and lighting." Proc. Annu. Meet.-Am. Sect. Int. Sol. Energy Soc.;(United States) **6**(CONF-810925-).

Al-Amri, F. G. and M. A. El-Shaarawi (2012). "Mixed convection with surface radiation between two asymmetrically heated vertical parallel plates." International Journal of Thermal Sciences **58**: 70-78.

Al-Sallal, K. A. (2007). "Testing glare in universal space design studios in Al-Ain, UAE desert climate and proposed improvements." Renewable Energy **32**(6): 1033-1044.

Ansys, A. F. (2011). "14.0 Theory Guide." ANSYS inc.

ANSYS, F. T. S. (2009). ANSYS Fluent 14.0 Theory Guide. Lebanon, NH, USA, ANSYS Inc.

Atif, M. R. and A. D. Galasiu (2003). "Energy performance of daylight-linked automatic lighting control systems in large atrium spaces: report on two field-monitored case studies." Energy and Buildings **35**(5): 441-461.

Awbi, H. B. (1998). "Calculation of convective heat transfer coefficients of room surfaces for natural convection." Energy and Buildings **28**(2): 219-227.

Awbi, H. B. (2013). Ventilation of buildings, Routledge.

Aydin, O. (2000). "Determination of optimum air-layer thickness in double-pane windows." Energy and Buildings **32**(3): 303-308.

Aydın, O. (2006). "Conjugate heat transfer analysis of double pane windows." Building and Environment **41**(2): 109-116.

Aynsley, R. M. (1997). "A resistance approach to analysis of natural ventilation airflow networks." Journal of wind engineering and industrial aerodynamics **67**: 711-719.

Baker, P. and M. McEvoy (2000). "Test cell analysis of the use of a supply air window as a passive solar component." Solar Energy **69**(2): 113-130.

Bakker, A. (2012, 04/03/2014). "Applied Computational Fluid Dynamics: Lecture 10 - Turbulence Model." from http://www.bakker.org/dartmouth06/engs150/10-rans.pdf.

Balocco, C. (2002). "A simple model to study ventilated facades energy performance." Energy and Buildings **34**(5): 469-475.

Balocco, C. (2004). "A non-dimensional analysis of a ventilated double façade energy performance." Energy and Buildings **36**(1): 35-40.

Balocco, C. and M. Colombari (2006). "Thermal behaviour of interactive mechanically ventilated double glazed façade: Non-dimensional analysis." Energy and Buildings **38**(1): 1-7.

Barakat, S. A. (1987). Thermal performance of a supply-air window, National Research Council Canada, Institute for Research in Construction.

BEJAN, A. (2003). "Forced convection: Internal flows." Heat Transfer Handbook: 395-438.

Bellia, L.,F. Bisegna and G. Spada (2011). "Lighting in indoor environments: Visual and non-visual effects of light sources with different spectral power distributions." Building and Environment.

Bhamjee, M. (2012). A computational fluid dynamics and experimental investigation of an airflow window. Mechanical Engineering. Johannesburg, South Africa, Univesirty of Johannesburg. **Master Degree**.

Bhamjee, M.,A. Nurick and D. Madyira (2012). "An experimentally validated mathematical and CFD model of a supply air window: Forced and natural flow." Energy and Buildings.

Blevins, R. D. (1984). "Applied fluid dynamics handbook." New York, Van Nostrand Reinhold Co., 1984, 568 p. **1**.

Blok, K. (2004). "Improving Energy Efficiency by Five Percent and More per Year?" Journal of Industrial Ecology **8**(4): 87-99.

Blok, K.,D. de Jager,C. Hendriks,N. Kouvaritakis and L. Mantzos (2001). "Economic evaluation of sectoral emission reduction objectives for climate change–Comparison of topdown and bottom-up analysis of emission reduction opportunities for CO2 in the European Union." Ecofys, AEA and NTUA, Report for European Commission, DG Environment, Brussels, September.

Carlos, J. S.,H. Corvacho,P. D. Silva and J. Castro-Gomes (2010). "Real climate experimental study of two double window systems with preheating of ventilation air." Energy and Buildings **42**(6): 928-934.

Carlos, J. S.,H. Corvacho,P. D. Silva and J. Castro-Gomes (2011). "Modelling and simulation of a ventilated double window." Applied thermal engineering **31**(1): 93-102.

Carmody, J.,S. Selkowitz,E. Lee,D. Arasteh and T. Willmert (2004). Window systems for high-performance buildings, Norton New York.

Charron, R. and A. K. Athienitis (2006). "Optimization of the performance of double-facades with integrated photovoltaic panels and motorized blinds." Solar Energy **80**(5): 482-491.

Chel, A.,G. Tiwari and A. Chandra (2009). "A model for estimation of daylight factor for skylight: An experimental validation using pyramid shape skylight over vault roof mud-house in New Delhi (India)." Applied Energy **86**(11): 2507-2519.

Chel, A.,G. Tiwari and H. Singh (2010). "A modified model for estimation of daylight factor for skylight integrated with dome roof structure of mud-house in New Delhi (India)." Applied Energy **87**(10): 3037-3050.

Chen, H. J.,C. M. Chiang,R. S. Horng and S. K. Lee (2012). "Thermal and optical properties of semi-transparent amorphous silicon BIPV for building application." Advanced Materials Research **343**: 199-204.

Chen, Q. (1995). "Comparison of different k-ε models for indoor air flow computations." Numerical Heat Transfer, Part B Fundamentals **28**(3): 353-369.

Chow, T.-t.,C. Li and Z. Lin (2010). "Innovative solar windows for cooling-demand climate." Solar Energy Materials and Solar Cells **94**(2): 212-220.

Chow, T.-t.,Z. Lin,K.-f. Fong,L.-s. Chan and M.-m. He (2009a). "Thermal performance of natural airflow window in subtropical and temperate climate zones – A comparative study." Energy Conversion and Management **50**(8): 1884-1890.

Chow, T.-T.,Z. Qiu and C. Li (2009b). "Potential application of “see-through” solar cells in ventilated glazing in Hong Kong." Solar Energy Materials and Solar Cells **93**(2): 230-238.

Chow, T.,K. Fong,W. He,Z. Lin and A. Chan (2007). "Performance evaluation of a PV ventilated window applying to office building of Hong Kong." Energy and Buildings **39**(6): 643-650.

Chow, T. T.,G. Pei,L. Chan,Z. Lin and K. Fong (2009c). "A comparative study of PV glazing performance in warm climate." Indoor and Built Environment **18**(1): 32-40.

Churchill, S. W. and H. Ozoe (1973a). "Correlations for laminar forced convection in flow over an isothermal flat plate and in developing and fully developed flow in an isothermal tube." Journal of Heat Transfer **95**: 416.

Churchill, S. W. and H. Ozoe (1973b). "Correlations for laminar forced convection with uniform heating in flow over a plate and in developing and fully developed flow in a tube." Journal of Heat Transfer **95**: 78.

CIBSE, G. A. (2006). "Environmental design." The Chartered Institution of Building Services Engineers, London.

Clarke, J. A.,J. W. Hand,C. M. Johnstone,N. Kelly and P. A. Strachan (1996). "Photovoltaic-integrated building facades." Renewable Energy **8**(1–4): 475-479.

Colsmann, A.,A. Puetz,A. Bauer,J. Hanisch,E. Ahlswede and U. Lemmer (2011). "Efficient Semi-Transparent Organic Solar Cells with Good Transparency Color Perception and Rendering Properties." Advanced Energy Materials **1**(4): 599-603.

Congress, I. B. (2008). Practical Handbook on Energy Conservation in Buidlings New Delhi, Nabhi Publications.

Corgnati, S. P.,M. Perino and V. Serra (2007). "Experimental assessment of the performance of an active transparent façade during actual operating conditions." Solar Energy **81**(8): 993-1013.

Crawley, D. B.,J. W. Hand,M. Kummert and B. T. Griffith (2008). "Contrasting the capabilities of building energy performance simulation programs." Building and Environment **43**(4): 661-673.

Curry, R. (1998). PV Insider's Report, Vol, XVII.

Dalal, R.,D. Naylor and D. Roeleveld (2009). "A CFD study of convection in a double glazed window with an enclosed pleated blind." Energy and Buildings **41**(11): 1256-1262.

De Boer, B. and W. van Helden (2001). PV MOBI, PV Modules Optimised for Building Integration, Netherlands Energy Research Foundation ECN.

Diomidov, M. V.,M. I. Nizovtsev and V. I. Terekhov (2002). "Ventilation of window interpane cavity aimed at a higher temperature of the inner pane." Thermal science **6**(1): 15-22.

Edwards, D. (1977). "Solar absorption by each element in an absorber-coverglass array." Solar Energy **19**: 401.

Eicker, U.,V. Fux,U. Bauer,L. Mei and D. Infield (2008). "Facades and summer performance of buildings." Energy and Buildings **40**(4): 600-611.

Eicker, U.,V. Fux,D. Infield and L. Mei (2000). Heating and cooling potential combined photovoltaic-solar air collector façade.

Eicker, U.,V. Fux,D. Infield,L. Mei and K. Vollmer (1999). Thermal performance of building integrated ventilated PV facades.

Evans, D. (1981). "Simplified method for predicting photovoltaic array output." Solar Energy **27**(6): 555-560.

Faggembauu, D.,M. Costa,M. Soria and A. Oliva (2003a). "Numerical analysis of the thermal behaviour of glazed ventilated facades in Mediterranean climates. Part II: applications and analysis of results." Solar Energy **75**(3): 229-239.

Faggembauu, D.,M. Costa,M. Soria and A. Oliva (2003b). "Numerical analysis of the thermal behaviour of ventilated glazed facades in Mediterranean climates. Part I: development and validation of a numerical model." Solar Energy **75**(3): 217-228.

Fallahi, A.,F. Haghighat and H. Elsadi (2010). "Energy performance assessment of double-skin façade with thermal mass." Energy and Buildings **42**(9): 1499-1509.

Fluent, A. (2009). "12.0 User's Guide." User Inputs for Porous Media: 6.

Fuliotto, R.,F. Cambuli,N. Mandas,N. Bacchin,G. Manara and Q. Chen (2010). "Experimental and numerical analysis of heat transfer and airflow on an interactive building facade." Energy and Buildings **42**(1): 23-28.

Fung, T. Y. Y. and H. Yang (2008). "Study on thermal performance of semi-transparent building-integrated photovoltaic glazings." Energy and Buildings **40**(3): 341-350.

Gan, G. (2006). "Simulation of buoyancy-induced flow in open cavities for natural ventilation." Energy and Buildings **38**(5): 410-420.

Gan, G. (2009a). "Effect of air gap on the performance of building-integrated photovoltaics." Energy **34**(7): 913-921.

Gan, G. (2009b). "Numerical determination of adequate air gaps for building-integrated photovoltaics." Solar Energy **83**(8): 1253-1273.

Gan, G. (2010a). "Impact of computational domain on the prediction of buoyancy-driven ventilation cooling." Building and Environment **45**(5): 1173-1183.

Gan, G. (2010b). "Interaction Between Wind and Buoyancy Effects in Natural Ventilation of Buildings." Open Construction and Building Technology Journal **4**(1874-8368, 1874-8368): 134-145.

Gan, G. and S. B. Riffat (2004). "CFD modelling of air flow and thermal performance of an atrium integrated with photovoltaics." Building and Environment **39**(7): 735-748.

Garimella, S.,W. J. Dowling,M. Van derVeen and J. D. Killion (2000). "Heat transfer coefficients for simultaneously developing flow in rectangular tubes." ASME-PUBLICATIONS-HTD **366**: 3-12.

Gosselin, J. R. and Q. Chen (2008a). "A computational method for calculating heat transfer and airflow through a dual-airflow window." Energy and Buildings **40**(4): 452-458.

Gosselin, J. R. and Q. Chen (2008b). "A dual airflow window for indoor air quality improvement and energy conservation in buildings." HVAC&R Research **14**(3): 359-372.

Gosselin, J. R. and Q. Y. Chen (2008c). "A computational method for calculating heat transfer and airflow through a dual-airflow window." Energy and Buildings **40**(4): 452-458.

Gratia, E. and A. De Herde (2004a). "Is day natural ventilation still possible in office buildings with a double-skin façade?" Building and Environment **39**(4): 399-409.

Gratia, E. and A. De Herde (2004b). "Natural cooling strategies efficiency in an office building with a double-skin façade." Energy and Buildings **36**(11): 1139-1152.

Gratia, E. and A. De Herde (2004c). "Natural ventilation in a double-skin facade." Energy and Buildings **36**(2): 137-146.

Gratia, E. and A. De Herde (2004d). "Optimal operation of a south double-skin facade." Energy and Buildings **36**(1): 41-60.

Gratia, E. and A. De Herde (2007a). "Are energy consumptions decreased with the addition of a double-skin?" Energy and Buildings **39**(5): 605-619.

Gratia, E. and A. De Herde (2007b). "Greenhouse effect in double-skin facade." Energy and Buildings **39**(2): 199-211.

Gratia, E. and A. De Herde (2007c). "Guidelines for improving natural daytime ventilation in an office building with a double-skin facade." Solar Energy **81**(4): 435-448.

Gratia, E. and A. De Herde (2007d). "The most efficient position of shading devices in a double-skin facade." Energy and Buildings **39**(3): 364-373.

Guardo, A.,M. Coussirat,E. Egusquiza,P. Alavedra and R. Castilla (2009). "A CFD approach to evaluate the influence of construction and operation parameters on the performance of Active Transparent Façades in Mediterranean climates." Energy and Buildings **41**(5): 534-542.

Haase, M. and A. Amato (2009a). "A study of the effectiveness of different control strategies in double skin facades in warm and humid climates." Journal of Building Performance Simulation **2**(3): 179-187.

Haase, M.,F. Marques da Silva and A. Amato (2009b). "Simulation of ventilated facades in hot and humid climates." Energy and Buildings **41**(4): 361-373.

Hadlock, C. (2006). Modelling and optimization of an airflow window with between-the-panes shading device. Mechanical Engineering. Waterloo, Ontario, Canada, University of Waterloo **Master Degree**

Hall, K. (2008). The Green Building Bible, Green Building Press.

Hamdan, M. O. (2013). "An empirical correlation for isothermal parallel plate channel completely filled with porous media." Thermal science(00): 15-15.

Hammond, G. P.,H. A. Harajli,C. I. Jones and A. B. Winnett (2012). "Whole systems appraisal of a UK Building Integrated Photovoltaic (BIPV) system: energy, environmental, and economic evaluations." Energy Policy **40**: 219-230.

Han, J.-C. (2012). Analytical heat transfer, CRC Press.

Han, J.,L. Lu and H. Yang (2009). "Thermal behavior of a novel type see-through glazing system with integrated PV cells." Building and Environment **44**(10): 2129-2136.

Han, J.,L. Lu and H. Yang (2010). "Numerical evaluation of the mixed convective heat transfer in a double-pane window integrated with see-through a-Si PV cells with low-e coatings." Applied Energy **87**(11): 3431-3437.

Handbook, A. (2009). "Fundamentals." American Society of Heating, Refrigerating and Air Conditioning Engineers, Atlanta.

Henríquez, J. R. (2002). Modelagem e análise de janelas térmicas. Campinas-SP, Brazil, Universidade Estadual de Campinas. **Doctoral thesis**.

Hensen, J.,M. Bartak and F. Drkal (2002). "Modeling and simulation of a double-skin façade system." ASHRAE Transactions **108**(2): 1251-1259.

Hien, W. N.,W. Liping,A. N. Chandra,A. R. Pandey and W. Xiaolin (2005). "Effects of double glazed facade on energy consumption, thermal comfort and condensation for a typical office building in Singapore." Energy and Buildings **37**(6): 563-572.

Hollands, K. G. T.,J. L. Wright and C. G. Granqvist (2001). Ch. 2 (Glazings and Coatings). Solar Energy – The state of the Art ISES position papers, James and James Ltd.**:** 29-107.

Høseggen, R.,B. Wachenfeldt and S. Hanssen (2008). "Building simulation as an assisting tool in decision making: Case study: With or without a double-skin façade?" Energy and Buildings **40**(5): 821-827.

Hviid, C. A.,T. R. Nielsen and S. Svendsen (2008). "Simple tool to evaluate the impact of daylight on building energy consumption." Solar Energy **82**(9): 787-798.

IEA (1998). "Photovoltaic Power Systems Programme-Strategy Document 1998-2002." International Energy Agency (IEA)(Final draft): p2.

Incropera, F. and D. DeWitt (1990). "Fundamentals of Heat and Mass Transfer, John Wiley and Sons, New York, 1990." p. 524.

Infield, D.,L. Mei and U. Eicker (2004). "Thermal performance estimation for ventilated PV facades." Solar Energy **76**(1): 93-98.

Infield, D.,L. Mei,U. Eicker and V. Fux (1999). Understanding the potential of ventilated PV facades.

Institute, B. B. R. (2002). Source Book for a Better Understanding of Conceptual and Operational Aspects of Active Facades.

Institution, B. S. (2014). Ventilation for non-residential buildings. Performance requirements for ventilation and room-conditioning systems. London, BSI. **BS EN 13779:2004:** 56.

Ismail, K. and J. Henríquez (2006). "Simplified model for a ventilated glass window under forced air flow conditions." Applied thermal engineering **26**(2): 295-302.

Ismail, K. A. R. and J. R. Henríquez (2005). "Two-dimensional model for the double glass naturally ventilated window." International Journal of Heat and Mass Transfer **48**(3–4): 461-475.

Ji, Y.,M. Cook,V. Hanby,D. Infield,D. Loveday and L. Mei (2008). "CFD modelling of naturally ventilated double-skin facades with venetian blinds." Journal of Building Performance Simulation **1**(3): 185-196.

Jiru, T. E. and F. Haghighat (2008). "Modeling ventilated double skin façade—A zonal approach." Energy and Buildings **40**(8): 1567-1576.

Judkoff, R. and J. Neymark (1995). International energy agency building energy simulation test (BESTEST) and diagnostic method, National Renewable Energy Lab., Golden, CO (US).

K.T. Hollands, J. W., C. Ganqvist (2001). Solar Energy: The State of the Art, ISES Position Papers ISES International Solar Energy Society, James and James (Science Publisher) Ltd.

Keshock, E. and R. Siegel (1963). "Combined radiation and convection in an asymmetrically heated parallel plate flow channel."

Kim, Y.-M.,S.-Y. Kim,S.-W. Shin and J.-Y. Sohn (2009). "Contribution of natural ventilation in a double skin envelope to heating load reduction in winter." Building and Environment **44**(11): 2236-2244.

Klein, S.,W. Beckman,J. Mitchell,J. Duffie,N. Duffie,T. Freeman,J. Mitchell,J. Braun,B. Evans and J. Kummer (2004). "TRNSYS 16–A TRaNsient system simulation program, user manual." Solar Energy Laboratory. Madison: University of Wisconsin-Madison.

Krarti, M.,P. M. Erickson and T. C. Hillman (2005). "A simplified method to estimate energy savings of artificial lighting use from daylighting." Building and Environment **40**(6): 747-754.

Krauter, S.,R. G. Araújo,S. Schroer,R. Hanitsch,M. J. Salhi,C. Triebel and R. Lemoine (1999). "Combined photovoltaic and solar thermal systems for facade integration and building insulation." Solar Energy **67**(4): 239-248.

Larsson, U.,B. Moshfegh and M. Sandberg (1999). "Thermal analysis of super insulated windows (numerical and experimental investigations)." Energy and Buildings **29**(2): 121-128.

Lechner, N. (2014). Heating, cooling, lighting: sustainable design methods for architects, John wiley & sons.

Lee, E. and A. Tavil (2007). "Energy and visual comfort performance of electrochromic windows with overhangs." Building and Environment **42**(6): 2439-2449.

Lee, E. S. and S. E. Selkowitz (2006). "The New York Times Headquarters daylighting mockup: Monitored performance of the daylighting control system." Energy and Buildings **38**(7): 914-929.

Li, D. H. W. and J. C. Lam (2001). "Evaluation of lighting performance in office buildings with daylighting controls." Energy and Buildings **33**(8): 793-803.

Li, D. H. W.,T. N. T. Lam,W. W. H. Chan and A. H. L. Mak (2009). "Energy and cost analysis of semi-transparent photovoltaic in office buildings." Applied Energy **86**(5): 722-729.

Li, D. H. W.,T. N. T. Lam and S. Wong (2006). "Lighting and energy performance for an office using high frequency dimming controls." Energy Conversion and Management **47**(9): 1133-1145.

Liao, L.,A. K. Athienitis,L. Candanedo,K. W. Park,Y. Poissant and M. Collins (2007). "Numerical and Experimental Study of Heat Transfer in a BIPV-Thermal System." Journal of Solar Energy Engineering **129**(4): 423-430.

Lloret, A.,J. Andreu,J. Merten,O. Aceves,L. Sabata,F. Sen,J. Puigdollers,C. Person,M. Chantant and J. Servant (1995). The Mataro public library: a 53 kW p grid connected building with integrated PV-thermal multifunctional modules. 13th European Photovoltaic Solar Energy Conference.

López, F. P.,R. L. Jensen,P. Heiselberg and M. Ruiz de Adana Santiago (2012). "Experimental analysis and model validation of an opaque ventilated facade." Building and Environment **56**: 265-275.

Lou, W.,M. Huang,M. Zhang and N. Lin (2012). "Experimental and zonal modeling for wind pressures on double-skin facades of a tall building." Energy and Buildings **54**: 179-191.

Loutzenhiser, P. G.,G. M. Maxwell and H. Manz (2007). "An empirical validation of the daylighting algorithms and associated interactions in building energy simulation programs using various shading devices and windows." Energy **32**(10): 1855-1870.

Lu, L. and K. M. Law (2013). "Overall energy performance of semi-transparent single-glazed photovoltaic (PV) window for a typical office in Hong Kong." Renewable Energy **49**: 250-254.

Lynn, N.,L. Mohanty and S. Wittkopf (2012). "Color rendering properties of semi-transparent thin-film PV modules." Building and Environment **54**: 148-158.

Manav, B. (2007). "An experimental study on the appraisal of the visual environment at offices in relation to colour temperature and illuminance." Building and Environment **42**(2): 979-983.

Manz, H.,A. Schaelin and H. Simmler (2004). "Airflow patterns and thermal behavior of mechanically ventilated glass double façades." Building and Environment **39**(9): 1023-1033.

Marsh, A. J. (1996). Survey of simulation modeling into initial stages of design. ANZAScA Conference Proceedings, Hong Kong, China, University of Hong Kong.

McEvoy, M. and R. Southall (2000). Validation of a computational fluid dynamics simulation of a supply air 'ventilated'window. CISBE Conference, Dublin, Ireland.

McEvoy, M.,R. Southall and P. Baker (2003). "Test cell evaluation of supply air windows to characterise their optimum performance and its verification by the use of modelling techniques." Energy and Buildings **35**(10): 1009-1020.

Mei, L.,U. Eicker and V. Fux (2002). "Parameter estimation for ventilated photovoltaic facades." Building services engineering research and technology **23**(2): 81-96.

Mei, L.,D. Infield,U. Eicker and V. Fux (2003). "Thermal modelling of a building with an integrated ventilated PV façade." Energy and Buildings **35**(6): 605-617.

Mei, L.,D. Loveday,D. Infield,V. Hanby,M. Cook,Y. Ji,M. Holmes and J. Bates (2007). "The influence of blinds on temperatures and air flows within ventilated double-skin façades." Proceedings of Clima 2007 WellBeing Indoors.

Menter, F. R. (1994). "Two-equation eddy-viscosity turbulence models for engineering applications." AIAA journal **32**(8): 1598-1605.

Miyazaki, T.,A. Akisawa and T. Kashiwagi (2005). "Energy savings of office buildings by the use of semi-transparent solar cells for windows." Renewable Energy **30**(3): 281-304.

Moshfegh, B. and M. Sandberg (1996). "Investigation of fluid flow and heat transfer in a vertical channel heated from one side by PV elements, part I - Numerical Study." Renewable Energy **8**(1–4): 248-253.

Moshfegh, B. and M. Sandberg (1998). "Flow and heat transfer in the air gap behind photovoltaic panels." Renewable and Sustainable Energy Reviews **2**(3): 287-301.

Nakahara, N. and J. Monbusho (1995). Proceedings of Pan Pacific Symposium on Building and Urban Environmental Conditioning in Asia, March 16-18, Nagoya, Japan, Organizing Committee of the Pan Pacific Symposium on Building and Urban Environmental Conditioning in Asia.

Nemati, O. (2009). Analysis of a Mechanically Ventilated Multiple-skin Facade with Between-the-Panes Venetian Blinds. Mechanical Engineering. Waterloo, Ontario, Canada, University of Waterloo. **Master Degree**.

Neymark, J. and R. Judkoff (2002). International Energy Agency Building Energy Simulation Test and Diagnostic Method for Heating, Ventilating, and Air-Conditioning Equipment Models (HVAC BESTEST); Volume 1: Cases E100-E200, National Renewable Energy Lab., Golden, CO.(US).

Nickolay, M. and H. Martin (2002). "Improved approximation for the Nusselt number for hydrodynamically developed laminar flow between parallel plates." International Journal of Heat and Mass Transfer **45**(15): 3263-3266.

Nielsen, T.,T. R. Nielsen and S. Svendsen (2005). Calculation of daylight distribution and utilization in rooms with solar shadings and light redirecting devices. Proceedings of 7th Symposium on Building Physics in the Nordic Countries.

Oelhafen, P.,R. Steiner,G. Reber,A. Romanyuk,B. Heimann,M. Steinacher and P. Juchli (2005). "Database for optical and thermal properties of insulating glasses." CISBAT 2005 Proceedings, Lausanne.

Offices, B. C. f. (2009). 2009 guide to specification / British Council for Offices. London, British Council for Offices.

P.F. Abreu,A.F. Roydon,H.F. Sullivan and J. L. Wright (1998). A 2-D numerical model for heat transfer calculations in multipane windows. in: Proc VII Encontro Nacional de Ciências Térmicas-ENCIT, Rio de Janeiro, Brazil.

Pappas, A. and Z. Zhai (2008). "Numerical investigation on thermal performance and correlations of double skin facade with buoyancy-driven airflow." Energy and Buildings **40**(4): 466-475.

Parida, B.,S. Iniyan and R. Goic (2011). "A review of solar photovoltaic technologies." Renewable and Sustainable Energy Reviews **15**(3): 1625-1636.

Park, C.-S.,G. Augenbroe,T. Messadi,M. Thitisawat and N. Sadegh (2004a). "Calibration of a lumped simulation model for double-skin façade systems." Energy and Buildings **36**(11): 1117-1130.

Park, C.-S.,G. Augenbroe,N. Sadegh,M. Thitisawat and T. Messadi (2004b). "Real-time optimization of a double-skin facade based on lumped modeling and occupant preference." Building and Environment **39**(8): 939-948.

Pasut, W. and M. De Carli (2012). "Evaluation of various CFD modelling strategies in predicting airflow and temperature in a naturally ventilated double skin façade." Applied thermal engineering **37**: 267-274.

Patankar, S. V. (1980). Numerical heat transfer and fluid flow, Taylor & Francis Group.

Peng, C.,Y. Huang and Z. Wu (2011). "Building-integrated photovoltaics (BIPV) in architectural design in China." Energy and Buildings **43**(12): 3592-3598.

Perez-Lombard, L.,J. Ortiz and C. Pout (2008). "A review on buildings energy consumption information." Energy and Buildings **40**(3): 394-398.

Petter Jelle, B.,C. Breivik and H. Drolsum Røkenes (2012). "Building integrated photovoltaic products: A state-of-the-art review and future research opportunities." Solar Energy Materials and Solar Cells **100**(0): 69-96.

Posner, J.,C. Buchanan and D. Dunn-Rankin (2003). "Measurement and prediction of indoor air flow in a model room." Energy and Buildings **35**(5): 515-526.

Ramos, G. and E. Ghisi (2010). "Analysis of daylight calculated using the EnergyPlus programme." Renewable and Sustainable Energy Reviews **14**(7): 1948-1958.

Reijenga, T. and W. Bottger (1997). Glass roof integrated photovoltaic system De Kleine Aarde Boxtel (NL). Proceedings from the 14th European Photovoltaic Solar Energy Conference, Barcelona, France June.

Reinhart, C. and P. Breton (2009). "Experimental Validation of Autodesk® 3ds Max® Design 2009 and Daysim 3.0." Leukos **6**: 1.

Reinhart, C. and A. Fitz (2006). "Findings from a survey on the current use of daylight simulations in building design." Energy and Buildings **38**(7): 824-835.

Reinhart, C. F. and S. Herkel (2000). "The simulation of annual daylight illuminance distributions—a state-of-the-art comparison of six RADIANCE-based methods." Energy and Buildings **32**(2): 167-187.

Roberts, S. and N. Guariento (2009). Building integrated photovoltaics: a handbook, Birkhauser.

Robinson, L. and A. Athienitis (2009). "Design methodology for optimization of electricity generation and daylight utilization for façade with semi-transparent photovoltaics." Proceedings of Building Simulation 2009.

S. Belharat,G. Desrayaud and G. Lauriat (1996). Naturalconvection-radiationinteraction in venteddoubleglazing. in: Proceeding of the 2nd European Thermal-Sciences and 14th UIT National Heat Transfer Conference, , Roma, Italy.

Saelens, D.,S. Roels and H. Hens (2004). "The inlet temperature as a boundary condition for multiple-skin facade modelling." Energy and Buildings **36**(8): 825-835.

Saelens, D.,S. Roels and H. Hens (2008). "Strategies to improve the energy performance of multiple-skin facades." Building and Environment **43**(4): 638-650.

Safer, N.,M. Woloszyn and J. J. Roux (2005). "Three-dimensional simulation with a CFD tool of the airflow phenomena in single floor double-skin facade equipped with a venetian blind." Solar Energy **79**(2): 193-203.

Sandberg, M. and B. Moshfegh (1998). "Ventilated-solar roof air flow and heat transfer investigation." Renewable Energy **15**(1): 287-292.

Sandberg, M. and B. Moshfegh (2002). "Buoyancy-induced air flow in photovoltaic facades: effect of geometry of the air gap and location of solar cell modules." Building and Environment **37**(3): 211-218.

Seo, D.,P. Ihm and M. Krarti (2011). "Development of an optimal daylighting controller." Building and Environment **46**(5): 1011-1022.

Serra, V.,F. Zanghirella and M. Perino (2010). "Experimental evaluation of a climate façade: Energy efficiency and thermal comfort performance." Energy and Buildings **42**(1): 50-62.

Shia-hui, P. and F. Peterson (1995). "Convection from a cold window with simulated floor heating by means of a transiently heated flat unit." Energy and Buildings **23**(2): 95-103.

Southall, R. and M. McEvoy (2000). Results from a validated CFD simulation of a supply air 'ventilated'window. RoomVent 2000-7th International Conference on Air Distribution in Rooms.

Southall, R. and M. McEvoy (2006). "Investigations into the functioning of a supply air window in relation to solar energy as determined by experiment and simulation." Solar Energy **80**(5): 512-523.

Stapleton, G. and G. Milne (2005). Australia's guide to environmentally sustainable homes–6.7 photovoltaic systems.

Stec, W. and A. Van Paassen (2005). "Symbiosis of the double skin facade with the HVAC system." Energy and Buildings **37**(5): 461-469.

Strachan, P. and L. Vandaele (2008a). "Case studies of outdoor testing and analysis of building components." Building and Environment **43**(2): 129-142.

Strachan, P. A. and P. Baker (2008b). "Outdoor testing, analysis and modelling of building components." Building and Environment **43**(2): 127-128.

Takeoka, A.,S. Kouzuma,H. Tanaka,H. Inoue,K. Murata,M. Morizane,N. Nakamura,H. Nishiwaki,M. Ohnishi and S. Nakano (1993). "Development and application of see-through a-Si solar cells." Solar Energy Materials and Solar Cells **29**(3): 243-252.

Tanaka, H.,M. Okumiya,H. Tanaka,G. Young Yoon and K. Watanabe (2009). "Thermal characteristics of a double-glazed external wall system with roll screen in cooling season." Building and Environment **44**(7): 1509-1516.

Tanimoto, J. and K.-i. Kimura (1997). "Simulation study on an air flow window system with an integrated roll screen." Energy and Buildings **26**(3): 317-325.

Till, P. (2004). "Natural ventilation in high-rise buildings with double facades, saving or waste of energy." Energy and Buildings **36**(4): 381-389.

Vangimalla, P.,S. Olbina,R. Issa and J. Hinze (2011). Validation of Autodesk Ecotect™ accuracy for thermal and daylighting simulations. Simulation Conference (WSC), Proceedings of the 2011 Winter, IEEE.

Vartiainen, E.,K. Peippo and P. Lund (2000). "Daylight optimization of multifunctional solar facades." Solar Energy **68**(3): 223-235.

Vats, K. and G. Tiwari (2011). "Performance evaluation of a building integrated semitransparent photovoltaic thermal system for roof and facade." Energy and Buildings.

Vats, K. and G. N. Tiwari "Energy and exergy analysis of a building integrated semitransparent photovoltaic thermal (BISPVT) system." Applied Energy(0).

Versteeg, H. K. and W. Malalasekera (2007). An introduction to computational fluid dynamics: the finite volume method, Prentice Hall.

Wah, W. P.,Y. Shimoda,M. Nonaka,M. Inoue and M. Mizuno (2005). "Field study and modeling of semi-transparent PV in power, thermal and optical aspects." Journal of Asian Architecture and Building Engineering **4**(2): 549-556.

Ward, G. and R. Shakespeare (1998). "Rendering with Radiance." The Art.

Wei, J.,J. Zhao and Q. Chen (2010). "Energy performance of a dual airflow window under different climates." Energy and Buildings **42**(1): 111-122.

Wigginton, M. and B. McCarthy (2000). "Environmental Second Skin Systems." Retrieved 05/25, 2012, from http://www.battlemccarthy.com/external%20site_double%20skin%20website/index.htm.

Wilson, H. R. (2006). "High-Performance Windows." ISES Solar Academy. from http://www.aisglass.com/insulated-glass-units/High-Performance_Windows.pdf.

Winkelmann, F.,B. Birdsall,W. Buhl,K. Ellington,A. Erdem,J. Hirsch and S. Gates (1993). "DOE–2 Supplement, Version 2.1 E, LBL-34947, November 1993, Lawrence Berkeley National Laboratory." Springfield, Virginia: National Technical Information Service.

Wong, P.,D. Prasad and M. Behnia (2008a). "A new type of double-skin façade configuration for the hot and humid climate." Energy and Buildings **40**(10): 1941-1945.

Wong, P. W.,Y. Shimoda,M. Nonaka,M. Inoue and M. Mizuno (2008b). "Semi-transparent PV: Thermal performance, power generation, daylight modelling and energy saving potential in a residential application." Renewable Energy **33**(5): 1024-1036.

Wright, J. L.,M. R. Collins and N. Y. T. Huang (2008). "Thermal resistance of a window with an enclosed Venetian blind: a simplified model." ASHRAE Transactions **114**(1): 471-482.

Xamán, J.,G. Álvarez,L. Lira and C. Estrada (2005). "Numerical study of heat transfer by laminar and turbulent natural convection in tall cavities of facade elements." Energy and Buildings **37**(7): 787-794.

Xu, L. and T. Ojima (2007). "Field experiments on natural energy utilization in a residential house with a double skin façade system." Building and Environment **42**(5): 2014-2023.

Xu, X.-l. and Z. Yang (2008). "Natural ventilation in the double skin facade with venetian blind." Energy and Buildings **40**(8): 1498-1504.

Yamawaki, T.,S. Mizukami,T. Masui and H. Takahashi (2001). "Experimental investigation on generated power of amorphous PV module for roof azimuth." Solar Energy Materials and Solar Cells **67**(1): 369-377.

Ye, P.,S. Harrison,P. Oosthuizen and D. Naylor (1999). Convective heat transfer from a window with a Venetian blind: Detailed modeling, Interautomation Inc., Oakville, Ontario (CA).

Yoon, J.-H.,J. Song and S.-J. Lee (2011). "Practical application of building integrated photovoltaic (BIPV) system using transparent amorphous silicon thin-film PV module." Solar Energy **85**(5): 723-733.

Yovanovich, M. (2004). "Laminar forced convection heat transfer in the combined entry region of non-circular ducts."

Zain-Ahmed, A. (2000). "Daylighting and shading for thermal comfort in Malaysian buildings." Department of Engineering. 2000, University of Hertfordshire.

Zöllner, A.,E. Winter and R. Viskanta (2002). "Experimental studies of combined heat transfer in turbulent mixed convection fluid flows in double-skin-facades." International Journal of Heat and Mass Transfer **45**(22): 4401-4408.

APPENDICES

APPENDIX A INPUTS DATA FOR CHAPTER 3

APPENDIX A-1 VARIATION VALUES OF PARAMETERS FOR SUMMER SEASON

Jun 21st	G [W/m2]	v [m/s]	m [m/s]	Tamb °c	d [m]	hc W/(m2K)	H [m]
05h	62.16	0.10	0.04	16.80	0.06	1.53	1.1
06h	91.52	0.15	0.06	18.50	0.14	2.08	2.2
07h	107.53	0.20	0.07	20.10	0.22	2.60	3.4
08h	210.21	0.30	0.11	21.50	0.30	3.55	4.5
09h	342.32	0.35	0.13	22.70	0.38	4.00	5.6
10h	448.98	0.40	0.15	23.60	0.46	4.44	6.7
11h	516.95	0.50	0.19	24.40	0.54	5.27	7.8
12h	538.62	0.55	0.20	24.50	0.62	5.67	8.9
13h	511.66	0.60	0.22	24.40	0.70	6.07	10
14h	438.96	0.70	0.26	24.20	0.78	6.84	11.1
15h	328.76	0.75	0.22	23.50	0.86	7.21	12.2
16h	194.93	0.80	0.30	22.50	0.94	7.58	13.3
17h	106.16	0.90	0.33	19.30	1.02	8.31	14.4
18h	89.22	0.95	0.35	17.90	1.10	8.66	15.6
19h	57.52	1.00	0.37	16.80	1.18	9.01	16.7

APPENDIX A-2 VARIATION VALUES OF PARAMETERS FOR WINTER SEASON

Jan 29th	G [W/m2]	v [m/s]	m [m/s]	Tamb °c	d [m]	hc W/(m2K)	H [m]
05h	0	0.10	0.04	0.70	0.06	1.59	1.1
06h	0	0.15	0.06	0.70	0.14	2.17	2.2
07h	0	0.20	0.08	1.80	0.22	2.71	3.4
08h	18.3	0.30	0.12	2.30	0.30	3.71	4.5
09h	300.09	0.35	0.14	3.70	0.38	4.18	5.6
10h	523.18	0.40	0.16	4.70	0.46	4.63	6.7
11h	656.16	0.50	0.20	5.50	0.54	5.50	7.8
12h	707.36	0.55	0.22	5.90	0.62	5.93	8.9
13h	678.58	0.60	0.24	5.80	0.70	6.34	10
14h	568.99	0.70	0.28	5.30	0.78	7.14	11.1
15h	372.94	0.75	0.30	4.30	0.86	7.53	12.2
16h	24.52	0.80	0.32	3.70	0.94	7.92	13.3
17h	0	0.90	0.36	3.30	1.02	8.68	14.4
18h	0	0.95	0.38	3.00	1.10	9.05	15.6
19h	0	1.00	0.40	2.70	1.18	9.42	16.7

APPENDIX B RESULTS FOR CHAPTER 3

APPENDIX B-1 RESULTS OF THE EFFECT OF DIFFERENT GAP SIZES IN WINTER SEASON

Energy Balance For Pv Panel For London For One Hour In Winter With Different Gap Sizes						
Jan 29th	Ti	**Tp**	Gp	G	QE	hcp
13h	5.9	**28.03**	282.94	707.36	28.294	7.68
13h	5.9	**29.64**	282.94	707.36	28.294	6.33
13h	5.9	**30.82**	282.94	707.36	28.294	5.72
13h	5.9	**31.73**	282.94	707.36	28.294	5.34
13h	5.9	**32.49**	282.94	707.36	28.294	5.06
13h	5.9	**33.11**	282.94	707.36	28.294	4.85
13h	5.9	**33.64**	282.94	707.36	28.294	4.68
13h	5.9	**34.11**	282.94	707.36	28.294	4.54
13h	5.9	**34.52**	282.94	707.36	28.294	4.42
13h	5.9	**34.92**	282.94	707.36	28.294	4.31
13h	5.9	**35.26**	282.94	707.36	28.294	4.22
13h	5.9	**35.56**	282.94	707.36	28.294	4.14
13h	5.9	**35.84**	282.94	707.36	28.294	4.07
13h	5.9	**36.12**	282.94	707.36	28.294	4
13h	5.9	**36.37**	282.94	707.36	28.294	3.94
Energy Balance For Double Glazing For London For One Hour In Winter With Different Gap Sizes						
Jan 29th	Troom	**Tg**	Gg	G	Tamb	hcg
13h	21	**17.90**	22.64	707.36	5.9	7.68
13h	21	**18.90**	22.64	707.36	5.9	6.33
13h	21	**19.83**	22.64	707.36	5.9	5.72
13h	21	**20.60**	22.64	707.36	5.9	5.34
13h	21	**21.27**	22.64	707.36	5.9	5.06
13h	21	**21.82**	22.64	707.36	5.9	4.85
13h	21	**22.31**	22.64	707.36	5.9	4.68
13h	21	**22.74**	22.64	707.36	5.9	4.54
13h	21	**23.12**	22.64	707.36	5.9	4.42
13h	21	**23.50**	22.64	707.36	5.9	4.31
13h	21	**23.81**	22.64	707.36	5.9	4.22
13h	21	**24.10**	22.64	707.36	5.9	4.14
13h	21	**24.37**	22.64	707.36	5.9	4.07
13h	21	**24.64**	22.64	707.36	5.9	4
13h	21	**24.88**	22.64	707.36	5.9	3.94
Energy Balance For Airflow Rate For London For One Hour In Winter With Different Gap Sizes							
Jan 29th	Tm	**To**	m	v	H	d	hr
13h	8.40	**10.90**	0.1	0.6	2.2	0.06	5.320
13h	7.01	**8.12**	0.22	0.6	2.2	0.14	5.391
13h	6.58	**7.27**	0.35	0.6	2.2	0.22	5.448
13h	6.39	**6.88**	0.48	0.6	2.2	0.3	5.494
13h	6.29	**6.67**	0.6	0.6	2.2	0.38	5.534
13h	6.21	**6.53**	0.73	0.6	2.2	0.46	5.566
13h	6.16	**6.43**	0.86	0.6	2.2	0.54	5.595
13h	6.13	**6.35**	0.99	0.6	2.2	0.62	5.620
13h	6.10	**6.30**	1.11	0.6	2.2	0.7	5.642
13h	6.08	**6.26**	1.24	0.6	2.2	0.78	5.664
13h	6.06	**6.22**	1.37	0.6	2.2	0.86	5.682
13h	6.05	**6.19**	1.5	0.6	2.2	0.94	5.699
13h	6.03	**6.17**	1.62	0.6	2.2	1.02	5.714
13h	6.02	**6.15**	1.75	0.6	2.2	1.1	5.730
13h	6.01	**6.13**	1.88	0.6	2.2	1.18	5.744

APPENDIX B-2 RESULTS OF THE EFFECT OF DIFFERENT GAP SIZES IN SUMMER SEASON

Energy Balance For PV Panel For London For One Hour In Summer With Different Gap Sizes						
Jan 29th	Ti	**Tp**	Gp	G	QE	hcp
13h	24.5	**40.79**	215.45	538.62	21.545	7.37
13h	24.5	**41.99**	215.45	538.62	21.545	6.07
13h	24.5	**42.85**	215.45	538.62	21.545	5.48
13h	24.5	**43.49**	215.45	538.62	21.545	5.12
13h	24.5	**44.04**	215.45	538.62	21.545	4.85
13h	24.5	**44.48**	215.45	538.62	21.545	4.65
13h	24.5	**44.86**	215.45	538.62	21.545	4.49
13h	24.5	**45.21**	215.45	538.62	21.545	4.35
13h	24.5	**45.49**	215.45	538.62	21.545	4.24
13h	24.5	**45.76**	215.45	538.62	21.545	4.14
13h	24.5	**46.01**	215.45	538.62	21.545	4.05
13h	24.5	**46.24**	215.45	538.62	21.545	3.97
13h	24.5	**46.44**	215.45	538.62	21.545	3.9
13h	24.5	**46.65**	215.45	538.62	21.545	3.83
13h	24.5	**46.80**	215.45	538.62	21.545	3.78
Energy Balance For Double Glazing For London For One Hour In Summer With Different Gap Sizes						
Jan 29th	Troom	**Tg**	Gg	G	Tamb	hcg
13h	24	**32.65**	17.24	538.62	24.5	7.37
13h	24	**33.38**	17.24	538.62	24.5	6.07
13h	24	**34.05**	17.24	538.62	24.5	5.48
13h	24	**34.58**	17.24	538.62	24.5	5.12
13h	24	**35.05**	17.24	538.62	24.5	4.85
13h	24	**35.44**	17.24	538.62	24.5	4.65
13h	24	**35.77**	17.24	538.62	24.5	4.49
13h	24	**36.08**	17.24	538.62	24.5	4.35
13h	24	**36.34**	17.24	538.62	24.5	4.24
13h	24	**36.59**	17.24	538.62	24.5	4.14
13h	24	**36.82**	17.24	538.62	24.5	4.05
13h	24	**37.03**	17.24	538.62	24.5	3.97
13h	24	**37.22**	17.24	538.62	24.5	3.9
13h	24	**37.42**	17.24	538.62	24.5	3.83
13h	24	**37.56**	17.24	538.62	24.5	3.78
Energy Balance For Airflow Rate For London For One Hour In Summer With Different Gap Sizes							
Jan 29th	Tm	**To**	m	v	H	d	hr
13h	26.22	**27.95**	0.1	0.6	2.2	0.06	6.096793
13h	25.26	**26.03**	0.22	0.6	2.2	0.14	6.153609
13h	24.97	**25.44**	0.35	0.6	2.2	0.22	6.199155
13h	24.84	**25.17**	0.48	0.6	2.2	0.3	6.234301
13h	24.77	**25.03**	0.6	0.6	2.2	0.38	6.26499
13h	24.72	**24.93**	0.73	0.6	2.2	0.46	6.289778
13h	24.68	**24.86**	0.86	0.6	2.2	0.54	6.311138
13h	24.66	**24.81**	0.99	0.6	2.2	0.62	6.331056
13h	24.64	**24.78**	1.11	0.6	2.2	0.7	6.347502
13h	24.62	**24.75**	1.24	0.6	2.2	0.78	6.363071
13h	24.61	**24.72**	1.37	0.6	2.2	0.86	6.377637
13h	24.60	**24.70**	1.5	0.6	2.2	0.94	6.391031
13h	24.59	**24.68**	1.62	0.6	2.2	1.02	6.403123
13h	24.58	**24.67**	1.75	0.6	2.2	1.1	6.415561
13h	24.58	**24.66**	1.88	0.6	2.2	1.18	6.424611

APPENDIX B-3 RESULTS OF THE EFFECT OF DIFFERENT HEIGHTS IN WINTER SEASON

Energy Balance For PV Panel For London For One Hour In Winter With Different Heights						
Jan 29th	Ti	**Tp**	Gp	G	QE	hcp
13h	5.9	**30.16**	282.94	707.36	28.294	5.93
13h	5.9	**30.51**	282.94	707.36	28.294	5.93
13h	5.9	**30.90**	282.94	707.36	28.294	5.93
13h	5.9	**31.24**	282.94	707.36	28.294	5.93
13h	5.9	**31.58**	282.94	707.36	28.294	5.93
13h	5.9	**31.92**	282.94	707.36	28.294	5.93
13h	5.9	**32.25**	282.94	707.36	28.294	5.93
13h	5.9	**32.58**	282.94	707.36	28.294	5.93
13h	5.9	**32.90**	282.94	707.36	28.294	5.93
13h	5.9	**33.22**	282.94	707.36	28.294	5.93
13h	5.9	**33.53**	282.94	707.36	28.294	5.93
13h	5.9	**33.84**	282.94	707.36	28.294	5.93
13h	5.9	**34.15**	282.94	707.36	28.294	5.93
13h	5.9	**34.48**	282.94	707.36	28.294	5.93
13h	5.9	**34.78**	282.94	707.36	28.294	5.93
Energy Balance For Double Glazing For London For One Hour In Winter With Different Heights						
Jan 29th	Troom	**Tg**	Gg	G	Tamb	hcg
13h	21	**19.23**	22.64	707.36	5.9	5.93
13h	21	**19.62**	22.64	707.36	5.9	5.93
13h	21	**20.05**	22.64	707.36	5.9	5.93
13h	21	**20.43**	22.64	707.36	5.9	5.93
13h	21	**20.81**	22.64	707.36	5.9	5.93
13h	21	**21.18**	22.64	707.36	5.9	5.93
13h	21	**21.55**	22.64	707.36	5.9	5.93
13h	21	**21.91**	22.64	707.36	5.9	5.93
13h	21	**22.27**	22.64	707.36	5.9	5.93
13h	21	**22.62**	22.64	707.36	5.9	5.93
13h	21	**22.97**	22.64	707.36	5.9	5.93
13h	21	**23.32**	22.64	707.36	5.9	5.93
13h	21	**23.66**	22.64	707.36	5.9	5.93
13h	21	**24.02**	22.64	707.36	5.9	5.93
13h	21	**24.36**	22.64	707.36	5.9	5.93
Energy Balance For Airflow Rate For London For One Hour In Winter With Different Heights							
Jan 29th	Tm	**To**	m	v	H	d	hr
13h	6.41	**6.91**	0.239	0.6	1.1	0.14	5.413
13h	6.90	**7.91**	0.239	0.6	2.2	0.14	5.434
13h	7.44	**8.98**	0.239	0.6	3.4	0.14	5.456
13h	7.93	**9.95**	0.239	0.6	4.5	0.14	5.476
13h	8.41	**10.91**	0.239	0.6	5.6	0.14	5.496
13h	8.88	**11.85**	0.239	0.6	6.7	0.14	5.516
13h	9.34	**12.79**	0.239	0.6	7.8	0.14	5.535
13h	9.80	**13.71**	0.239	0.6	8.9	0.14	5.554
13h	10.26	**14.62**	0.239	0.6	10	0.14	5.573
13h	10.71	**15.51**	0.239	0.6	11.1	0.14	5.592
13h	11.15	**16.40**	0.239	0.6	12.2	0.14	5.610
13h	11.59	**17.27**	0.239	0.6	13.3	0.14	5.629
13h	12.02	**18.14**	0.239	0.6	14.4	0.14	5.647
13h	12.48	**19.07**	0.239	0.6	15.6	0.14	5.666
13h	12.90	**19.91**	0.239	0.6	16.7	0.14	5.684

APPENDIX B-4 RESULTS OF THE EFFECT OF DIFFERENT HEIGHTS IN SUMMER SEASON

Energy Balance For PV Panel For London For One Hour In Summer With Different Heights						
Jan 29th	Ti	**Tp**	Gp	G	QE	hcp
13h	24.5	**42.42**	215.45	538.36	21.545	5.67
13h	24.5	**42.68**	215.45	538.36	21.545	5.67
13h	24.5	**42.96**	215.45	538.36	21.545	5.67
13h	24.5	**43.21**	215.45	538.36	21.545	5.67
13h	24.5	**43.46**	215.45	538.36	21.545	5.67
13h	24.5	**43.70**	215.45	538.36	21.545	5.67
13h	24.5	**43.95**	215.45	538.36	21.545	5.67
13h	24.5	**44.18**	215.45	538.36	21.545	5.67
13h	24.5	**44.42**	215.45	538.36	21.545	5.67
13h	24.5	**44.65**	215.45	538.36	21.545	5.67
13h	24.5	**44.88**	215.45	538.36	21.545	5.67
13h	24.5	**45.11**	215.45	538.36	21.545	5.67
13h	24.5	**45.33**	215.45	538.36	21.545	5.67
13h	24.5	**45.57**	215.45	538.36	21.545	5.67
13h	24.5	**45.79**	215.45	538.36	21.545	5.67
Energy Balance For Double Glazing For London For One Hour In Summer With Different Heights						
Jan 29th	Troom	**Tg**	Gg	G	Tamb	hcg
13h	24	**33.67**	17.24	538.36	24.5	5.67
13h	24	**33.95**	17.24	538.36	24.5	5.67
13h	24	**34.26**	17.24	538.36	24.5	5.67
13h	24	**34.53**	17.24	538.36	24.5	5.67
13h	24	**34.81**	17.24	538.36	24.5	5.67
13h	24	**35.07**	17.24	538.36	24.5	5.67
13h	24	**35.34**	17.24	538.36	24.5	5.67
13h	24	**35.60**	17.24	538.36	24.5	5.67
13h	24	**35.86**	17.24	538.36	24.5	5.67
13h	24	**36.11**	17.24	538.36	24.5	5.67
13h	24	**36.36**	17.24	538.36	24.5	5.67
13h	24	**36.61**	17.24	538.36	24.5	5.67
13h	24	**36.85**	17.24	538.36	24.5	5.67
13h	24	**37.11**	17.24	538.36	24.5	5.67
13h	24	**37.35**	17.24	538.36	24.5	5.67
Energy Balance For Airflow Rate For London For One Hour In Summer With Different Heights							
Jan 29th	Tm	**To**	m	v	H	d	hr
13h	24.87	**25.24**	0.223	0.6	1.1	0.14	6.175
13h	25.24	**25.98**	0.223	0.6	2.2	0.14	6.191
13h	25.63	**26.77**	0.223	0.6	3.4	0.14	6.209
13h	25.99	**27.48**	0.223	0.6	4.5	0.14	6.224
13h	26.34	**28.18**	0.223	0.6	5.6	0.14	6.240
13h	26.69	**28.88**	0.223	0.6	6.7	0.14	6.255
13h	27.03	**29.56**	0.223	0.6	7.8	0.14	6.271
13h	27.37	**30.24**	0.223	0.6	8.9	0.14	6.286
13h	27.70	**30.90**	0.223	0.6	10	0.14	6.301
13h	28.03	**31.56**	0.223	0.6	11.1	0.14	6.315
13h	28.35	**32.20**	0.223	0.6	12.2	0.14	6.330
13h	28.67	**32.84**	0.223	0.6	13.3	0.14	6.344
13h	28.99	**33.47**	0.223	0.6	14.4	0.14	6.358
13h	29.33	**34.15**	0.223	0.6	15.6	0.14	6.374
13h	29.63	**34.76**	0.223	0.6	16.7	0.14	6.387

APPENDIX B-5 RESULTS OF THE EFFECT OF DIFFERENT SOLAR RADIATIONS IN WINTER SEASON

Energy Balance For PV Panel Using The Climate Data Of London With Different Solar Radiation						
Jan 29th	Ti	**Tp**	Gp	G	QE	hcp
13h	5.9	6.78	0.00	0	0	5.93
13h	5.9	6.78	0.00	0	0	5.93
13h	5.9	6.78	0.00	0	0	5.93
13h	5.9	**7.41**	7.32	18.3	0.732	5.93
13h	5.9	**16.99**	120.04	300.09	12.004	5.93
13h	5.9	**24.44**	209.27	523.18	20.927	5.93
13h	5.9	**28.83**	262.46	656.16	26.246	5.93
13h	5.9	**30.51**	282.94	707.36	28.294	5.93
13h	5.9	**29.57**	271.43	678.58	27.143	5.93
13h	5.9	**25.96**	227.60	568.99	22.76	5.93
13h	5.9	**19.44**	149.18	372.94	14.918	5.93
13h	5.9	**7.63**	9.81	24.52	0.981	5.93
13h	5.9	6.78	0.00	0	0	5.93
13h	5.9	6.78	0.00	0	0	5.93
13h	5.9	6.78	0.00	0	0	5.93
Energy Balance For Double Glazing Using The Climate Data Of London With Different Solar Radiation						
Jan 29th	Troom	**Tg**	Gg	G	Tamb	hcg
13h	21	8.56	0.00	0	5.9	5.93
13h	21	8.56	0.00	0	5.9	5.93
13h	21	8.56	0.00	0	5.9	5.93
13h	21	**8.83**	0.59	18.3	5.9	5.93
13h	21	**13.07**	9.60	300.09	5.9	5.93
13h	21	**16.60**	16.74	523.18	5.9	5.93
13h	21	**18.78**	21.00	656.16	5.9	5.93
13h	21	**19.62**	22.64	707.36	5.9	5.93
13h	21	**19.15**	21.71	678.58	5.9	5.93
13h	21	**17.35**	18.21	568.99	5.9	5.93
13h	21	**14.21**	11.93	372.94	5.9	5.93
13h	21	**8.92**	0.78	24.52	5.9	5.93
13h	21	8.56	0.00	0	5.9	5.93
13h	21	8.56	0.00	0	5.9	5.93
13h	21	8.56	0.00	0	5.9	5.93
Energy Balance For Airflow Rate Using The Climate Data Of London With Different Solar Radiation							
Jan 29th	Tm	**To**	m	v	H	d	hr
13h	5.98	6.07	0.239	0.6	2.2	0.14	4.536
13h	5.98	6.07	0.239	0.6	2.2	0.14	4.536
13h	5.98	6.07	0.239	0.6	2.2	0.14	4.536
13h	6.01	**6.12**	0.239	0.6	2.2	0.14	4.558
13h	6.37	**6.85**	0.239	0.6	2.2	0.14	4.904
13h	6.66	**7.43**	0.239	0.6	2.2	0.14	5.190
13h	6.84	**7.78**	0.239	0.6	2.2	0.14	5.366
13h	6.90	**7.91**	0.239	0.6	2.2	0.14	5.435
13h	6.87	**7.83**	0.239	0.6	2.2	0.14	5.396
13h	6.72	**7.55**	0.239	0.6	2.2	0.14	5.251
13h	6.47	**7.04**	0.239	0.6	2.2	0.14	4.997
13h	6.02	**6.13**	0.239	0.6	2.2	0.14	4.565
13h	5.98	6.07	0.239	0.6	2.2	0.14	4.536
13h	5.98	6.07	0.239	0.6	2.2	0.14	4.536
13h	5.98	6.07	0.239	0.6	2.2	0.14	4.536

APPENDIX B-6 RESULTS OF THE EFFECT OF DIFFERENT SOLAR RADIATIONS IN SUMMER SEASON

Energy Balance For PV Panel For London For One Hour In Summer With Different Solar Radiation						
Jan 29th	Ti	**Tp**	Gp	G	QE	hcp
13h	24.5	**26.60**	24.86	62.16	2.486	5.67
13h	24.5	**27.61**	36.61	91.52	3.661	5.67
13h	24.5	**28.16**	43.01	107.53	4.301	5.67
13h	24.5	**31.65**	84.08	210.21	8.408	5.67
13h	24.5	**36.12**	136.93	342.32	13.693	5.67
13h	24.5	**39.69**	179.59	448.98	17.959	5.67
13h	24.5	**41.96**	206.78	516.95	20.678	5.67
13h	24.5	**42.68**	215.45	538.62	21.545	5.67
13h	24.5	**41.78**	204.66	511.66	20.466	5.67
13h	24.5	**39.36**	175.58	438.96	17.558	5.67
13h	24.5	**35.66**	131.50	328.76	13.15	5.67
13h	24.5	**31.13**	77.97	194.93	7.797	5.67
13h	24.5	**28.11**	42.46	106.16	4.246	5.67
13h	24.5	**27.53**	35.69	89.22	3.569	5.67
13h	24.5	**26.44**	23.01	57.52	2.301	5.67

Energy Balance For Double Glazing For London For One Hour In Summer With Different Solar Radiation						
Jan 29th	Troom	**Tg**	Gg	G	Tamb	hcg
13h	24	**25.68**	1.99	62.16	24.5	5.67
13h	24	**26.17**	2.93	91.52	24.5	5.67
13h	24	**26.44**	3.44	107.53	24.5	5.67
13h	24	**28.18**	6.73	210.21	24.5	5.67
13h	24	**30.46**	10.95	342.32	24.5	5.67
13h	24	**32.35**	14.37	448.98	24.5	5.67
13h	24	**33.56**	16.54	516.95	24.5	5.67
13h	24	**33.95**	17.24	538.62	24.5	5.67
13h	24	**33.47**	16.37	511.66	24.5	5.67
13h	24	**32.17**	14.05	438.96	24.5	5.67
13h	24	**30.23**	10.52	328.76	24.5	5.67
13h	24	**27.92**	6.24	194.93	24.5	5.67
13h	24	**26.41**	3.40	106.16	24.5	5.67
13h	24	**26.13**	2.86	89.22	24.5	5.67
13h	24	**25.60**	1.84	57.52	24.5	5.67

Energy Balance For Airflow Rate For London For One Hour In Winter With Different Solar Radiation							
Jan 29th	Tm	**To**	m	v	H	d	hr
13h	24.58	**24.67**	0.223	0.6	2.2	0.14	5.493
13h	24.62	**24.75**	0.223	0.6	2.2	0.14	5.534
13h	24.65	**24.79**	0.223	0.6	2.2	0.14	5.557
13h	24.79	**25.07**	0.223	0.6	2.2	0.14	5.704
13h	24.97	**25.44**	0.223	0.6	2.2	0.14	5.897
13h	25.12	**25.73**	0.223	0.6	2.2	0.14	6.056
13h	25.21	**25.92**	0.223	0.6	2.2	0.14	6.158
13h	25.24	**25.98**	0.223	0.6	2.2	0.14	6.191
13h	25.20	**25.90**	0.223	0.6	2.2	0.14	6.150
13h	25.10	**25.70**	0.223	0.6	2.2	0.14	6.041
13h	24.95	**25.40**	0.223	0.6	2.2	0.14	5.877
13h	24.77	**25.03**	0.223	0.6	2.2	0.14	5.682
13h	24.64	**24.79**	0.223	0.6	2.2	0.14	5.555
13h	24.62	**24.74**	0.223	0.6	2.2	0.14	5.531
13h	24.58	**24.65**	0.223	0.6	2.2	0.14	5.486

APPENDIX B-7 RESULTS OF THE EFFECT OF DIFFERENT TEMPERATURES IN WINTER SEASON

Energy Balance For PV Panel Of London With Different Temperatures In Winter						
Jan 29th	Ti	**Tp**	Gp	G	QE	hcp
13h	0.7	25.77	282.94	707.36	28.294	5.93
13h	0.7	25.77	282.94	707.36	28.294	5.93
13h	1.8	26.77	282.94	707.36	28.294	5.93
13h	2.3	**27.23**	282.94	707.36	28.294	5.93
13h	3.7	**28.51**	282.94	707.36	28.294	5.93
13h	4.7	**29.42**	282.94	707.36	28.294	5.93
13h	5.5	**30.15**	282.94	707.36	28.294	5.93
13h	5.9	**30.51**	282.94	707.36	28.294	5.93
13h	5.8	**30.42**	282.94	707.36	28.294	5.93
13h	5.3	**29.97**	282.94	707.36	28.294	5.93
13h	4.3	**29.06**	282.94	707.36	28.294	5.93
13h	3.7	**28.51**	282.94	707.36	28.294	5.93
13h	3.3	28.14	282.94	707.36	28.294	5.93
13h	3	27.87	282.94	707.36	28.294	5.93
13h	2.7	27.60	282.94	707.36	28.294	5.93

Energy Balance For Double Glazing Of London With Different Temperatures In Winter						
Jan 29th	Troom	**Tg**	Gg	G	Tamb	hcg
13h	21	15.07	22.64	707.36	0.7	5.93
13h	21	15.07	22.64	707.36	0.7	5.93
13h	21	16.03	22.64	707.36	1.8	5.93
13h	21	**16.47**	22.64	707.36	2.3	5.93
13h	21	**17.69**	22.64	707.36	3.7	5.93
13h	21	**18.57**	22.64	707.36	4.7	5.93
13h	21	**19.27**	22.64	707.36	5.5	5.93
13h	21	**19.62**	22.64	707.36	5.9	5.93
13h	21	**19.54**	22.64	707.36	5.8	5.93
13h	21	**19.10**	22.64	707.36	5.3	5.93
13h	21	**18.22**	22.64	707.36	4.3	5.93
13h	21	**17.69**	22.64	707.36	3.7	5.93
13h	21	17.34	22.64	707.36	3.3	5.93
13h	21	17.08	22.64	707.36	3	5.93
13h	21	16.82	22.64	707.36	2.7	5.93

Energy Balance For Airflow Rate Of London With Different Temperatures In Winter							
Jan 29th	Tm	**To**	m	v	H	d	hr
13h	1.73	2.77	0.239	0.6	2.2	0.14	5.184
13h	1.73	2.77	0.239	0.6	2.2	0.14	5.184
13h	2.83	3.85	0.239	0.6	2.2	0.14	5.236
13h	3.32	**4.35**	0.239	0.6	2.2	0.14	5.260
13h	4.72	**5.73**	0.239	0.6	2.2	0.14	5.327
13h	5.71	**6.72**	0.239	0.6	2.2	0.14	5.376
13h	6.51	**7.51**	0.239	0.6	2.2	0.14	5.415
13h	6.90	**7.91**	0.239	0.6	2.2	0.14	5.434
13h	6.81	**7.81**	0.239	0.6	2.2	0.14	5.429
13h	6.31	**7.32**	0.239	0.6	2.2	0.14	5.405
13h	5.31	**6.33**	0.239	0.6	2.2	0.14	5.356
13h	4.72	**5.73**	0.239	0.6	2.2	0.14	5.327
13h	4.32	5.34	0.239	0.6	2.2	0.14	5.308
13h	4.02	5.04	0.239	0.6	2.2	0.14	5.294
13h	3.72	4.75	0.239	0.6	2.2	0.14	5.279

APPENDIX B-8 RESULTS OF THE EFFECT OF DIFFERENT TEMPERATURES IN SUMMER SEASON

Energy Balance For PV Panel Of London With Different Temperatures In Summer						
Jan 29th	Ti	**Tp**	Gp	G	QE	hcp
13h	16.8	**35.66**	215.45	538.62	21.54	5.67
13h	18.5	**37.21**	215.45	538.62	21.54	5.67
13h	20.1	**38.67**	215.45	538.62	21.54	5.67
13h	21.5	**39.95**	215.45	538.62	21.54	5.67
13h	22.7	**41.04**	215.45	538.62	21.54	5.67
13h	23.6	**41.86**	215.45	538.62	21.54	5.67
13h	24.4	**42.59**	215.45	538.62	21.54	5.67
13h	24.5	**42.68**	215.45	538.62	21.54	5.67
13h	24.4	**42.59**	215.45	538.62	21.54	5.67
13h	24.2	**42.41**	215.45	538.62	21.54	5.67
13h	23.5	**41.77**	215.45	538.62	21.54	5.67
13h	22.5	**40.86**	215.45	538.62	21.54	5.67
13h	19.3	**37.94**	215.45	538.62	21.54	5.67
13h	17.9	**36.67**	215.45	538.62	21.54	5.67
13h	16.8	**35.66**	215.45	538.62	21.54	5.67
Energy Balance For Double Glazing Of London With Different Temperatures In Summer						
Jan 29th	Troom	**Tg**	Gg	G	Tamb	hcg
13h	24	**27.26**	17.24	538.62	16.8	5.67
13h	24	**28.73**	17.24	538.62	18.5	5.67
13h	24	**30.12**	17.24	538.62	20.1	5.67
13h	24	**31.34**	17.24	538.62	21.5	5.67
13h	24	**32.38**	17.24	538.62	22.7	5.67
13h	24	**33.17**	17.24	538.62	23.6	5.67
13h	24	**33.86**	17.24	538.62	24.4	5.67
13h	24	**33.95**	17.24	538.62	24.5	5.67
13h	24	**33.86**	17.24	538.62	24.4	5.67
13h	24	**33.69**	17.24	538.62	24.2	5.67
13h	24	**33.08**	17.24	538.62	23.5	5.67
13h	24	**32.21**	17.24	538.62	22.5	5.67
13h	24	**29.43**	17.24	538.62	19.3	5.67
13h	24	**28.21**	17.24	538.62	17.9	5.67
13h	24	**27.26**	17.24	538.62	16.8	5.67
Energy Balance For Air flow Rates Of London With Different Temperatures In Summer							
Jan 29th	Tm	**To**	m	v	H	d	hr
13h	17.58	**18.37**	0.223	0.6	2.2	0.14	5.790
13h	19.27	**20.05**	0.223	0.6	2.2	0.14	5.877
13h	20.87	**21.63**	0.223	0.6	2.2	0.14	5.959
13h	22.26	**23.01**	0.223	0.6	2.2	0.14	6.032
13h	23.45	**24.20**	0.223	0.6	2.2	0.14	6.096
13h	24.34	**25.09**	0.223	0.6	2.2	0.14	6.143
13h	25.14	**25.88**	0.223	0.6	2.2	0.14	6.186
13h	25.24	**25.98**	0.223	0.6	2.2	0.14	6.191
13h	25.14	**25.88**	0.223	0.6	2.2	0.14	6.186
13h	24.94	**25.68**	0.223	0.6	2.2	0.14	6.175
13h	24.25	**24.99**	0.223	0.6	2.2	0.14	6.138
13h	23.25	**24.00**	0.223	0.6	2.2	0.14	6.085
13h	20.07	**20.84**	0.223	0.6	2.2	0.14	5.918
13h	18.68	**19.46**	0.223	0.6	2.2	0.14	5.846
13h	17.58	**18.37**	0.223	0.6	2.2	0.14	5.790

APPENDIX B-9 RESULTS OF THE EFFECT OF DIFFERENT VELOCITIES IN WINTER SEASON

Energy Balance For PV Panel For London For One Hour In Winter With Different Velocities						
Jan 29th	Ti	**Tp**	Gp	G	QE	hcp
13h	5.9	53.82	282.94	707.36	28.294	1.59
13h	5.9	48.12	282.94	707.36	28.294	2.17
13h	5.9	44.03	282.94	707.36	28.294	2.71
13h	5.9	**38.38**	282.94	707.36	28.294	3.71
13h	5.9	**36.31**	282.94	707.36	28.294	4.18
13h	5.9	**34.56**	282.94	707.36	28.294	4.63
13h	5.9	**31.75**	282.94	707.36	28.294	5.50
13h	5.9	**30.59**	282.94	707.36	28.294	5.93
13h	5.9	**29.56**	282.94	707.36	28.294	6.34
13h	5.9	**27.80**	282.94	707.36	28.294	7.14
13h	5.9	**27.04**	282.94	707.36	28.294	7.53
13h	5.9	**26.34**	282.94	707.36	28.294	7.92
13h	5.9	25.10	282.94	707.36	28.294	8.68
13h	5.9	24.56	282.94	707.36	28.294	9.05
13h	5.9	24.04	282.94	707.36	28.294	9.42
Energy Balance For Double Glazing For London For One Hour In Winter With Different Velocities						
Jan 29th	Troom	**Tg**	Gg	G	Tamb	hcg
13h	21	43.16	22.64	707.36	5.9	1.59
13h	21	37.02	22.64	707.36	5.9	2.17
13h	21	32.72	22.64	707.36	5.9	2.71
13h	21	**26.98**	22.64	707.36	5.9	3.71
13h	21	**24.96**	22.64	707.36	5.9	4.18
13h	21	**23.30**	22.64	707.36	5.9	4.63
13h	21	**20.73**	22.64	707.36	5.9	5.50
13h	21	**19.70**	22.64	707.36	5.9	5.93
13h	21	**18.82**	22.64	707.36	5.9	6.34
13h	21	**17.35**	22.64	707.36	5.9	7.14
13h	21	**16.73**	22.64	707.36	5.9	7.53
13h	21	**16.18**	22.64	707.36	5.9	7.92
13h	21	15.24	22.64	707.36	5.9	8.68
13h	21	14.83	22.64	707.36	5.9	9.05
13h	21	14.45	22.64	707.36	5.9	9.42
Energy Balance For Airflow Rate For London For One Hour In Winter With Different Velocities							
Jan 29th	Tm	**To**	m	v	H	d	hr
13h	9.35	12.80	0.040	0.1	2.2	0.14	6.806
13h	8.63	11.36	0.060	0.15	2.2	0.14	6.440
13h	8.18	10.45	0.080	0.2	2.2	0.14	6.189
13h	7.63	**9.35**	0.119	0.3	2.2	0.14	5.858
13h	7.44	**8.99**	0.139	0.35	2.2	0.14	5.742
13h	7.30	**8.70**	0.159	0.4	2.2	0.14	5.647
13h	7.08	**8.26**	0.199	0.5	2.2	0.14	5.498
13h	6.99	**8.09**	0.219	0.55	2.2	0.14	5.438
13h	6.92	**7.94**	0.239	0.6	2.2	0.14	5.386
13h	6.80	**7.70**	0.279	0.7	2.2	0.14	5.299
13h	6.75	**7.60**	0.299	0.75	2.2	0.14	5.262
13h	6.71	**7.52**	0.319	0.8	2.2	0.14	5.229
13h	6.63	7.36	0.358	0.9	2.2	0.14	5.171
13h	6.60	7.30	0.378	0.95	2.2	0.14	5.146
13h	6.57	7.24	0.398	1	2.2	0.14	5.122

APPENDIX B-10 RESULTS OF THE EFFECT OF DIFFERENT VELOCITIES IN SUMMER SEASON

Energy Balance For PV Panel For London For One Hour In Summer With Different Velocities						
Jan 29th	Ti	**Tp**	Gp	G	QE	hcp
13h	24.5	**59.13**	215.45	538.62	21.54	1.53
13h	24.5	**55.15**	215.45	538.62	21.54	2.08
13h	24.5	**52.27**	215.45	538.62	21.54	2.60
13h	24.5	**48.27**	215.45	538.62	21.54	3.55
13h	24.5	**46.80**	215.45	538.62	21.54	4.00
13h	24.5	**45.55**	215.45	538.62	21.54	4.44
13h	24.5	**43.55**	215.45	538.62	21.54	5.27
13h	24.5	**42.72**	215.45	538.62	21.54	5.67
13h	24.5	**41.98**	215.45	538.62	21.54	6.07
13h	24.5	**40.72**	215.45	538.62	21.54	6.84
13h	24.5	**40.29**	215.45	538.62	21.54	7.21
13h	24.5	**39.67**	215.45	538.62	21.54	7.58
13h	24.5	**38.78**	215.45	538.62	21.54	8.31
13h	24.5	**38.39**	215.45	538.62	21.54	8.66
13h	24.5	**38.02**	215.45	538.62	21.54	9.01
Energy Balance For Double Glazing For London For One Hour In Summer With Different Velocities						
Jan 29th	Troom	**Tg**	Gg	G	Tamb	hcg
13h	24	**50.18**	17.24	538.62	24.5	1.53
13h	24	**45.99**	17.24	538.62	24.5	2.08
13h	24	**43.03**	17.24	538.62	24.5	2.60
13h	24	**39.07**	17.24	538.62	24.5	3.55
13h	24	**37.67**	17.24	538.62	24.5	4.00
13h	24	**36.51**	17.24	538.62	24.5	4.44
13h	24	**34.71**	17.24	538.62	24.5	5.27
13h	24	**34.00**	17.24	538.62	24.5	5.67
13h	24	**33.38**	17.24	538.62	24.5	6.07
13h	24	**32.35**	17.24	538.62	24.5	6.84
13h	24	**32.04**	17.24	538.62	24.5	7.21
13h	24	**31.53**	17.24	538.62	24.5	7.58
13h	24	**30.86**	17.24	538.62	24.5	8.31
13h	24	**30.58**	17.24	538.62	24.5	8.66
13h	24	**30.32**	17.24	538.62	24.5	9.01
Energy Balance For Air flow Rate For London For One Hour In Summer With Different Velocities							
Jan 29th	Tm	**To**	m	v	H	d	hr
13h	27.01	**29.51**	0.037	0.1	2.2	0.14	7.210
13h	26.49	**28.48**	0.056	0.15	2.2	0.14	6.946
13h	26.16	**27.83**	0.074	0.2	2.2	0.14	6.761
13h	25.77	**27.03**	0.111	0.3	2.2	0.14	6.514
13h	25.64	**26.77**	0.130	0.35	2.2	0.14	6.427
13h	25.53	**26.56**	0.148	0.4	2.2	0.14	6.354
13h	25.37	**26.24**	0.186	0.5	2.2	0.14	6.240
13h	25.31	**26.11**	0.204	0.55	2.2	0.14	6.194
13h	25.25	**26.01**	0.223	0.6	2.2	0.14	6.153
13h	25.17	**25.83**	0.260	0.7	2.2	0.14	6.086
13h	25.28	**26.07**	0.223	0.75	2.2	0.14	6.064
13h	25.10	**25.69**	0.297	0.8	2.2	0.14	6.031
13h	25.04	**25.58**	0.334	0.9	2.2	0.14	5.985
13h	25.02	**25.53**	0.353	0.95	2.2	0.14	5.965
13h	25.00	**25.49**	0.371	1	2.2	0.14	5.947

APPENDIX C RESULTS AND PARAMETERS OF CFD MODELS VALIDATION FOR CHAPTER 4

APPENDIX C-1 RESULTS AND PARAMETERS OF K-ε WITH ENHANCED WALL TREATMENT CFD MODEL (TI = 288.15K, TO = 323.15K)

k-ε Model & Enhanced Wall Treatment with Ti = 288.15K, To = 323.15K				
Original Mesh				
Cases	**Velocities**	**ΔT**	**ΔT Rakes**	**Error**
1	**5.22**	**30.27**	**29.02**	4.13%
2	**5.17**	**30.27**	**29.02**	4.13%
Refined Mesh 1				
Cases	**Velocities**	**ΔT**	**ΔT Rakes**	**Error**
1	**5.22**	**30.62**	**29.34**	4.18%
2	**5.17**	**30.62**	**29.34**	4.18%
Refined Mesh 2				
Cases	**Velocities**	**ΔT**	**ΔT Rakes**	**Error**
1	**5.22**	**30.65**	**29.34**	4.27%
2	**5.17**	**30.65**	**29.34**	4.27%

APPENDIX C-2 RESULTS AND PARAMETERS OF K-ε WITH ENHANCED WALL TREATMENT CFD MODEL (TI = 286K, TO = 306K)

k-ε Model & Enhanced Wall Treatment with Ti = 286K, To = 306K				
Original Mesh				
Cases	**Velocities**	**ΔT**	**ΔT Rakes**	**Error**
1	**5.22**	**17.49**	**17.04**	2.57%
2	**5.17**	**17.46**	**16.80**	3.78%
Refined Mesh 1				
Cases	**Velocities**	**ΔT**	**ΔT Rakes**	**Error**
1	**5.22**	**15.54**	**14.89**	4.18%
2	**5.17**	**15.53**	**14.82**	4.57%
Refined Mesh 2				
Cases	**Velocities**	**ΔT**	**ΔT Rakes**	**Error**
1	**5.22**	**17.45**	**16.95**	2.87%
2	**5.17**	**17.53**	**16.98**	3.14%

APPENDIX C-3 RESULTS AND PARAMETERS OF SST K-ω CFD MODEL (TI = 288.15K, TO = 323.15K)

SST k-ω with Ti = 288.15K, To = 323.15K				
Original Mesh				
Cases	**Velocities**	**ΔT**	**ΔT Rakes**	**Error**
1	**5.2233**	**30.45**	**29.17**	4.20%
2	**5.1719**	**30.49**	**28.81**	5.51%
Refined Mesh 1				
Cases	**Velocities**	**ΔT**	**ΔT Rakes**	**Error**
1	**5.2233**	**29.56**	**28.04**	5.14%
2	**5.1719**	**29.69**	**28.32**	4.61%
Refined Mesh 2				
Cases	**Velocities**	**ΔT**	**ΔT Rakes**	**Error**
1	**5.2233**	**29.76**	**28.74**	3.43%
2	**5.1719**	**29.89**	**28.96**	3.11%

APPENDIX C-4 RESULTS AND PARAMETERS OF SST K-ω CFD MODEL (TI = 286K, TO = 306K)

SST k-ω with Ti = 286K, To = 306K				
Original Mesh				
Cases	**Velocities**	**ΔT**	**ΔT Rakes**	**Error**
1	**5.2233**	**16.49**	**16.56**	0.42%
2	**5.1719**	**16.95**	**17.18**	1.36%
Refined Mesh 1				
Cases	**Velocities**	**ΔT**	**ΔT Rakes**	**Error**
1	**5.2233**	**17.27**	**16.39**	5.10%
2	**5.1719**	**17.41**	**16.88**	3.04%
Refined Mesh 2				
Cases	**Velocities**	**ΔT**	**ΔT Rakes**	**Error**
1	**5.2233**	**18.09**	**17.55**	2.99%
2	**5.1719**	**18.39**	**17.13**	6.85%

APPENDIX C-5 RESULTS AND PARAMETERS OF TRANSITION SST CFD MODEL (TI = 288.15K, TO = 323.15K)

Transition SST with Ti = 288.15K, To = 323.15K				
Original Mesh				
Cases	**Velocities**	**ΔT**	**ΔT Rakes**	**Error**
1	**5.2233**	**26.76**	**24.78**	7.40%
2	**5.1719**	**30.45**	**29.67**	2.56%
Refined Mesh 1				
Cases	**Velocities**	**ΔT**	**ΔT Rakes**	**Error**
1	**5.2233**	**29.94**	**28.79**	3.84%
2	**5.1719**	**30.66**	**29.74**	3.00%
Refined Mesh 2				
Cases	**Velocities**	**ΔT**	**ΔT Rakes**	**Error**
1	**5.2233**	**30.42**	**29.59**	2.73%
2	**5.1719**	**30.71**	**29.72**	3.22%

APPENDIX C-6 RESULTS AND PARAMETERS OF TRANSITION SST CFD MODEL (TI = 286K, TO = 306K)

Transition SST with Ti = 286K, To = 306K				
Original Mesh				
Cases	**Velocities**	**ΔT**	**ΔT Rakes**	**Error**
1	**5.2233**	**17.45**	**17.06**	2.23%
2	**5.1719**	**17.42**	**16.99**	2.47%
Refined Mesh 1				
Cases	**Velocities**	**ΔT**	**ΔT Rakes**	**Error**
1	**5.2233**	**17.50**	**16.68**	4.69%
2	**5.1719**	**17.64**	**17.30**	1.93%
Refined Mesh 2				
Cases	**Velocities**	**ΔT**	**ΔT Rakes**	**Error**
1	**5.2233**	**17.53**	**16.98**	3.14%
2	**5.1719**	**17.68**	**17.41**	1.53%

APPENDIX C-7 RESULTS AND PARAMETERS OF OVERALL NUSSELT NUMBER OBTAINED FROM CFD MODEL AND BENCHMARK AT THE ORIGINAL MESH, 1ST MESH REFINEMENT, AND 2ND MESH REFINEMENT

k-ε (original mesh) and wall Temperature 333.15k						
Velocity	q (k-ε)	Nu Pred (k-ε)	Nu Meas	Percentage Errors	Re	Flow type
0.1	33.61	0.77	1.03	26	137.34	Laminar
0.15	49.22	1.12	1.42	21	206.01	Laminar
0.2	64.53	1.47	1.79	18	274.68	Laminar
0.25	79.29	1.81	2.14	16	343.35	Laminar
0.3	93.46	2.13	2.48	14	412.02	Laminar
0.35	107.08	2.44	2.80	13	480.69	Laminar
0.4	120.23	2.74	3.12	12	549.36	Laminar
0.45	132.97	3.03	3.43	12	618.03	Laminar
0.5	145.34	3.31	3.73	11	686.70	Laminar
0.55	157.38	3.59	4.02	11	755.37	Laminar
0.6	169.14	3.86	4.32	11	824.05	Laminar
0.65	180.65	4.12	4.60	10	892.72	Laminar
0.7	191.94	4.37	4.88	10	961.39	Laminar
0.75	203.02	4.63	5.16	10	1030.06	Laminar
0.8	213.93	4.88	5.43	10	1098.73	Laminar
0.85	224.68	5.12	5.70	10	1167.40	Laminar
0.9	235.30	5.36	5.97	10	1236.07	Laminar
0.95	245.79	5.60	6.23	10	1304.74	Laminar
1	256.16	5.84	6.49	10	1373.41	Laminar

k-ε (1st refined mesh) and wall Temperature 333.15k						
Velocity	q (k-ε)	Nu Pred (k-ε)	Nu Meas	Percentage Errors	Re	Flow type
0.1	34.09	0.78	1.03	24	137.34	Laminar
0.15	49.61	1.13	1.42	21	206.01	Laminar
0.2	64.85	1.48	1.79	17	274.68	Laminar
0.25	79.55	1.81	2.14	15	343.35	Laminar
0.3	93.66	2.14	2.48	14	412.02	Laminar
0.35	107.46	2.45	2.80	13	480.69	Laminar
0.4	120.56	2.75	3.12	12	549.36	Laminar
0.45	133.25	3.04	3.43	11	618.03	Laminar
0.5	145.57	3.32	3.73	11	686.70	Laminar
0.55	157.61	3.59	4.02	11	755.37	Laminar
0.6	169.37	3.86	4.32	11	824.05	Laminar
0.65	180.80	4.12	4.60	10	892.72	Laminar
0.7	192.07	4.38	4.88	10	961.39	Laminar
0.75	203.12	4.63	5.16	10	1030.06	Laminar
0.8	214.03	4.88	5.43	10	1098.73	Laminar
0.85	224.87	5.13	5.70	10	1167.40	Laminar
0.9	235.34	5.37	5.97	10	1236.07	Laminar
0.95	245.67	5.60	6.23	10	1304.74	Laminar
1	255.92	5.84	6.49	10	1373.41	Laminar
k-ε (2nd refined mesh) and wall Temperature 333.15k						
Velocity	q (k-ε)	Nu Pred (k-ε)	Nu Meas	Percentage Errors	Re	Flow type
0.1	35.14	0.80	1.03	22	137.34	Laminar
0.15	49.90	1.14	1.42	20	206.01	Laminar
0.2	65.15	1.49	1.79	17	274.68	Laminar
0.25	79.95	1.82	2.14	15	343.35	Laminar
0.3	94.05	2.14	2.48	13	412.02	Laminar
0.35	107.82	2.46	2.80	12	480.69	Laminar
0.4	120.79	2.75	3.12	12	549.36	Laminar
0.45	133.61	3.05	3.43	11	618.03	Laminar
0.5	145.82	3.33	3.73	11	686.70	Laminar
0.55	158.03	3.60	4.02	10	755.37	Laminar
0.6	169.77	3.87	4.32	10	824.05	Laminar
0.65	181.10	4.13	4.60	10	892.72	Laminar
0.7	192.47	4.39	4.88	10	961.39	Laminar
0.75	203.47	4.64	5.16	10	1030.06	Laminar
0.8	214.36	4.89	5.43	10	1098.73	Laminar
0.85	225.03	5.13	5.70	10	1167.40	Laminar
0.9	235.63	5.37	5.97	10	1236.07	Laminar
0.95	245.97	5.61	6.23	10	1304.74	Laminar
1	256.25	5.84	6.49	10	1373.41	Laminar

APPENDIX D RESULTS AND PARAMETERS OF DAYLIGHTING VALIDATION FOR CHAPTER 5

APPENDIX D-1 RESULTS AND PARAMETERS OF DAYLIGHT FACTOR OF 5*5 MODEL

Daylight Factors 5*5 Model				
ECOTECT	**Daysim/Radiance**	**TropLux**	**Change with Daysim/Radiance**	**Change with Troplux**
28.8	24	18.8	5	10
14.28	19.8	15.4	6	1
8.87	12	10.7	3	2
7.3	9	8.3	2	1
7	7.7	6.2	1	1

APPENDIX D-2 RESULTS AND PARAMETERS OF DAYLIGHT FACTOR OF 5*10 MODEL

Daylight Factors 5*10 Model				
ECOTECT	**Daysim/Radiance**	**TropLux**	**Change with Daysim/Radiance**	**Change with Troplux**
21	24	17.5	3	10
6.9	8	7	1	1
3.6	4.7	4	1	1
2.3	4.2	3.5	2	1
1.9	3.9	2.5	2	2

Model A		
Experiment	**ECOTECT**	**Change with Experiment**
26.1	22.66	3.44
23.6	16.12	7.48
14.8	10.98	3.82
8.8	6.42	2.38
6.1	4.96	1.14
4.4	4.36	0.04
3.3	3.29	0.01
2.4	2.81	0.41
2.1	2.43	0.33
1.8	2.27	0.47
1.7	2.12	0.42
Model B		
Experiment	**ECOTECT**	**Change with Experiment**
29	19.96	9.04
17	12.57	4.43
11	7.97	3.03
7	4.13	2.87
4	3.62	0.38
3	3	0
2	2.4	0.4
2	2.2	0.2
1	1.9	0.9
1	1.78	0.78
1	1.7	0.7

APPENDIX D-4 RESULTS AND PARAMETERS OF DAYLIGHT FACTORS FROM CIE STANDARD OVERCAST SKY MODEL AND CLEAR DOUBLE GLAZING WITH LOW-E COATING

Daylight factor from CIE standard overcast sky model and a clear double glazing with Low-E coating			
DF ECOTECT	DF Radiance	DF BC/LC	Change %
23.14	22.5	20.7	1
15.6	13	13	3
9.89	8.3	8.3	2
6.55	5	5	2
3.95	4.1	4.1	0
2.65	3.2	3.2	1
1.8	3	3	1
1.53	2.3	2.3	1
1.2	2	2	1
1.14	1.9	1.9	1
1	1.8	1.8	1

APPENDIX D-5 RESULTS AND PARAMETERS OF ILLUMINANCE LEVELS OF THE BLIND LOWERED CASE

Comparison with screen lowered case			
Illuminance ECOTECT	Illuminanace Radiance	Illuminanace BC/LC	Change %
61.7	630	600	90
53.59	225	225	76
47.52	148	148	68
45.29	102	102	56
43.29	78	78	45
41.61	66	66	37
40.65	63	63	35
42.18	61	61	31
41.95	59	59	29
43.68	54	54	19
48.44	50	50	3

APPENDIX D-6 RESULTS AND PARAMETERS OF ILLUMINANCE LEVELS OF SCREEN LOWERED CASE

Comparison with blind lowered case				
Illuminance ECOTECT	Illuminanace Radiance	Illuminanace BC/LC	Change with Radiance %	Change with BC/LC%
956.23	843	890	13	7
654.42	759	750	14	13
540.23	645	580	16	7
355.6	550	495	35	28
243.73	435	380	44	36
196.08	385	350	49	44
154.34	367	305	58	49
122.77	350	260	65	53
94	344	210	73	55
84.77	340	200	75	58
77.37	325	200	76	61

APPENDIX E PARAMETERS OF TRANSIENT ANALYSIS FOR CHAPTER 10

APPENDIX E-1 PARAMETERS OF TRANSIENT ANALYSIS FROM 8-9AM IN WINTER

8		Gp	Gg1	Gg2	Gfloor	9		Gp	Gg1	Gg2	Gfloor
8.00	**18.3**	3.81	0.15	0.12	0.66	9.00	**300.09**	62.42	2.40	1.92	10.76
8.01	21.12	4.39	0.17	0.14	0.76	9.01	302.32	62.88	2.42	1.93	10.84
8.02	23.94	4.98	0.19	0.15	0.86	9.02	304.55	63.35	2.44	1.95	10.92
8.03	26.75	5.56	0.21	0.17	0.96	9.03	306.78	63.81	2.45	1.96	11.00
8.04	29.57	6.15	0.24	0.19	1.06	9.04	309.01	64.27	2.47	1.98	11.08
8.05	32.39	6.74	0.26	0.21	1.16	9.05	311.24	64.74	2.49	1.99	11.16
8.06	35.21	7.32	0.28	0.23	1.26	9.06	313.48	65.20	2.51	2.01	11.23
8.07	38.03	7.91	0.30	0.24	1.36	9.07	315.71	65.67	2.53	2.02	11.31
8.08	40.84	8.50	0.33	0.26	1.46	9.08	317.94	66.13	2.54	2.03	11.39
8.09	43.66	9.08	0.35	0.28	1.56	9.09	320.17	66.59	2.56	2.05	11.47
8.1	46.48	9.67	0.37	0.30	1.67	9.1	322.40	67.06	2.58	2.06	11.55
8.11	49.30	10.25	0.39	0.32	1.77	9.11	324.63	67.52	2.60	2.08	11.63
8.12	52.11	10.84	0.42	0.33	1.87	9.12	326.86	67.99	2.61	2.09	11.71
8.13	54.93	11.43	0.44	0.35	1.97	9.13	329.09	68.45	2.63	2.11	11.79
8.14	57.75	12.01	0.46	0.37	2.07	9.14	331.32	68.92	2.65	2.12	11.87
8.15	60.57	12.60	0.48	0.39	2.17	9.15	333.55	69.38	2.67	2.13	11.95
8.16	63.39	13.18	0.51	0.41	2.27	9.16	335.78	69.84	2.69	2.15	12.03
8.17	66.20	13.77	0.53	0.42	2.37	9.17	338.02	70.31	2.70	2.16	12.11
8.18	69.02	14.36	0.55	0.44	2.47	9.18	340.25	70.77	2.72	2.18	12.19
8.19	71.84	14.94	0.57	0.46	2.57	9.19	342.48	71.24	2.74	2.19	12.27
8.2	74.66	15.53	0.60	0.48	2.68	9.2	344.71	71.70	2.76	2.21	12.35
8.21	77.48	16.11	0.62	0.50	2.78	9.21	346.94	72.16	2.78	2.22	12.43
8.22	80.29	16.70	0.64	0.51	2.88	9.22	349.17	72.63	2.79	2.23	12.51
8.23	83.11	17.29	0.66	0.53	2.98	9.23	351.40	73.09	2.81	2.25	12.59
8.24	85.93	17.87	0.69	0.55	3.08	9.24	353.63	73.56	2.83	2.26	12.67
8.25	88.75	18.46	0.71	0.57	3.18	9.25	355.86	74.02	2.85	2.28	12.75
8.26	91.57	19.05	0.73	0.59	3.28	9.26	358.09	74.48	2.86	2.29	12.83
8.27	94.38	19.63	0.76	0.60	3.38	9.27	360.32	74.95	2.88	2.31	12.91
8.28	97.20	20.22	0.78	0.62	3.48	9.28	362.56	75.41	2.90	2.32	12.99
8.29	100.02	20.80	0.80	0.64	3.58	9.29	364.79	75.88	2.92	2.33	13.07
8.3	102.84	21.39	0.82	0.66	3.69	9.3	367.02	76.34	2.94	2.35	13.15
8.31	105.65	21.98	0.85	0.68	3.79	9.31	369.25	76.80	2.95	2.36	13.23
8.32	108.47	22.56	0.87	0.69	3.89	9.32	371.48	77.27	2.97	2.38	13.31
8.33	111.29	23.15	0.89	0.71	3.99	9.33	373.71	77.73	2.99	2.39	13.39
8.34	114.11	23.73	0.91	0.73	4.09	9.34	375.94	78.20	3.01	2.41	13.47
8.35	116.93	24.32	0.94	0.75	4.19	9.35	378.17	78.66	3.03	2.42	13.55
8.36	119.74	24.91	0.96	0.77	4.29	9.36	380.40	79.12	3.04	2.43	13.63
8.37	122.56	25.49	0.98	0.78	4.39	9.37	382.63	79.59	3.06	2.45	13.71

8.38	125.38	26.08	1.00	0.80	4.49	9.38	384.86	80.05	3.08	2.46	13.79
8.39	128.20	26.67	1.03	0.82	4.59	9.39	387.10	80.52	3.10	2.48	13.87
8.4	131.02	27.25	1.05	0.84	4.70	9.4	389.33	80.98	3.11	2.49	13.95
8.41	133.83	27.84	1.07	0.86	4.80	9.41	391.56	81.44	3.13	2.51	14.03
8.42	136.65	28.42	1.09	0.87	4.90	9.42	393.79	81.91	3.15	2.52	14.11
8.43	139.47	29.01	1.12	0.89	5.00	9.43	396.02	82.37	3.17	2.53	14.19
8.44	142.29	29.60	1.14	0.91	5.10	9.44	398.25	82.84	3.19	2.55	14.27
8.45	145.11	30.18	1.16	0.93	5.20	9.45	400.48	83.30	3.20	2.56	14.35
8.46	147.92	30.77	1.18	0.95	5.30	9.46	402.71	83.76	3.22	2.58	14.43
8.47	150.74	31.35	1.21	0.96	5.40	9.47	404.94	84.23	3.24	2.59	14.51
8.48	153.56	31.94	1.23	0.98	5.50	9.48	407.17	84.69	3.26	2.61	14.59
8.49	156.38	32.53	1.25	1.00	5.60	9.49	409.40	85.16	3.28	2.62	14.67
8.5	159.19	33.11	1.27	1.02	5.71	9.5	411.63	85.62	3.29	2.63	14.75
8.51	162.01	33.70	1.30	1.04	5.81	9.51	413.87	86.08	3.31	2.65	14.83
8.52	164.83	34.28	1.32	1.05	5.91	9.52	416.10	86.55	3.33	2.66	14.91
8.53	167.65	34.87	1.34	1.07	6.01	9.53	418.33	87.01	3.35	2.68	14.99
8.54	170.47	35.46	1.36	1.09	6.11	9.54	420.56	87.48	3.36	2.69	15.07
8.55	173.28	36.04	1.39	1.11	6.21	9.55	422.79	87.94	3.38	2.71	15.15
8.56	176.10	36.63	1.41	1.13	6.31	9.56	425.02	88.40	3.40	2.72	15.23
8.57	178.92	37.22	1.43	1.15	6.41	9.57	427.25	88.87	3.42	2.73	15.31
8.58	181.74	37.80	1.45	1.16	6.51	9.58	429.48	89.33	3.44	2.75	15.39
8.59	184.56	38.39	1.48	1.18	6.61	9.59	431.71	89.80	3.45	2.76	15.47

APPENDIX E-2 PARAMETERS OF TRANSIENT ANALYSIS FROM 10-11AM IN WINTER

10		**Gp**	**Gg1**	**Gg2**	**Gfloor**	**11**		**Gp**	**Gg1**	**Gg2**	**Gfloor**
10.00	**523.18**	Gp	Gg1	Gg2	Gfloor	11.00	**656.16**	Gp	Gg1	Gg2	Gfloor
10.01	524.51	109.10	4.20	3.36	18.80	11.01	656.67	136.59	5.25	4.20	23.54
10.02	525.84	109.37	4.21	3.37	18.85	11.02	657.18	136.69	5.26	4.21	23.55
10.03	527.17	109.65	4.22	3.37	18.89	11.03	657.70	136.80	5.26	4.21	23.57
10.04	528.50	109.93	4.23	3.38	18.94	11.04	658.21	136.91	5.27	4.21	23.59
10.05	529.83	110.20	4.24	3.39	18.99	11.05	658.72	137.01	5.27	4.22	23.61
10.06	531.16	110.48	4.25	3.40	19.04	11.06	659.23	137.12	5.27	4.22	23.63
10.07	532.49	110.76	4.26	3.41	19.08	11.07	659.74	137.23	5.28	4.22	23.65
10.08	533.82	111.03	4.27	3.42	19.13	11.08	660.26	137.33	5.28	4.23	23.66
10.09	535.15	111.31	4.28	3.42	19.18	11.09	660.77	137.44	5.29	4.23	23.68
10.1	536.48	111.59	4.29	3.43	19.23	11.1	661.28	137.55	5.29	4.23	23.70
10.11	537.81	111.86	4.30	3.44	19.28	11.11	661.79	137.65	5.29	4.24	23.72
10.12	539.14	112.14	4.31	3.45	19.32	11.12	662.30	137.76	5.30	4.24	23.74
10.13	540.47	112.42	4.32	3.46	19.37	11.13	662.82	137.87	5.30	4.24	23.76
10.14	541.80	112.69	4.33	3.47	19.42	11.14	663.33	137.97	5.31	4.25	23.77
10.15	543.13	112.97	4.35	3.48	19.47	11.15	663.84	138.08	5.31	4.25	23.79
10.16	544.46	113.25	4.36	3.48	19.51	11.16	664.35	138.19	5.31	4.25	23.81
10.17	545.79	113.52	4.37	3.49	19.56	11.17	664.86	138.29	5.32	4.26	23.83
10.18	547.12	113.80	4.38	3.50	19.61	11.18	665.38	138.40	5.32	4.26	23.85

10.19	548.45	114.08	4.39	3.51	19.66	11.19	665.89	138.50	5.33	4.26	23.87
10.2	549.78	114.35	4.40	3.52	19.70	11.2	666.40	138.61	5.33	4.26	23.88
10.21	551.11	114.63	4.41	3.53	19.75	11.21	666.91	138.72	5.34	4.27	23.90
10.22	552.44	114.91	4.42	3.54	19.80	11.22	667.42	138.82	5.34	4.27	23.92
10.23	553.77	115.18	4.43	3.54	19.85	11.23	667.94	138.93	5.34	4.27	23.94
10.24	555.10	115.46	4.44	3.55	19.89	11.24	668.45	139.04	5.35	4.28	23.96
10.25	556.43	115.74	4.45	3.56	19.94	11.25	668.96	139.14	5.35	4.28	23.98
10.26	557.75	116.01	4.46	3.57	19.99	11.26	669.47	139.25	5.36	4.28	23.99
10.27	559.08	116.29	4.47	3.58	20.04	11.27	669.98	139.36	5.36	4.29	24.01
10.28	560.41	116.57	4.48	3.59	20.09	11.28	670.50	139.46	5.36	4.29	24.03
10.29	561.74	116.84	4.49	3.60	20.13	11.29	671.01	139.57	5.37	4.29	24.05
10.3	563.07	117.12	4.50	3.60	20.18	11.3	671.52	139.68	5.37	4.30	24.07
10.31	564.40	117.40	4.52	3.61	20.23	11.31	672.03	139.78	5.38	4.30	24.09
10.32	565.73	117.67	4.53	3.62	20.28	11.32	672.54	139.89	5.38	4.30	24.10
10.33	567.06	117.95	4.54	3.63	20.32	11.33	673.06	140.00	5.38	4.31	24.12
10.34	568.39	118.23	4.55	3.64	20.37	11.34	673.57	140.10	5.39	4.31	24.14
10.35	569.72	118.50	4.56	3.65	20.42	11.35	674.08	140.21	5.39	4.31	24.16
10.36	571.05	118.78	4.57	3.65	20.47	11.36	674.59	140.32	5.40	4.32	24.18
10.37	572.38	119.06	4.58	3.66	20.51	11.37	675.10	140.42	5.40	4.32	24.20
10.38	573.71	119.33	4.59	3.67	20.56	11.38	675.62	140.53	5.40	4.32	24.21
10.39	575.04	119.61	4.60	3.68	20.61	11.39	676.13	140.63	5.41	4.33	24.23
10.4	576.37	119.89	4.61	3.69	20.66	11.4	676.64	140.74	5.41	4.33	24.25
10.41	577.70	120.16	4.62	3.70	20.70	11.41	677.15	140.85	5.42	4.33	24.27
10.42	579.03	120.44	4.63	3.71	20.75	11.42	677.66	140.95	5.42	4.34	24.29
10.43	580.36	120.72	4.64	3.71	20.80	11.43	678.18	141.06	5.43	4.34	24.31
10.44	581.69	120.99	4.65	3.72	20.85	11.44	678.69	141.17	5.43	4.34	24.32
10.45	583.02	121.27	4.66	3.73	20.90	11.45	679.20	141.27	5.43	4.35	24.34
10.46	584.35	121.54	4.67	3.74	20.94	11.46	679.71	141.38	5.44	4.35	24.36
10.47	585.68	121.82	4.69	3.75	20.99	11.47	680.22	141.49	5.44	4.35	24.38
10.48	587.01	122.10	4.70	3.76	21.04	11.48	680.74	141.59	5.45	4.36	24.40
10.49	588.34	122.37	4.71	3.77	21.09	11.49	681.25	141.70	5.45	4.36	24.42
10.5	589.67	122.65	4.72	3.77	21.13	11.5	681.76	141.81	5.45	4.36	24.43
10.51	591.00	122.93	4.73	3.78	21.18	11.51	682.27	141.91	5.46	4.37	24.45
10.52	592.33	123.20	4.74	3.79	21.23	11.52	682.78	142.02	5.46	4.37	24.47
10.53	593.66	123.48	4.75	3.80	21.28	11.53	683.30	142.13	5.47	4.37	24.49
10.54	594.99	123.76	4.76	3.81	21.32	11.54	683.81	142.23	5.47	4.38	24.51
10.55	596.32	124.03	4.77	3.82	21.37	11.55	684.32	142.34	5.47	4.38	24.53
10.56	597.65	124.31	4.78	3.82	21.42	11.56	684.83	142.45	5.48	4.38	24.54
10.57	598.98	124.59	4.79	3.83	21.47	11.57	685.34	142.55	5.48	4.39	24.56
10.58	600.31	124.86	4.80	3.84	21.52	11.58	685.86	142.66	5.49	4.39	24.58
10.59	601.64	125.14	4.81	3.85	21.56	11.59	686.37	142.76	5.49	4.39	24.60

APPENDIX E-3 PARAMETERS OF TRANSIENT ANALYSIS FROM 12-13PM IN WINTER

12		Gp	Gg1	Gg2	Gfloor	13		Gp	Gg1	Gg2	Gfloor
12.00	**707.36**	Gp	Gg1	Gg2	Gfloor	13.00	**678.58**	Gp	Gg1	Gg2	Gfloor
12.01	707.07	147.07	5.66	4.53	25.34	13.01	677.48	140.92	5.42	4.34	24.28
12.02	706.78	147.01	5.65	4.52	25.33	13.02	676.39	140.69	5.41	4.33	24.24
12.03	706.50	146.95	5.65	4.52	25.32	13.03	675.29	140.46	5.40	4.32	24.20
12.04	706.21	146.89	5.65	4.52	25.31	13.04	674.20	140.23	5.39	4.31	24.16
12.05	705.92	146.83	5.65	4.52	25.30	13.05	673.10	140.00	5.38	4.31	24.12
12.06	705.63	146.77	5.65	4.52	25.29	13.06	672.00	139.78	5.38	4.30	24.08
12.07	705.35	146.71	5.64	4.51	25.28	13.07	670.91	139.55	5.37	4.29	24.05
12.08	705.06	146.65	5.64	4.51	25.27	13.08	669.81	139.32	5.36	4.29	24.01
12.09	704.77	146.59	5.64	4.51	25.26	13.09	668.72	139.09	5.35	4.28	23.97
12.1	704.48	146.53	5.64	4.51	25.25	13.1	667.62	138.87	5.34	4.27	23.93
12.11	704.19	146.47	5.63	4.51	25.24	13.11	666.53	138.64	5.33	4.27	23.89
12.12	703.91	146.41	5.63	4.51	25.23	13.12	665.43	138.41	5.32	4.26	23.85
12.13	703.62	146.35	5.63	4.50	25.22	13.13	664.33	138.18	5.31	4.25	23.81
12.14	703.33	146.29	5.63	4.50	25.21	13.14	663.24	137.95	5.31	4.24	23.77
12.15	703.04	146.23	5.62	4.50	25.20	13.15	662.14	137.73	5.30	4.24	23.73
12.16	702.76	146.17	5.62	4.50	25.19	13.16	661.05	137.50	5.29	4.23	23.69
12.17	702.47	146.11	5.62	4.50	25.18	13.17	659.95	137.27	5.28	4.22	23.65
12.18	702.18	146.05	5.62	4.49	25.17	13.18	658.85	137.04	5.27	4.22	23.61
12.19	701.89	145.99	5.62	4.49	25.16	13.19	657.76	136.81	5.26	4.21	23.57
12.2	701.60	145.93	5.61	4.49	25.15	13.2	656.66	136.59	5.25	4.20	23.53
12.21	701.32	145.87	5.61	4.49	25.14	13.21	655.57	136.36	5.24	4.20	23.50
12.22	701.03	145.81	5.61	4.49	25.12	13.22	654.47	136.13	5.24	4.19	23.46
12.23	700.74	145.75	5.61	4.48	25.11	13.23	653.37	135.90	5.23	4.18	23.42
12.24	700.45	145.69	5.60	4.48	25.10	13.24	652.28	135.67	5.22	4.17	23.38
12.25	700.17	145.63	5.60	4.48	25.09	13.25	651.18	135.45	5.21	4.17	23.34
12.26	699.88	145.57	5.60	4.48	25.08	13.26	650.09	135.22	5.20	4.16	23.30
12.27	699.59	145.51	5.60	4.48	25.07	13.27	648.99	134.99	5.19	4.15	23.26
12.28	699.30	145.45	5.59	4.48	25.06	13.28	647.89	134.76	5.18	4.15	23.22
12.29	699.01	145.39	5.59	4.47	25.05	13.29	646.80	134.53	5.17	4.14	23.18
12.3	698.73	145.34	5.59	4.47	25.04	13.3	645.70	134.31	5.17	4.13	23.14
12.31	698.44	145.28	5.59	4.47	25.03	13.31	644.61	134.08	5.16	4.13	23.10
12.32	698.15	145.22	5.59	4.47	25.02	13.32	643.51	133.85	5.15	4.12	23.06
12.33	697.86	145.16	5.58	4.47	25.01	13.33	642.42	133.62	5.14	4.11	23.02
12.34	697.57	145.10	5.58	4.46	25.00	13.34	641.32	133.39	5.13	4.10	22.98
12.35	697.29	145.04	5.58	4.46	24.99	13.35	640.22	133.17	5.12	4.10	22.95
12.36	697.00	144.98	5.58	4.46	24.98	13.36	639.13	132.94	5.11	4.09	22.91
12.37	696.71	144.92	5.57	4.46	24.97	13.37	638.03	132.71	5.10	4.08	22.87
12.38	696.42	144.86	5.57	4.46	24.96	13.38	636.94	132.48	5.10	4.08	22.83
12.39	696.14	144.80	5.57	4.46	24.95	13.39	635.84	132.25	5.09	4.07	22.79
12.4	695.85	144.74	5.57	4.45	24.94	13.4	634.74	132.03	5.08	4.06	22.75
12.41	695.56	144.68	5.56	4.45	24.93	13.41	633.65	131.80	5.07	4.06	22.71
12.42	695.27	144.62	5.56	4.45	24.92	13.42	632.55	131.57	5.06	4.05	22.67

12.43	694.98	144.56	5.56	4.45	24.91	13.43	631.46	131.34	5.05	4.04	22.63
12.44	694.70	144.50	5.56	4.45	24.90	13.44	630.36	131.11	5.04	4.03	22.59
12.45	694.41	144.44	5.56	4.44	24.89	13.45	629.26	130.89	5.03	4.03	22.55
12.46	694.12	144.38	5.55	4.44	24.88	13.46	628.17	130.66	5.03	4.02	22.51
12.47	693.83	144.32	5.55	4.44	24.87	13.47	627.07	130.43	5.02	4.01	22.47
12.48	693.55	144.26	5.55	4.44	24.86	13.48	625.98	130.20	5.01	4.01	22.44
12.49	693.26	144.20	5.55	4.44	24.85	13.49	624.88	129.98	5.00	4.00	22.40
12.5	692.97	144.14	5.54	4.44	24.84	13.5	623.79	129.75	4.99	3.99	22.36
12.51	692.68	144.08	5.54	4.43	24.83	13.51	622.69	129.52	4.98	3.99	22.32
12.52	692.39	144.02	5.54	4.43	24.82	13.52	621.59	129.29	4.97	3.98	22.28
12.53	692.11	143.96	5.54	4.43	24.81	13.53	620.50	129.06	4.96	3.97	22.24
12.54	691.82	143.90	5.53	4.43	24.79	13.54	619.40	128.84	4.96	3.96	22.20
12.55	691.53	143.84	5.53	4.43	24.78	13.55	618.31	128.61	4.95	3.96	22.16
12.56	691.24	143.78	5.53	4.42	24.77	13.56	617.21	128.38	4.94	3.95	22.12
12.57	690.96	143.72	5.53	4.42	24.76	13.57	616.11	128.15	4.93	3.94	22.08
12.58	690.67	143.66	5.53	4.42	24.75	13.58	615.02	127.92	4.92	3.94	22.04
12.59	690.38	143.60	5.52	4.42	24.74	13.59	613.92	127.70	4.91	3.93	22.00

APPENDIX E-4 PARAMETERS OF TRANSIENT ANALYSIS FROM 14-15PM IN WINTER

14		**Gp**	**Gg1**	**Gg2**	**Gfloor**	**15**		**Gp**	**Gg1**	**Gg2**	**Gfloor**
14.00	**568.99**	Gp	Gg1	Gg2	Gfloor	15.00	**372.94**	Gp	Gg1	Gg2	Gfloor
14.01	567.03	117.94	4.54	3.63	20.32	15.01	369.46	76.85	2.96	2.36	13.24
14.02	565.07	117.53	4.52	3.62	20.25	15.02	365.97	76.12	2.93	2.34	13.12
14.03	563.11	117.13	4.50	3.60	20.18	15.03	362.49	75.40	2.90	2.32	12.99
14.04	561.15	116.72	4.49	3.59	20.11	15.04	359.00	74.67	2.87	2.30	12.87
14.05	559.19	116.31	4.47	3.58	20.04	15.05	355.52	73.95	2.84	2.28	12.74
14.06	557.23	115.90	4.46	3.57	19.97	15.06	352.03	73.22	2.82	2.25	12.62
14.07	555.27	115.50	4.44	3.55	19.90	15.07	348.55	72.50	2.79	2.23	12.49
14.08	553.31	115.09	4.43	3.54	19.83	15.08	345.07	71.77	2.76	2.21	12.37
14.09	551.35	114.68	4.41	3.53	19.76	15.09	341.58	71.05	2.73	2.19	12.24
14.1	549.39	114.27	4.40	3.52	19.69	15.1	338.10	70.32	2.70	2.16	12.12
14.11	547.42	113.86	4.38	3.50	19.62	15.11	334.61	69.60	2.68	2.14	11.99
14.12	545.46	113.46	4.36	3.49	19.55	15.12	331.13	68.87	2.65	2.12	11.87
14.13	543.50	113.05	4.35	3.48	19.48	15.13	327.65	68.15	2.62	2.10	11.74
14.14	541.54	112.64	4.33	3.47	19.41	15.14	324.16	67.43	2.59	2.07	11.62
14.15	539.58	112.23	4.32	3.45	19.34	15.15	320.68	66.70	2.57	2.05	11.49
14.16	537.62	111.83	4.30	3.44	19.27	15.16	317.19	65.98	2.54	2.03	11.37
14.17	535.66	111.42	4.29	3.43	19.20	15.17	313.71	65.25	2.51	2.01	11.24
14.18	533.70	111.01	4.27	3.42	19.13	15.18	310.22	64.53	2.48	1.99	11.12
14.19	531.74	110.60	4.25	3.40	19.06	15.19	306.74	63.80	2.45	1.96	10.99
14.2	529.78	110.19	4.24	3.39	18.99	15.2	303.26	63.08	2.43	1.94	10.87
14.21	527.82	109.79	4.22	3.38	18.92	15.21	299.77	62.35	2.40	1.92	10.74
14.22	525.86	109.38	4.21	3.37	18.85	15.22	296.29	61.63	2.37	1.90	10.62
14.23	523.90	108.97	4.19	3.35	18.78	15.23	292.80	60.90	2.34	1.87	10.49

14.24	521.94	108.56	4.18	3.34	18.71	15.24	289.32	60.18	2.31	1.85	10.37
14.25	519.98	108.16	4.16	3.33	18.64	15.25	285.84	59.45	2.29	1.83	10.24
14.26	518.02	107.75	4.14	3.32	18.57	15.26	282.35	58.73	2.26	1.81	10.12
14.27	516.06	107.34	4.13	3.30	18.50	15.27	278.87	58.00	2.23	1.78	9.99
14.28	514.10	106.93	4.11	3.29	18.43	15.28	275.38	57.28	2.20	1.76	9.87
14.29	512.14	106.52	4.10	3.28	18.35	15.29	271.90	56.55	2.18	1.74	9.74
14.3	510.18	106.12	4.08	3.27	18.28	15.3	268.41	55.83	2.15	1.72	9.62
14.31	508.21	105.71	4.07	3.25	18.21	15.31	264.93	55.11	2.12	1.70	9.50
14.32	506.25	105.30	4.05	3.24	18.14	15.32	261.45	54.38	2.09	1.67	9.37
14.33	504.29	104.89	4.03	3.23	18.07	15.33	257.96	53.66	2.06	1.65	9.25
14.34	502.33	104.49	4.02	3.21	18.00	15.34	254.48	52.93	2.04	1.63	9.12
14.35	500.37	104.08	4.00	3.20	17.93	15.35	250.99	52.21	2.01	1.61	9.00
14.36	498.41	103.67	3.99	3.19	17.86	15.36	247.51	51.48	1.98	1.58	8.87
14.37	496.45	103.26	3.97	3.18	17.79	15.37	244.02	50.76	1.95	1.56	8.75
14.38	494.49	102.85	3.96	3.16	17.72	15.38	240.54	50.03	1.92	1.54	8.62
14.39	492.53	102.45	3.94	3.15	17.65	15.39	237.06	49.31	1.90	1.52	8.50
14.4	490.57	102.04	3.92	3.14	17.58	15.4	233.57	48.58	1.87	1.49	8.37
14.41	488.61	101.63	3.91	3.13	17.51	15.41	230.09	47.86	1.84	1.47	8.25
14.42	486.65	101.22	3.89	3.11	17.44	15.42	226.60	47.13	1.81	1.45	8.12
14.43	484.69	100.82	3.88	3.10	17.37	15.43	223.12	46.41	1.78	1.43	8.00
14.44	482.73	100.41	3.86	3.09	17.30	15.44	219.64	45.68	1.76	1.41	7.87
14.45	480.77	100.00	3.85	3.08	17.23	15.45	216.15	44.96	1.73	1.38	7.75
14.46	478.81	99.59	3.83	3.06	17.16	15.46	212.67	44.23	1.70	1.36	7.62
14.47	476.85	99.18	3.81	3.05	17.09	15.47	209.18	43.51	1.67	1.34	7.50
14.48	474.89	98.78	3.80	3.04	17.02	15.48	205.70	42.79	1.65	1.32	7.37
14.49	472.93	98.37	3.78	3.03	16.95	15.49	202.21	42.06	1.62	1.29	7.25
14.5	470.97	97.96	3.77	3.01	16.88	15.5	198.73	41.34	1.59	1.27	7.12
14.51	469.00	97.55	3.75	3.00	16.81	15.51	195.25	40.61	1.56	1.25	7.00
14.52	467.04	97.15	3.74	2.99	16.74	15.52	191.76	39.89	1.53	1.23	6.87
14.53	465.08	96.74	3.72	2.98	16.67	15.53	188.28	39.16	1.51	1.20	6.75
14.54	463.12	96.33	3.70	2.96	16.60	15.54	184.79	38.44	1.48	1.18	6.62
14.55	461.16	95.92	3.69	2.95	16.53	15.55	181.31	37.71	1.45	1.16	6.50
14.56	459.20	95.51	3.67	2.94	16.46	15.56	177.82	36.99	1.42	1.14	6.37
14.57	457.24	95.11	3.66	2.93	16.39	15.57	174.34	36.26	1.39	1.12	6.25
14.58	455.28	94.70	3.64	2.91	16.32	15.58	170.86	35.54	1.37	1.09	6.12
14.59	453.32	94.29	3.63	2.90	16.25	15.59	167.37	34.81	1.34	1.07	6.00

APPENDIX E-5 PARAMETERS OF TRANSIENT ANALYSIS FROM 16PM-17PM IN WINTER

16		Gp	Gg1	Gg2	Gfloor
16.00	**24.52**	Gp	Gg1	Gg2	Gfloor
16.01	24.27	5.05	0.19	0.16	0.87
16.02	24.03	5.00	0.19	0.15	0.86
16.03	23.78	4.95	0.19	0.15	0.85
16.04	23.54	4.90	0.19	0.15	0.84
16.05	23.29	4.85	0.19	0.15	0.83
16.06	23.05	4.79	0.18	0.15	0.83
16.07	22.80	4.74	0.18	0.15	0.82
16.08	22.56	4.69	0.18	0.14	0.81
16.09	22.31	4.64	0.18	0.14	0.80
16.1	22.07	4.59	0.18	0.14	0.79
16.11	21.82	4.54	0.17	0.14	0.78
16.12	21.58	4.49	0.17	0.14	0.77
16.13	21.33	4.44	0.17	0.14	0.76
16.14	21.09	4.39	0.17	0.13	0.76
16.15	20.84	4.34	0.17	0.13	0.75
16.16	20.60	4.28	0.16	0.13	0.74
16.17	20.35	4.23	0.16	0.13	0.73
16.18	20.11	4.18	0.16	0.13	0.72
16.19	19.86	4.13	0.16	0.13	0.71
16.2	19.62	4.08	0.16	0.13	0.70
16.21	19.37	4.03	0.15	0.12	0.69
16.22	19.13	3.98	0.15	0.12	0.69
16.23	18.88	3.93	0.15	0.12	0.68
16.24	18.64	3.88	0.15	0.12	0.67
16.25	18.39	3.83	0.15	0.12	0.66
16.26	18.14	3.77	0.15	0.12	0.65
16.27	17.90	3.72	0.14	0.11	0.64
16.28	17.65	3.67	0.14	0.11	0.63
16.29	17.41	3.62	0.14	0.11	0.62
16.3	17.16	3.57	0.14	0.11	0.62
16.31	16.92	3.52	0.14	0.11	0.61
16.32	16.67	3.47	0.13	0.11	0.60
16.33	16.43	3.42	0.13	0.11	0.59
16.34	16.18	3.37	0.13	0.10	0.58
16.35	15.94	3.32	0.13	0.10	0.57
16.36	15.69	3.26	0.13	0.10	0.56
16.37	15.45	3.21	0.12	0.10	0.55
16.38	15.20	3.16	0.12	0.10	0.54
16.39	14.96	3.11	0.12	0.10	0.54
16.4	14.71	3.06	0.12	0.09	0.53
16.41	14.47	3.01	0.12	0.09	0.52
16.42	14.22	2.96	0.11	0.09	0.51

16.43	13.98	2.91	0.11	0.09	0.50
16.44	13.73	2.86	0.11	0.09	0.49
16.45	13.49	2.81	0.11	0.09	0.48
16.46	13.24	2.75	0.11	0.08	0.47
16.47	13.00	2.70	0.10	0.08	0.47
16.48	12.75	2.65	0.10	0.08	0.46
16.49	12.51	2.60	0.10	0.08	0.45
16.5	12.26	2.55	0.10	0.08	0.44
16.51	12.01	2.50	0.10	0.08	0.43
16.52	11.77	2.45	0.09	0.08	0.42
16.53	11.52	2.40	0.09	0.07	0.41
16.54	11.28	2.35	0.09	0.07	0.40
16.55	11.03	2.30	0.09	0.07	0.40
16.56	10.79	2.24	0.09	0.07	0.39
16.57	10.54	2.19	0.08	0.07	0.38
16.58	10.30	2.14	0.08	0.07	0.37
16.59	10.05	2.09	0.08	0.06	0.36

APPENDIX E-6 PARAMETERS OF TRANSIENT ANALYSIS FROM 5-6AM IN SUMMER

5		Gp	Gg1	Gg2	Gfloor	6		Gp	Gg1	Gg2	Gfloor
5.00	**62.16**	13.92	0.37	0.30	1.67	6.00	**91.52**	20.50	0.55	0.44	2.46
5.01	62.45	13.99	0.37	0.30	1.68	6.01	91.68	20.54	0.55	0.44	2.46
5.02	62.75	14.06	0.38	0.30	1.69	6.02	91.84	20.57	0.55	0.44	2.47
5.03	63.04	14.12	0.38	0.30	1.69	6.03	92.00	20.61	0.55	0.44	2.47
5.04	63.33	14.19	0.38	0.30	1.70	6.04	92.16	20.64	0.55	0.44	2.48
5.05	63.63	14.25	0.38	0.31	1.71	6.05	92.32	20.68	0.55	0.44	2.48
5.06	63.92	14.32	0.38	0.31	1.72	6.06	92.48	20.72	0.55	0.44	2.49
5.07	64.22	14.38	0.39	0.31	1.73	6.07	92.64	20.75	0.56	0.44	2.49
5.08	64.51	14.45	0.39	0.31	1.73	6.08	92.80	20.79	0.56	0.45	2.49
5.09	64.80	14.52	0.39	0.31	1.74	6.09	92.96	20.82	0.56	0.45	2.50
5.1	65.10	14.58	0.39	0.31	1.75	6.1	93.12	20.86	0.56	0.45	2.50
5.11	65.39	14.65	0.39	0.31	1.76	6.11	93.28	20.89	0.56	0.45	2.51
5.12	65.68	14.71	0.39	0.32	1.77	6.12	93.44	20.93	0.56	0.45	2.51
5.13	65.98	14.78	0.40	0.32	1.77	6.13	93.60	20.97	0.56	0.45	2.52
5.14	66.27	14.84	0.40	0.32	1.78	6.14	93.76	21.00	0.56	0.45	2.52
5.15	66.56	14.91	0.40	0.32	1.79	6.15	93.92	21.04	0.56	0.45	2.52
5.16	66.86	14.98	0.40	0.32	1.80	6.16	94.08	21.07	0.56	0.45	2.53
5.17	67.15	15.04	0.40	0.32	1.81	6.17	94.24	21.11	0.57	0.45	2.53
5.18	67.44	15.11	0.40	0.32	1.81	6.18	94.40	21.15	0.57	0.45	2.54
5.19	67.74	15.17	0.41	0.33	1.82	6.19	94.56	21.18	0.57	0.45	2.54
5.2	68.03	15.24	0.41	0.33	1.83	6.2	94.72	21.22	0.57	0.45	2.55
5.21	68.33	15.30	0.41	0.33	1.84	6.21	94.88	21.25	0.57	0.46	2.55
5.22	68.62	15.37	0.41	0.33	1.84	6.22	95.04	21.29	0.57	0.46	2.55
5.23	68.91	15.44	0.41	0.33	1.85	6.23	95.20	21.33	0.57	0.46	2.56
5.24	69.21	15.50	0.42	0.33	1.86	6.24	95.36	21.36	0.57	0.46	2.56

5.25	69.50	15.57	0.42	0.33	1.87	6.25	95.52	21.40	0.57	0.46	2.57
5.26	69.79	15.63	0.42	0.34	1.88	6.26	95.68	21.43	0.57	0.46	2.57
5.27	70.09	15.70	0.42	0.34	1.88	6.27	95.84	21.47	0.58	0.46	2.58
5.28	70.38	15.77	0.42	0.34	1.89	6.28	96.00	21.50	0.58	0.46	2.58
5.29	70.67	15.83	0.42	0.34	1.90	6.29	96.16	21.54	0.58	0.46	2.58
5.3	70.97	15.90	0.43	0.34	1.91	6.3	96.32	21.58	0.58	0.46	2.59
5.31	71.26	15.96	0.43	0.34	1.92	6.31	96.48	21.61	0.58	0.46	2.59
5.32	71.56	16.03	0.43	0.34	1.92	6.32	96.64	21.65	0.58	0.46	2.60
5.33	71.85	16.09	0.43	0.34	1.93	6.33	96.80	21.68	0.58	0.46	2.60
5.34	72.14	16.16	0.43	0.35	1.94	6.34	96.96	21.72	0.58	0.47	2.61
5.35	72.44	16.23	0.43	0.35	1.95	6.35	97.12	21.76	0.58	0.47	2.61
5.36	72.73	16.29	0.44	0.35	1.95	6.36	97.28	21.79	0.58	0.47	2.61
5.37	73.02	16.36	0.44	0.35	1.96	6.37	97.44	21.83	0.58	0.47	2.62
5.38	73.32	16.42	0.44	0.35	1.97	6.38	97.60	21.86	0.59	0.47	2.62
5.39	73.61	16.49	0.44	0.35	1.98	6.39	97.76	21.90	0.59	0.47	2.63
5.4	73.90	16.55	0.44	0.35	1.99	6.4	97.92	21.93	0.59	0.47	2.63
5.41	74.20	16.62	0.45	0.36	1.99	6.41	98.08	21.97	0.59	0.47	2.64
5.42	74.49	16.69	0.45	0.36	2.00	6.42	98.24	22.01	0.59	0.47	2.64
5.43	74.78	16.75	0.45	0.36	2.01	6.43	98.40	22.04	0.59	0.47	2.65
5.44	75.08	16.82	0.45	0.36	2.02	6.44	98.56	22.08	0.59	0.47	2.65
5.45	75.37	16.88	0.45	0.36	2.03	6.45	98.72	22.11	0.59	0.47	2.65
5.46	75.67	16.95	0.45	0.36	2.03	6.46	98.88	22.15	0.59	0.47	2.66
5.47	75.96	17.01	0.46	0.36	2.04	6.47	99.04	22.19	0.59	0.48	2.66
5.48	76.25	17.08	0.46	0.37	2.05	6.48	99.20	22.22	0.60	0.48	2.67
5.49	76.55	17.15	0.46	0.37	2.06	6.49	99.36	22.26	0.60	0.48	2.67
5.5	76.84	17.21	0.46	0.37	2.07	6.5	99.52	22.29	0.60	0.48	2.68
5.51	77.13	17.28	0.46	0.37	2.07	6.51	99.69	22.33	0.60	0.48	2.68
5.52	77.43	17.34	0.46	0.37	2.08	6.52	99.85	22.37	0.60	0.48	2.68
5.53	77.72	17.41	0.47	0.37	2.09	6.53	100.01	22.40	0.60	0.48	2.69
5.54	78.01	17.48	0.47	0.37	2.10	6.54	100.17	22.44	0.60	0.48	2.69
5.55	78.31	17.54	0.47	0.38	2.10	6.55	100.33	22.47	0.60	0.48	2.70
5.56	78.60	17.61	0.47	0.38	2.11	6.56	100.49	22.51	0.60	0.48	2.70
5.57	78.90	17.67	0.47	0.38	2.12	6.57	100.65	22.54	0.60	0.48	2.71
5.58	79.19	17.74	0.48	0.38	2.13	6.58	100.81	22.58	0.60	0.48	2.71
5.59	79.48	17.80	0.48	0.38	2.14	6.59	100.97	22.62	0.61	0.48	2.71

APPENDIX E-7 PARAMETERS OF TRANSIENT ANALYSIS FROM 7-8AM IN SUMMER

7		Gp	Gg1	Gg2	Gfloor	8		Gp	Gg1	Gg2	Gfloor
7.00	**107.53**	24.09	0.65	0.52	2.89	8.00	**210.21**	47.09	1.26	1.01	5.65
7.01	108.56	24.32	0.65	0.52	2.92	8.01	211.53	47.38	1.27	1.02	5.69
7.02	109.58	24.55	0.66	0.53	2.95	8.02	212.85	47.68	1.28	1.02	5.72
7.03	110.61	24.78	0.66	0.53	2.97	8.03	214.17	47.97	1.29	1.03	5.76
7.04	111.64	25.01	0.67	0.54	3.00	8.04	215.49	48.27	1.29	1.03	5.79
7.05	112.66	25.24	0.68	0.54	3.03	8.05	216.82	48.57	1.30	1.04	5.83
7.06	113.69	25.47	0.68	0.55	3.06	8.06	218.14	48.86	1.31	1.05	5.86
7.07	114.72	25.70	0.69	0.55	3.08	8.07	219.46	49.16	1.32	1.05	5.90
7.08	115.74	25.93	0.69	0.56	3.11	8.08	220.78	49.45	1.32	1.06	5.93
7.09	116.77	26.16	0.70	0.56	3.14	8.09	222.10	49.75	1.33	1.07	5.97
7.1	117.80	26.39	0.71	0.57	3.17	8.1	223.42	50.05	1.34	1.07	6.01
7.11	118.82	26.62	0.71	0.57	3.19	8.11	224.74	50.34	1.35	1.08	6.04
7.12	119.85	26.85	0.72	0.58	3.22	8.12	226.06	50.64	1.36	1.09	6.08
7.13	120.88	27.08	0.73	0.58	3.25	8.13	227.38	50.93	1.36	1.09	6.11
7.14	121.91	27.31	0.73	0.59	3.28	8.14	228.71	51.23	1.37	1.10	6.15
7.15	122.93	27.54	0.74	0.59	3.30	8.15	230.03	51.53	1.38	1.10	6.18
7.16	123.96	27.77	0.74	0.60	3.33	8.16	231.35	51.82	1.39	1.11	6.22
7.17	124.99	28.00	0.75	0.60	3.36	8.17	232.67	52.12	1.40	1.12	6.25
7.18	126.01	28.23	0.76	0.60	3.39	8.18	233.99	52.41	1.40	1.12	6.29
7.19	127.04	28.46	0.76	0.61	3.41	8.19	235.31	52.71	1.41	1.13	6.33
7.2	128.07	28.69	0.77	0.61	3.44	8.2	236.63	53.01	1.42	1.14	6.36
7.21	129.09	28.92	0.77	0.62	3.47	8.21	237.95	53.30	1.43	1.14	6.40
7.22	130.12	29.15	0.78	0.62	3.50	8.22	239.27	53.60	1.44	1.15	6.43
7.23	131.15	29.38	0.79	0.63	3.53	8.23	240.60	53.89	1.44	1.15	6.47
7.24	132.17	29.61	0.79	0.63	3.55	8.24	241.92	54.19	1.45	1.16	6.50
7.25	133.20	29.84	0.80	0.64	3.58	8.25	243.24	54.49	1.46	1.17	6.54
7.26	134.23	30.07	0.81	0.64	3.61	8.26	244.56	54.78	1.47	1.17	6.57
7.27	135.25	30.30	0.81	0.65	3.64	8.27	245.88	55.08	1.48	1.18	6.61
7.28	136.28	30.53	0.82	0.65	3.66	8.28	247.20	55.37	1.48	1.19	6.64
7.29	137.31	30.76	0.82	0.66	3.69	8.29	248.52	55.67	1.49	1.19	6.68
7.3	138.33	30.99	0.83	0.66	3.72	8.3	249.84	55.96	1.50	1.20	6.72
7.31	139.36	31.22	0.84	0.67	3.75	8.31	251.16	56.26	1.51	1.21	6.75
7.32	140.39	31.45	0.84	0.67	3.77	8.32	252.49	56.56	1.51	1.21	6.79
7.33	141.41	31.68	0.85	0.68	3.80	8.33	253.81	56.85	1.52	1.22	6.82
7.34	142.44	31.91	0.85	0.68	3.83	8.34	255.13	57.15	1.53	1.22	6.86
7.35	143.47	32.14	0.86	0.69	3.86	8.35	256.45	57.44	1.54	1.23	6.89
7.36	144.49	32.37	0.87	0.69	3.88	8.36	257.77	57.74	1.55	1.24	6.93
7.37	145.52	32.60	0.87	0.70	3.91	8.37	259.09	58.04	1.55	1.24	6.96
7.38	146.55	32.83	0.88	0.70	3.94	8.38	260.41	58.33	1.56	1.25	7.00
7.39	147.58	33.06	0.89	0.71	3.97	8.39	261.73	58.63	1.57	1.26	7.04
7.4	148.60	33.29	0.89	0.71	3.99	8.4	263.05	58.92	1.58	1.26	7.07
7.41	149.63	33.52	0.90	0.72	4.02	8.41	264.38	59.22	1.59	1.27	7.11
7.42	150.66	33.75	0.90	0.72	4.05	8.42	265.70	59.52	1.59	1.28	7.14

7.43	151.68	33.98	0.91	0.73	4.08	8.43	267.02	59.81	1.60	1.28	7.18
7.44	152.71	34.21	0.92	0.73	4.10	8.44	268.34	60.11	1.61	1.29	7.21
7.45	153.74	34.44	0.92	0.74	4.13	8.45	269.66	60.40	1.62	1.29	7.25
7.46	154.76	34.67	0.93	0.74	4.16	8.46	270.98	60.70	1.63	1.30	7.28
7.47	155.79	34.90	0.93	0.75	4.19	8.47	272.30	61.00	1.63	1.31	7.32
7.48	156.82	35.13	0.94	0.75	4.22	8.48	273.62	61.29	1.64	1.31	7.35
7.49	157.84	35.36	0.95	0.76	4.24	8.49	274.94	61.59	1.65	1.32	7.39
7.5	158.87	35.59	0.95	0.76	4.27	8.5	276.26	61.88	1.66	1.33	7.43
7.51	159.90	35.82	0.96	0.77	4.30	8.51	277.59	62.18	1.67	1.33	7.46
7.52	160.92	36.05	0.97	0.77	4.33	8.52	278.91	62.48	1.67	1.34	7.50
7.53	161.95	36.28	0.97	0.78	4.35	8.53	280.23	62.77	1.68	1.35	7.53
7.54	162.98	36.51	0.98	0.78	4.38	8.54	281.55	63.07	1.69	1.35	7.57
7.55	164.00	36.74	0.98	0.79	4.41	8.55	282.87	63.36	1.70	1.36	7.60
7.56	165.03	36.97	0.99	0.79	4.44	8.56	284.19	63.66	1.71	1.36	7.64
7.57	166.06	37.20	1.00	0.80	4.46	8.57	285.51	63.95	1.71	1.37	7.67
7.58	167.08	37.43	1.00	0.80	4.49	8.58	286.83	64.25	1.72	1.38	7.71
7.59	168.11	37.66	1.01	0.81	4.52	8.59	288.15	64.55	1.73	1.38	7.75

APPENDIX E-8 PARAMETERS OF TRANSIENT ANALYSIS FROM 9-10AM IN SUMMER

9		Gp	Gg1	Gg2	Gfloor	10		Gp	Gg1	Gg2	Gfloor
9.00	**342.32**	76.68	2.05	1.64	9.20	10.00	**448.98**	100.57	2.69	2.16	12.07
9.01	343.39	76.92	2.06	1.65	9.23	10.01	449.66	100.72	2.70	2.16	12.09
9.02	344.45	77.16	2.07	1.65	9.26	10.02	450.34	100.88	2.70	2.16	12.11
9.03	345.52	77.40	2.07	1.66	9.29	10.03	451.02	101.03	2.71	2.16	12.12
9.04	346.59	77.64	2.08	1.66	9.32	10.04	451.70	101.18	2.71	2.17	12.14
9.05	347.65	77.87	2.09	1.67	9.34	10.05	452.38	101.33	2.71	2.17	12.16
9.06	348.72	78.11	2.09	1.67	9.37	10.06	453.06	101.49	2.72	2.17	12.18
9.07	349.79	78.35	2.10	1.68	9.40	10.07	453.74	101.64	2.72	2.18	12.20
9.08	350.85	78.59	2.11	1.68	9.43	10.08	454.42	101.79	2.73	2.18	12.21
9.09	351.92	78.83	2.11	1.69	9.46	10.09	455.10	101.94	2.73	2.18	12.23
9.1	352.99	79.07	2.12	1.69	9.49	10.1	455.78	102.09	2.73	2.19	12.25
9.11	354.05	79.31	2.12	1.70	9.52	10.11	456.46	102.25	2.74	2.19	12.27
9.12	355.12	79.55	2.13	1.70	9.55	10.12	457.14	102.40	2.74	2.19	12.29
9.13	356.19	79.79	2.14	1.71	9.57	10.13	457.82	102.55	2.75	2.20	12.31
9.14	357.25	80.02	2.14	1.71	9.60	10.14	458.50	102.70	2.75	2.20	12.32
9.15	358.32	80.26	2.15	1.72	9.63	10.15	459.18	102.86	2.76	2.20	12.34
9.16	359.39	80.50	2.16	1.73	9.66	10.16	459.86	103.01	2.76	2.21	12.36
9.17	360.45	80.74	2.16	1.73	9.69	10.17	460.53	103.16	2.76	2.21	12.38
9.18	361.52	80.98	2.17	1.74	9.72	10.18	461.21	103.31	2.77	2.21	12.40
9.19	362.59	81.22	2.18	1.74	9.75	10.19	461.89	103.46	2.77	2.22	12.42
9.2	363.65	81.46	2.18	1.75	9.77	10.2	462.57	103.62	2.78	2.22	12.43
9.21	364.72	81.70	2.19	1.75	9.80	10.21	463.25	103.77	2.78	2.22	12.45
9.22	365.79	81.94	2.19	1.76	9.83	10.22	463.93	103.92	2.78	2.23	12.47
9.23	366.85	82.17	2.20	1.76	9.86	10.23	464.61	104.07	2.79	2.23	12.49
9.24	367.92	82.41	2.21	1.77	9.89	10.24	465.29	104.23	2.79	2.23	12.51

9.25	368.98	82.65	2.21	1.77	9.92	10.25	465.97	104.38	2.80	2.24	12.53
9.26	370.05	82.89	2.22	1.78	9.95	10.26	466.65	104.53	2.80	2.24	12.54
9.27	371.12	83.13	2.23	1.78	9.98	10.27	467.33	104.68	2.80	2.24	12.56
9.28	372.18	83.37	2.23	1.79	10.00	10.28	468.01	104.83	2.81	2.25	12.58
9.29	373.25	83.61	2.24	1.79	10.03	10.29	468.69	104.99	2.81	2.25	12.60
9.3	374.32	83.85	2.25	1.80	10.06	10.3	469.37	105.14	2.82	2.25	12.62
9.31	375.38	84.09	2.25	1.80	10.09	10.31	470.05	105.29	2.82	2.26	12.63
9.32	376.45	84.33	2.26	1.81	10.12	10.32	470.73	105.44	2.82	2.26	12.65
9.33	377.52	84.56	2.27	1.81	10.15	10.33	471.41	105.60	2.83	2.26	12.67
9.34	378.58	84.80	2.27	1.82	10.18	10.34	472.09	105.75	2.83	2.27	12.69
9.35	379.65	85.04	2.28	1.82	10.21	10.35	472.77	105.90	2.84	2.27	12.71
9.36	380.72	85.28	2.28	1.83	10.23	10.36	473.45	106.05	2.84	2.27	12.73
9.37	381.78	85.52	2.29	1.83	10.26	10.37	474.13	106.20	2.84	2.28	12.74
9.38	382.85	85.76	2.30	1.84	10.29	10.38	474.81	106.36	2.85	2.28	12.76
9.39	383.92	86.00	2.30	1.84	10.32	10.39	475.49	106.51	2.85	2.28	12.78
9.4	384.98	86.24	2.31	1.85	10.35	10.4	476.17	106.66	2.86	2.29	12.80
9.41	386.05	86.48	2.32	1.85	10.38	10.41	476.85	106.81	2.86	2.29	12.82
9.42	387.12	86.71	2.32	1.86	10.41	10.42	477.53	106.97	2.87	2.29	12.84
9.43	388.18	86.95	2.33	1.86	10.43	10.43	478.21	107.12	2.87	2.30	12.85
9.44	389.25	87.19	2.34	1.87	10.46	10.44	478.89	107.27	2.87	2.30	12.87
9.45	390.32	87.43	2.34	1.87	10.49	10.45	479.57	107.42	2.88	2.30	12.89
9.46	391.38	87.67	2.35	1.88	10.52	10.46	480.25	107.58	2.88	2.31	12.91
9.47	392.45	87.91	2.35	1.88	10.55	10.47	480.93	107.73	2.89	2.31	12.93
9.48	393.52	88.15	2.36	1.89	10.58	10.48	481.61	107.88	2.89	2.31	12.95
9.49	394.58	88.39	2.37	1.89	10.61	10.49	482.29	108.03	2.89	2.31	12.96
9.5	395.65	88.63	2.37	1.90	10.64	10.5	482.97	108.18	2.90	2.32	12.98
9.51	396.72	88.86	2.38	1.90	10.66	10.51	483.64	108.34	2.90	2.32	13.00
9.52	397.78	89.10	2.39	1.91	10.69	10.52	484.32	108.49	2.91	2.32	13.02
9.53	398.85	89.34	2.39	1.91	10.72	10.53	485.00	108.64	2.91	2.33	13.04
9.54	399.92	89.58	2.40	1.92	10.75	10.54	485.68	108.79	2.91	2.33	13.06
9.55	400.98	89.82	2.41	1.92	10.78	10.55	486.36	108.95	2.92	2.33	13.07
9.56	402.05	90.06	2.41	1.93	10.81	10.56	487.04	109.10	2.92	2.34	13.09
9.57	403.12	90.30	2.42	1.93	10.84	10.57	487.72	109.25	2.93	2.34	13.11
9.58	404.18	90.54	2.43	1.94	10.86	10.58	488.40	109.40	2.93	2.34	13.13
9.59	405.25	90.78	2.43	1.95	10.89	10.59	489.08	109.55	2.93	2.35	13.15

APPENDIX E-9 PARAMETERS OF TRANSIENT ANALYSIS FROM 11-12PM IN SUMMER

11		Gp	Gg1	Gg2	Gfloor	12		Gp	Gg1	Gg2	Gfloor
11.00	**516.95**	115.80	3.10	2.48	13.90	12.00	**538.62**	120.65	3.23	2.59	14.48
11.01	517.17	115.85	3.10	2.48	13.90	12.01	538.35	120.59	3.23	2.58	14.47
11.02	517.38	115.89	3.10	2.48	13.91	12.02	538.08	120.53	3.23	2.58	14.46
11.03	517.60	115.94	3.11	2.48	13.91	12.03	537.81	120.47	3.23	2.58	14.46
11.04	517.82	115.99	3.11	2.49	13.92	12.04	537.54	120.41	3.23	2.58	14.45
11.05	518.03	116.04	3.11	2.49	13.92	12.05	537.27	120.35	3.22	2.58	14.44
11.06	518.25	116.09	3.11	2.49	13.93	12.06	537.00	120.29	3.22	2.58	14.43
11.07	518.47	116.14	3.11	2.49	13.94	12.07	536.73	120.23	3.22	2.58	14.43
11.08	518.68	116.19	3.11	2.49	13.94	12.08	536.46	120.17	3.22	2.58	14.42
11.09	518.90	116.23	3.11	2.49	13.95	12.09	536.19	120.11	3.22	2.57	14.41
11.1	519.12	116.28	3.11	2.49	13.95	12.1	535.92	120.05	3.22	2.57	14.41
11.11	519.33	116.33	3.12	2.49	13.96	12.11	535.65	119.99	3.21	2.57	14.40
11.12	519.55	116.38	3.12	2.49	13.97	12.12	535.38	119.93	3.21	2.57	14.39
11.13	519.77	116.43	3.12	2.49	13.97	12.13	535.12	119.87	3.21	2.57	14.38
11.14	519.98	116.48	3.12	2.50	13.98	12.14	534.85	119.81	3.21	2.57	14.38
11.15	520.20	116.52	3.12	2.50	13.98	12.15	534.58	119.75	3.21	2.57	14.37
11.16	520.42	116.57	3.12	2.50	13.99	12.16	534.31	119.68	3.21	2.56	14.36
11.17	520.63	116.62	3.12	2.50	13.99	12.17	534.04	119.62	3.20	2.56	14.35
11.18	520.85	116.67	3.13	2.50	14.00	12.18	533.77	119.56	3.20	2.56	14.35
11.19	521.07	116.72	3.13	2.50	14.01	12.19	533.50	119.50	3.20	2.56	14.34
11.2	521.28	116.77	3.13	2.50	14.01	12.2	533.23	119.44	3.20	2.56	14.33
11.21	521.50	116.82	3.13	2.50	14.02	12.21	532.96	119.38	3.20	2.56	14.33
11.22	521.72	116.86	3.13	2.50	14.02	12.22	532.69	119.32	3.20	2.56	14.32
11.23	521.93	116.91	3.13	2.51	14.03	12.23	532.42	119.26	3.19	2.56	14.31
11.24	522.15	116.96	3.13	2.51	14.04	12.24	532.15	119.20	3.19	2.55	14.30
11.25	522.37	117.01	3.13	2.51	14.04	12.25	531.88	119.14	3.19	2.55	14.30
11.26	522.58	117.06	3.14	2.51	14.05	12.26	531.61	119.08	3.19	2.55	14.29
11.27	522.80	117.11	3.14	2.51	14.05	12.27	531.34	119.02	3.19	2.55	14.28
11.28	523.02	117.16	3.14	2.51	14.06	12.28	531.07	118.96	3.19	2.55	14.28
11.29	523.23	117.20	3.14	2.51	14.06	12.29	530.80	118.90	3.18	2.55	14.27
11.3	523.45	117.25	3.14	2.51	14.07	12.3	530.53	118.84	3.18	2.55	14.26
11.31	523.67	117.30	3.14	2.51	14.08	12.31	530.26	118.78	3.18	2.55	14.25
11.32	523.88	117.35	3.14	2.51	14.08	12.32	529.99	118.72	3.18	2.54	14.25
11.33	524.10	117.40	3.14	2.52	14.09	12.33	529.72	118.66	3.18	2.54	14.24
11.34	524.32	117.45	3.15	2.52	14.09	12.34	529.45	118.60	3.18	2.54	14.23
11.35	524.53	117.50	3.15	2.52	14.10	12.35	529.18	118.54	3.18	2.54	14.22
11.36	524.75	117.54	3.15	2.52	14.11	12.36	528.91	118.48	3.17	2.54	14.22
11.37	524.97	117.59	3.15	2.52	14.11	12.37	528.64	118.42	3.17	2.54	14.21
11.38	525.18	117.64	3.15	2.52	14.12	12.38	528.38	118.36	3.17	2.54	14.20
11.39	525.40	117.69	3.15	2.52	14.12	12.39	528.11	118.30	3.17	2.53	14.20
11.4	525.62	117.74	3.15	2.52	14.13	12.4	527.84	118.24	3.17	2.53	14.19
11.41	525.83	117.79	3.16	2.52	14.13	12.41	527.57	118.17	3.17	2.53	14.18
11.42	526.05	117.84	3.16	2.53	14.14	12.42	527.30	118.11	3.16	2.53	14.17

11.43	526.27	117.88	3.16	2.53	14.15	12.43	527.03	118.05	3.16	2.53	14.17
11.44	526.48	117.93	3.16	2.53	14.15	12.44	526.76	117.99	3.16	2.53	14.16
11.45	526.70	117.98	3.16	2.53	14.16	12.45	526.49	117.93	3.16	2.53	14.15
11.46	526.92	118.03	3.16	2.53	14.16	12.46	526.22	117.87	3.16	2.53	14.14
11.47	527.13	118.08	3.16	2.53	14.17	12.47	525.95	117.81	3.16	2.52	14.14
11.48	527.35	118.13	3.16	2.53	14.18	12.48	525.68	117.75	3.15	2.52	14.13
11.49	527.57	118.18	3.17	2.53	14.18	12.49	525.41	117.69	3.15	2.52	14.12
11.5	527.79	118.22	3.17	2.53	14.19	12.5	525.14	117.63	3.15	2.52	14.12
11.51	528.00	118.27	3.17	2.53	14.19	12.51	524.87	117.57	3.15	2.52	14.11
11.52	528.22	118.32	3.17	2.54	14.20	12.52	524.60	117.51	3.15	2.52	14.10
11.53	528.44	118.37	3.17	2.54	14.20	12.53	524.33	117.45	3.15	2.52	14.09
11.54	528.65	118.42	3.17	2.54	14.21	12.54	524.06	117.39	3.14	2.52	14.09
11.55	528.87	118.47	3.17	2.54	14.22	12.55	523.79	117.33	3.14	2.51	14.08
11.56	529.09	118.52	3.17	2.54	14.22	12.56	523.52	117.27	3.14	2.51	14.07
11.57	529.30	118.56	3.18	2.54	14.23	12.57	523.25	117.21	3.14	2.51	14.07
11.58	529.52	118.61	3.18	2.54	14.23	12.58	522.98	117.15	3.14	2.51	14.06
11.59	529.74	118.66	3.18	2.54	14.24	12.59	522.71	117.09	3.14	2.51	14.05

APPENDIX E-10 PARAMETERS OF TRANSIENT ANALYSIS FROM 13-14PM IN SUMMER

13		Gp	Gg1	Gg2	Gfloor	14		Gp	Gg1	Gg2	Gfloor
13.00	**511.66**	114.61	3.07	2.46	13.75	14.00	**438.96**	98.33	2.63	2.11	11.80
13.01	510.93	114.45	3.07	2.45	13.73	14.01	437.86	98.08	2.63	2.10	11.77
13.02	510.21	114.29	3.06	2.45	13.71	14.02	436.76	97.83	2.62	2.10	11.74
13.03	509.48	114.12	3.06	2.45	13.69	14.03	435.65	97.59	2.61	2.09	11.71
13.04	508.75	113.96	3.05	2.44	13.68	14.04	434.55	97.34	2.61	2.09	11.68
13.05	508.03	113.80	3.05	2.44	13.66	14.05	433.45	97.09	2.60	2.08	11.65
13.06	507.30	113.63	3.04	2.44	13.64	14.06	432.35	96.85	2.59	2.08	11.62
13.07	506.57	113.47	3.04	2.43	13.62	14.07	431.25	96.60	2.59	2.07	11.59
13.08	505.84	113.31	3.04	2.43	13.60	14.08	430.14	96.35	2.58	2.06	11.56
13.09	505.12	113.15	3.03	2.42	13.58	14.09	429.04	96.11	2.57	2.06	11.53
13.1	504.39	112.98	3.03	2.42	13.56	14.1	427.94	95.86	2.57	2.05	11.50
13.11	503.66	112.82	3.02	2.42	13.54	14.11	426.84	95.61	2.56	2.05	11.47
13.12	502.94	112.66	3.02	2.41	13.52	14.12	425.74	95.36	2.55	2.04	11.44
13.13	502.21	112.49	3.01	2.41	13.50	14.13	424.63	95.12	2.55	2.04	11.41
13.14	501.48	112.33	3.01	2.41	13.48	14.14	423.53	94.87	2.54	2.03	11.38
13.15	500.76	112.17	3.00	2.40	13.46	14.15	422.43	94.62	2.53	2.03	11.35
13.16	500.03	112.01	3.00	2.40	13.44	14.16	421.33	94.38	2.53	2.02	11.33
13.17	499.30	111.84	3.00	2.40	13.42	14.17	420.23	94.13	2.52	2.02	11.30
13.18	498.57	111.68	2.99	2.39	13.40	14.18	419.12	93.88	2.51	2.01	11.27
13.19	497.85	111.52	2.99	2.39	13.38	14.19	418.02	93.64	2.51	2.01	11.24
13.2	497.12	111.35	2.98	2.39	13.36	14.2	416.92	93.39	2.50	2.00	11.21
13.21	496.39	111.19	2.98	2.38	13.34	14.21	415.82	93.14	2.49	2.00	11.18
13.22	495.67	111.03	2.97	2.38	13.32	14.22	414.72	92.90	2.49	1.99	11.15
13.23	494.94	110.87	2.97	2.38	13.30	14.23	413.61	92.65	2.48	1.99	11.12
13.24	494.21	110.70	2.97	2.37	13.28	14.24	412.51	92.40	2.48	1.98	11.09

13.25	493.49	110.54	2.96	2.37	13.26	14.25	411.41	92.16	2.47	1.97	11.06
13.26	492.76	110.38	2.96	2.37	13.25	14.26	410.31	91.91	2.46	1.97	11.03
13.27	492.03	110.21	2.95	2.36	13.23	14.27	409.21	91.66	2.46	1.96	11.00
13.28	491.30	110.05	2.95	2.36	13.21	14.28	408.10	91.42	2.45	1.96	10.97
13.29	490.58	109.89	2.94	2.35	13.19	14.29	407.00	91.17	2.44	1.95	10.94
13.3	489.85	109.73	2.94	2.35	13.17	14.3	405.90	90.92	2.44	1.95	10.91
13.31	489.12	109.56	2.93	2.35	13.15	14.31	404.80	90.67	2.43	1.94	10.88
13.32	488.40	109.40	2.93	2.34	13.13	14.32	403.70	90.43	2.42	1.94	10.85
13.33	487.67	109.24	2.93	2.34	13.11	14.33	402.59	90.18	2.42	1.93	10.82
13.34	486.94	109.08	2.92	2.34	13.09	14.34	401.49	89.93	2.41	1.93	10.79
13.35	486.22	108.91	2.92	2.33	13.07	14.35	400.39	89.69	2.40	1.92	10.76
13.36	485.49	108.75	2.91	2.33	13.05	14.36	399.29	89.44	2.40	1.92	10.73
13.37	484.76	108.59	2.91	2.33	13.03	14.37	398.19	89.19	2.39	1.91	10.70
13.38	484.03	108.42	2.90	2.32	13.01	14.38	397.08	88.95	2.38	1.91	10.67
13.39	483.31	108.26	2.90	2.32	12.99	14.39	395.98	88.70	2.38	1.90	10.64
13.4	482.58	108.10	2.90	2.32	12.97	14.4	394.88	88.45	2.37	1.90	10.61
13.41	481.85	107.94	2.89	2.31	12.95	14.41	393.78	88.21	2.36	1.89	10.58
13.42	481.13	107.77	2.89	2.31	12.93	14.42	392.68	87.96	2.36	1.88	10.56
13.43	480.40	107.61	2.88	2.31	12.91	14.43	391.57	87.71	2.35	1.88	10.53
13.44	479.67	107.45	2.88	2.30	12.89	14.44	390.47	87.47	2.34	1.87	10.50
13.45	478.95	107.28	2.87	2.30	12.87	14.45	389.37	87.22	2.34	1.87	10.47
13.46	478.22	107.12	2.87	2.30	12.85	14.46	388.27	86.97	2.33	1.86	10.44
13.47	477.49	106.96	2.86	2.29	12.83	14.47	387.17	86.73	2.32	1.86	10.41
13.48	476.76	106.80	2.86	2.29	12.82	14.48	386.06	86.48	2.32	1.85	10.38
13.49	476.04	106.63	2.86	2.28	12.80	14.49	384.96	86.23	2.31	1.85	10.35
13.5	475.31	106.47	2.85	2.28	12.78	14.5	383.86	85.98	2.30	1.84	10.32
13.51	474.58	106.31	2.85	2.28	12.76	14.51	382.76	85.74	2.30	1.84	10.29
13.52	473.86	106.14	2.84	2.27	12.74	14.52	381.66	85.49	2.29	1.83	10.26
13.53	473.13	105.98	2.84	2.27	12.72	14.53	380.55	85.24	2.28	1.83	10.23
13.54	472.40	105.82	2.83	2.27	12.70	14.54	379.45	85.00	2.28	1.82	10.20
13.55	471.68	105.66	2.83	2.26	12.68	14.55	378.35	84.75	2.27	1.82	10.17
13.56	470.95	105.49	2.83	2.26	12.66	14.56	377.25	84.50	2.26	1.81	10.14
13.57	470.22	105.33	2.82	2.26	12.64	14.57	376.15	84.26	2.26	1.81	10.11
13.58	469.49	105.17	2.82	2.25	12.62	14.58	375.04	84.01	2.25	1.80	10.08
13.59	468.77	105.00	2.81	2.25	12.60	14.59	373.94	83.76	2.24	1.79	10.05

APPENDIX E-11 PARAMETERS OF TRANSIENT ANALYSIS FROM 15-16PM IN SUMMER

15		Gp	Gg1	Gg2	Gfloor	16		Gp	Gg1	Gg2	Gfloor
15.00	**328.76**	73.64	1.97	1.58	8.84	16.00	**194.93**	43.66	1.17	0.94	5.24
15.01	327.42	73.34	1.96	1.57	8.80	16.01	194.04	43.47	1.16	0.93	5.22
15.02	326.08	73.04	1.96	1.57	8.77	16.02	193.15	43.27	1.16	0.93	5.19
15.03	324.75	72.74	1.95	1.56	8.73	16.03	192.27	43.07	1.15	0.92	5.17
15.04	323.41	72.44	1.94	1.55	8.69	16.04	191.38	42.87	1.15	0.92	5.14
15.05	322.07	72.14	1.93	1.55	8.66	16.05	190.49	42.67	1.14	0.91	5.12
15.06	320.73	71.84	1.92	1.54	8.62	16.06	189.60	42.47	1.14	0.91	5.10
15.07	319.39	71.54	1.92	1.53	8.59	16.07	188.72	42.27	1.13	0.91	5.07
15.08	318.05	71.24	1.91	1.53	8.55	16.08	187.83	42.07	1.13	0.90	5.05
15.09	316.72	70.94	1.90	1.52	8.51	16.09	186.94	41.87	1.12	0.90	5.02
15.1	315.38	70.64	1.89	1.51	8.48	16.1	186.05	41.68	1.12	0.89	5.00
15.11	314.04	70.34	1.88	1.51	8.44	16.11	185.17	41.48	1.11	0.89	4.98
15.12	312.70	70.04	1.88	1.50	8.41	16.12	184.28	41.28	1.11	0.88	4.95
15.13	311.36	69.75	1.87	1.49	8.37	16.13	183.39	41.08	1.10	0.88	4.93
15.14	310.02	69.45	1.86	1.49	8.33	16.14	182.50	40.88	1.10	0.88	4.91
15.15	308.69	69.15	1.85	1.48	8.30	16.15	181.61	40.68	1.09	0.87	4.88
15.16	307.35	68.85	1.84	1.48	8.26	16.16	180.73	40.48	1.08	0.87	4.86
15.17	306.01	68.55	1.84	1.47	8.23	16.17	179.84	40.28	1.08	0.86	4.83
15.18	304.67	68.25	1.83	1.46	8.19	16.18	178.95	40.09	1.07	0.86	4.81
15.19	303.33	67.95	1.82	1.46	8.15	16.19	178.06	39.89	1.07	0.85	4.79
15.2	301.99	67.65	1.81	1.45	8.12	16.2	177.18	39.69	1.06	0.85	4.76
15.21	300.66	67.35	1.80	1.44	8.08	16.21	176.29	39.49	1.06	0.85	4.74
15.22	299.32	67.05	1.80	1.44	8.05	16.22	175.40	39.29	1.05	0.84	4.71
15.23	297.98	66.75	1.79	1.43	8.01	16.23	174.51	39.09	1.05	0.84	4.69
15.24	296.64	66.45	1.78	1.42	7.97	16.24	173.63	38.89	1.04	0.83	4.67
15.25	295.30	66.15	1.77	1.42	7.94	16.25	172.74	38.69	1.04	0.83	4.64
15.26	293.96	65.85	1.76	1.41	7.90	16.26	171.85	38.49	1.03	0.82	4.62
15.27	292.63	65.55	1.76	1.40	7.87	16.27	170.96	38.30	1.03	0.82	4.60
15.28	291.29	65.25	1.75	1.40	7.83	16.28	170.07	38.10	1.02	0.82	4.57
15.29	289.95	64.95	1.74	1.39	7.79	16.29	169.19	37.90	1.02	0.81	4.55
15.3	288.61	64.65	1.73	1.39	7.76	16.3	168.30	37.70	1.01	0.81	4.52
15.31	287.27	64.35	1.72	1.38	7.72	16.31	167.41	37.50	1.00	0.80	4.50
15.32	285.93	64.05	1.72	1.37	7.69	16.32	166.52	37.30	1.00	0.80	4.48
15.33	284.60	63.75	1.71	1.37	7.65	16.33	165.64	37.10	0.99	0.80	4.45
15.34	283.26	63.45	1.70	1.36	7.61	16.34	164.75	36.90	0.99	0.79	4.43
15.35	281.92	63.15	1.69	1.35	7.58	16.35	163.86	36.70	0.98	0.79	4.40
15.36	280.58	62.85	1.68	1.35	7.54	16.36	162.97	36.51	0.98	0.78	4.38
15.37	279.24	62.55	1.68	1.34	7.51	16.37	162.09	36.31	0.97	0.78	4.36
15.38	277.90	62.25	1.67	1.33	7.47	16.38	161.20	36.11	0.97	0.77	4.33
15.39	276.57	61.95	1.66	1.33	7.43	16.39	160.31	35.91	0.96	0.77	4.31
15.4	275.23	61.65	1.65	1.32	7.40	16.4	159.42	35.71	0.96	0.77	4.29
15.41	273.89	61.35	1.64	1.31	7.36	16.41	158.53	35.51	0.95	0.76	4.26
15.42	272.55	61.05	1.64	1.31	7.33	16.42	157.65	35.31	0.95	0.76	4.24

15.43	271.21	60.75	1.63	1.30	7.29	16.43	156.76	35.11	0.94	0.75	4.21
15.44	269.87	60.45	1.62	1.30	7.25	16.44	155.87	34.92	0.94	0.75	4.19
15.45	268.54	60.15	1.61	1.29	7.22	16.45	154.98	34.72	0.93	0.74	4.17
15.46	267.20	59.85	1.60	1.28	7.18	16.46	154.10	34.52	0.92	0.74	4.14
15.47	265.86	59.55	1.60	1.28	7.15	16.47	153.21	34.32	0.92	0.74	4.12
15.48	264.52	59.25	1.59	1.27	7.11	16.48	152.32	34.12	0.91	0.73	4.09
15.49	263.18	58.95	1.58	1.26	7.07	16.49	151.43	33.92	0.91	0.73	4.07
15.5	261.85	58.65	1.57	1.26	7.04	16.5	150.55	33.72	0.90	0.72	4.05
15.51	260.51	58.35	1.56	1.25	7.00	16.51	149.66	33.52	0.90	0.72	4.02
15.52	259.17	58.05	1.56	1.24	6.97	16.52	148.77	33.32	0.89	0.71	4.00
15.53	257.83	57.75	1.55	1.24	6.93	16.53	147.88	33.13	0.89	0.71	3.98
15.54	256.49	57.45	1.54	1.23	6.89	16.54	146.99	32.93	0.88	0.71	3.95
15.55	255.15	57.15	1.53	1.22	6.86	16.55	146.11	32.73	0.88	0.70	3.93
15.56	253.82	56.85	1.52	1.22	6.82	16.56	145.22	32.53	0.87	0.70	3.90
15.57	252.48	56.55	1.51	1.21	6.79	16.57	144.33	32.33	0.87	0.69	3.88
15.58	251.14	56.26	1.51	1.21	6.75	16.58	143.44	32.13	0.86	0.69	3.86
15.59	249.80	55.96	1.50	1.20	6.71	16.59	142.56	31.93	0.86	0.68	3.83

APPENDIX E-12 PARAMETERS OF TRANSIENT ANALYSIS FOR 17PM-18PM IN SUMMER

17		Gp	Gg1	Gg2	Gfloor
17.00	**106.16**	23.78	0.64	0.51	2.85
17.01	105.99	23.74	0.64	0.51	2.85
17.02	105.82	23.70	0.63	0.51	2.84
17.03	105.65	23.67	0.63	0.51	2.84
17.04	105.48	23.63	0.63	0.51	2.84
17.05	105.31	23.59	0.63	0.51	2.83
17.06	105.14	23.55	0.63	0.50	2.83
17.07	104.97	23.51	0.63	0.50	2.82
17.08	104.80	23.48	0.63	0.50	2.82
17.09	104.64	23.44	0.63	0.50	2.81
17.1	104.47	23.40	0.63	0.50	2.81
17.11	104.30	23.36	0.63	0.50	2.80
17.12	104.13	23.32	0.62	0.50	2.80
17.13	103.96	23.29	0.62	0.50	2.79
17.14	103.79	23.25	0.62	0.50	2.79
17.15	103.62	23.21	0.62	0.50	2.79
17.16	103.45	23.17	0.62	0.50	2.78
17.17	103.28	23.13	0.62	0.50	2.78
17.18	103.11	23.10	0.62	0.49	2.77
17.19	102.94	23.06	0.62	0.49	2.77
17.2	102.77	23.02	0.62	0.49	2.76
17.21	102.60	22.98	0.62	0.49	2.76
17.22	102.43	22.95	0.61	0.49	2.75
17.23	102.26	22.91	0.61	0.49	2.75
17.24	102.09	22.87	0.61	0.49	2.74

17.25	101.93	22.83	0.61	0.49	2.74
17.26	101.76	22.79	0.61	0.49	2.74
17.27	101.59	22.76	0.61	0.49	2.73
17.28	101.42	22.72	0.61	0.49	2.73
17.29	101.25	22.68	0.61	0.49	2.72
17.3	101.08	22.64	0.61	0.49	2.72
17.31	100.91	22.60	0.61	0.48	2.71
17.32	100.74	22.57	0.60	0.48	2.71
17.33	100.57	22.53	0.60	0.48	2.70
17.34	100.40	22.49	0.60	0.48	2.70
17.35	100.23	22.45	0.60	0.48	2.69
17.36	100.06	22.41	0.60	0.48	2.69
17.37	99.89	22.38	0.60	0.48	2.69
17.38	99.72	22.34	0.60	0.48	2.68
17.39	99.55	22.30	0.60	0.48	2.68
17.4	99.38	22.26	0.60	0.48	2.67
17.41	99.21	22.22	0.60	0.48	2.67
17.42	99.05	22.19	0.59	0.48	2.66
17.43	98.88	22.15	0.59	0.47	2.66
17.44	98.71	22.11	0.59	0.47	2.65
17.45	98.54	22.07	0.59	0.47	2.65
17.46	98.37	22.03	0.59	0.47	2.64
17.47	98.20	22.00	0.59	0.47	2.64
17.48	98.03	21.96	0.59	0.47	2.64
17.49	97.86	21.92	0.59	0.47	2.63
17.5	97.69	21.88	0.59	0.47	2.63
17.51	97.52	21.84	0.59	0.47	2.62
17.52	97.35	21.81	0.58	0.47	2.62
17.53	97.18	21.77	0.58	0.47	2.61
17.54	97.01	21.73	0.58	0.47	2.61
17.55	96.84	21.69	0.58	0.46	2.60
17.56	96.67	21.65	0.58	0.46	2.60
17.57	96.50	21.62	0.58	0.46	2.59
17.58	96.33	21.58	0.58	0.46	2.59
17.59	96.17	21.54	0.58	0.46	2.58